2008

Elucidating marine pore water exchange and fresh aquifer sources in estimates of submarine groundwater discharge to a coastal lagoon

Christopher Gerald Smith
Louisiana State University and Agricultural and Mechanical College

ELUCIDATING MARINE PORE WATER EXCHANGE AND FRESH AQUIFER SOURCES IN ESTIMATES OF SUBMARINE GROUNDWATER DISCHARGE TO A COASTAL LAGOON

A Dissertation

Submitted to the Graduate Faculty of the
Louisiana State University and
Agricultural and Mechanical College
in partial fulfillment of the
requirements for the degree of
Doctor of Philosophy

in

The Department of Oceanography and Coastal Sciences

by
Christopher Gerald Smith
B.S., East Carolina University, 2001
M.S., East Carolina University, 2004
August 2008

ACKNOWLEDGMENTS

I would like to extend my deepest respect and gratitude to all of my committee members, past and present. I would like to thank my graduate advisor, Jaye Cable, for her limitless support, flexibility, and patience; you have bestowed upon me a wealth of knowledge that I will inevitably spend the rest of my life interpreting and re-interpreting. To Jonathan "Jon" Martin, it has been great working with you in the field; the conversations we shared concerning my work provided insurmountable insight to the "bigger picture". To Drs. William "Bill" Blanford and Chunyan Li, I thank you for reminding me how important mathematics are in modern scientific research and the patience for teaching me quantitative techniques. To the remainder of my official (Drs. Robert Gambrell and Frank Tsai) and unofficial (Dr. Samuel Bentley) committee members, thank you for answering any and all questions that I asked and for your help in developing this document.

I would like to thank Dr. Jennifer Cherrier (FAMU), Amanda Dorsett, Kevin Hartl, Dr. John Jaeger (UF), Puja Jasrotia, Dr. Christof Meile (UGA), Kelly McGowan, Dr. John Trefry (FIT), Dylan Miner, and Sarakeith Valentine for their field and technical support. A special thanks is extended to my friend Moutusi Roy; our conversation about "SGD", "seepage faces", and "subterranean estuaries" were fundamental in the development of this document. I would like to thank Julia Wheatley for her assistance in the lab. To Peter "Pete" Cable, you were truly the light at the end of the chemistry lab. Whenever I thought something was chemically impossible, you were there to show me the way. I express gratitude to Hilary Collis and Gregg Snedden for showing me the ropes of Baton Rouge and the lab. Also, I would like to thank Dr. Michael Bizimis of Florida State University-National High Magentic Field Laboratory as well as Drs. Bin Huang of Louisiana State University for their analytical assistance. I acknowledge all students, staff, and faculty of the Department of Oceanography and Coastal Sciences here at

Louisiana State University to whom I have interacted with in the hallways, offices, and classrooms. This research would not have been possible without the continued financial support from the National Science Foundation. Additional funding was provided by the Geological Society of America in the form of a student research grant. I would like to thank St. Johns River Water Management District and United States Geological Survey for access to data.

Now I would like to thank those people who reach beyond my time here at Louisiana State University. To my wife and the mother of my daughter, Jeanna Taylor-Smith, you are truly an amazing woman. You have been the common thread in my life for the last eight years, no matter where I wanted to go or what I wanted to do. To you I say thank you and I love you. To my daughter, Alana Smith, you have shown me what it truly means to be unselfish. I would like to thank my parents, Gerald Jr. and Myra Smith; my brother, Brad; and my paternal grandparents, Gerald and Mavis Smith; all of you have been a constant emotional support no matter how far I venture away from Duplin County. Finally I would like to thank Mr. Ricky Houston, my high school trigonometry and calculus teacher; if not for your academic encouragement early in life I would not be where I am today.

TABLE OF CONTENTS

LIST OF TABLES

LIST OF FIGURES

ABSTRACT

Dynamic balances between fresh groundwater, saline groundwater, and surface water control the physics and chemistry of subterranean estuaries. Investigations were performed in a subterranean estuary on physical processes contributing to fresh groundwater and saline water mixing, vertical and lateral positioning of this mixing zone, and how this mixing affects spatial and temporal distributions of $^{234,238}U$, ^{226}Ra, and ^{222}Rn. The subterranean estuary is located in an unconfined aquifer beneath Indian River Lagoon, Florida, USA, where I could examine redox responses to altered flow regimes. Continuous groundwater and surface water level measurements suggest a strong hydrologic connection between this lagoon and the groundwater-aquifer system. Periodic forces (e.g. tides, frontal passages) represent a minor contribution to water level variations; however, forcing by tropical cyclones creates large variations in mixing within the seepage outflow. Hurricane Wilma and Tropical Storm Tammy caused hydraulic gradients to reverse, causing lagoon water to recharge the aquifer and shifting the seepage face and subterranean estuary landward about seven meters. Additionally, seasonal distributions of dissolved ^{222}Rn, ^{226}Ra, and $^{234,238}U$ in pore and surface waters revealed sensitivity to temporal and spatial mixing and geological heterogeneity. Processes affecting the distribution of these elements include U redox cycling, heterogeneous production of ^{222}Rn from sediments, and ^{226}Ra release during Mn-hydroxide reduction and/or surface exchange. Uranium cycling within the subterranean estuary resulted in a flux of approximately 54 μmol U m^{-2} y^{-1} to the lagoon. A one-dimensional ^{222}Rn transport model was used to quantify fresh and marine sources to submarine groundwater discharge (SGD) through incorporation of heterogeneous production, diffusive, advective, and nonlocal transport mechanisms, and Monte Carlo simulations. Model-based volumetric estimates of fresh and marine SGD components yield ranges of 1.01 to 1.85 and 1.69 to 3.43 m^3 d^{-1} m^{-1} of shoreline, respectively, suggesting fresh SGD contributes approximately

one-third of total discharge measured within this subterranean estuary. The 30% fresh component in discharge and the uranium source to coastal lagoon demonstrates SGDs role in global ocean freshwater and elemental inputs. This study highlights the significance of distinguishing fresh and marine groundwater sources and the hydrogeological and chemical complexity of these dynamic subterranean mixing zones.

CHAPTER 1.

INTRODUCTION

This introductory chapter provides a brief background on the relevance of submarine groundwater discharge research to larger coastal issues (e.g. eutrophication and water resources), provide conventional definitions for submarine groundwater discharge (SGD) and the subterranean estuary, describes some of the current conundrums with respect to source and measurement of submarine groundwater discharge, and provides an outline for the remainder of the dissertation.

Submarine Groundwater Discharge and the Subterranean Estuary

Nutrient and containment transport to coastal systems (wetlands, estuaries, and the shelf) occurs via rivers, runoff, groundwater, and precipitation, and these inputs are a constant threat to maintaining coastal ecological health and diversity. In particular, the benthos is identified as one of the critical zones where material flux as both external loading (e.g. rivers and groundwater discharge) and internal cycling (e.g. sediment resuspension, shallow pore water exchange) of buried organic matter occurs (Simmons 1992, Moore 1999, Slomp and Van Cappellen 2004; Collis 2006). While benthic fluxes are ubiquitous natural processes occurring on the seafloor, they may have deleterious effects on the biogeochemistry of the coastal system (Simmons 1992; Church 1996; Paerl 1997); the effect ultimately depends on the source and composition of the pore fluid as well as the geochemical framework of the benthic sediments. Over the last decade submarine groundwater discharge has been recognized as an important vector of benthic flux to coastal systems. Quantifying this vector is important not only for the ecology of the coastal system but also for understanding groundwater resources in coastal systems.

Coastal groundwater resources have become increasingly stressed by the continuous development of coastal regions for human occupation and recreation. Water resource managers

have long struggled with balancing groundwater demand with supply in coastal regions to prevent aquifer salinization. In general, groundwater-aquifer systems connect recharge, storativity, transmissivity, and discharge; consequently understanding one or more of these hydrogeologic traits helps better predict responses to disturbances, such as drought, sea level rise, and salt water intrusion (Bredehoeft 2007). Benthic fluid fluxes to coastal systems may contain both marine and fresh water components, of which the fresh component is significant as a groundwater sink from terrestrial aquifers and as a source to surface waters. The relative fractions of marine and fresh components are critical to water resource and water quality managers considering approximately 23% of the world's population now lives within 100 km of the coast, thus stressing regional freshwater resources. Population and resource pressures will likely be exacerbated considering the alarming predictions for climate change consequences to the hydrologic cycle (IPCC 2007). Thus, identifying areas where fresh groundwater discharge to coastal regions occurs and quantifying this discharge would provide coastal managers with valuable information concerning groundwater availability and potential locations for nearshore benthic constituent loading. In this dissertation, I examine the magnitude of fresh groundwater entering a back-barrier lagoon located on a marine carbonate platform and consider the response of this subterranean discharge zone to physical perturbations and redox and cation exchange conditions.

This discussion highlights the implications for submarine groundwater discharge (SGD). Burnett et al. (2003) defines submarine groundwater discharge as "any and all flow of water on continental margins from the seabed to the coastal ocean, regardless of fluid composition or driving force." SGD can be subdivided based on fluid composition and origin as: 1) meteoric fresh submarine groundwater, 2) recirculated or marine submarine groundwater, and 3) connate water; each water type exerts a distinct influence on the biogeochemical processes occurring

within the sediment and across the sediment-water interface (Burnett et al. 2003). Meteoric groundwater and recirculated seawater are the two main processes contributing to most SGD measurements. To date, most SGD research has focused on quantifying the total SGD flux, evaluating the primary physical processes, and deducing the biogeochemical impact to the coastal water bodies (e.g., Church 1996; Moore 1996; Younger 1996; Li et al. 1999; Moore 1999; Burnett et al. 2001; Taniguchi et al. 2002; Burnett et al. 2003).

Meteoric-derived or fresh SGD is driven by the hydraulic gradient within an aquifer with the terminus of the flow paths occurring along the shoreline and some distance offshore (Figure 1.1). The offshore extent of seepage has been shown to decrease exponentially from the shoreline (Mcbride and Pfannkuch 1975, Bokuniewicz 1995), with the greatest volume of freshwater occurring within the outflow gap or seepage face (Bokuniewicz 1995). The magnitude of fresh submarine groundwater discharge is dependent on the aquifer hydraulic conductivity and the hydraulic gradient (Freeze and Cherry 1979; Bokuniewicz 1995; Fetter 2001; Burnett et al. 2006), thus varying over different hydrogeologic settings. Consequently, meteoric groundwater acts as an allochthonous source of freshwater and dissolved constituents to coastal systems and creates a dynamic mixing zone for biogeochemical transformations at the coastline.

Submarine groundwater derived from the circulation of seawater into and out of the seafloor is generated at a variety of scales; the two most commonly identified scales of (re)circulation are shallow surface water-pore water exchange and deep, convective mixing. The most common processes responsible for the shallow surface water-pore water exchange include tidal and wave pumping (Riedl et al. 1972; Precht and Huettel 2003; Robinson et al. 2007), density- and/or thermally-driven convection (Rasmussen 1998; Wilson 2005), and bioirrigation (Hammond and Fuller 1979; Martens et al. 1980; Emerson et al. 1984; Martin and Banta 1992;

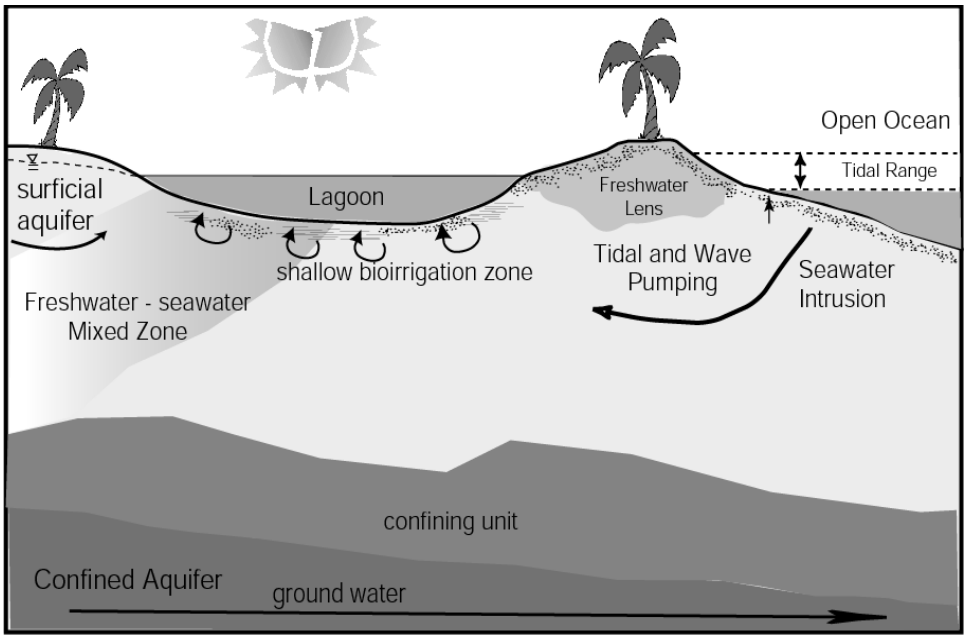

Figure 1.1. Schematic cross-section through a coastal barrier island setting showing the processes that influence the discharge of pore water into overlying water bodies, namely the lagoon (modified from Cable et al. 2006a).

Cable et al. 2004; Martin et al. 2004; Martin et al. 2006; Martin et al. 2007) (Figure 1.1). In contrast, density- and/or thermally-driven convection are the primary mechanisms responsible for deep (re)circulation of seawater into and out of the seafloor and deeper extents of coastal aquifers (Cooper 1959; Glover 1959; Senger and Fogg 1990b; Senger and Fogg 1990a; Smith 2004; Wilson 2005). This (re)circulated seawater may be enriched in oxygen relative to meteoric groundwater, and subsequently, their interaction affects redox conditions and elemental cycling (e.g., metals, nutrients, and contaminants) within shallow sediments (Simmons 1992; Moore 1999).

Connate water provides a non-local source to the coastal water budget similar to meteoric groundwater. The water chemistry reflects the paleoenvironmental conditions under which the aquifer was deposited and subsequent alteration of the aquifer and pore fluid through time. This water can be more saline and denser than modern seawater and have a completely different

geochemistry than recently recharged inland aquifer water; thus connate water may provide allochthonous chemical constituents to the modern coastal system if an exchange pathway exists. The influence of connate water is often limited to areas where hydrothermal processes occur or where the surface water body is hydrologically contacted to very old geologic materials through a breach or truncation in a confining unit.

Biogeochemical transformations associated with SGD are influenced by the composition of these end-member water sources and the interaction between these different sources. This interaction is manifested as a subsurface mixing zone defined by Moore (1999) as the subterranean estuary, due to its similarities to surface water estuaries (Table 1.1). Specifically, the subterranean estuary is a mixing zone between fresh groundwater and saline waters (i.e. deeper saline groundwater or marine surface water). Contrasts in the oxidation-reduction potential (redox), pH, and ionic strength between fresh and saline end-members exert a significant influence on the biogeochemistry of dissolved constituents transported through this zone as well as the aquifer matrix. Depending upon the local geology, aquifer composition, and human consumption pressures, subterranean estuaries may contribute significantly to local-, regional-, and global-scale elemental budgets, and subsequently, affect the application of certain geochemical tracers used to quantify SGD.

Measuring Submarine Groundwater Discharge

To date, geochemical tracers (e.g., Ra-isotopes, ^{222}Rn, ^{3}H, Cl^{-}), seepage meters, and water budgets are the most commonly employed techniques for quantifying SGD (e.g. Cable et al. 1996a; Moore 1996; Burnett 1999; Burnett et al. 2001; Burnett et al. 2002; Burnett et al. 2003, Taniguchi and Iwakawa 2004). One of the largest problems with current SGD research is the corroboration among the different measurement techniques; several researchers suggest that these discrepancies reside in the component of SGD being measured (Martin et al. 2002;

Table 1.1 Comparison of surface and subterranean estuaries, modified from Moore (1999).

Characteristic	Surface estuaries	Subterranean estuaries
Interaction	Mixing zone of continental rivers and sea water	Mixing zone of meteoric groundwater and sea water
Physical Forcing Mechanisms	Tidal forces and river discharge, estuarine circulation	Aquifer hydraulic head and coastal tidal forces, seawater re-circulation through sediments,
Residence Time	Relatively short residence time (order of hours to months)	Longer residence time due to slower flow rates(order of weeks to years)
Residual Flow	Residual flow to sea	Residual flow may occur as either salt water intrusion or groundwater discharge
Particle and Ionic Strength Interactions	High particulate loads lead to strong particle–water interactions. Major ions dominated by sea salts. Sea level exerts a major control.	Large surface area contact with solids leads to strong particle–water interactions. Major ions reflect pore water exchange and diagenesis. Sea level exerts a major control.
Atmospheric Influence	In contact with atmosphere, high oxygen, oxidized Fe and Mn-sediments.	No direct contact with atmosphere, responds to barometric pressure, hypoxic to anoxic conditions, high pCO_2, Fe and Mn may be reduced
Biology	Low diversity, high abundance biological systems	Burrowing organisms and bacteria are primary life
Human Influence	Human impact is often significant	Human impact is likely significant

Shinn et al. 2002; Burnett et al. 2003; Oberdorfer 2003; Taniguchi et al. 2003; Cable et al. 2004; Martin et al. 2004; Cable et al. 2006b). The Scientific Committee on Oceanic Research (SCOR) Working Group 112 conducted several intercomparison studies between 2000 and 2005, through a jointly funded UNESCO/IAEA project, to understand discrepancies among measurement techniques; these studies were conducted in several hydrogeologic settings including karst (Florida), glacial till sand (New York), volcanic island (Mauritius), and mixed, fractured igneous and alluvium (Brazil) aquifer systems. The premise for these intercomparisons was to address measurement differences (i.e., improve accuracy and corroboration) to allow better estimates of material flux while simultaneously testing whether coastal typology could be used to estimate discharge in similar geologic environments.

Direct Measurement

Seepage meters and measured total heads and hydraulic gradients are the only direct methods of measuring SGD. Some studies have disagreed about the utility of seepage meters (e.g. Shinn et al. 2002; Spinelli et al. 2002; Corbett and Cable 2003; Murdoch and Kelly 2003; Cable et al. 2006a). Numerous lake studies and a few marine studies have documented the sensitivity of seepage meter measurements to background fluxes (e.g. Shaw and Prepas 1989; Cable et al. 1997). Shinn et al. (2002) found the most egregious effect on seepage meters to be the pressure differential between the sides and top of the seepage device, which they called "Bernoulli's Revenge". Shinn et al. (2002) noted this phenomenon after conducting a study using several seepage meter designs where all seepage meters recorded positive (vertically upward) fluxes even when a negative hydraulic gradient existed between surface water and groundwater. While their experiments were all conducted well beyond any subterranean freshwater discharge zone, the study does point to some limitations of seepage meters and has a basis in observations of flow over ripple beds. Laboratory studies (e.g., Huettel et al. 1996;

Precht and Huettel 2003) and field observations (e.g., Riedl et al. 1972) have noted pressure gradients sufficient enough to cause shallow (5-10 cm) surface water/pore water exchange due to the passage of waves over irregular sea bottoms (e.g., ripples and sediment mounds). However, Cable et al. (2006a) demonstrated seepage meters are more likely responding to numerous environmental conditions, including wind and wave driven currents, bioirrigation, and fresh groundwater discharge. Seepage meters have been the most widely used direct measurement technique in the marine science community, and some studies have provided strong evidence that a fresh water component is present in the seepage volume (e.g. Bokuniewicz 1992; Burnett et al. 2006; Martin et al. 2007). However given the uncertainties of seepage meters and the lack of any specific cause for the anomalous responses in flow, the hydraulic gradient (Darcy) method may be the most reliable technique for directly measuring terrestrial (fresh) SGD. Below, I present studies where both seepage meters and wells were used to estimate SGD.

Although the hydraulic gradient method is not truly a direct measurement of SGD, it provides a means of computing SGD (using Darcy's Law for specific discharge $q = -Ki$) through a direct measurement of fluid potential. Head measurements and hydraulic gradient (*i*) techniques are commonly implemented in hydrogeologic studies to investigate the movement of groundwater (Freeze and Cherry 1979; Heath 1987; Winter et al. 1988; Fetter 2001; Li and Jiao 2001a). Hydraulic conductivity (*K*) spans twelve orders of magnitude and is dependent on both the nature of the porous medium (*k*, intrinsic permeability) as well as fluid properties (i.e., dynamic viscosity and fluid density). Various techniques (slug tests, tidal dampening methods, rising/falling and constant head permeameters, and grain size based estimates) are used to estimate hydraulic conductivity of porous medium. Despite the more complex set of background measurements required for a Darcy flow estimate, this technique is more representative of fresh

groundwater discharge and makes it possible to observe the size and shape of the subterranean estuary if conductivity measurements are collected simultaneously.

The relationship between SGD flux and water fluctuations due to wave/tidal oscillation is ultimately tied to pressure (head) differences between the surface water and groundwater; upward flux from the sediment occurs when the groundwater head is greater than surface water levels. Surface and gravity waves invoke pressure gradients between the water column and pore water/groundwater, subsequently enhancing pore water exchange (Nielsen 1990; Rasmussen 1998; Uchiyama et al. 2000; Wang and Tsay 2001; Kim and Hwang 2002; Li and Jiao 2002b; Li et al. 2004; Mango et al. 2004). Various studies have looked at the influence of these pressure contrasts to inshore groundwater fluctuations (e.g., Carr and Van Der Kamp 1969; Nielsen 1990; Li and Jiao 2001a; Li and Jiao 2001b; Li and Jiao 2002b; Li and Jiao 2002a; Li et al. 2002; Jhan et al. 2003; Li and Jiao 2003; Li et al. 2004; see following section on groundwater models for more details) as well as the impact to SGD (Corbett et al. 1999; Corbett et al. 2000; Uchiyama et al. 2000; Chanton et al. 2003; Taniguchi and Iwakawa 2004). Pressure gradients have typically been evaluated using well transects, while fluxes are determined by seepage meters; however, it is possible to perform both using nested wells.

Working in the Florida Keys carbonate island chain, Chanton et al. (2003) documented a direct relationship between Atlantic tide on the east side of the islands and seepage to Florida Bay, Florida, on the west side of the islands. They employed three different techniques, automated seepage meters, wells, and continuous radon measurements, to estimate SGD fluxes. In their study, water level in Florida Bay remained fairly static over a 12-hour period while groundwater responded to Atlantic tidal oscillations; SGD fluxes to Florida Bay in response to this oscillation ranged from 10 cm d^{-1} during high tide to 2 cm d^{-1} during low tide (see Figure 3 of Chanton et al. 2003). In a similar study (also using seepage meters to evaluate total SGD),

Taniguchi and Iwakawa (2004) noted a inverse relationship between tidal fluctuations in Osaka Bay, Japan and SGD; time lag between surface water fluctuations and maximum SGD was 4 hours. By coupling flux data with head measurements, they found approximately 4 to 29% of the total SGD was fresh groundwater.

Numerical Groundwater Flow Models

Water budgets and numerical flow models have proven useful in determining the contribution of fresh SGD on both local and regional scales (Langevin 2001; Destouni and Prieto 2003; Langevin 2003; Oberdorfer 2003; Smith and Nield 2003; Smith and Zawadzki 2003). In addition to measuring meteoric-derived SGD, numerical models are now being used to address freshwater-saltwater mixing processes and the separation of SGD into fresh and marine components. Scale and validation have become the major issues for corroborating these models and water budgets. With a majority of literature reporting total SGD (not resolved by water origin), validating model estimates of fresh SGD to other techniques has proven difficult. Cross-sectional flow models and water budgets have been the most useful in addressing complex processes (e.g., density-driven convection and surface water-groundwater interactions) that occur in coastal settings (Rasmussen 1998; Uchiyama et al. 2000; Spinelli et al. 2002; Smith and Zawadzki 2003; Smith 2004). At the regional-scale, three-dimensional models and water budgets generally neglect such processes reducing their reliability (Smith and Nield 2003). Experiments conducted by the SCOR WG-112 compared flow model SGD estimates to other measurement techniques. To date, no field method appears to replicate numerical flow models or vice versa. Oberdorfer (2003) suggested seepage meter studies measuring only freshwater discharge may be the only comparable scenario.

Currently, a limited number of three-dimensional, regional scale models have been constructed to evaluate SGD (e.g., Langevin 2001; Langevin 2003; Smith and Nield 2003).

Smith and Nield (2003) modeled the fresh groundwater discharge into Cockburn Sound, Australia, using MODFLOW-2000. Their model incorporated various assumptions that limited the reliability of the discharge flux estimates: 1) outflow gap represented as a set of shore-parallel drain cells, 2) neglected density contrasts between freshwater and salt water, 3) no surface water-groundwater interactions. The representation of the outflow gap as a set of drain cells forces all groundwater flow paths out at this point; suggesting all fresh groundwater is discharged along this narrow zone. Cross-sectional models have shown that this drain-cell approach is not a reasonable assumption and overestimates fresh goundwater fluxes (Smith 2004). Shallow groundwater flow paths generally discharge near the shoreline, while deeper flow paths mix at depth with the intruding saline water.

Langevin (2003) produced the most thorough model to evaluate SGD in the Biscayne Aquifer, near Miami, Florida, and used the variable-density USGS SEAWAT-2000 code (refer to Guo and Langevin 2002 for details on the program). By using a variable-density code such as SEAWAT, Langevin (2003) was able to simulate density-driven convection within the aquifer. Langevin (2003) also simulated the entire Biscayne Bay as an open water body allowing for surface water-groundwater interaction and wider discharge zones. Fresh groundwater discharge estimates were made by evaluating total vertical flow and solute concentration from the uppermost cells and computing the freshwater contribution based on a linear two end-member mixing model. Estimates of the SGD into Biscayne Bay averaged 3.7×10^5 m^3/day, which is approximately 10% of the surface water input and only 2% of annual rainfall total for the Biscayne Bay area (Langevin 2003).

Radioisotopic Tracers

Radionuclides of the U-Th decay series (Figure 1.2) have proven to be valuable geochemical tracers due to their natural occurrence in aquifer matrices, chemical behavior, and

predictive radiochemical behavior. Specific applications of these radionuclides include evaluating sedimentation rates (^{234}Th, ^{210}Pb) and dating geologic events ($^{234, 238}$U, ^{232}Th), assessing boundary layer fluxes ($^{223, 224, 226, 228}$Ra, ^{222}Rn), and determining water-rock interaction ($^{234, 238}$U). Of the 39 or so radionuclides associated with the three decay series, only $^{234, 238}$U, the Ra-quartet ($^{223, 224, 226, 228}$Ra), and ^{222}Rn are used in evaluating submarine groundwater discharge and surface water-groundwater interactions.

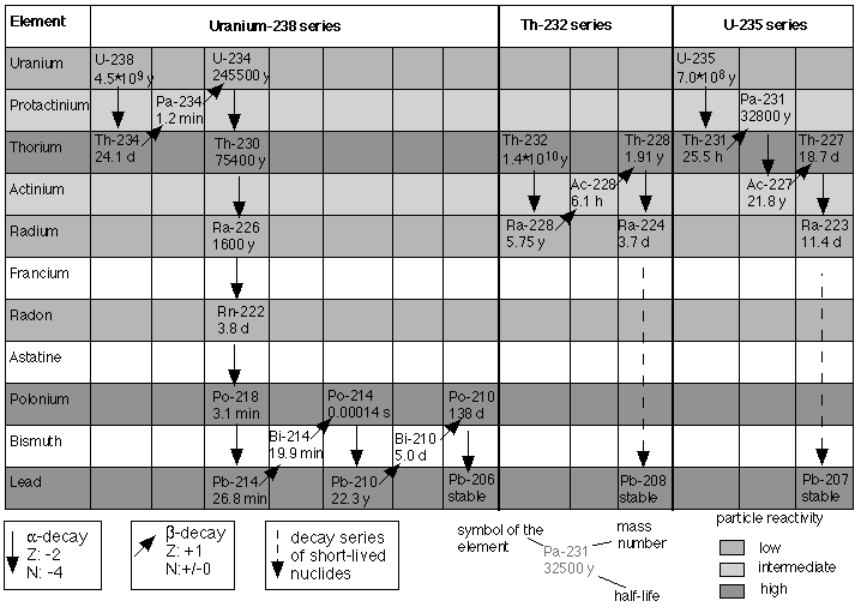

Figure 1.2. Flow chart of the U-Th decay series showing all radionuclides, the parent and daughter relationships and the mode of decay (modified from internet image located at http://www.es.mq.edu.au/GEMOC/Participants/Research/ADosseto/decay_chains.gif).

Uranium – Uranium occurs predominantly in natural systems as either U(IV) or U(VI). The oxidized state forms soluble complexes with carbonates, phosphates, sulfates, and chlorides (Gascoyne 1992), while the reduced state forms relatively insoluble oxides and hydroxides. Groundwater uranium concentrations are highly variable due to contrasting chemical behavior of the two valence states, but also depend on the mineral source and complexation with anionic ligands (Osmond and Cowart 1976). Windom and Niencheski (2003) used U to assess mixing

and redox conditions along the freshwater-saltwater interface beneath a barrier spit in southern Brazil. U enrichment was observed between 2 and 6 m below land surface due to phosphate mineral dissolution, while U depletion was observed below 6 m commensurate with iron and sulfate reduction (Windom and Niencheski 2003). Durand et al. (2005) used activity ratios between ^{234}U and ^{238}U to evaluate deep groundwater inputs into the Upper Rhine River. Dissimilar $^{234}U/^{238}U$ activity ratios between river water and drainage area sediments and rocks and similar activity ratios between river water and groundwater from various surrounding aquifers suggested groundwater inputs rather than weathering supplied most of the U to the Upper Rhine River. This distinction among U sources allowed them to construct mixing diagrams to determine volumetric inputs of groundwater from the different aquifers to each of the Rhine tributaries.

Radium – Like U, Ra is found in a variety of geologic materials. Ra^{2+} is an alkaline earth metal and behaves chemically similar to barium; it is observed in the crystal lattices of minerals as well as adsorbed onto clays and surface coatings. Ra desorption has been observed by Webster et al. (1995) to be directly correlated with salinity (e.g. ionic strength) of the solution. The Ra-quartet ($^{223, 224, 226, 228}Ra$) has been widely used to assess groundwater input into coastal water bodies (e.g., Webster et al. 1994; Rama and Moore 1996; Moore 2000; Charette et al. 2003; Krest and Harvey 2003; Moore 2003). The $^{223, 224, 226, 228}Ra$ sources occur from alpha decay of the strongly particle reactive, sediment-derived, $^{227, 228, 230, 232}Th$ parents that precede them in the decay series. The contrasting chemical behavior between Ra and Th generally leads to excess levels of Ra in pore waters. The half-life of each Ra isotope is significantly different (^{228}Ra-5.75 yrs, ^{226}Ra-1620 yrs, ^{224}Ra-3.66 days, and ^{223}Ra-11.4 days) making them a useful set of radionuclides to assess water mass mixing and chemical fluxes at a variety of timescales.

Rama and Moore (1996) observed fluxes of ^{226}Ra and ^{228}Ra into a tidal creek at North Inlet near Georgetown, SC, that could not be explained by the sediment supported ^{230}Th and ^{232}Th activities, respectively, from the nearby marsh. They concluded that groundwater inputs enriched in desorbed Ra were combining with the infiltrating marsh water and discharging into the nearby tidal creek. A similar finding was observed at Great Sippewissett Marsh, West Falmouth, MA, by Charette et al. (2003). In this study they were able to use excess ^{226}Ra activities to determine the required flux of ^{226}Ra due to groundwater inputs to sustain the activity observed in the marsh; water flux estimates ranged between 2700 and 5000 $m^3\ d^{-1}$.

Radon – Radon-222 is found wherever its progenitor ^{226}Ra is present. Radon is a inert gas which behaves conservatively in all chemical reactions in the sediments and water column. The exception to the conservative behavior results from its decay and production. Radon gas is found in the atmosphere, trapped in mineral grains. or dissolved in solution (gas solubility constant of radon in water, $K = 10^{-2.03}$ M or in radioactivity units $K = 10^{17.84}$ dpm L^{-1}). Radon accumulates in groundwater due to production from and recoil processes associated with its parent, ^{226}Ra, which may result in excess quantities of ^{222}Rn with respect to locally supported ^{226}Ra. The inert behavior and higher mobility as a gas result in disequilibrium between ^{222}Rn and ^{226}Ra and enable the usage of ^{222}Rn as a groundwater tracer.

Both excess and deficit disequilibrium of ^{222}Rn (with respect to ^{226}Ra activity) are observed in natural environments. Excess ^{222}Rn is more common in coastal environments where groundwater enrichment occurs, while deficit ^{222}Rn is observed offshore and in marine environments. Burnett et al. (1996) characterized the benefits of ^{222}Rn as a groundwater tracer as 1) 2 to 4 orders of magnitude higher concentration in groundwater than surface water, 2) conservative behavior, 3) inputs and outputs can be estimated relatively precisely by known production and decay terms, 4) easily measured even at low concentrations. Specific examples

where excess ^{222}Rn has been successfully used as groundwater tracer include northeast Gulf of Mexico (Cable et al. 1996b), Par Pond near the Savannah River, Georgia (Corbett et al. 1997), Florida Bay, Florida (Corbett et al. 1999), and Ubatuba Coast, Brazil (Oliveira et al. 2003; Cable and Martin 2008). In contrast, deficit ^{222}Rn has been used to evaluate pore water exchange processes (i.e., bioirrigation) at the sediment-water interface in San Francisco Bay (Hammond and Fuller 1979), Hudson River estuary (Hammond et al. 1977), Buzzard Bay, MA (Martin and Sayles 1987; Martin and Banta 1992) and White Oak River estuary, NC (Gruebel and Martens 1984).

Dissertation Outline

My dissertation examines the role fresh groundwater and recirculated marine groundwater/pore water contribute to total submarine groundwater discharge. The specific location for the study took place in the Indian River Lagoon, Florida, USA. I also examine how the interaction of these distinct water sources within the submarine groundwater system influence the spatial and temporal distribution of $^{234, 238}$U, ^{226}Ra, and ^{222}Rn. In Chapter Two, I provide a general description of the submarine aquifer matrix and the physical flow regime of the submarine groundwater system. Comparison between surface water level and groundwater head in time- and frequency-domain are used to show the strong hydrologic connection between the lagoon and the submarine groundwater system. In Chapter Three, I examine how the physical flow regime and salinity framework of the subterranean estuary respond to episodic high intensity events (i.e. tropical cyclones). Continuous groundwater head and salinity measurements made along a piezometer transect prior to and during the 2005 Atlantic hurricane season show a significant perturbation in the salinity framework of the subterranean estuary commensurate with the passage of Tropical Storm Tammy and Hurricane Wilma. The processes associated with this perturbation are discussed in detail. In Chapter Four, I examine the spatial and temporal

variability of $^{234,238}U$, ^{226}Ra, and ^{222}Rn within the submarine groundwater system. The roles of redox-driven and surface exchange processes on the spatial distribution of these radionuclides are examined. The effects of episodic events (as described in Chapter Three) on these radionuclides are shown to impact their temporal distribution. In Chapter Five, I use ^{222}Rn to quantify spatial and temporal fluxes of both fresh groundwater and recirculated seawater. A one-dimensional transport model, which includes advection, diffusion, non-local exchange, and production/decay, is employed to quantify how groundwater advection and shallow sediment irrigation contribute to observed pore water ^{222}Rn distributions. Monte Carlo simulations are applied in the model to enhance statistical significance of predicted SGD rates. The model allows exploration of the role of non-local exchange in pore water ^{222}Rn distribution and separation of submarine groundwater discharge components. In the final concluding chapter, I summarize the findings of each study and show implications of these findings to water management scenarios and global constituent budgets (i.e. U).

References

Bokuniewicz, H. 1992. Analytical descriptions of subaqueous groundwater seepage. Estuaries **15:** 458-464.

---. 1995. Analytical descriptions of subaqueous groundwater seepage. Estuaries **15:** 458-464.

Bredehoeft, J. 2007. It Is the Discharge. Ground Water **45:** 523-523.

Burnett, W., J. Cable, D. R. Corbett, and J. Chanton. 1996. Tracing groundwater flow into surface waters using natural ^{222}Rn, p. 10. Proceedings of the Groundwater Symposium, Land-Ocean Interactions in the Coastal Zone.

Burnett, W. C. 1999. Offshore springs and seeps are focus of working group. EOS **80:** 13-15.

Burnett, W. C., M. Taniguchi, and J. Oberdorfer. 2001. Measurement and significance of the direct discharge of groundwater into the coastal zone. Journal of Sea Research **46:** 109-116.

Burnett, W. C., J. P. Chanton, J. Christoff, E. Kontiar, S. Krupa, M. J. Lambert, W. S. Moore, D. O'rourke, R. Paulsen, C. Smith, L. Smith, and M. Taniguchi. 2002. Assessing methodologies for measuring groundwater discharge to the ocean. EOS **83:** 120-123.

Burnett, W. C., M. H. Bokuniewicz, W. S. Moore, and M. Taniguchi. 2003. Groundwater and pore water inputs to the coastal zone. Biogeochemistry **66:** 3-33.

Burnett, W. C., P. K. Aggarwal, A. Aureli, H. Bokuniewicz, J. E. Cable, M. A. Charette, E. Kontar, S. Krupa, K. M. Kulkarni, A. Loveless, W. S. Moore, J. A. Oberdorfer, J. Oliveira, N. Ozyurt, P. Povinec, A. M. G. Privitera, R. Rajar, R. T. Ramassur, J. Scholten, T. Stieglitz, M. Taniguchi, and J. V. Turner. 2006. Quantifying submarine groundwater discharge in the coastal zone via multiple methods. Sci. Total Environ. **367:** 498-543.

Cable, J. E., G. C. Bugna, W. C. Burnett, and J. P. Chanton. 1996a. Application of Rn-222 and CH4 for assessment of groundwater discharge to the coastal ocean. Limnology and Oceanography **41:** 1347-1353.

Cable, J. E., W. C. Burnett, J. P. Chanton, and G. L. Weatherly. 1996b. Estimating groundwater discharge into the northeastern Gulf of Mexico using Radon-222. Earth and Planetary Science Letters **144:** 591-604.

Cable, J. E., W. C. Burnett, J. P. Chanton, D. R. Corbett, and P. H. Cable. 1997. Field evaluation of seepage meters in the coastal marine environment. Estuarine Coastal and Shelf Science **45:** 367-375.

Cable, J. E., J. B. Martin, P. W. Swarzenski, M. K. Lindenberg, and J. Steward. 2004. Advection Within Shallow Pore Waters of a Coastal Lagoon, Florida. Ground Water **42:** 1011-1020.

Cable, J. E., J. B. Martin, and J. Jaeger. 2006a. Exonerating Bernoulli? On evaluating the physical and biological processes affecting marine seepage meter measurements. Limnol. Oceanogr. Meth. **4:** 172-183.

Cable, J. E., J. B. Martin, and M. Taniguchi. 2006b. A review of submarine ground water discharge: biogeochemical inputs and leaky coastlines, p. 22-41. *In* I. S. Zektser, R. G. Dzhamalov and L. G. Everett [eds.], Submarine Groundwater. CRC Press, 512 pp.

Cable, J. E., and J. B. Martin. 2008. In situ evaluation of nearshore marine and fresh pore water transport into Flamengo Bay, Brazil. Estuarine Coastal and Shelf Science **76:** 473-483.

Carr, P. A., and G. S. Van Der Kamp. 1969. Determining aquifer characteristics by the tidal method. Water Resources Research **5:** 1023-1031.

Chanton, J. P., W. C. Burnett, H. Bulaviova, D. R. Corbett, and M. Taniguchi. 2003. Seepage rate variability in Florida Bay driven by Atlantic tidal height. Biogeochemistry **66:** 187-202.

Charette, M. A., R. Splivallo, C. Herbold, M. S. Bollinger, and W. S. Moore. 2003. Salt marsh submarine groundwater discharge as traced by radium isotopes. Marine Chemistry **84:** 113-121.

Church, T. M. 1996. An underground route for the water cycle. Nature **380:** 579-580.

Collis, H. A. 2006. Application of Short-Term Sediment Dynamics and Particle-Bound Phosphorus Fractionation Methods (SEDEX) to Estimate the Benthic Nutrient Loading Potential in Upper Newport Estuary, California. Master. Louisiana State University.

Cooper, H. H. 1959. A Hypothesis Concerning the Dynamic Balance of Fresh Water and Salt Water in a Coastal Aquifer. Journal of Geophysical Research **64:** 461-467.

Corbett, D. R., W. C. Burnett, P. H. Cable, and S. B. Clark. 1997. Radon tracing of groundwater input into Par Pond, Savannah River Site. Journal of Hydrology **203:** 209-227.

Corbett, D. R., J. Chanton, W. Burnett, K. Dillon, C. Rutkowski, and J. W. Fourqurean. 1999. Patterns of groundwater discharge into Florida Bay. Limnology and oceanography **44:** 1045-1055.

Corbett, D. R., K. Dillon, and W. Burnett. 2000. Tracing groundwater flow on a barrier island in the north-east Gulf of Mexico. Estuarine, Coastal and Shelf Science **51:** 227-242.

Corbett, D. R., and J. E. Cable. 2003. Seepage meters and advective transport in coastal environments: Comments on "Seepage meters and Bernoulli's revenge" by E. A. Shinn, C. D. Reich, and T. D. Hickey. 2002. Estuaries 25 : 126-132. Estuaries **26:** 1383-1387.

Destouni, G., and C. Prieto. 2003. On the possibility for generic modeling of submarine groundwater discharge. Biogeochemistry **66:** 171-186.

Durand, S., F. Chabaux, S. Rihs, P. Duringer, and P. Elsass. 2005. U isotope ratios as tracers of groundwater inputs into surface waters: Example of the Upper Rhine hydrosystem. Chemical Geology **220:** 1-19.

Emerson, S., R. Jahnke, and D. Heggie. 1984. Sediment-water exchange in shallow water estuarine sediments. Journal of Marine Research **42:** 709-730.

Fetter, C. W. 2001. Applied Hydrogeology, 4th ed. Prentice-Hall, Inc.

Freeze, R. A., and J. A. Cherry. 1979. Groundwater. Prentice Hall.

Gascoyne, M. 1992. Geochemistry of the actinides and their daughters, p. 34-61. *In* M. Ivanovich and R. S. Harmon [eds.], Uranium series disequilibrium: applications to Earth, marine, and environmental sciences. Clarendon Press : Oxford, United Kingdom.

Glover, R. E. 1959. The pattern of fresh-water flow in a coastal aquifer. Journal of Geophysical Research **64:** 457-459.

Gruebel, K. A., and C. S. Martens. 1984. Radon-222 tracing of sediment-water chemical Transport in an Estuarine sediment. Limnology and oceanography **29:** 587-597.

Guo, W., and C. D. Langevin. 2002. User's guide to SEAWAT: a computer program for simulation of three-dimensional variable-density ground-water flow, p. 77. U.S. Geological Survey.

Hammond, D. E., H. J. Simpson, and G. Mathieu. 1977. Radon 222 distribution and transport across the sediment-water interface in the Hudson River estuary. Journal of Geophysical Research **82:** 3913-3920.

Hammond, D. E., and C. Fuller. 1979. The use of Radon-222 to estimate benthic exchange and atmospheric exchange rates in San Francisco Bay. San Fransisco Bay: The Urbanized Estuary **The Pacific Division of the American Association for the Advancement of Science:** 213-229.

Heath, R. C. 1987. Basic Ground-Water Hydrology, p. 81.

Huettel, M., W. Ziebis, and S. Forster. 1996. Flow-induced uptake of particulate matter in permeable sediments. Limnology and Oceanography **41:** 309-322.

Ipcc. 2007. *Climate Change 2007: Impacts, Adaptation and Vulnerability. Contribution of Working Group II to the Fourth Assessment Report of the Intergovernmental Panel on Climate Change* [M.L. Parry, O.F. Canziani, J.P. Palutikof, P.J. van der Linden and C.E. Hanson (eds)], p. 976.

Jhan, M. K., Y. Kamii, and K. Chikamori. 2003. On the estimation of phreatic aquifer parameters by the tidal response technique. Water Resources Management **17:** 69-88.

Kim, G., and D.-W. Hwang. 2002. Tidal pumping of groundwater into the coastal ocean revealed from submarine ^{222}Rn and CH_4 monitoring. Geophysical Research Letters **29:** 23-21 - 23-24.

Krest, J. M., and J. W. Harvey. 2003. Using natural distribtuions of short-lived radium isotopes to quantify groundwater discharge and recharge. Limnology and Oceanography **48:** 290-298.

Langevin, C. D. 2001. Simulation of Ground-Water Discharge to Biscayne Bay, Southeastern Florida, p. 127. U.S. Geological Survey.

---. 2003. Simulation of submarine ground water discharge to a marine esutary: Biscayne Bay, Florida. Ground Water **41:** 758-771.

Li, H., and J. J. Jiao. 2001a. Analytical studies of groundwater-head fluctuation in a coastal confined aquifer overlain by a semi-permeable layer with storage. Advances in Water Resources **24:** 565-573.

---. 2001b. Tide-induced groundwater fluctuation in a coastal leaky confined aquifer system extending under the sea. Water Resources Research **37, No 5:** 1165-1171.

---. 2002a. Tidal groundwater level fluctuations in L-shaped leaky coastal aquifer system. Jouranl of Hydrology **268:** 234-243.

---. 2002b. Analytical solutions of tidal groundwater flow in coastal two-aquifer system. Advances in Water Resources **25:** 417-426.

Li, H., J. J. Jiao, M. Luk, and K. Cheung. 2002. Tide-induced groundwater level fluctuation in coastal aquifers bounded by L-shaped coastlines. Water Resources Research **38, No 3:** 10.1029/2001WR000556.

Li, H., and J. J. Jiao. 2003. Tide-induced seawater-groundwater circulation in a multi-layered coastal leaky aquifer system. Journal of Hydrology **274:** 211-224.

Li, L., D. A. Barry, F. Stagnitti, and J. Y. Parlange. 1999. Submarine groundwater discharge and associated chemical input to a coastal sea. Water Resources Research **35:** 3253-3259.

Li, L., D. A. Barry, D.-S. Jeng, and H. Prommer. 2004. Tidal dynamics of groundwater flow and contaminant transport in coastal aquifers, p. 115-141. *In* A. H.-D. Cheng and D. Ouazar [eds.], Coastal Aquifer Management: Monitoring, Modeling, and Case Studies. CRC Press LLC.

Mango, A. J., M. W. Schmeeckle, and D. J. Furbish. 2004. Tidally induced groundwater circulation in an unconfined coastal aquifer modeled with a Hele-Shaw cell. Geology **32:** 233-236.

Martens, C. S., G. W. Kipphut, and J. V. Klump. 1980. Sediment-water chemical exchange in the coastal zone traced by in situ Radon-222 flux measurements. Science **208:** 285-288.

Martin, J. B., J. Cable, and P. W. Swarzenski. 2002. Quantification of ground water discharge and nutrient loading to the Indian River Lagoon. St. Johns River Water Management District Final Report.

Martin, J. B., J. E. Cable, P. W. Swarzenski, and M. K. Lindenberg. 2004. Enhanced submarine ground water discharge from mixing of pore water and estuarine water. Ground Water (special Ocean issue) **42:** 1001-1010.

Martin, J. B., J. E. Cable, J. Jaeger, K. Hartl, and C. G. Smith. 2006. Thermal and chemical evidence for rapid water exchange across the sediment-water interface by bioirrigation in the Indian River Lagoon, Florida. Limnology and Oceanography **51:** 1332-1341.

Martin, J. B., J. E. Cable, C. Smith, M. Roy, and J. Cherrier. 2007. Magnitudes of submarine groundwater discharge from marine and terrestrial sources: Indian River Lagoon, Florida. Water Resources Research **43:** -.

Martin, W. R., and F. L. Sayles. 1987. Seasonal cycles of particle and solute transport processes in nearshore sediments: $^{222}Rn/^{226}Ra$ and $^{234}Th/^{238}U$ disequilibrium at a site in Buzzards Bay, MA. Geochimica et Cosmochimica Acta **51:** 927-943.

Martin, W. R., and G. T. Banta. 1992. The measurement of sediment irrigation rates: A comparison of the Br^- tracer and $^{222}Rn/^{226}Ra$ disequilibrium techniques. Journal of Marine Research **50:** 125-154.

Mcbride, M. S., and H. O. Pfannkuch. 1975. Distribution of seepage within lakebeds. Journal of Research of the US Geological Survey **3:** 505-512.

Moore, W. S. 1996. Large groundwater inputs to coastal waters revealed by Ra-226 enrichments. Nature **380:** 612-614.

---. 1999. The subterranean estuary: a reaction zone of ground water and sea water. Marine Chemistry **65:** 111-125.

---. 2000. Determining coastal mixing rates using radium isotopes. Continental Shelf Research **20:** 1993-2007.

---. 2003. Sources and fluxes of submarine groundwater discharge delineated by radium isotopes. Biogeochemistry **66:** 75-93.

Murdoch, L. C., and S. E. Kelly. 2003. Factors affecting the performance of conventional seepage meters. Water Resources Research **39:** 1163, doi:1110.1029/2002WR001347.

Nielsen, P. 1990. Tidal dynamics of the water table in beaches. Water Resources Research **26:** 2127-2134.

Oberdorfer, J. A. 2003. Hydrogeologic modeling of submarine groundwater discharge: comparison to other quantitative methods. Biogeochemistry **66:** 159-169.

Oliveira, J., W. C. Burnett, P. P. Mazzilli, E. S. Braga, L. A. Farias, J. Christoff, and V. V. Furtado. 2003. Reconnaissance of submarine groundwater discharge at Ubatuba coast, Brazil, using Rn as a natural tracer. Journal of Environmental Radioactivity **69:** 37-52.

Osmond, J. K., and J. B. Cowart. 1976. The theory and uses of natural uranium isotopic variations in hydrology. Atomic Energy Review **144:** 621-679.

Paerl, H. W. 1997. Coastal eutrophication and harmful algal blooms: importance of atmospheric deposition and groundwater as "new" nitrogen and other nutrient sources. Limnology and oceanography **42:** 1154-1165.

Precht, E., and M. Huettel. 2003. Advective pore-water exchange driven by surface gravity waves and its ecological implications. Limnology and Oceanography **48:** 1674-1684.

Rama, and W. S. Moore. 1996. Using the radium quartet for evaluating groundwater input and water exchange in salt marshes. Geochimica et Cosmochimica Acta **60:** 4645-4652.

Rasmussen, L. L. 1998. Groundwater Flow, Tidal Mixing and Haline Convection in Coastal Sediments. Master of Science. Florida State University.

Riedl, R. J., N. Huang, and R. Machan. 1972. The subtidal pump: a mechanism of interstital water exchange by wave action. Marine Biology **13:** 210-221.

Robinson, C., L. Li, and D. A. Barry. 2007. Effect of tidal forcing on a subterranean estuary. Advances in Water Resources **30:** 851-865.

Senger, R. K., and G. E. Fogg. 1990a. Stream Functions and Equivalent Fresh-Water Heads for Modeling Regional Flow of Variable-Density Groundwater: 2. Application and Implications for Modeling Strategy. Water Resources Research **26:** 2097-2106.

---. 1990b. Stream functions and equivalent freshwater heads for modeling regional flow of variable-density groundwater: 1. Review of Theory and Verification. Water Resources Research **26:** 2089-2096.

Shaw, J. F. H., and E. E. Prepas. 1989. Temporal and Spatial Patterns of Porewater Phosphorus in Shallow Sediments, and Its Potential Transport into Narrow-Lake, Alberta. Canadian Journal of Fisheries and Aquatic Sciences **46:** 981-988.

Shinn, E. A., C. D. Reich, and T. D. Hickey. 2002. Seepage meters and Bernoulli's revenge. Estuaries **25:** 126-132.

Simmons, J., G.M. 1992. Importance of submarine groundwater discharge (SGWD) and seawater cycling to material flux across sediment/water interfaces in marine environments. Marine Ecology Progress Series **84:** 173-184.

Slomp, C. P., and P. Van Cappellen. 2004. Nutrient inputs to the coastal ocean through submarine groundwater discharge: controls and potential impact. Journal of Hydrology **295:** 64-86.

Smith, A. J., and S. P. Nield. 2003. Groundwater discharge from the superficial aquifer into Cockburn Sound Western Australia:estimation by inshore water balance. Biogeochemistry **66:** 125-144.

Smith, A. J. 2004. Mixed convection and density-dependent seawater circulation in coastal aquifers. Water Resources Research **40**.

Smith, L., and W. Zawadzki. 2003. A hydrogeologic model of submarine groundwater discharge: Florida intercomparison experiment. Biogeochemistry **66:** 95-110.

Spinelli, G. A., A. T. Fisher, C. G. Wheat, M. D. Tryon, K. M. Brown, and A. R. Flegal. 2002. Groundwater seepage into northern San Francisco Bay: Implications for dissolved metals budgets. Water Resources Research **38**.

Taniguchi, M., W. C. Burnett, J. E. Cable, and J. V. Turner. 2002. Investigation of submarine groundwater discharge. Hydrological processes **16:** 2115-2129.

Taniguchi, M., W. C. Burnett, C. F. Smith, R. J. Paulsen, D. O'rourke, S. L. Krupa, and J. L. Christoff. 2003. Spatial and temporal distribuions of submarine groundwater discharge rates obtained from various types of seepage meters at a site in the Northeastern Gulf of Mexico. Biogeochemistry **66:** 35-53.

Taniguchi, M., and H. Iwakawa. 2004. Submarine groundwater discharge in Osaka Bay, Japan. Limnology **5:** 25-32.

Uchiyama, Y., K. Nadaoka, P. Rolke, K. Adachi, and H. Yagi. 2000. Submarine groundwater discharge into the sea and associated nutrient transport in a sandy beach. Water Resources Research **36:** 1467-1479.

Wang, J., and T. K. Tsay. 2001. Tidal effects on groundwater motions. Transport in Porous Media **43:** 159-178.

Webster, I. T., G. J. Hancock, and A. S. Murray. 1994. Use of radium isotopes to examine pore-water exchange in an estuary. Limnology and Oceanography **39:** 1917-1927.

---. 1995. Modelling the effect of salinity on radium desorption from sediments. Geochimica et Cosmochimica Acta **59:** 2469-2476.

Wilson, A. M. 2005. Fresh and saline groundwater discharge to the ocean: A regional perspective. Water Resources Research **41:** W02016, doi: 02010.01029/02004WR003399.

Windom, H., and F. Niencheski. 2003. Biogeochemical processes in a freshwater-seawater mixing zone in permeable sediments along the coast of Southern Brazil. Marine Chemistry **83:** 121-130.

Winter, T. C., J. W. Labaugh, and D. O. Rosenberry. 1988. The design and use of a hydraulic potentiomanometer for direct measurement of differences in hydraulic head between groundwater and surface water. Limnology and oceanography **33:** 1209-1214.

Younger, P. L. 1996. Submarine groundwater discharge. Nature **382:** 121-122.

CHAPTER 2.

FAIR WEATHER INTERACTIONS BETWEEN SURFACE WATER AND GROUNDWATER IN A COASTAL SUBMARINE AQUIFER

Introduction

Surface water-groundwater interactions are driven by vertical gradients between piezometric groundwater head and the surface water levels. In one dimension, when piezometric head rises above surface water levels, transport is vertically upward and discharge occurs, whereas when this hydraulic gradient is reversed, surface water is recharged to the aquifer. These gradients can reverse frequently in coastal systems by tides and wind waves (e.g. Robinson et al. 2007; Smith et al. 2008), thereby reversing the exchange of groundwater and surface water and influencing the mixing of discharging fresh water and saline surface water. In two and three dimensions, lateral or longitudinal head gradients also contribute to coastal surface water-groundwater interactions by controlling the horizontal extent of the discharge zone (e.g. Glover 1959; Martin et al. 2007). Groundwater discharging to coastal surface water bodies carries an allochthonous signal (e.g., chemical constituents such as nutrients or pollutants), which may have adverse consequences for ecological and biogeochemical processes of the receiving waters. Conversely, recharge of surface water into shallow sediments can increase pore water oxygen levels and affect metal, organic carbon, and nutrient chemistry and distributions. Controls on the distribution, transport, and timing of surface water-groundwater interactions must be understood to characterize the bio-geochemical transformations and fluxes in these dynamic systems.

Many studies have focused on surface water-groundwater interactions in a variety of coastal geological settings with the purpose of estimating the magnitude of the groundwater component in local and regional water and nutrient budgets (e.g. Simmons 1992; Bokuniewicz

1995; Cable et al. 1996; Church 1996; Huettel et al. 1998; Li et al. 1999; Bokuniewicz et al. 2003; Burnett et al. 2003; Windom and Niencheski 2003; Cable et al. 2004; Burnett et al. 2006). These studies collectively demonstrate that estimates of groundwater discharge are generally site specific and limited by the application of different measurement techniques in that particular environment. For example, Moore (1996) used a radium (Ra) mass balance to suggest that the volume of water discharging from coastal aquifers along the South Carolina continental shelf is as high as 40% of local riverine discharge. However, local head gradients and volume of recharge do not substantiate such large fluxes (Younger 1996). The discrepancy in estimated magnitude derives from the inclusion of highly variable pore water-surface water exchange in the total SGD estimate made by the tracer. Both exchange and discharge produce a benthic flux from the sediments to the water column, and compositions of these water sources may be chemically indistinguishable due to long residence times and mixing between fresh groundwater and infiltrated salt water within the sediment pore spaces. Inclusion of the outflow fraction of this marine SGD exchange in the total SGD term may be biogeochemically significant but volumetrically it is not a new addition. Fluxes also vary depending on the techniques used to measure them, resulting in total SGD observations at a single site that often vary between a factor of five and an order of magnituide (e.g. Burnett 1999; Burnett et al. 2002; Shinn et al. 2002; Burnett et al. 2003; Burnett et al. 2006).

In addition to measurement discrepancies, the interpretation of what constitutes SGD has been a barrier for communication among scientists who study this phenomena (e.g., Burnett 1999; Burnett et al. 2001; Burnett et al. 2002; Taniguchi et al. 2002; Burnett et al. 2003; Cable et al. 2004; Martin et al. 2004; Martin et al. 2007). Burnett et al. (2003) formally defines SGD as "... any and all water that passes across the sediment water interface, despite its origin or composition...." Two most prominent sources of SGD are generally considered: 1) aquifer

water and 2) recirculated seawater. This definition unifies the concept of SGD, but it reinforces the importance of separating fresh groundwater discharge from the recirculated seawater component (Taniguchi et al. 2002; Cable et al., 2004; Martin et al. 2007). Quantification of these two water sources is critical for environmental impact assessment and water resources management in coastal systems.

Traditional groundwater studies use piezometric head gradients to predict and evaluate groundwater flow in aquifers, but this approach is not often employed among scientists studying SGD because long term studies may be required, monitoring wells are difficult to install, and typically only local estimates are obtained. Water column tracers offer the advantage of more regional SGD estimates, but the disadvantages include the inability to distinguish fresh and marine water sources in SGD. One of the few studies where fluid potential was measured simultaneously with seepage meter measurements of SGD was conducted in Florida Bay, FL, to the west of the Florida Keys, where little to no tidal exchange occurs with the Atlantic Ocean (Chanton et al. 2003). In a similar study, Harvey et al. (2004) noted interior wetlands of the Florida Everglades acted as both discharge and recharge sites, varying cyclically in response to local precipitation and the operation of water-control structures. Discharge from the wetlands occurred during generally dry conditions, while the wetlands functioned as recharge sites during wetter periods (Harvey et al. 2004). These studies point out the general utility of standard hydrogeologic techniques in understanding submarine groundwater discharge in coastal systems with generally low-gradients.

This chapter provides general information concerning the physical flow regime of the subterranean estuary observed in the Surficial aquifer discharging to the Indian River Lagoon, Florida, USA (see Appendix A for general description of Indian River Lagoon and the local hydrogeology). Two distinct periods of water level measurements are considered which I

interpret as representative of long-term response or fair-weather conditions. In this text, "fair-weather conditions" refers to time periods when no major storm event (tropical or extra-tropical cyclones) influenced the field site; the effects of these storms are discussed in Chapter 3. Temporal variability of surface water and groundwater levels are considered to verify this interpretation. Aquifer attributes are examined both qualitatively using standard sediment characterization techniques and quantitatively using frequency-domain analysis of water level data to investigate attenuation of periodic surface water perturbations as they are propagated into the submarine groundwater/aquifer system.

Methods

Water Level Measurements

Surface water level and groundwater head were measured in piezometers installed along a transect in Indian River Lagoon, FL, at four locations: 1) about 10 m onshore (EGNW-OS), (2) at the shoreline (EGNW-0), (3) 15 m offshore (EGNW-15), and (4) 30 m offshore (EGNW-30; Figure 2.1). Measurements were conducted to assess the physical conditions of the coastal seepage face/subterranean estuary under inherently "fair-weather" conditions. All offshore piezometers were installed manually using a fence-post driver and consisted of 3.8 cm (1.5 in) outer diameter schedule 40 or 80 PVC tubing coupled with 15 to 20 cm long, 0.254 mm slotted PVC screening. The onshore piezometer, of the same construction type as the offshore piezometers, was installed inside of 10.2 cm (4 in) diameter PVC casing emplaced using a manual auger. Piezometers were surveyed to a common (local) datum (average lagoon water level) on 10-Feb-05; all head measurements are referenced to this datum. At 0, 15, and 30 m offshore, two nested piezometers, separated laterally by 0.3 m, were installed at sediment depths of 1.5 m (EGNW-0s, 15s, and -30s) and 2.5 m (EGNW-0d, 15d, and -30d) below the local datum. The onshore piezometer (EGNW-OS) was installed to a depth of 2.25 m below datum.

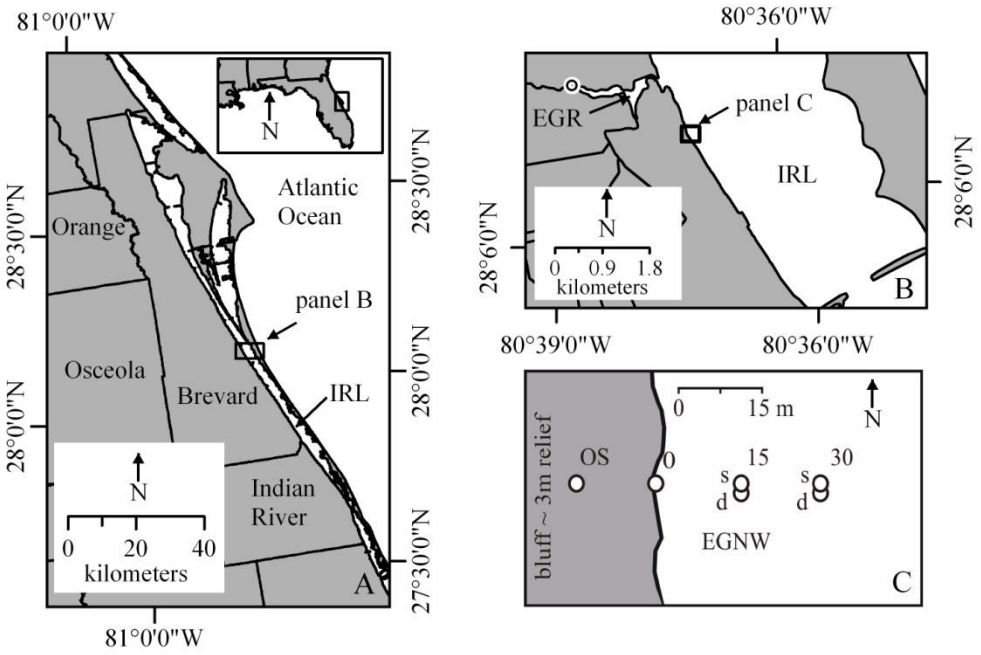

Figure 2.1. (A) Map of east-central Florida showing the location of the field site within the Indian River Lagoon, (B) relative to Eau Gallie River and USGS gaging station 02449007, (C) and the piezometer transect; labels above the piezometers (i.e., OS, 0, 5, 15, and 30) denote their position relative to the shoreline in meters. At 15 and 30 m offshore, two piezometers are installed at each location; the shallow piezometer (s) is screened at 1.5 m and the deep piezometer (d) is screened at 2.5 m.

All piezometers were installed with top of casing (TOC) approximately 1 m (range of 0.98 to 1.02 m) above the local datum and with a vent (1 mm wide, 1 cm long) approximately 2 cm below the TOC.

Two separate monitoring studies were conducted: 1) 22-Nov-04 to 20-Jul-05 and 2) 06-Oct-06 to 27-Dec-06; hereafter referred to as ST1 and ST2, respectively. During ST1, ultra-sonic water level recorders (*Infinites USA, Inc.*) were used to monitor water levels in a stilling well (EGNSW-35) 35 m offshore and in three offshore piezometers (EGNW-0s, EGNW-15d, and EGNW-30d). Sampling frequency (f_s) was 12 cycles per day (cpd) (sampling period, T_s, of 2 h) for all wellsexcept EGN-15d and EGN-30d which were not monitored during 2006. Fresh

water equivalent head was computed using synoptic salinity measurements made during Nov-04, Feb-05, May-05, and Jul-05; relative standard deviation of salinity measurements were less than 5% between these time periods.

During the shorter duration measurement period of ST2, absolute pressure (water and atmospheric), temperature, and conductivity were continuously recorded (f_s = 72 cpd; T_s = 20 min) in EGNW-OS, -0s, -15s, and -30s and a stilling well (EGNSW-20) using Solinst LTC loggers (*Solinst Canada, Inc.*). Sensors were in contact with the upper 4 to 6 cm of screening. Absolute water pressure was corrected for barometric pressure to obtain groundwater pressure head; a constant aquifer barometric efficiency of 95% was used in the correction. Salinity and water density were computed from water pressure, conductivity, and temperature using SEAWATER 3.0 (Morgan and Jankowski 2004). Pressure head was corrected for density variations and normalized to freshwater (0 salinity). All water levels are presented as freshwater equivalent head.

Analysis of Water Level Data

Times-series data were reduced using standard statistical and frequency analysis techniques (Bendat and Piersol 1971). Trends and means were removed from the raw time series using a raised-cosine (Hanning) window technique with a cut-off frequency of 0.01 cpd. One-sided auto- (S_{xx}) and cross-spectral (S_{xy}) density functions were computed using the fast-Fourier transform technique outlined by Bendat and Piersol (1971), which represented discretely is

$$S_{xx}(f_k) = \frac{2}{T_s}|X(f_k)|^2 = \frac{2}{T_s}\left|\sum_{k=0}^{N-1} x_k e^{-\frac{i2mn}{N}}\right|^2 \quad (2.1)$$

and

$$S_{xy}(f_k) = \frac{2}{T_s}|X^*(f_k)Y(f_k)| = \frac{2}{T_s}\left|\left(\sum_{k=0}^{N-1} x_k e^{-i2mn/N}\right)\left(\sum_{k=0}^{N-1} y_k e^{-i2mn/N}\right)\right| \quad (2.2)$$

where T_s is the temporal length of the data series, *X (f)*or *Y(f)* are the Fourier transform of *x(t)* and *y(t)* time-series data sets, respectively, *N* is the number of samples, $2\pi mm/N$ is frequency, *i* is the imaginary number ($\sqrt{-1}$), and * denotes the complex conjugate. The approximations include spectral smoothing using a raised-cosine window with 50% overlap to increase the reliability of the data. The exact degrees of freedom varied between data sets (between 20 and 30) due to the variability in length of the records. Mean squared coherence

$$\gamma^2{}_{xy}(f_k) = \frac{\left|S_{xy}(f_k)\right|^2}{S_{xx}(f_k)S_{yy}(f_k)} \tag{2.3}$$

were computed to evaluate input-output relationships between surface water and groundwater.

Aquifer Characterization

Sediment cores were collected from the shore-normal transect at 0, 10, 17.5, 20and 30 m offshore to characterize the aquifer. Whole sediment cores were analyzed for bulk density with a multi-sensor core logger (*Geotek, LTD* MSCL-S), split, and then photographed using the core logger imaging system (*Geotek, LTD* MSCL-CIS). The core logger measures the attenuation of gamma rays from a ^{137}Cs source as a proxy for gamma bulk density (Gunn and Best). Gamma bulk density is assumed to be equivalent to wet bulk density (e.g. Gerland and Villinger). Fractional porosity was computed from gamma/wet bulk density measurements by assuming a constant sediment grain density (2.65 g cm^{-3}) and pore water density (1.000 to 1.013 g cm^{-3} depending on coring location). After core surfaces were prepared, cores were photographed using GEOSCAN II line scan imaging system on the multi-sensor core logger. Fluorescent light is reflected off the sediment surface and detected using red, green, and blue detectors. Mosaic photographs were constructed using Geotek MSCL 6.2 (*Geotek, LTD*) software and red-green-blue (RGB) color intensities were extracted from the images. Cores were examined macroscopically (10 cm scale) and 10x hand lens to provide descriptive qualitative core logs.

Sediment sections (approximately 5 cm long) were sub-sampled from the vibracores with mid-point depths of 7, 15, 25, 35, 55, 75, 95, 115, 145, 175, 205, and 230 cm below the seafloor (cmbsf). Grain size was measured on 50 g of dry sediment using standard sieving techniques at 0.5 ϕ intervals (Folk 1974). An additional 20 g of dry sediment was wet sieved through a 4 ϕ (63 µm) sieve with 25% sodium metaphosphate ($Na_6O_{18}P_6$) solution to determine percent sand and mud.

Hydraulic conductivity (*K*) of the aquifer was assessed using a field bail-down test, a vertical constant-head permeameter in the laboratory, and grain-size. Bail-down tests were performed using a pressure transducer placed at the base of each piezometer and a peristaltic pump to extract water from the piezometer; total displacement was determined by water levels measured prior to and following 20 min of pumping or until the well was pumped dry. Recovery data were analyzed using both the Hvorslev (Hvorslev 1951) and KGS (Hyder et al. 1994) slug test solutions to determine estimates for hydraulic conductivity. Vertical hydraulic conductivity was measured on the mid-section (~100 cmbsf) of each vibracore using a Trautwein constant-head permeameter (*Trautwein-GeoTAC*). Measurements were conducted at four constant heads (20, 30, 40, and 50 cm). Grain size data were reduced following the suggestions of Dullien (1979) and Panda and Lake (1994) to determine an effective mean grain size diameter, D_{eff} (cm); this effective diameter accounts for the effects of variance and skewness in grain size(Appendix B). Hydraulic conductivity (cm s^{-1}) was computed using a modified Carmen-Kozeny (CK) equation from Panda and Lake (1994)

$$K = \left(\frac{\rho g}{\mu}\right)\left(\frac{{D_{eff}}^2 \varphi^3}{72\tau(1-\varphi)^2}\right) \tag{2.4}$$

where ρ is the density of water (g cm^{-3}), g is acceleration due to gravity (cm s^{-2}), μ is viscosity (g cm^{-1} s^{-1}), φ is porosity, and τ is sediment tortousity.

Results

Aquifer Matrix

Macroscopic examination of the sediments and quantitative measurements of color intensity, porosity, texture, and hydraulic conductivity provide the basis for the aquifer matrix characterization (Figure 2.2). The sediments collected from the field site can be qualitatively divided into three lithologic units (bottom to top): (LU-1) orange, thinly to thickly laminated, fine to medium quartz sand; (LU-2) gray to grayish-tan, massively bedded, moderately sorted fine quartz sand with an occasional burrow or root; and (LU-3) grayish-tan to black, normal graded, fine to coarse quartz sand with some shell fragments, mud, and organic matter. Although the lithologic contact between LU-1 and LU-2 is gradational, the color contrast between the two units makes the contact easily discernible. The base of LU-3 consists of coarse-grained quartz sand with some shell fragments producing a sharp lithologic contact between LU-2 and LU-3.

The major distinction between LU-1 and LU-2 is fine-scale laminar bedding or laminations observed in LU-1. Although a detailed mineralogic study was not conducted on these sediments, the laminations are composed primarily of ferric-bearing heavy minerals (e.g. magnetite or maghematite) as indicated by their attraction to a weak magnet. The mean and effective grain sizes for all samples collected from this unit are 112±45 μm and 220±50 μm, respectively, indicating a very fine to medium sand. Mud content in LU-1 is generally low (less than 1%); the mud-size fraction collected during grain size analysis was ferric-rich and strongly resembled the surface coatings on the sand. Porosity of the unit is between 0.37 and 0.42 with a slight increase in the offshore direction. Since all piezometers are screened in the L1 unit, slug-tests provide an effective hydraulic conductivity of the LU-1 sediment-type only. The average

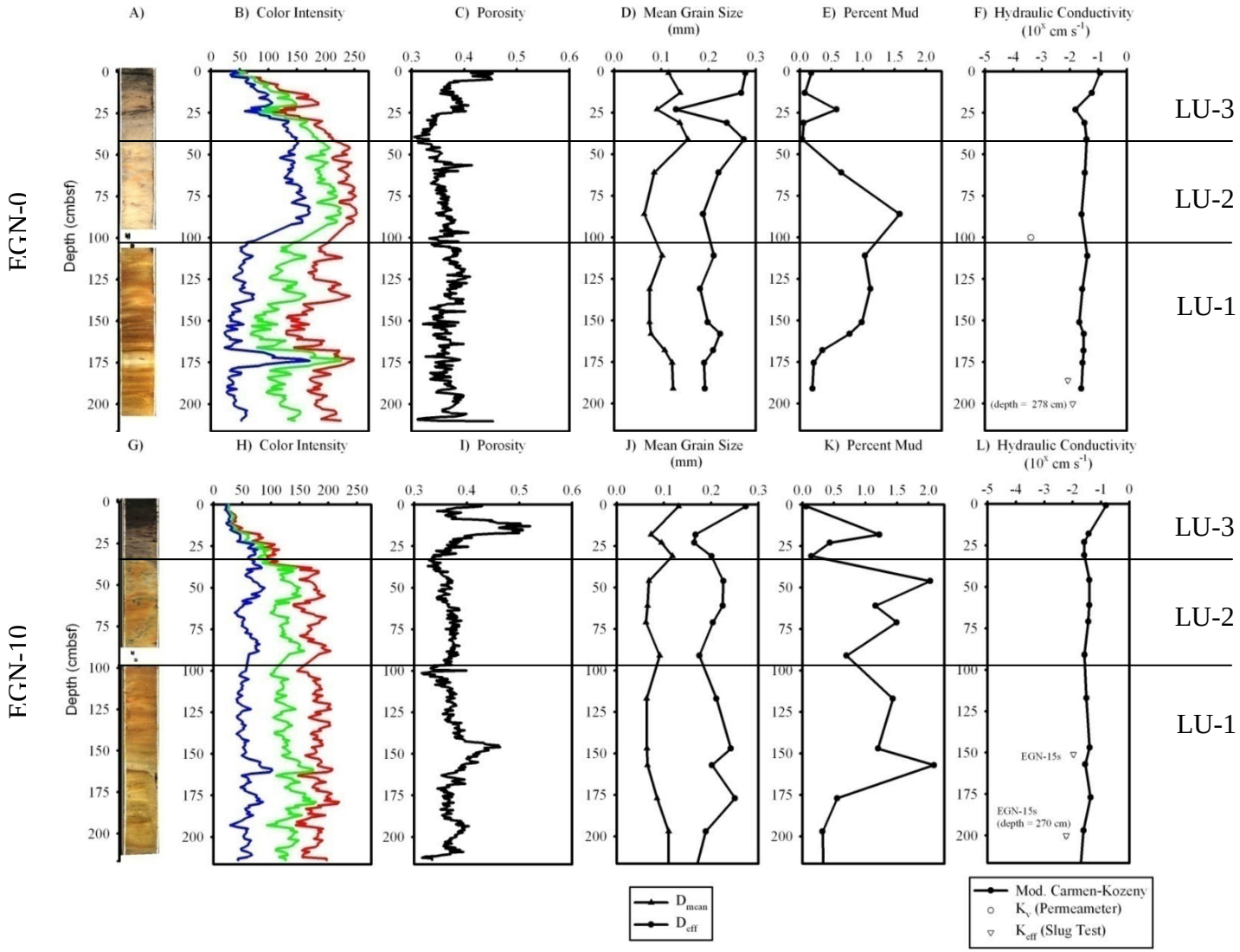

Figure 2.2. Core photographs, color intensity, porosity, grain size, percent mud, and hydraulic conductivity plotted as a function of depth below the seafloor (cmbsf) obtained from the four vibracores: (A – F) EGN-0, (G – L) EGN-10, (M – R) EGN-20, and (S – X) EGN-30. The missing section in each core is associated with the vertical hydraulic conductivity analysis.

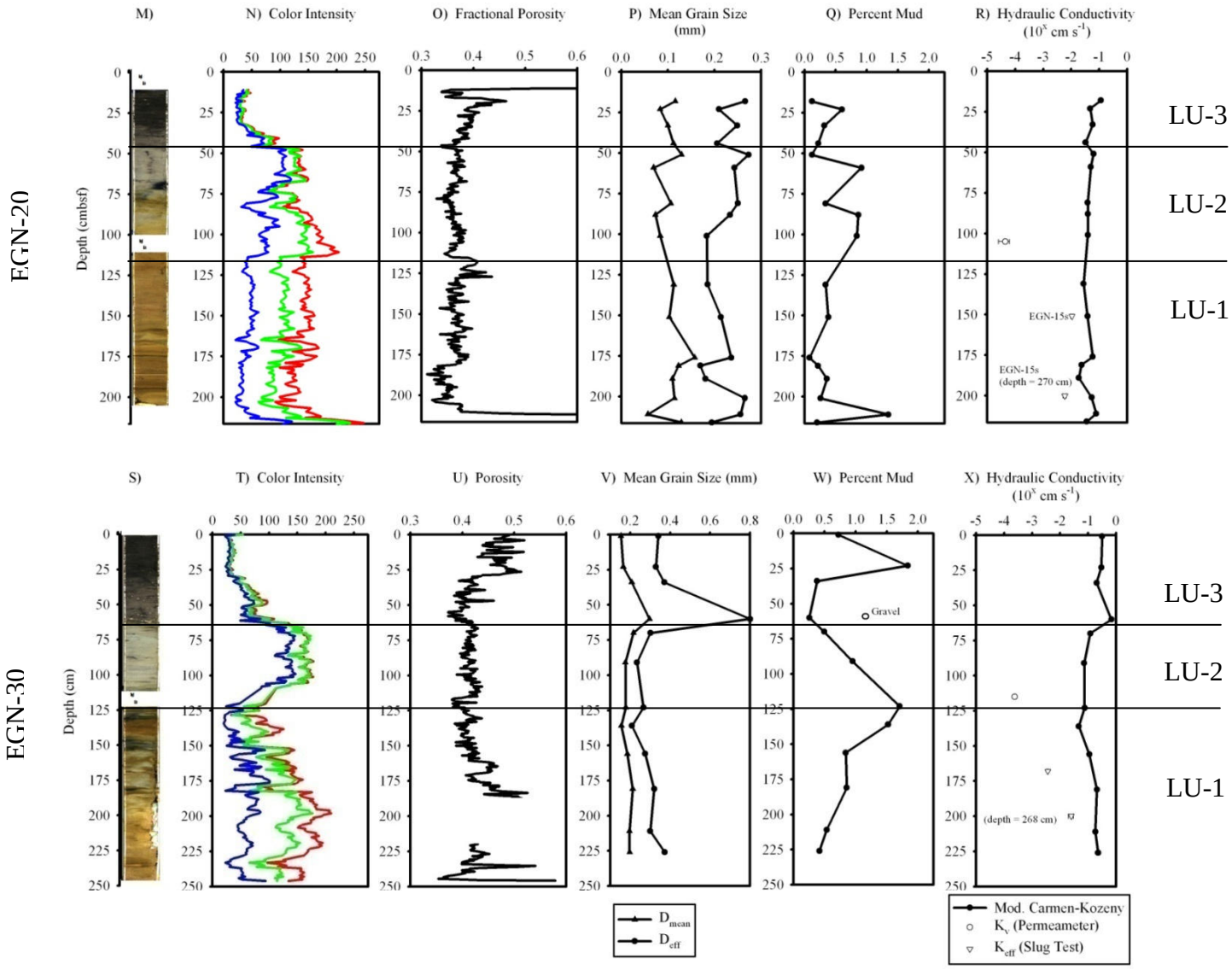
EGN-20
M)
N) Color Intensity
O) Fractional Porosity
P) Mean Grain Size (mm)
Q) Percent Mud
R) Hydraulic Conductivity (10^x cm s^{-1})
Depth (cmbsf)
LU-3
LU-2
LU-1
EGN-15s
EGN-15s (depth = 270 cm)
EGN-30
S)
T) Color Intensity
U) Porosity
V) Mean Grain Size (mm)
W) Percent Mud
X) Hydraulic Conductivity (10^x cm s^{-1})
Depth (cm)
Gravel
(depth = 268 cm)
D_{mean}
D_{eff}
Mod. Carmen-Kozeny
K_v (Permeameter)
K_{eff} (Slug Test)

(fig. con'd)

hydraulic conductivity from bail-tests is $10^{-1.96}$ cm s^{-1}, which is comparable to the average hydraulic conductivity ($K = 10^{-1.23}$ cm s^{-1}) derived from grain size data and CK-equation (Table 2.1).

LU-2 has physical properties similar to LU-1. Porosity, mean and effective grain size, and the grain-size based hydraulic conductivity are similar between LU-2 and LU-1; however, the absence of heavy mineral lamina in LU-2 distinguishes it from LU-1. The color of LU-2 sediments varies significantly among the four cores: orangish-yellow (high, closely spaced RGB intensities) at the shoreline; yellowish-orange to orange (high, closely spaced RG intensities and low B intensity) at 10 m offshore; and yellowish-gray to gray (low, closely spaced RGB intensities) at 20 and 30 m offshore. Percent mud is also generally higher in LU-2 relative to LU-1 sediments; mud fractions exceeding 1% are observed in all cores. Similar to LU-1, the mud size particles have an orange coloration and probably reflect disaggregation of surface coatings during sieving. Vertical hydraulic conductivity (K_v) measurements are primarily from the LU-2 sediment type or the gradational contact between LU-1 and LU-2 sediments; the average K_v is $10^{-3.63}$ cm s^{-1}, more than two orders of magnitude less than CK-based hydraulic conductivity (Table 2.1). Hartl (2006) noted a similar low (vertical) permeability, transition zone from cores collected 300 to 500 m offshore from our study site. The offshore hydraulic conductivity was approximately $10^{-3.2}$ cm s^{-1} while the depth-averaged hydraulic conductivity was on the order of $10^{-2.3}$ cm s^{-1}.

LU-3 is the most lithologically distinct of the three units; macroscopically, it is normal-graded from slightly-shelly, medium quartz sand with trace amounts of mud at the base to a fine to medium grain quartz sand with variable amounts of mud and organic matter at the top. The cmbsf at the shoreline to approximately 55 cmbsf at 30 m offshore. The mean and effective

Table 2.1. Summary of hydraulic conductivity obtained from the various measurement techniques.

	LU-1	LU-2	LU-3
	Hydraulic Conductivity, K (cm s^{-1})		
Slug Test	0.011		
Vertical Permeameter		0.00023	
modified Carmen-Kozeny	0.059	0.049	0.14
Hartl (2006)		0.0050	

sharp contact between LU-2 and LU-3 dips offshore and LU-3 thickness increases from 30 grain sizes for this unit are 133±50 and 280±150 µm. While the mean grain size for LU-3 is indistinguishable from the mean grain size from LU-1 and LU-2 sediments, the variability in the effective grain size (relative standard deviation of 0.55) shows the dissimilarity of this unit relative to LU-1 and -2 sediments. This dissimilarity is also apparent by the slightly higher porosity observed in LU-3 relative to LU-1 and LU-2. Both of these factors (i.e. higher D_{eff} and porosity) contribute to the higher CK-derived hydraulic conductivity in LU-3 relative LU-1 and -2 (Table 2.1).

Salinity Distribution

Temporally-discrete salinity measurements from the piezometers made during ST1 (Table 2.2) and the continuous salinity record obtained during ST2 (Table 2.3) concur with the salinity framework found by other researchers (Martin et al, 2007). Fresh groundwater (salinity less than 0.5) extends to approximately 10 m offshore, low brackish water (salinity between 0.5 to 6) extends from approximately 10 m to 20 m offshore, and brackish water (salinity of 6 to near lagoon water salinity, ~20) occurs beyond 20 m offshore. This portion of the coastal aquifer is the offshore freshwater seepage face, which interacts with more saline groundwater and surface water and is often referred to as the subterranean estuary (Moore 1999) or the dispersive mixing

zone (Cooper Jr. et al. 1964). More detail on the structure of the EGN subterranean estuary is provided in subsequent chapters.

Physical Flow Regime

Groundwater and surface water time-series data for ST1 and ST2 are presented in Figure 2.3. During both sampling trips, groundwater fluctuations correlate well with surface water fluctuations. The (cross) correlation coefficients (r_{xy}) between the various piezometric head measurements and surface water levels during both studies are between 0.940 and 0.999, assuming no time lag effects (Tables 2.2 – 2.3). Groundwater-surface water fluctuations occur on a number of time-scales, and the longer duration of ST1 provides insight to time-variant water level fluctuations. For example during ST1, relative high groundwater and surface water levels (> 10 cm above the long-term average) occur on the time-scale of a month as observed from 15-Jan-05 to 15-Feb-05 and from 01-Jun-05 to 01-Jul-05 (Fig. 2.3A). Variability occurs during ST1 and ST2 at intervals of less than a month as indicated by daily to weekly increases and decreases (spikes) in water level. Such short-term fluctuations include, but are not limited to, 26-Dec-04, 08-May-05, 04-Nov-06, 06-Dec-06, and 14-Dec-06 (Figure 2.3).

Vertical and horizontal hydraulic gradients can be extracted from the various water level measurements and these gradients provide information about the physical flow regime of the system as suggested by Darcy's Law (i.e. $q = -Ki$ where q is specific discharge or Darcy flux [L/T], K is hydraulic conductivity [L/T], and i is the hydraulic gradient [L/L]). Vertical gradients (i_v) are the difference between surface water and groundwater water levels (dh_v) normalized by the difference in depth between the two sampling points (dz), such that negative gradients indicate vertical upward flow and vice versa. Similarly, horizontal gradients (i_h) are the difference between head in the piezometers (dh_h) normalized by the horizontal distance between

Table 2.2. Statistical summary of salinity, water level data, hydraulic gradients, and discharge for 22-Nov-04 to 20-Jul-05.

22-Nov-04 to 20-Jul-05	EGNW-OS	EGNW-0s	EGNW-15d	EGNW-30d	EGNW-SW
Salinity					
Mean	N/A	0.1	1.5	21.0	18.0
2σ	N/A	0.01	0.1	1.5	2.0
Water level or Piezometric Head (cm relative to field datum)					
Mean	N/A	20	6	3	7
2σ	N/A	16	14	20	16
Max	N/A	44	23	32	35
Min	N/A	-11	-16	-15	-16
Correlation Coefficient (wrt Surface Water)	N/A	0.956	0.963	0.999	1.000
Vertical hydraulic gradient, i_v (relative to surface water)					
Mean	N/A	-0.070	0.0037	0.015	N/A
2σ	N/A	0.026	0.014	0.0036	N/A
Vertical specific discharge, q_v (cm d^{-1})					
Mean	N/A	30	-1.1	-6.5	N/A
2σ	N/A	11	6.0	1.5	N/A
Horizontal hydraulic gradient, i_h (relative to EGNW-0s)					
Mean	N/A	N/A	0.0096	0.0043	N/A
2σ	N/A	N/A	0.0041	0.0016	N/A
Horizontal specific discharge, q_h (cm d^{-1})					
Mean	N/A	N/A	-9.1	-4.1	N/A
2σ	N/A	N/A	3.9	1.5	N/A

Table 2.3. Statistical summary of salinity, water level data, hydraulic gradients, and discharge for 06-Oct-06 to 27-Dec-06.

06-Oct-06 to 27-Dec-06	EGNW-OS	EGN-0s	EGN-15s	EGNW-30s	EGNW-SW
Salinity					
Mean	0.2	0.1	1.0	20.2	14.4
2σ	0.0	0.01	0.1	2.2	5.9
Water level or Piezometric Head (cm)					
Mean	69	40	31	41	34
2σ	13	15	15	15	14
Max	86	59	51	61	55
Min	52	22	14	24	18
Correlation Coefficient (wrt Surface Water)	0.940	0.958	0.967	0.968	1.000
Vertical hydraulic gradient, i_v (relative to surface water)					
Mean	N/A	-0.027	0.021	-0.036	N/A
2σ	N/A	0.023	0.025	0.023	N/A
Vertical specific discharge, q_v (cm d^{-1})					
Mean	N/A	12	-9.2	16	N/A
2σ	N/A	9.9	10.9	10	N/A
Horizontal hydraulic gradient, i_h (relative to EGNW-0s)					
Mean	0.029	N/A	0.0055	-0.00033	N/A
2σ	0.0044	N/A	0.0022	0.0012	N/A
Horizontal specific discharge, q_h (cm d^{-1})					
Mean	-27	N/A	-5.3	0.32	N/A
2σ	4.2	N/A	2.1	1.1	N/A

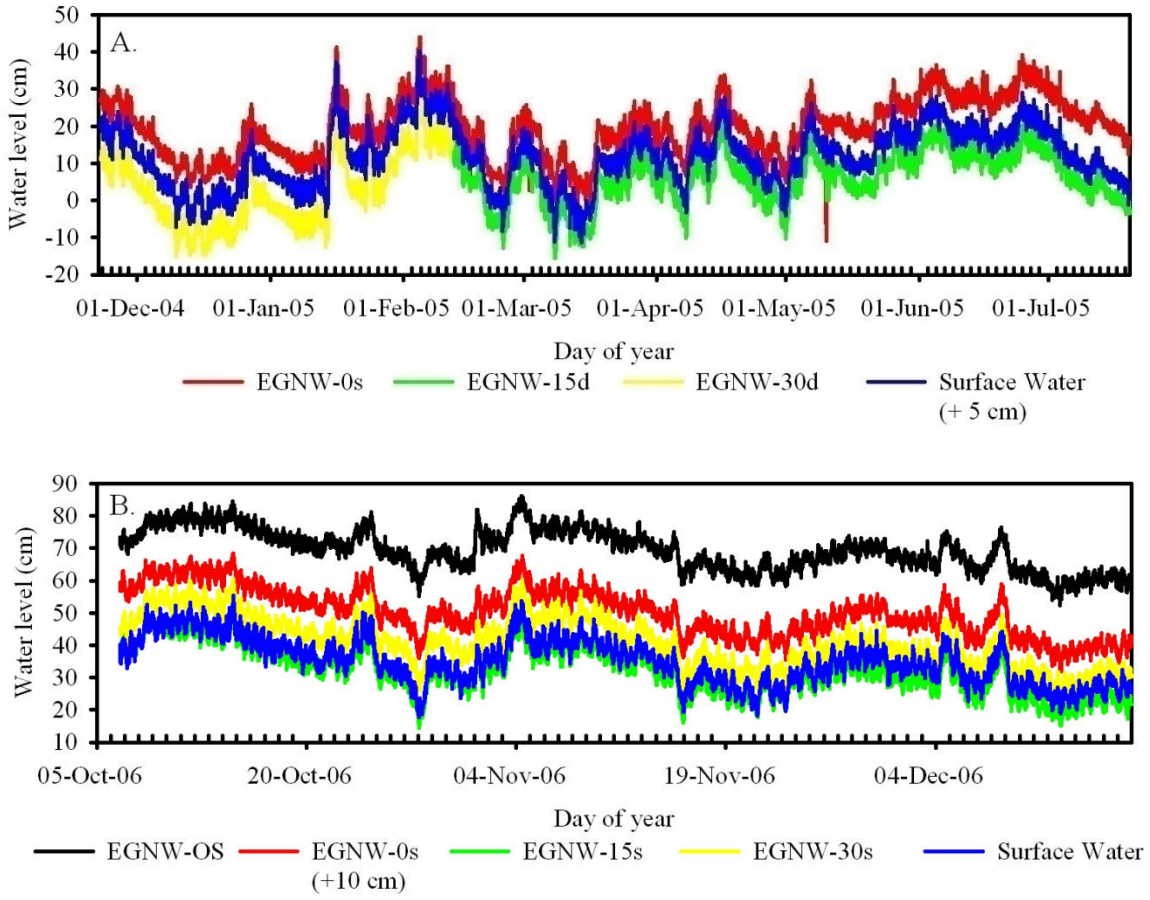

Figure 2.3. (A) Raw water level data obtained during ST1 (22-Nov-04 to 15-Jul-05). Note that the surface water data has been offset by 5 cm to prevent significant overlap with EGNW-15d and EGNW-30d. (B) Raw water level data obtained during ST2 (06-Oct-06 to 27-Dec-06). Note that the groundwater head for EGNW-0s has been offset by 10 cm to prevent significant overlap with EGNW-30s.

the two sampling points (*dx*). In this study, all horizontal gradients are referenced to the shoreline well (Table 2.2) such that positive gradients indicate seaward flow and vice versa. In the following paragraphs, the hydraulic gradients are described to evaluate the physical flow regime; vertical and horizontal discharge are estimated using the depth-average K_v ($10^{-2.3}$ cm s^{-1}; reported by Hartl 2006) and the average K_h from the bail-down tests ($10^{-1.96}$), respectively (Tables 2.2 – 2.3).

The strong correlation between piezometric head(s) and surface water suggests a comparison between long-term average hydraulic gradients should be sufficient in characterizing the system (Table 2.2; Figure 2.3A). During ST1, the average vertical hydraulic gradients between the groundwater and surface water at 0, 15 and 30 m offshore are -0.070±0.026 (2σ, n = 2878), 0.0037±0.014 (2σ, n = 1894), and 0.013±0.0036 (2σ, n = 984), respectively. These gradients suggest discharge is occurring at the shoreline at a rate of 30±11 cm d^{-1} (2). In contrast, recharge is occurring 15 and 30 m offshore at rates of 1.6±6.0 and 5.5±1.5 cm d^{-1} (2σ), respectively. As indicated by the variations in the rates, EGNW-15d experiences both recharge and discharge. Horizontal hydraulic gradients for EGNW-15 and EGNW-30 with respect to EGNW-0 for ST1 are 0.0096±0.0041 (2σ, n = 1894) and 0.0043±0.0016 (2σ, n = 984), respectively. These horizontal gradients suggest seaward flow on the order of 4 to 9 cm d^{-1}; however, care should be taken in interpreting this generalization because the piezometers are screened at different depths.

The long-term average vertical hydraulic gradients obtained from the ST2 data set share similarities and differences with those from ST1 (*cf.* Tables 2.2 and 2.3). During ST2, the average vertical hydraulic gradients between the groundwater and surface water at 0, 15 and 30 m offshore are -0.027±0.023, 0.021±0.025, and -0.036±0.023 (2σ, n = 5898 for all), respectively.

As with ST1, the i_v at the shoreline during ST2 indicates discharge, however, the rate (12±9.9 cm d^{-1}; 2σ, n = 5898) is approximately one-third of that observed during ST1 (Table 2.2). During ST2, the average i_v at 15 m offshore suggests recharge; however as with ST1, the site appears to be a point of both recharge and discharge (Table 2.3). In contrast to ST1, the vertical hydraulic gradient at 30 m offshore during ST2 suggests both discharge and recharge are probable at rates ranging from -26 to 5.5 cm d^{-1}. Horizontal hydraulic gradients from EGNW-OS, EGNW-15s, and EGNW-30s relative to EGN-0s are 0.029±0.0044, 0.0055±0.0022, and -0.00033±0.0012 (2σ, n = 5898 for all), respectively, which equate to Darcy velocities of -27±4.2, -5.3±2.1, and 0.32±1.1 cm d^{-1}, respectively. These rates show that the horizontal groundwater flow does occur seaward of the shoreline, however, given the current piezometer configuration it cannot be determined whether the horizontal or vertical component of flow is more dominant.

Periodic Surface Water-Groundwater Interactions

Correlation between surface water and groundwater head is high suggesting a significant causal relationship between the two data sets. By comparing the data sets in the frequency domain, a better understanding of how periodic forces imposed by surface water fluctuations are propagated through the saturated aquifer. Auto-spectra were computed from individual water level records to identify consistent periodic forces among the data sets and cross-spectra and mean-squared coherency were computed to quantitatively justify these general observations.

Power spectra for ST1 and ST2 for each of the water level data sets are shown in Figures 2.4 and 2.5, respectively. In general, most of the power occurs at the lower end of the frequency spectrum (less than 3 cpd). The higher resolution sampling (Nyquist frequency of 36 cpd) conducted during ST2 does not show any significant power inputs at the higher end of the frequency spectrum. The most prominent, resolvable power signals for both monitoring periods

and all the data sets are at frequencies of 1.000 and 1.933 cpd (T_p = 1 and 0.52 d; Figures 2.4 – 2.5); these frequencies are consistent with the K1 and M2 tidal constituents. Additional resolvable power peaks during ST1 occur between frequencies of 0.048 and 0.1680 cpd (T_p = 20.8 and 6.0 cpd; Figure 2.4); whereas during ST2, the only additional resolvable power peak occurs at a frequency of 0.36 cpd (T_p = 2.8 d; Figure 2.5). The lack of significant astronomical forces acting on these time-scales suggests that atmospheric forcing is the primary mechanism.

Cross-spectra between surface water and the various groundwater data sets collected during ST1 and ST2 are presented in Figures 2.6 and 2.7, respectively. Following the suggestion of Shih et al. (1999), the significance of the cross-spectra are evaluated by the mean-squared coherency relative to the 95% confidence of the non-zero coherency (NZC) for a given frequency. As foreshadowed by the auto-spectra, a significant power relationship exists between surface water and groundwater at the frequencies mentioned above. This analysis confirms that periodic forces affecting the surface water are propagated into the aquifer; the question remains how much attenuation of these signals is induced by the aquifer matrix.

The propagation of energy/power signal can be assessed using the gain/attenuation factor, $H(f)$,

$$|H(f)|^2 = \frac{S_{xx}(f)}{S_{yy}(f)} \tag{2.5}$$

where S_{yy} and S_{xx} are the one-sided, power spectra for an input (i.e. surface water) and an output (i.e. groundwater) signal, respectively. Instead of the entire power spectra, I concentrate on those frequencies with significant cross-spectral/coherent relationships as indicated above; a summary of attenuation factors are presented in Table 2.4. These data show the aquifer is very efficient in transmitting perturbations in the surface water into the groundwater. In addition, it

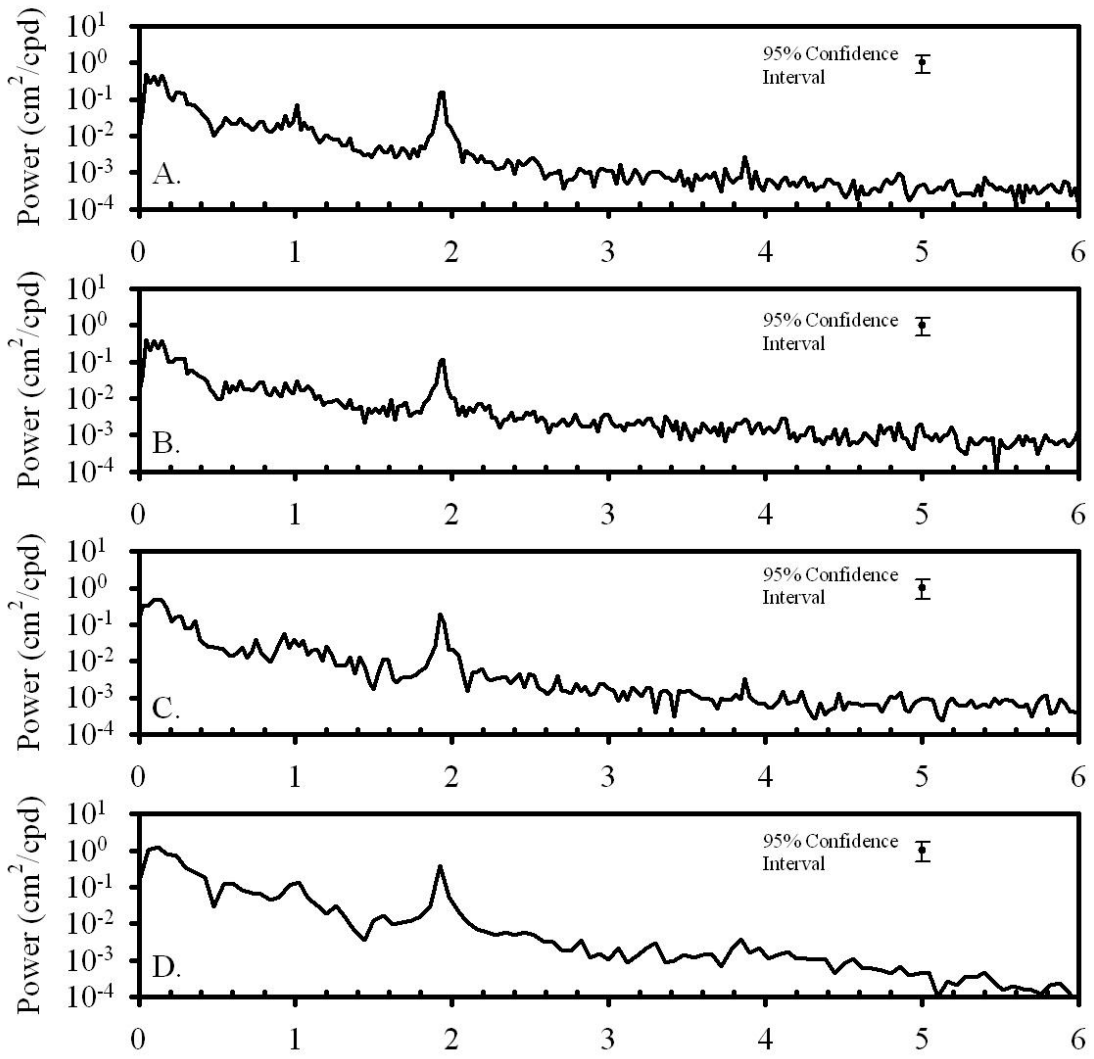

Figure 2.4. Power auto-spectra density functions computed for (A) surface water, (B) EGNW-0s, (C) EGNW-15d, and (D) EGNW-30d for time-series data collected during ST1 (22-Nov-04 to 15-Jul-05).

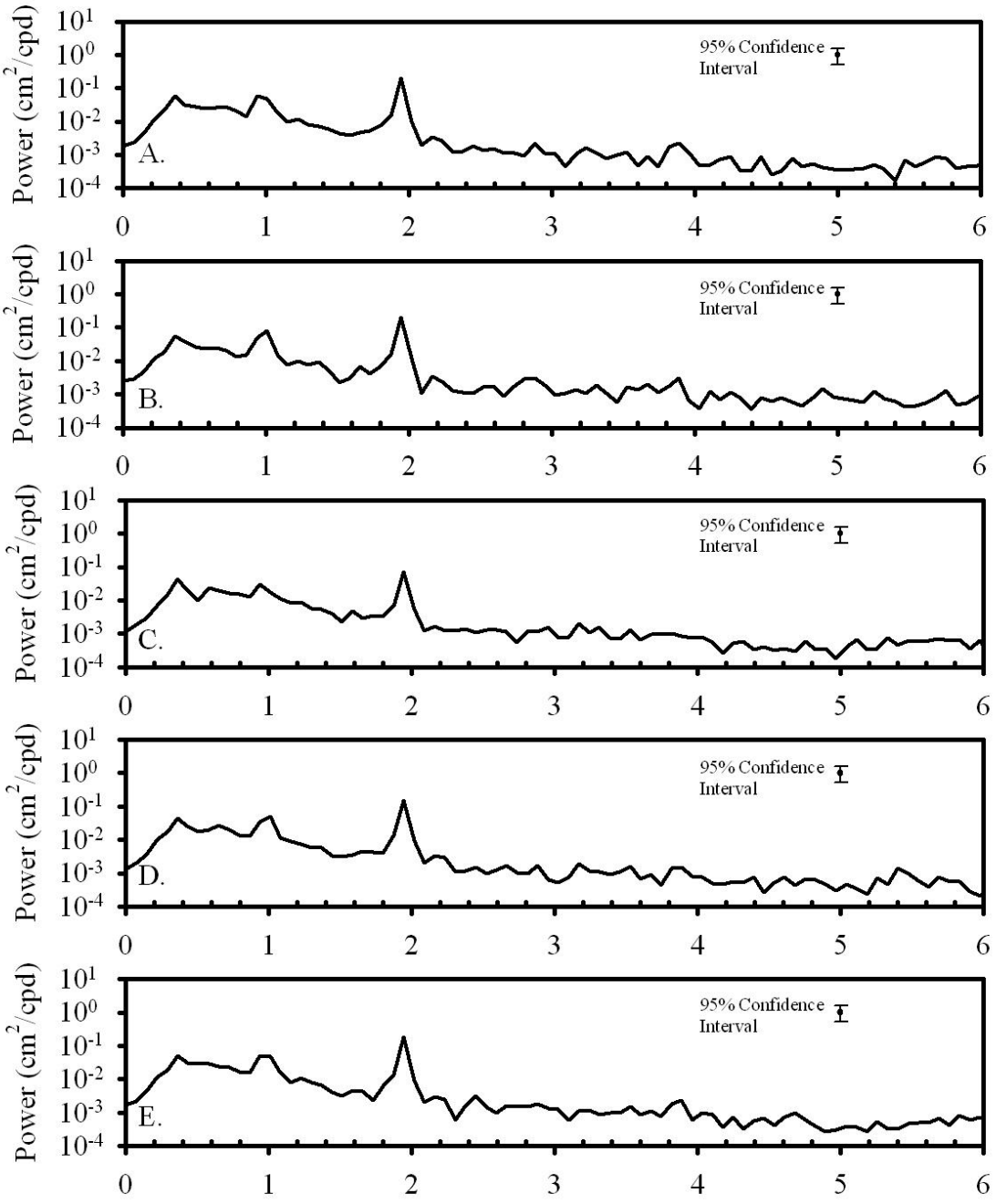

Figure 2.5. Power auto-spectra density functions computed for (A) surface water, (B) EGNW-OS, (C) EGNW-0s, (D) EGNW-15s, and (E) EGNW-30d for time-series data collected during ST2 (06-Oct-06 to 27-Dec-06).

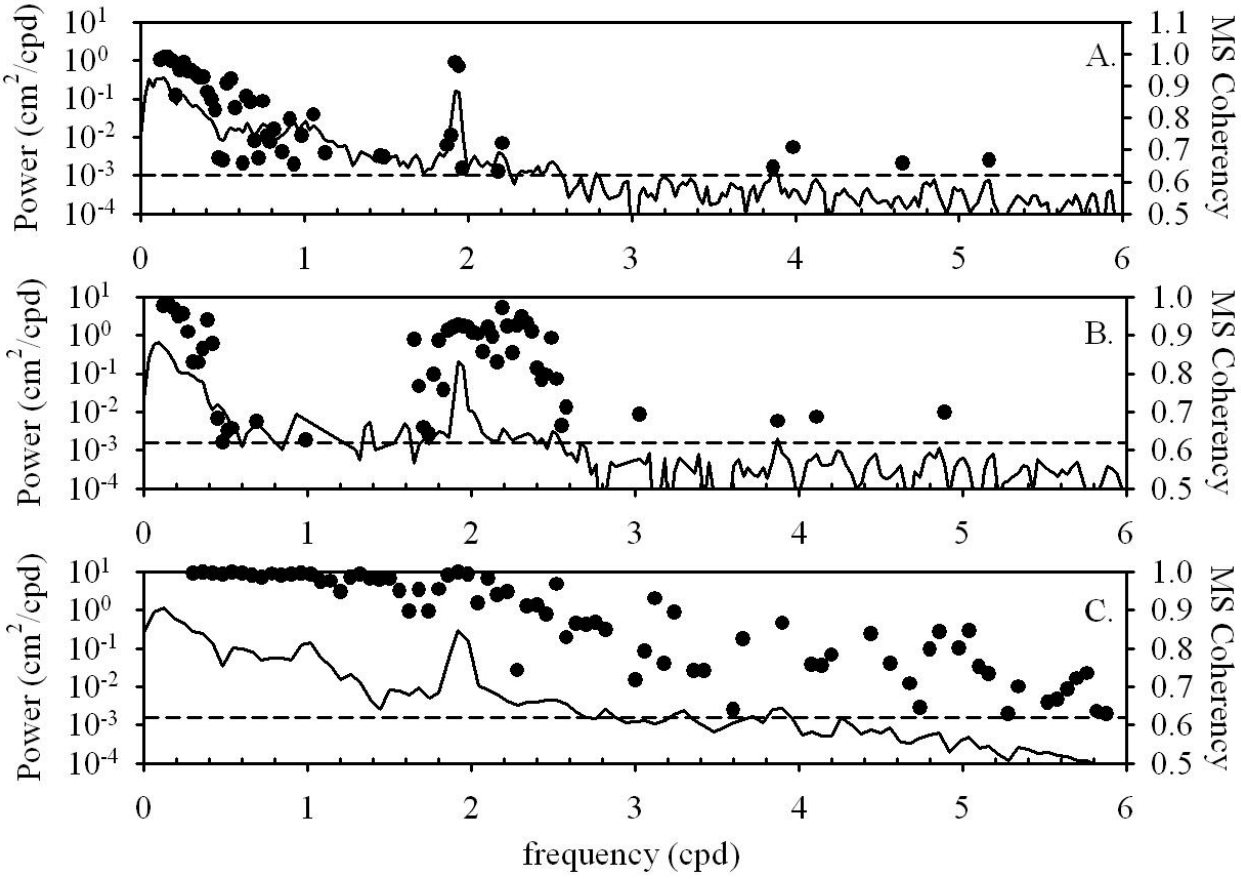

Figure 2.6. Power cross-spectra density functions computed using surface water as an input and (A) EGNW-0s, (B) EGNW-15d, and (C) EGNW-30d as output for time-series data collected during ST1 (22-Nov-04 to 15-Jul-05). Mean squared coherence that is greater than the 95% non-zero coherence (NZC) is plotted as scatter points to indicate frequencies were coherent relationship existed between input and output.

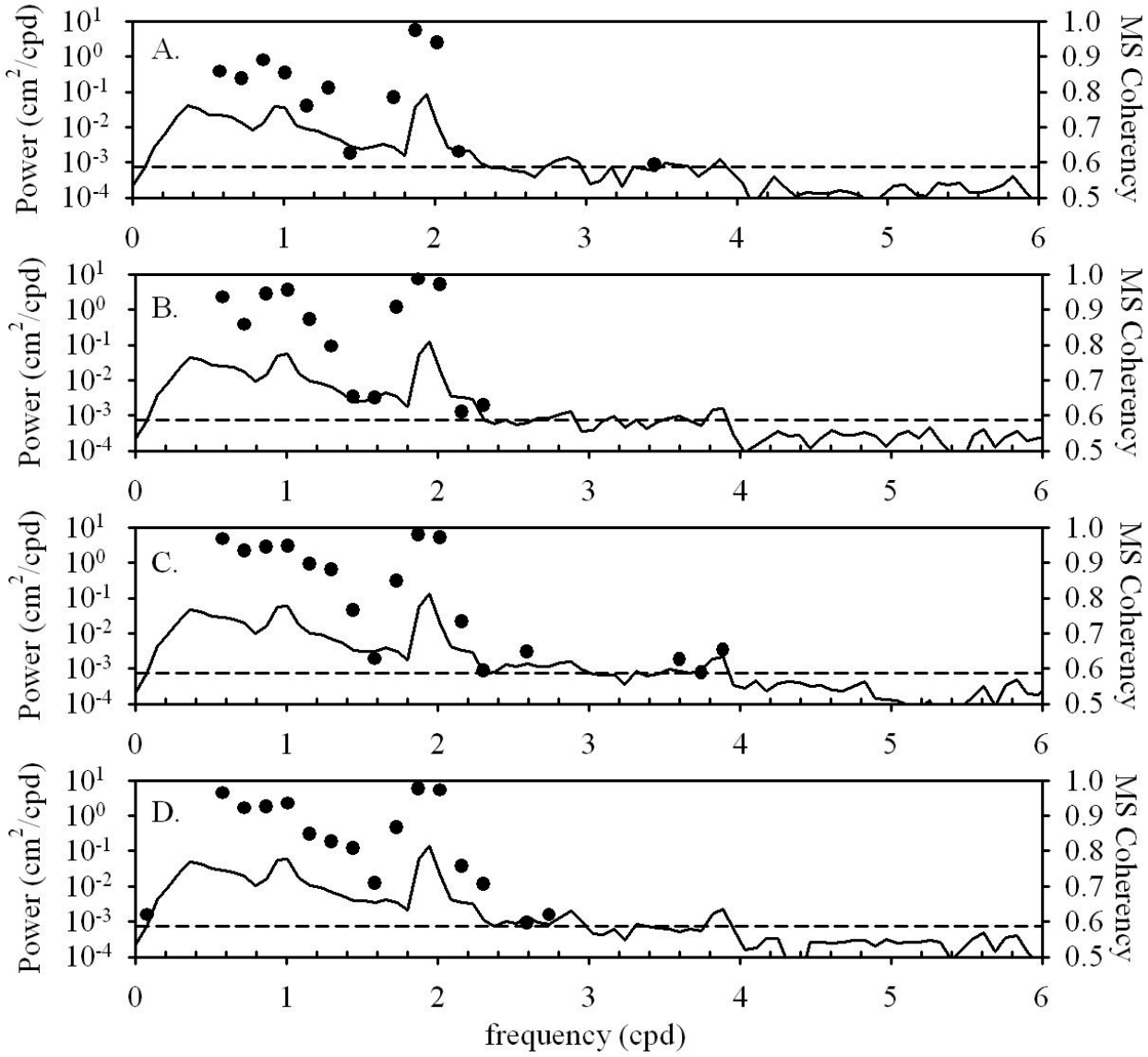

Figure 2.7. Power cross-spectra density functions computed using surface water as an input and (A) EGNW-OS, (B) EGNW-0s, (C) EGNW-15d, and (D) EGNW-30d as output for time-series data collected during ST2 (06-Oct-06 to 27-Dec-06). Mean squared coherence that is greater than the 95% non-zero coherence (NZC) is plotted as scatter points to indicate frequencies were coherent relationship existed between input and output.

Table 2.4. Attenuation factor of discrete frequencies that demonstrated high coherency.

Sampling Trip	frequency	Attenuation Factor, *H(f)* for different piezometers 0	15	30	SW
ST1	0.048	0.846			1.000
	1	0.449	0.381	0.689	1.000
	1.933	0.758	0.807	0.818	1.000
ST2	0.36	0.749	0.777	0.868	1.000
	1	0.509	0.711	0.826	1.000
	1.933	0.363	0.773	0.835	1.000

appears the lower frequency signals experience the least attenuation, which could play a significant role if the system is perturbed by non-periodic events (e.g. hurricanes).

Discussion

The open hydrologic connection between the lagoon and the submarine aquifer is apparent from the strong correlation between surface water level and piezometric head(s). Even with this open connection, the vertical and horizontal hydraulic gradients and subsequently the physical flow regime remain fairly constant through time. Based on the piezometer configuration of this study, the physical flow regime does not appear to be dominated by either vertical or horizontal flow. At 15 m offshore, the ratio between horizontal and vertical flow rates derived from horizontal hydraulic gradients between EGNW-0 and -15 and the vertical hydraulic gradient between EGNW-15 and surface water, respectively, is approximately 1:1 during both ST1 and ST2. However, a subsequent study conducted between Jul-05 and Mar-06 (see Table 3.1 of Chapter 3) using nested piezometers suggests the ratio between horizontal flow rate (estimated by the horizontal hydraulic gradient between EGNW-0d and -15d) and vertical flow rates (estimated from vertical hydraulic gradients between EGNW-15d and -15s) is 1:5, which implies vertical flow is dominant. The discrepancy between these two observations is not clear and may be related to a number of factors, including the similarity in lagoon water level and head

at 15 m offshore during ST1 and ST2, changes in the overall water balance in the fresh groundwater system (i.e. recharge, withdrawal) during the various sampling trips, and/or the treatment of data (i.e. usage of long-term averages and comparison of horizontal and vertical flows for EGNW-15) to examine the physical flow regime. However, a vertically-dominated physical flow regime is more consistent with the theory of groundwater hydraulics at a seepage or exit face (Cooper 1959; Glover 1959; Harr 1962; Bear 1972).

In general, the dominance of vertical flow in submarine seepage faces stems from the fact that surface water body (i.e. the lagoon or sea) acts as a prescribed head boundary. All such prescribed head boundary conditions (e.g. water-table divides and surface water bodies) are in fact an equipotential line (i.e. lines of equal head) for the groundwater flow system (Harr 1962). As these boundaries are approached (e.g. in the case of two-dimensional flow), hydraulic gradients and flow become pre-dominantly unidirectional (Harr 1962). In the case where the prescribed head boundary is a surface water body, the equipotential line is essentially horizontal and the groundwater flow is pre-dominantly vertical. Also important to coastal aquifers, as examined in this study, are density gradients. Contrasts in groundwater salinity create density gradients between seaward flowing fresh groundwater and landward flowing saline groundwater. The less dense fresh groundwater overlies the denser saline groundwater creating a curvilinear interface between the two water masses, which becomes progressively more vertical as you approach the top of the aquifer (i.e. Ghyben-Herzberg relation). Despite whether the interface between the two fluids is sharp (i.e. immiscible fluids) or transitional (i.e. miscible fluids), there is limited transport of fluid across the interface and the flow paths tend to parallel the interface (Cooper 1959; Glover 1959). The Indian River Lagoon acts as a prescribed head boundary for the submarine aquifer and salinity gradients occur between fresh groundwater and saline and groundwater, thus I argue that the vertically-dominated flow regime observed between Jul-05

Mar-06 is more consistent with the theory of coastal seepage faces. However, it should be noted that a 1:1 ratio implied by measurements from ST1 and ST2 still reflects the importance of vertical flow in this system and that flow will become increasingly more vertical as the sediment-water interface is approached (Cooper 1959; Glover 1959; Harr 1962; Nielsen 1990; Horn 2002; Mango et al. 2004).

Vertical discharge estimates derived from direct head measurements are somewhat consistent with observations made by Martin et al. (2007) using seepage meters and chloride concentration in the discharging fluid. For example, Martin et al. (2007) reported rates of fresh groundwater discharge at the shoreline that were 9.0±2.2 cm d^{-1}, which fall within the range derived from head measurements. However, the seepage meter and chloride data showed that fresh groundwater discharge occurred out to 20 m offshore. Based on water level measurements, the null point of fresh groundwater discharge may occur closer to the shoreline as indicated by the variable recharge/discharge scenario observed at 15 m offshore, especially during ST1. Seepage meter estimates of fresh groundwater discharge at 15 m offshore were on the order of 2.6 cm d^{-1} (Martin et al. 2007), which falls within the large range derived from head measurements. This discharge rate (2.6 cm d-1; Martin et al., 2007) suggests a head difference of 0.9 or 1.5 cm between the surface water and groundwater head, in either the shallow (1.5 m) or deep (2.5 m) piezometer, respectively, which is below the resolution of the probes used to measure head. Thus, the variability of the recharge/discharge rates at 15 m offshore could potentially be resolved by measuring water levels at various depths within the aquifer simultaneously or with instruments that have a resolution greater than ±1 cm. The discrepancy between the flow rates from Martin et al. (2007) and in this study using head measurements demonstrates importance of using multiple techniques but also the difficulties in their intercomparison.

Raw time-series water level data do not suggest any dominant periodic forces acting on the system; however, transforming the data into the frequency domain reveals both astronomic- and wind-tides are perturbing the system at consistent intervals. The main astronomical forces acting on this system include the diurnal K1 and semi-diurnal M2 tidal constituents; however, the amplitudes of these constituents are less than 1 cm. The influence of wind-tides is assumed from the additional resolvable peaks in the auto-spectra observed specifically at frequencies of 0.168 and 0.36. These frequencies correspond nicely with periodicity of frontal passages that occur on the order of 3 to 6 days. However, the amplitudes of these periodic wind-tides are generally less than 2 cm. Combined effects of these two periodic forces cannot explain the ~14 cm (2σ) variability observed in all water level data, because non-periodic or episodic forces also are influencing water levels in the Indian River Lagoon and submarine groundwater system. Such events are apparent in the raw data (e.g. 15-Jan-04; Figure 2.3) where surface water and groundwater levels increase almost 50 cm in a period of a 2 d.

Summary

The position of the subterranean estuary and fresh groundwater seepage face observed in Indian River Lagoon appears to be relatively stable during “fair weather conditions”. While periodic frontal systems appear in both groundwater and surface water data sets, limited attenuation is observed due to the effects of the aquifer matrix. The rapid response of groundwater to these periodic forces suggests an open hydrologic connection between the lagoon and the groundwater-aquifer system. Even with this open connection, the physical flow regime appears to remain fairly constant with time. Darcy velocities suggest the focus of fresh groundwater discharge is confined from the shoreline to approximately 15 m offshore. Vertical hydraulic gradients and Darcy velocities suggests vertical flow is a major component of the physical flow regime as is expected for a freshwater seepage face. While vertical flow is

significant during fair weather conditions, it could not be definitively shown that vertical flow dominates over horizontal flow.

References

Bear, J. 1972. Dynamics of Fluids in Porous Media. American Elsevier Publishing Co.

Bendat, J. S., and A. G. Piersol. 1971. Random Data: Analysis and Measurement Procedures. John Wiley & Sons, Inc.

Bokuniewicz, H. 1995. Analytical descriptions of subaqueous groundwater seepage. Estuaries **15:** 458-464.

Bokuniewicz, H., R. Buddemeier, B. Maxwell, and C. Smith. 2003. The typological approach to submarine groundwater discharge (SGD). Biogeochemistry **66:** 145-158.

Burnett, W. C. 1999. Offshore springs and seeps are focus of working group. EOS **80:** 13-15.

Burnett, W. C. and others 2006. Quantifying submarine groundwater discharge in the coastal zone via multiple methods. Sci. Total Environ. **367:** 498-543.

Burnett, W. C., M. H. Bokuniewicz, W. S. Moore, and M. Taniguchi. 2003. Groundwater and pore water inputs to the coastal zone. Biogeochemistry **66:** 3-33.

Burnett, W. C. and others 2002. Assessing methodologies for measuring groundwater discharge to the ocean. EOS **83:** 120-123.

Burnett, W. C., M. Taniguchi, and J. Oberdorfer. 2001. Measurement and significance of the direct discharge of groundwater into the coastal zone. Journal of Sea Research **46:** 109-116.

Cable, J. E., W. C. Burnett, J. P. Chanton, and G. L. Weatherly. 1996. Estimating groundwater discharge into the northeastern Gulf of Mexico using Radon-222. Earth and Planetary Science Letters **144:** 591-604.

Cable, J. E., J. B. Martin, P. W. Swarzenski, M. K. Lindenberg, and J. Steward. 2004. Advection Within Shallow Pore Waters of a Coastal Lagoon, Florida. Ground Water **42:** 1011-1020.

Chanton, J. P., W. C. Burnett, H. Bulaviova, D. R. Corbett, and M. Taniguchi. 2003. Seepage rate variability in Florida Bay driven by Atlantic tidal height. Biogeochemistry **66:** 187-202.

Church, T. M. 1996. An underground route for the water cycle. Nature **380:** 579-580.

Cooper, H. H. 1959. A Hypothesis Concerning the Dynamic Balance of Fresh Water and Salt Water in a Coastal Aquifer. Journal of Geophysical Research **64:** 461-467.

Cooper Jr., H. H., F. A. Kohout, H. R. Henry, and R. E. Glover. 1964. Sea Water in Coastal Aquifers, p. 84. United State Geological Survey.

Dullien, F. A. L. 1979. Porous media: fluid transport and pore structure, p. 110-155. Academic Press.

Folk, R. L. 1974. Petrology of Sedimentary Rocks. Hemphill Publishing Company.

Gerland, S., and H. Villinger. 1995. Nondestructive density determination on marine sediment cores from gamma-ray attenuation measurements. Geo-Mar. Lett. **15:** 111-118.

Glover, R. E. 1959. The pattern of fresh-water flow in a coastal aquifer. Journal of Geophysical Research **64:** 457-459.

Gunn, D. E., and A. I. Best. 1998. A new automated nondestructive system for high resolution multi sensor core logging of open sediment cores. Geo-Mar. Lett. **18:** 70-77.

Harr, M. E. 1962. Groundwater and Seepage. McGraw-Hill.

Hartl, K. 2006. Facies distribution and hydraulic conductivity of lagoonal sediments in a Holocene transgressive barrier island sequence, Indian River Lagoon, Florida. M.S. University of Florida.

Harvey, J. W., S. L. Krupa, and J. M. Krest. 2004. Ground Water Recharge and Discharge in the Central Everglades. Ground Water **42:** 1090-1102.

Horn, D. P. 2002. Beach groundwater dynamics. Geomorphology **48:** 121-146.

Huettel, M., W. Ziebis, S. Forster, and G. W. Luther. 1998. Advective transport affecting metal and nutrient distributions and interfacial fluxes in permeable sediments. Geochimica Et Cosmochimica Acta **62:** 613-631.

Hvorslev, M. J. 1951. Time Lag and Soil Permeability in Ground-Water Observations, p. 50. Waterways Experiment Station, U.S. Army Corp of Engineers.

Hyder, Z., J. J. Butler, C. D. Mcelwee, and W. Z. Liu. 1994. Slug Tests in Partially Penetrating Wells. Water Resources Research **30:** 2945-2957.

Li, L., D. A. Barry, F. Stagnitti, and J. Y. Parlange. 1999. Submarine groundwater discharge and associated chemical input to a coastal sea. Water Resources Research **35:** 3253-3259.

Mango, A. J., M. W. Schmeeckle, and D. J. Furbish. 2004. Tidally induced groundwater circulation in an unconfined coastal aquifer modeled with a Hele-Shaw cell. Geology **32:** 233-236.

Martin, J. B., J. E. Cable, C. Smith, M. Roy, and J. Cherrier. 2007. Magnitudes of submarine groundwater discharge from marine and terrestrial sources: Indian River Lagoon, Florida. Water Resources Research **43:** -.

Martin, J. B., J. E. Cable, P. W. Swarzenski, and M. K. Lindenberg. 2004. Enhanced submarine ground water discharge from mixing of pore water and estuarine water. Ground Water (special Ocean issue) **42:** 1001-1010.

Moore, W. S. 1996. Large groundwater inputs to coastal waters revealed by Ra-226 enrichments. Nature **380:** 612-614.

---. 1999. The subterranean estuary: a reaction zone of ground water and sea water. Marine Chemistry **65:** 111-125.

Morgan, K., and J. Jankowski. 2004. Saline groundwater seepage zones and their impact on soil and water resources in the Spicers Creek catchment, central west, New South Wales, Australia. Environmental Geology **46:** 273-285.

Nielsen, P. 1990. Tidal dynamics of the water table in beaches. Water Resources Research **26:** 2127-2134.

Panda, M. N., and L. W. Lake. 1994. Estimation of Single-Phase Permeability from Parameters of Particle-Size Distribution. Aapg Bulletin-American Association of Petroleum Geologists **78:** 1028-1039.

Robinson, C., L. Li, and D. A. Barry. 2007. Effect of tidal forcing on a subterranean estuary. Advances in Water Resources **30:** 851-865.

Shih, D. C. F., K. F. Chiou, C. D. Lee, and I. S. Wang. 1999. Spectral responses of water level in tidal river and groundwater. Hydrological Processes **13:** 889-911.

Shinn, E. A., C. D. Reich, and T. D. Hickey. 2002. Seepage meters and Bernoulli's revenge. Estuaries **25:** 126-132.

Simmons, J., G.M. 1992. Importance of submarine groundwater discharge (SGWD) and seawater cycling to material flux across sediment/water interfaces in marine environments. Marine Ecology Progress Series **84:** 173-184.

Smith, C. G., J. E. Cable, and J. B. Martin. 2008. Episodic high-intensity mixing events in a subterranean estuary: Effects of tropical cyclones. Limnology and Oceanography **53:** 666-674.

Smith, C. G., J. E. Cable, J. B. Martin, and M. Roy. in review. Evaluating the source and seasonality of submarine groundwater discharge using a Radon-222 pore water transport model. Earth and Planetary Science Letters.

Taniguchi, M., W. C. Burnett, J. E. Cable, and J. V. Turner. 2002. Investigation of submarine groundwater discharge. Hydrological processes **16:** 2115-2129.

Windom, H., and F. Niencheski. 2003. Biogeochemical processes in a freshwater-seawater mixing zone in permeable sediments along the coast of Southern Brazil. Marine Chemistry **83:** 121-130.

CHAPTER 3.

EPISODIC HIGH INTENSITY MIXING EVENTS IN A SUBTERRANEAN ESTUARY: EFFECTS OF TROPICAL CYCLONES[1]

Introduction

Fluid discharge from submarine aquifers and associated chemical loading to overlying surface water bodies have been the focus of a great deal of research over the last decade. The discharging fluid, collectively referred to as submarine groundwater discharge (SGD), is composed of terrestrially recharged groundwater and recirculated seawater. Within the aquifer, these two chemically contrasting fluids mix to form what is often referred to as the "subterranean estuary" (Moore 1999). A number of recent studies have investigated the role of the subterranean estuary on the biogeochemical cycling of metals, industrial or commercial groundwater contaminants, and macro- and micro-nutrients (e.g., Simmons 1992; Krest et al. 2000; Cable et al. 2002), thus providing the physical and chemical framework for these dynamic systems and their effects on chemical transport. Most studies are limited in temporal monitoring and many use synoptic data sets. Such measurement methods result in an incomplete understanding of how subterranean systems respond to perturbations (e.g., seasonal recharge, human consumption, storms, etc.).

Only a few studies have documented how SGD varies with changes in forcing mechanisms. Michael et al. (2005) noted a distinct seasonal pattern in SGD reflecting recharge of the surficial aquifer and changes in the position of the subterranean estuary in Waquoit Bay, MA. Extensive harmful algal blooms (HABs) in 2005 along the west-central Florida coast were blamed on the active 2004 Atlantic hurricane season, which dropped substantial rainfall on the

[1] Reprinted from Limnology and Oceanography **53**: 666-674. Copyright (2008) by the American Society of Limnology and Oceanography, Inc. Note: Minor changes were made to the presented chapter to conform to dissertation formatting requirements.

Tampa Bay region (Hu et al. 2006). These researchers hypothesized HABs were fed by large SGD-derived nitrogen fluxes driven to the coastal ocean by this precipitation and subsequent recharge. Along the North Carolina continental shelf, Moore and Wilson (2005) noted 1 to 2ºC temperature oscillations 4 m below seafloor following the passage of Hurricanes Dennis and Floyd in 1999. These temperature anomalies were attributed to enhanced pore water exchange between the permeable seafloor sediments and the ocean during the passage of large storm waves associated with these hurricanes. In this study, I investigate perturbations to the subterranean estuary associated with the passage of tropical cyclones and quantify how a subterranean estuary responds spatially and temporally to these episodic events.

Study Site

This study was conducted in Indian River Lagoon (IRL), a micro-tidal, back-barrier lagoon located in east-central Florida (Figure 3.1A). Astronomical tides decrease away from inlets, where amplitudes are ~10 to 15 cm, but winds can generate large water levels across the entire lagoon. Tidal amplitudes in this portion of the lagoon area are less than 2 cm, and non-tidal sea level variations are less than 30 cm (Smith 1993).

The hydrostratigraphy of the field site is associated with the Surficial aquifer because the Floridan aquifer is confined by the less conductive Hawthorne Group. The Surficial aquifer consists of interbedded and unconsolidated Pliocene to Holocene coquinas, sands, and clayey-silts. The hydraulically conductive regions of the aquifer, i.e. the sand and coquina portions, have hydraulic conductivities between 10 and 127 m d^{-1} (Toth 1988); hydraulic conductivities of silty and clayey units are estimated to be 0.01 to 0.1 m d^{-1} (Pandit and El-Khazen 1990). The shallow (< 2.5 m), nearshore sediments that compose the upper portion of the Surficial aquifer have average horizontal and vertical hydraulic conductivities of 8.3 and 0.20 m d^{-1}, respectively.

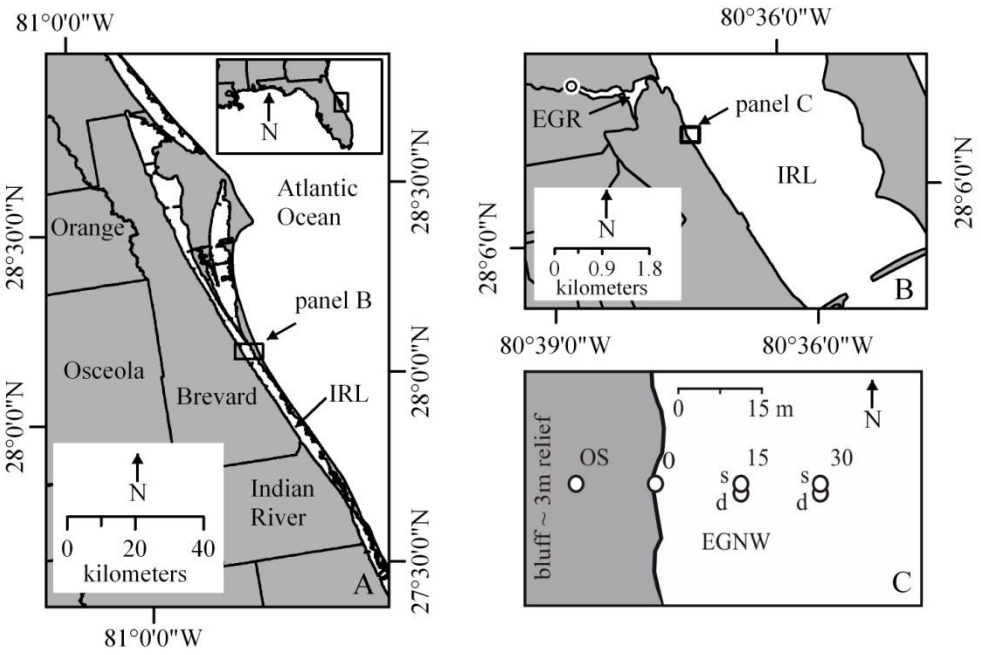

Figure 3.1. (A) Map of east-central Florida showing the location of the field site within the Indian River Lagoon, (B) relative to Eau Gallie River and USGS gaging station 02449007, (C) and the piezometer transect; labels above the piezometers (i.e., OS, 0, 5, 15, and 30) denote their position relative to the shoreline in meters. At 15 and 30 m offshore, two piezometers are installed at each location; the shallow piezometer (s) is screened at 1.5 m and the deep piezometer (d) is screened at 2.5 m.

Previous studies have shown that SGD may be an important component of the overall hydrologic budget of Indian River Lagoon (Cable et al., 2004; Martin et al., 2004; 2006); however, the significance is unclear because of large variations in discharge estimates and in sources of SGD (Martin et al., 2007). I consider here the concept of "fair-weather" versus "storm" conditions in the examination of SGD and the subterranean estuary. I define "fair-weather" as those conditions either averaged over an extended period of time (months to years) or based on data of limited temporal resolution.

Pandit and El-Khazen (1990) used a finite element groundwater flow model to estimate specific discharge of terrestrially-sourced groundwater that averaged 0.23 cm d^{-1} along the length of the lagoon. Martin et al. (2004; 2006) measured time-series of pore water temperature and Cl^-

concentrations in the north-central lagoon and reported offshore SGD rates as high as 150 cm d^{-1}; however, the fluid was determined to be recirculated lagoon water with no terrestrially-sourced groundwater. Nevertheless, both terrestrial groundwater and recirculated lagoon water are important to the formation and maintenance of subterranean estuaries. Along a pore water transect, 10 m north of the piezometer transect used in this study, Martin et al. (2007) used Cl^- concentrations to map the subterranean estuary in fair-weather conditions. A conceptual representation of the subterranean estuary during fair-weather conditions was derived from Martin et al.'s (2007) study (Figure 3.2A). Based on seepage meters, Cl^- concentrations, and Glover's analytical hydrostatic model, they determined freshwater inputs were restricted to about 22 m offshore. Within this 22 m wide zone, fresh water inputs were judged to decrease linearly with a net flux between 0.02 to 0.9 m^3 d^{-1} m^{-1} of shoreline. Approximately 250 m offshore, little to no terrestrial groundwater input was also judged to occur and recirculated lagoon water and/or saline groundwater are the dominant sources of SGD (Martin et al. 2007). These variations in fair-weather SGD rates can largely be attributed to the measurement technique and its ability to quantify the source of the fluid (i.e., terrestrial versus marine SGD; e.g., Cable et al. 2004).

2005 Atlantic Hurricane Season

The 2005 Atlantic hurricane season was one of the most active on record; a total of 27 named (and one unnamed) storms formed in the Atlantic Ocean. Of these storms, Hurricane Katrina (25 Aug), Tropical Storm Tammy (04-05 Oct) and Hurricane Wilma (24 Oct) passed directly over the Florida Peninsula; Hurricane Rita (20-21 Sep) and Hurricane Ophelia (08-09 Sep) also passed close to east-central Florida. Of these five storms, Tropical Storm Tammy and Hurricane Wilma had the most influence on east-central Florida and specifically the Indian River Lagoon. Tropical Storm Tammy moved north in the Atlantic Ocean paralleling the Florida coast

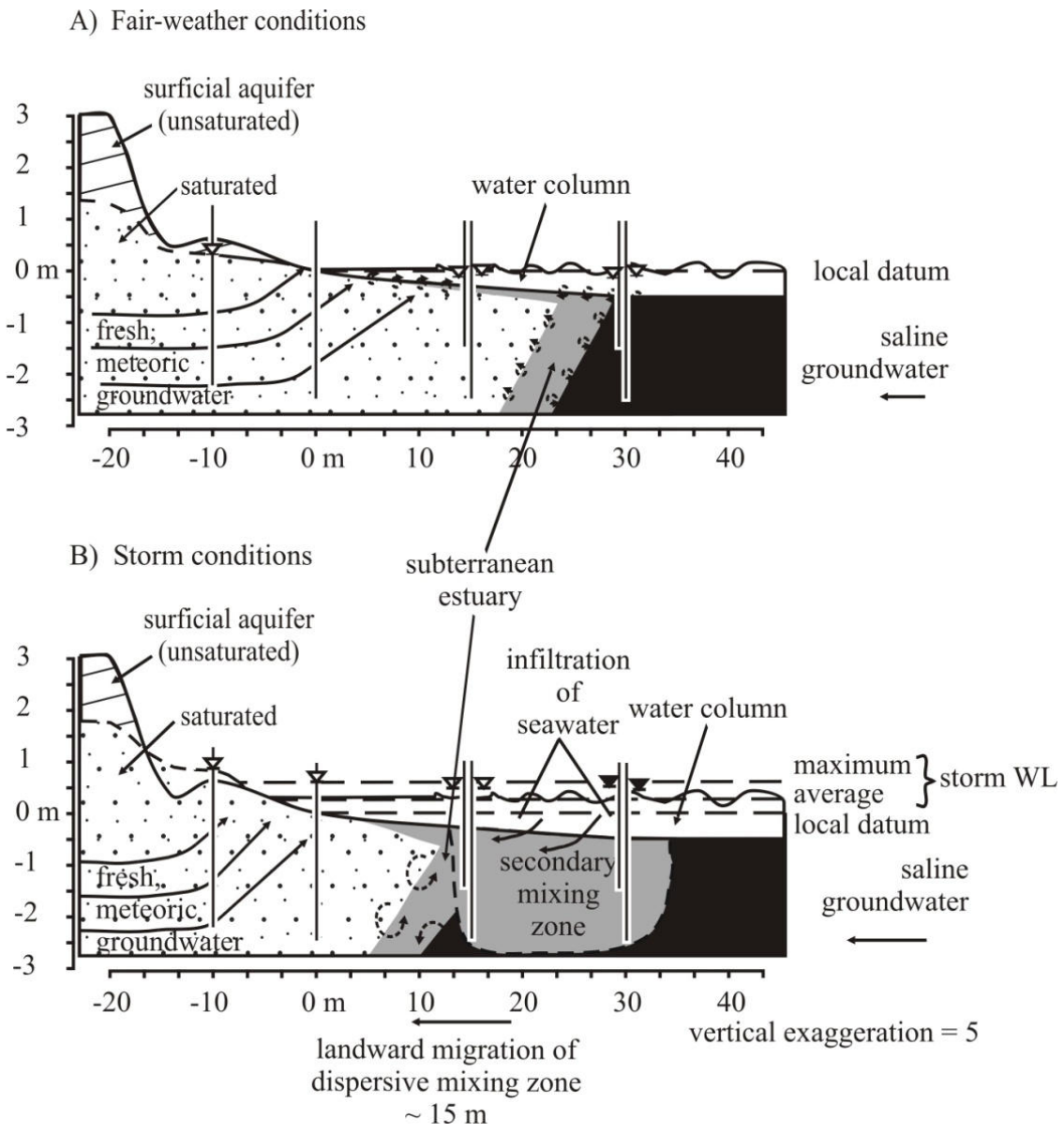

Figure 3.2. Conceptual model of the subterranean estuary showing the processes that contribute to its position during (A) fair-weather and (B) storm conditions. During fair-weather conditions, the subterranean estuary is located between 15 and 30 m offshore. During storm conditions, storm surge and waves cause the rapid infiltration of seawater into the upper portion of the aquifer, the dispersive mixing zone migrates landward, and secondary mixing zone extends to depths of 2.5 m. Flow lines are shown as solid lines with arrow heads, mixing lines are shown with dashed lines, and heads in the piezometers relative to the local datuam are shown as underlined, inverted solid triangles next to the respective piezometer.

and slowly passed over the field site with an average and maximum wind velocity of 10 and 18 m s^{-1}, respectively, on 04 and 05 October. During this time, the open ocean side of the barrier island system experienced a 25 to 50 cm storm surge (Stewart 2006) while the average and maximum increase in Eau Gallie River stage was 7 and 10 cm, respectively. Barometric setup in the lagoon and ocean would be of similar magnitude, while fetch limitation of the lagoon would prevent wind and wave setup comparable to the ocean (Figure 3.1). In contrast, Hurricane Wilma moved west out of the Gulf of Mexico, across the Florida peninsula, and into the Atlantic Ocean. The eye wall passed approximately 180 km south of the field site (near Jupiter, FL) as a category two storm with maximum winds of 48.8 m s^{-1}; official observations from Melbourne National Weather Service Station 5 km southeast of the current field site documented primarily westerly winds with an average wind velocity of 25 m s^{-1} and gusts of 33.4 m s^{-1} (Pasch et al. 2006). No official reports of storm surge during Hurricane Wilma exist for the ocean or lagoon proximal to my site; Eau Gallie River stage reached a maximum of 55 cm and averaged 20 cm.

Methods

Absolute pressure (water plus atmospheric) and temperature were continuously recorded in seven shallow piezometers from 20-Jul-05 to 14-Mar-06 along a shore-normal transect extending from 10 m onshore to 30 m offshore in the lagoon (Figure 3.1C). These measurements were collected along this east-west transect at 10 m onshore (EGNW-OS), at the shoreline (EGNW-0), 15 m offshore (EGNW-15), and 30 m offshore (EGNW-30; Figure 3.1C). All offshore piezometers were installed manually using a fence-post driver and consisted of 3.8 cm (1.5 in) outer diameter schedule 40 or 80 PVC tubing coupled with 15 to 20 cm long, 2.54 mm slotted PVC screening. The onshore piezometer, of the same construction type as the offshore piezometers, was installed inside of 10.2 cm (4 in) diameter PVC casing emplaced using a manual auger. Sensors were in contact with the upper 4 to 6 cm of screening. Piezometers were

surveyed to a common (local) datum (average lagoon water level) on 10-Feb-05; all head measurements are referenced to this datum. At 15 and 30 m offshore, two piezometers, separated laterally by 0.3 m, were installed to depths of 1.5 m (EGNW-15s and -30s) and 2.5 m (EGNW-15d and -30d) below the local datum. The piezometer at the shoreline (EGNW-0d) and onshore (EGN-OS) were installed to a depth of 2.5 and 2.25 m, respectively, below the local datum. All piezometers were installed with the top of the casing (TOC) approximately 1 m (range of 0.98 to 1.02 m) above the local datum and with a vent (1 mm wide, 1 cm long) approximately 2 cm below the TOC. The four offshore piezometers (EGNW-15s, EGNW-15d, EGNW-30s, and EGNW-30d) were also equipped with conductivity probes. All measurements were recorded at 20-minute intervals for the duration of the eight-month experiment. Absolute water pressure was corrected for barometric pressure to obtain groundwater pressure head; a constant aquifer barometric efficiency of 95 % was used in the correction. Stage data from Eau Gallie River (USGS Sta. 02449007), located less than 1 km north of the transect and 2.5 km upstream, was used as the best surrogate for lagoon water level. For reference, Eau Gallie River stage averaged 101.8 cm above NGVD29 datum on 10-Feb-05. I assume the difference between the Eau Gallie River stage and the NGVD29 datum on this date can be used to extrapolate changes in lagoon water level. Given the short distance between these sites, the likely error on this assumption is about 10%. Salinity and water density were computed from water pressure, conductivity, and temperature using SEAWATER 3.0 (Morgan 1994). Pressure head was corrected for density variations and normalized to freshwater (0 salinity) using the following equation:

$$h_{feq} = \left(\frac{\rho_s}{\rho_f}\right) h_s \tag{3.1}$$

where h_{feq} is the freshwater equivalent pressure head, ρ_s and ρ_f are the density of measured and fresh water, respectively, and h_s is measured pressure head.

The salinity records obtained from the offshore piezometers are the main data sources of episodic turnover or flushing of the subterranean estuary. Although salinity could be affected by contamination of the piezometers by overtopping from storm surge or waves, several physical observations suggest lagoon water did not contaminate the piezometers. Each peizometer was sealed with water-tight PVC caps, and thus contamination would have to occur either as water leakage along the skin of the piezometer (i.e., negative skin effect) or through the vent located 2 cm below the top of the piezometer. A significant wave height of 20 cm was computed for Tropical Storm Tammy using the CERC (1984) shallow water wave prediction model and input values of 3000 m, 1 m, and 10 m s^{-1}, for fetch, water depth, and average wind velocity, respectively. The increase in lagoon water level rise due to storm surge (10 cm) and waves (20 cm) would be insufficient to overtop the piezometer. During Hurricane Wilma, Eau Gallie River stage increased to a maximum of 55 cm but showed a strong correlation with precipitation, suggesting runoff and storm surge augmented the water levels. Thus, lagoon water level likely increased less than 55 cm during this storm. Using an average wind velocity of 25 m s^{-1}, and fetch and water depth from above, the predicted significant wave height is 40 cm, indicating lagoon water also would not have flowed into the piezometer during Hurricane Wilma.

Results

Spatial and Temporal Variations in Head

Total head in the piezometers measured from Jul-05 to Mar-06 reflects Florida's sub-tropical wet and dry seasonal climate (Figure 3.3A). All piezometers exhibit elevated head from 24-Aug-05 to 25-Nov-05, coinciding with the end of the wet season and the fall hurricane season. Average density-corrected, total hydraulic heads during this period for EGNW-15s, -15d, -30s, and -30d

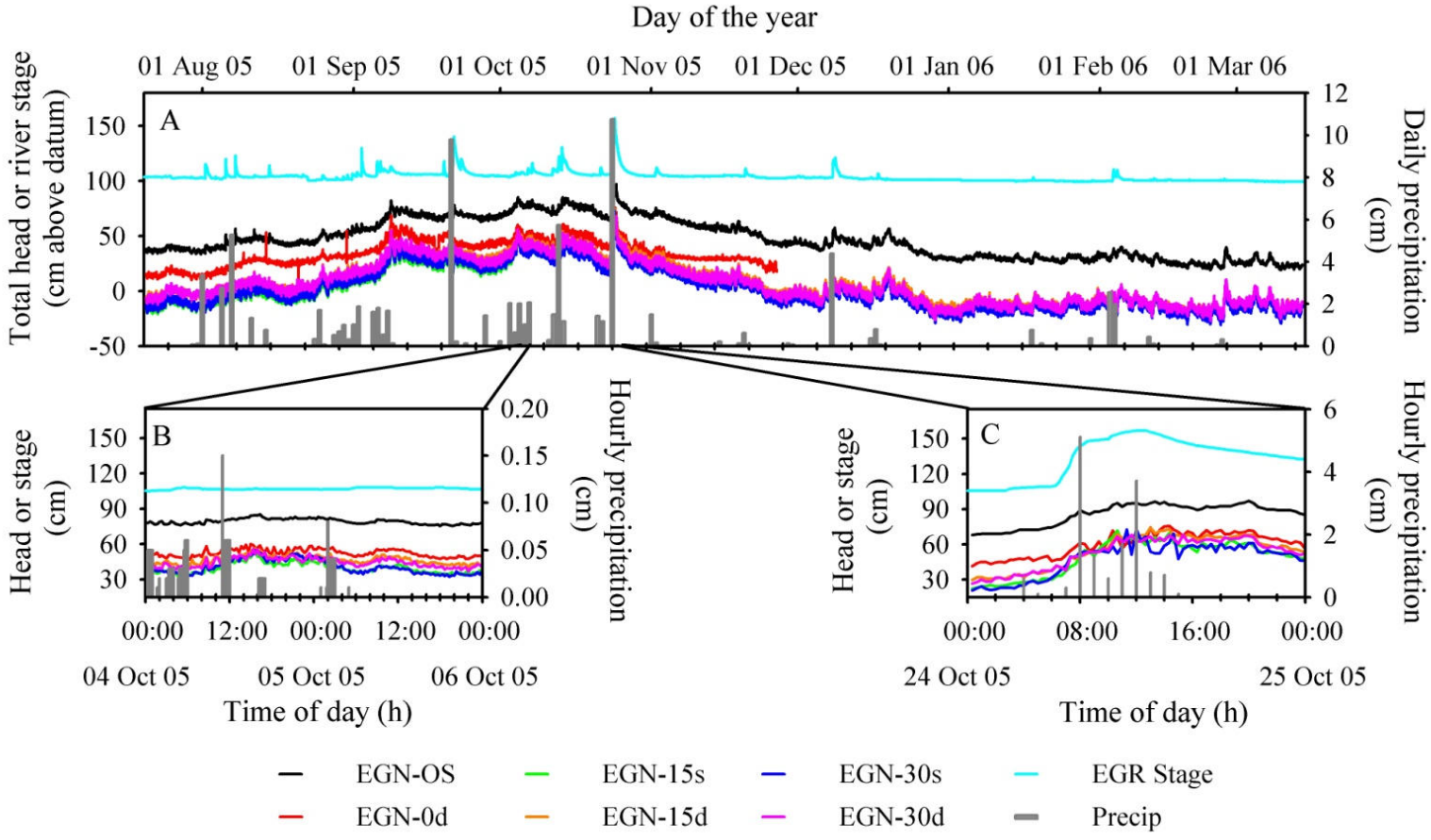

Figure 3.3. (A) Long-term time-series of freshwater equivalent head in piezometers recorded from 20-Jul-05 to 14-Mar-06. The piezometer name EGN-XXx represents the site name Eau Gallie North, XX the position with respect to the datum (OS = onshore, 0 = shoreline, 15 = 15 m offshore, and 30 = 30 m offshore), and x depth (s = shallow, 1.5 m; d = deep, 2.5 m). Water level and precipitation collected during (B) Tropical Storm Tammy and (C) Hurricane Wilma.

were 20.2±12.6, 28.4±12.7, 20.7±12.7, and 26.5±12.8 cm, respectively; heads in EGNW-OS and EGNW-0d averaged 65.4±9.9 and 39.7±9.9 cm, respectively (Table 3.1). Eau Gallie River stage averaged 107.4 cm during the same period.

Table 3.1. Average water levels (cm) observed in the piezometers and the Eau Gallie River. Maximum water levels during tropical cyclones are given in parentheses.

Sampling location	Dry season	Wet season	Tropical storm Tammy	Hurricane Wilma
Eau Gallie River	100.7	107.4	108.6 (112)	121.4 (156.9)
Indian River Lagoon Water Level*	-1.1	5.6	6.8 (10.2)	19.6 (55.1)
EGN-OS	32.2	65.4	79.3 (85.3)	83.4 (97.1)
EGN-0d	-	39.7	52.5 (60.2)	55.9 (75.8)
EGN-15s	-11.4	20.2	48.3 (53.2)	52.7 (72.0)
EGN-15d	-7.8	28.4	48.2 (56.2)	47.6 (74.2)
EGN-30s	-13.4	20.7	50.1 (54.9)	54.6 (73.0)
EGN-30d	-9.2	26.5	45.1 (55.9)	49.1 (68.1)

*Lagoon water level is estimated as the difference between reported Eau River Stage and river stage on 10-Feb-05 (101.8 cm).

Tropical cyclones during this period delivered 77 cm of precipitation to the region. The maximum head measurement in each piezometer coincides with the passage of Hurricane Wilma on 24-Oct-05, followed by a long recession period terminating in late December. Total head observed from 10-Dec-05 to 14-Mar-06 was relatively constant. The onshore piezometric head averaged 32.2±7.6 cm above the local datum while EGNW-15s, -15d, -30s, and -30d averaged 11.4±6.7, 7.8±7.5, 13.4±7.2, and 9.2±7.2 cm below the local datum, respectively. Eau Gallie River stage averaged 100.7 cm above the NGVD29 datum. This period of low head coincides with the onset of the dry season in the region; total precipitation during this period was 7 cm.

Based on long-term head averages, hydraulic gradients direct the flow of groundwater seaward and vertically upward along the piezometer transect during both wet and dry seasons. Analysis of hourly resolved head measurements in the piezometers show groundwater responded quickly to external forces such as the passage of frontal systems and/or tropical cyclones as indicated by precipitation and changes in river stage. Total head and river stage peaked on at least eight separate occasions during this period (Figure 3.3A). Two of the most notable changes in total head occurred during the passage of Tropical Storm Tammy (04-05 Oct-05) and Hurricane Wilma (24-Oct-05). During Tropical Storm Tammy, hydraulic heads in the onshore and shoreline piezometers increased 15 cm above the wet season average (Figure 3.3B), thus maintaining the offshore directed hydraulic gradient between these two piezometer. Heads observed in EGNW-15s, -15d, -30s, and -30d averaged 48.3±2.9, 48.2±2.8, 50.1±2.8, and 45.1±2.9 cm, respectively, suggesting a reversal in shallow to deep head gradients when compared to the long-term averages. Similarly, during Hurricane Wilma, heads in the onshore and shoreline piezometers increased on average 20 cm and a maximum of 25 cm above the wet season average . The uniform head increase suggests that the offshore-directed hydraulic gradient was maintained. During Hurricane Wilma, heads in the offshore piezometers demonstrated a similar reversal pattern as observed during Tropical Storm Tammy; the heads in EGNW-15s, -15d, -30s, and -30d averaged 52.7±3.5, 47.6±2.4, 54.6±3.6, and 49.1±2.5 cm, respectively. Reversals in the offshore head gradients indicate water percolated into the aquifer and flowed landward during both Tropical Storm Tammy and Hurricane Wilma.

Spatial and Temporal Variations in Pore Water Salinity

During the period of storm-related head changes (early August to late November 2005), only two significant changes in salinity were observed at or below the deep piezometer (2.5 m

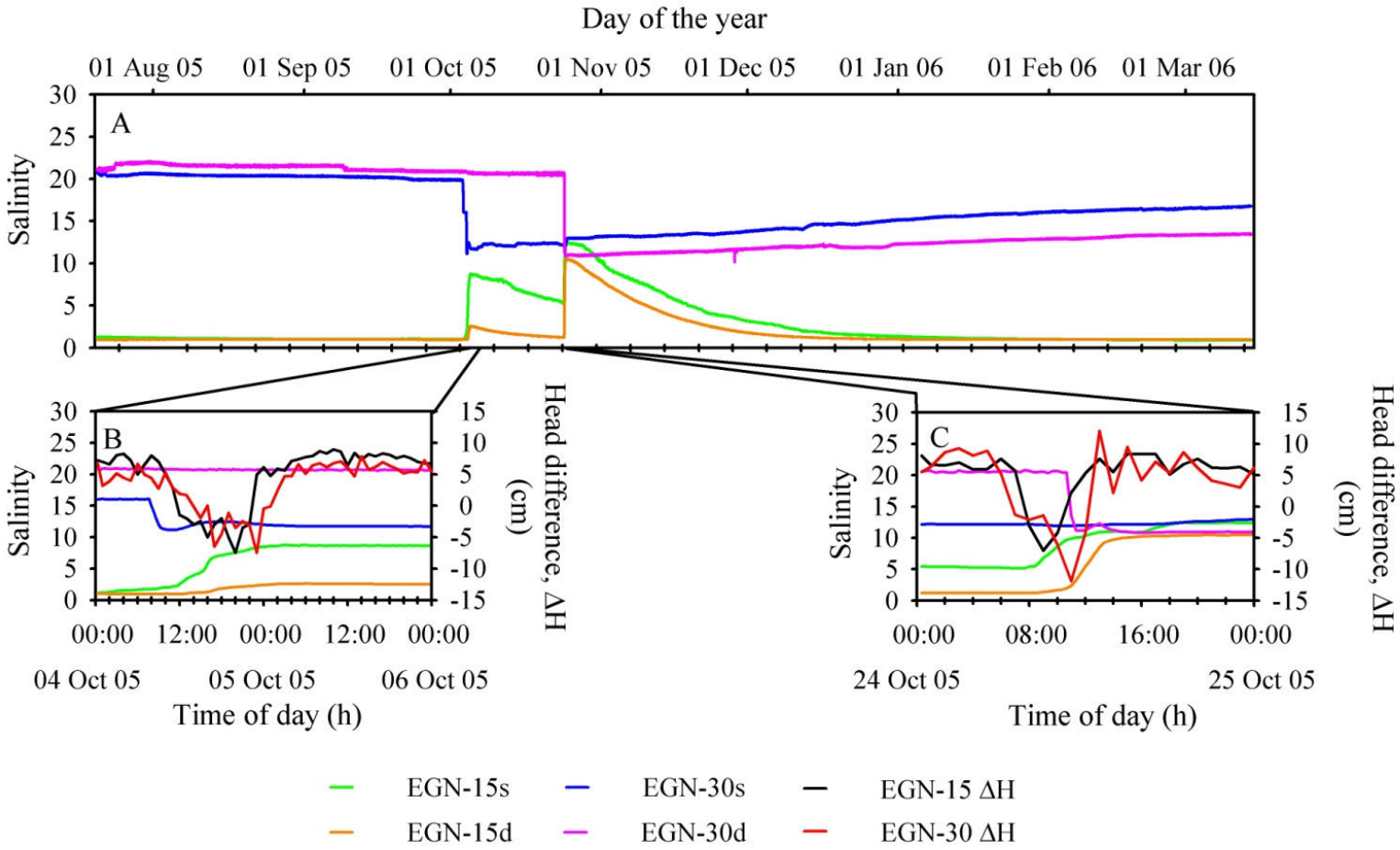

Figure 3.4. (A) Long-term time-series of salinity in the piezometers recorded from 20-Jul-05 to 14-Mar-06. The piezometer name EGN-XXx represents the site name Eau Gallie North, XX the position with respect to the datum (OS = onshore, 0 = shoreline, 15 = 15 m offshore, and 30 = 30 m offshore), and x depth (s = shallow, 1.5 m; d = deep, 2.5 m). Salinity and head differences between shallow and deep piezometers collected during (B) Tropical Storm Tammy and (C) Hurricane Wilma.

below the local datum); they occurred during the passage of Tropical Storm Tammy and Hurricane Wilma (Figure 3.4). As Tropical Storm Tammy passed over the field site, the salinity in the shallow piezometer 30 m offshore decreased by 6 to 7, while the shallow and deep piezometers at 15 m offshore increased in salinity by 7 and 2.5, respectively (Figure 3.4B). The subsequent pore water salinity recession back to pre-storm values was interrupted by the passage of Hurricane Wilma. Hurricane Wilma caused a similar perturbation in salinity, but more intense and deeper, in which all piezometer salinities converged to about 10 to 12 over a period of approximately six hours (Figure 3.4C). Breakthrough of the salinity perturbation was observed first in the shallow piezometers; three to six hours later the salinity perturbation reached the deeper piezometer at 15 m offshore. This result suggests that the effective transport rate (advective and dispersive) of dissolved salts, not fluid, was on the order of 4 to 8 m d^{-1}.

Discussion

Seasonal Submarine Groundwater Discharge and Tropical Cyclones

The long-term effect that tropical cyclones have on the magnitude of groundwater discharge can be examined with head measurements made at the onshore piezometer and using Glover's analytical solution to the seawater intrusion problem (Glover 1959; Cheng and Ouazar 1999). Glover's solution to the seawater intrusion problem is solved assuming steady-state flow; the passage of tropical cyclones are highly transient in nature, therefore, I choose to present only seasonal variations in groundwater discharge and discuss the role tropical cyclones have on this seasonal pattern. Using Glover's assumptions, the total freshwater discharge from the outflow face (seepage face) is approximated by

$$Q = \frac{\Delta h_f{}^2 K' \rho_f}{2(\rho_s - \rho_f)x} \tag{3.2}$$

where Q is total discharge per unit length of shoreline ($m^3\ d^{-1}\ m^{-1}$), Δh_f is the difference (m) between the head in the piezometer and the lagoon water level, x is the horizontal distance of the piezometer from the shoreline, K' is the effective hydraulic conductivity (1.3 m d^{-1}), and ρ_f (997 kg m^{-3}) and ρ_s (1014 kg m^{-3}) are the density of the fresh and saline groundwater end-members, respectively. By using the head difference between EGNW-OS and the lagoon, I have assumed that the head measurement from the piezometer is reflective of the water-table elevation at this point and thus vertical gradients at 10 m onshore are minor. This creates a vertical plane where total fresh groundwater discharge can be estimated. Conservation of volume requires the discharge across this vertical plane to be equal to the discharge exiting the seepage face.

During the wet season, the fair-weather onshore head averaged 65.4 cm above the local datum and the lagoon water level (estimated from change in Eau Gallie River stage; Table 3.1) increased 5.6 cm, resulting in a total freshwater discharge of 1.3 $m^3\ d^{-1}\ m^{-1}$ of shoreline. This estimate is relatively consistent with seepage meter estimates (0.9 $m^3\ d^{-1}\ m^{-1}$) made during the month of September 2005 (Martin et al. 2007). Using the average dry season head of 32.2 cm and estimated lagoon water level change of -1.1 cm (Table 3.1), computed total freshwater discharge is approximately 0.4 $m^3\ d^{-1}\ m^{-1}$ of shoreline. These discharge estimates suggest that fresh groundwater discharge from the Surficial aquifer varies by a factor 3.25 between the two seasons. These discharge variations are primarily controlled by precipitation and subsequently onshore recharge of the surficial aquifer. Based on the precipitation records (Figure 3.3), approximately 30% of the total (wet) seasonal precipitation occurred during the passage of Tropical Storm Tammy and Hurricane Wilma.

During the tropical cyclones, higher heads were observed in the onshore piezometer. Estimated values of h_f during Tropical Storm Tammy and Hurricane Wilma were 72.5 and 63.8

cm, respectively (Table 3.1), which based on the Glover model, suggests that discharge increased during the storms. However, this seems unlikely given the offshore head reversals and the salinity perturbations. I interpret these higher heads in the onshore piezometer as representing the water-table response to higher lagoon water levels (analogous to tidal effects), the infiltration of lagoon water into the aquifer, and the displacement of the subterranean estuary landward. Following the storms, the pressure gradients would relax and there would be a temporary increase in discharge of fresh groundwater and infiltrated lagoon water from the seepage face. Such effects have been observed in water-table aquifers at diurnal- and seasonal-scale (Mango et al. 2004; Michael et al. 2005) and thus are likely to occur at scales that are more episodic. Both the increase in precipitation during the tropical cyclones and the hypothesized water-table rebound would enhance groundwater discharge following the passage of tropical cyclones.

Mechanisms Driving Salinity Perturbations

The observed salinity perturbations are in response to several complex, and potentially interactive physical processes including: (1) pumping of lagoon water into the sediments by waves and storm surge; and (2) landward flow of saline groundwater due to barometric- and wind-setup in the lagoon and/or the ocean (Figure 3.2B). Given the complexity of the system, I attempt only to provide reasonable, qualitative assessments of processes that could have contributed to these salinity perturbations.

Locally, infiltration of seawater into the fresh water portion of the subterranean estuary can occur from wave- and tidal-induced pressure gradients in the nearshore and wave run-up or storm surging onto a sloping beach. As waves pass into shallow water, the wave orbitals interact with the seafloor, become oblong, and create pressure gradients between the surface and pore waters. Oscillating pressure gradients associated with waves have been shown experimentally to

enhance pore water and solute exchange by advective (Shum 1992; Precht and Huettel 2003) and diffusive/dispersive mechanisms (Webster 2003; Webster and Taylor, 1992). The effective flushing depths for such processes depend on sea-bed morphology (e.g., ripples), sediment permeability, and wave characteristics (i.e., amplitude, frequency, and length). The role of advection, due solely to pressure gradients between the pore and surface waters, can be considered assuming a maximum water level of 0.9 m (i.e., significant wave height plus storm surge) and average hydraulic head observed in the shallow offshore piezometers (~ 0.5 m). The maximum Darcy (advective) flux into the aquifer would be 0.4 m d^{-1}, which is 1 to 1.3 orders of magnitude less than the effective transport rate suggested by the lag of salinity between the shallow and deep piezometer. As suggested above, the effective rate includes both advective and dispersive transport of dissolved salts; the estimate based on head gradients reflects only advective flux and ignores dispersion. It is reasonable to suggest that dispersion of the dissolved salts, along with the imposed advective flow, contributed to the salinity perturbations observed during the storms; however, it is unlikely that this is the sole process.

Wave run-up and tidal or storm surging are other local mechanisms capable of delivering saline water into the freshwater portion of the aquifer (Nielsen 1990; Hegge and Masselink 1991; Robinson et al. 2006). The effects of wave run-up cannot be quantified with these data; however, the effects of tidal surging can be considered qualitatively. In a numerical experiment, Robinson et al. (2007) showed that tidal ranges of 1 to 2 m imposed on a beach face forced surface water into the aquifer and recirculated it 5 to 15 m below the sediment-water interface. This increase in sea level created a secondary mixing zone that occurred landward of the traditional dispersive mixing zone (Robinson et al. 2007). Unfortunately, Robinson et al. (2007) do not provide the time-scale for establishing these secondary mixing zones. Data do not reflect

the development of a secondary mixing zone during the tropical cyclones. It is hypothesized that a secondary mixing zone, extending to a depth less than 1 m, was established prior to the observed salinity perturbations as smaller frontal systems and tropical cyclones passed near the region. It was during Tropical Storm Tammy and Hurricane Wilma (where lagoon water level rose between 0.2 and 0.5 m plus wave-setup) that this secondary mixing zone expanded across the screening of the piezometers (e.g. Figure 3.4), but the distribution of the piezometers does not provide sufficient data to refute or support this hypothesis.

Increases in lagoon water level create landward-directed pressure gradients between the aquifer and the lagoon, which drives saline groundwater landward (Cooper Jr. et al. 1964; Nielsen 1990; Urish and Mckenna 2004). During tropical cyclones, sea level increases offshore as a result of barometric, wind, and wave set-up; the water-table responds with an onshore head increase (as observed in EGNW-OS; Figure 3.3B). Urish and McKenna (2004) provide a conceptual model describing this phenomenon. They suggest that during flooding tides and at high tides, groundwater flow is directed onshore and surface water infiltrates the aquifer. This seawater intrusion shifts the saltwater-freshwater interface and dispersive mixing zone landward during the elevated tide (Figure 3.3B). Higher sea level also increases the rate of recirculation of seawater in the main dispersive mixing zone (Mango et al. 2004; Prieto and Destouni 2005; Robinson et al. 2006). Field data, showing both horizontal and vertical head reversals, suggest that the landward migration of, and the enhanced mixing along, the subterranean estuary played an important role in the salinity perturbations observed during the 2005 hurricane season. Increases in ocean sea level should invoke the same general response as increases in the lagoon water level and should also be important for episodic mixing of the subterranean estuary. In contrast with localized changes in lagoon water levels, ocean sea level rise imposes a sustained

hydraulic gradient averaged over a much larger area. As observed along the mainland shoreline of Indian River Lagoon, its effects to the subterranean estuary would be less significant than the local increase in lagoon water level. As a result, several mechanisms appear to influence episodic turnover of the subterranean estuary observed during the tropical cyclones without any one process dominating.

Response Time of Subterranean Estuary to Storm Effects

The salinity perturbations permit us to assess the response time of subterranean estuaries as they return to pre-storm conditions. Based on the salinity response in the piezometers following Hurricane Wilma, the patterns are consistently different at 15 and 30 m offshore. The piezometers 15 m offshore demonstrate an exponential decrease in salinity with respect to time, similar to the response of a river following a peak in stage height. The recession curve suggests advective and dispersive inputs of lower salinity water slowly replace the water proximal to the piezometer screen. The salinity in the deep (2.5 m) and shallow (1.5 m) piezometer 15 m offshore returns to pre-storm conditions on a time-scale of 80 and 130 days, respectively. The longer replacement time of the shallower groundwater reflects the vertical upward flow of lower salinity groundwater. Also, the difference between these replacement times (50 days) suggests that groundwater inputs are on the order of 2 cm d^{-1}, similar to rates reported by Martin et al. (2007). In contrast, the salinity in the piezometers located 30 m offshore shows a linear response to the perturbation with a 210 day projected recovery. In this area, fresh terrestrially derived groundwater reaches approximately 22 m offshore (Martin et al. 2007). These results suggest a slow, more diffusive process controls changes in salinity beyond the seaward edge of the seepage face. Thus, the re-establishment of the "fair-weather" subterranean estuary strongly depends on the post-storm distribution of contaminated water masses (i.e. infiltrated lagoon water or

landward migrated saline groundwater), the influx of fresh groundwater into this region of the aquifer (i.e. recharge dynamics), and the breakdown of the secondary mixing zone, if present.

Conclusions

Subterranean estuaries are noted as highly geochemically reactive zones within aquifers (Moore 1999), representing sources of alkaline metals such as Ra^{2+} and Ba^{2+} (Moore 1996; Shaw et al. 1998) while acting as a sink for dissolved U^{6+}, Fe^{2+}, Mn^{2+}, (Charette and Sholkovitz 2006) and NO_3^- (Addy et al. 2005). Chemical transformations, namely cation exchange and redox reactions, within the subterranean estuary are driven by contrasting geochemistry between the surface water, fresh groundwater, and saline groundwater. To date, published data of the biogeochemical framework of subterranean estuaries originate from a single or temporally restricted data sets, limiting the general understanding of the dynamic nature of these systems. The episodic turnover of the subterranean estuary observed here would entail the infiltration of oxygen -rich seawater to depths much greater than during fair-weather conditions, greatly affecting the redox framework. An adjustment to the redox framework of the subterranean estuary could also affect the geochemistry of the overlying lagoon. With deeper penetration of oxygen into the sediments, metals and other constituents could be released by the dissolution of metal sulfides and/or by the oxidation of organic matter (metals absorbed to the organic matter). Likewise, the intrusion of saline water in zones previously occupied by freshwater would tend to liberate those constituents or ions favorable for exchange with Na or Ca; therefore providing a source of these constituents to the overlying lagoon. Thus, it is important to evaluate the context of the (bio)geochemical framework of these reactive subsurface estuaries at a variety of temporal scales.

Shallow mixing (tens to hundreds of centimeters) in a subterranean estuary is strongly influenced by episodic, high intensity events such as tropical storm systems. Other studies have documented coastal aquifer systems response to tides, waves, and seasonal forces; the data indicate these systems respond with time scales of 3 to 4 months to episodic perturbations such as hurricanes. The response time is dependent on the flow regime and source water entering the affected areas. In areas with advective freshwater inputs (e.g. from piezometers 15 m offshore), the response time is much shorter than areas where diffusive saltwater mixing controls the response (sampled at piezometers 30 m offshore). Furthermore, these time scale estimates are from different magnitude storms, Tropical Storm Tammy and Hurricane Wilma, in October 2005. Larger hurricanes may have greater effects that endure for longer periods of time. The replacement of pre-storm pore fluids, either by enhanced discharge along the seepage face or by increases in inland head, during these events could greatly influence the biogeochemical setting of the subterranean estuary as well as the overlying water body by shifting redox conditions in the wider dispersive mixing zone, greater short-term discharge potential of groundwater derived dissolved constituents, or changes in pore fluid residence time within the seepage face and along the mixing zone-seepage face front.

References

Addy, K., A. Gold, B. Nowicki, J. Mckenna, M. Stolt, and P. Groffman. 2005. Denitrification capacity in a subterranean estuary below a Rhode Island fringing salt marsh. Estuaries **28:** 896-908.

Cable, J. E., D. R. Corbett, and M. M. Walsh. 2002. Phosphate uptake in coastal limestone aquifers: a fresh look at wastewater management. Limnology and Oceanography Bulletin **11**: 29-32.

Cable, J. E., J. B. Martin, P. W. Swarzenski, M. K. Lindenberg, and J. Steward. 2004. Advection Within Shallow Pore Waters of a Coastal Lagoon, Florida. Ground Water **42:** 1011-1020.

Charette, M. A., and E. R. Sholkovitz. 2006. Trace element cycling in a subterranean estuary: Part 2. Geochemistry of the pore water. Geochimica et Cosmochimica Acta **70:** 811-826.

Cheng, A. H.-D., and D. Ouazar. 1999. Analytical Solutions, p. 163-191. *In* J. Bear, A. H.-D. Cheng, S. Sorek, D. Ouazar and I. Herrera [eds.], Seawater Intrusion in Coastal Aquifers - Concepts, Methods and Practices. Theory and Applications of Transport in Porous Media. Kluwer Academic Publishers.

Cooper Jr., H. H., F. A. Kohout, H. R. Henry, and R. E. Glover. 1964. Sea Water in Coastal Aquifers. United States Geological Survey. WSP 1613-C. 84 pp.

Glover, R. E. 1959. The pattern of fresh-water flow in a coastal aquifer. Journal of Geophysical Research **64**: 457-459.

Hegge, B. J., and G. Masselink. 1991. Groundwater-Table Responses to Wave Run-up – an Experimental-Study from Western Australia. J. Coastal Res 7: 623-634.

Hu, C. M., F. E. Muller-Karger, and P. W. Swarzenski. 2006. Hurricanes, submarine groundwater discharge, and Florida's red tides. Geophysical Research Letters **33**, L11601, doi:10.1029/2005GL025449.

Krest, J. M., W. S. Moore, L. R. Gardner, and J. T. Morris. 2000. Marsh nutrient export supplied by groundwater discharge: Evidence from radium measurements. Global Biogeochemical Cycles **14:** 167-176.

Mango, A. J., M. W. Schmeeckle, and D. J. Furbish. 2004. Tidally induced groundwater circulation in an unconfined coastal aquifer modeled with a Hele-Shaw cell. Geology **32:** 233-236.

Martin, J. B., J. E. Cable, C. G. Smith, M. Roy, and J. Cherrier. 2007. Magnitudes of submarine groundwater discharge from marine and terrestrial sources: Indian River Lagoon, Florida. Water Resources Research, **43**, W05440, doi:10.1029/2006WR005266.

Martin, J. B., J. E. Cable, J. Jaeger, K. Hartl, and C. G. Smith. 2006. Thermal and chemical evidence for rapid water exchange across the sediment-water interface by bioirrigation in the Indian River Lagoon, Florida. Limnology and Oceanography **51:** 1332-1341.

Martin, J. B., J. E. Cable, P. W. Swarzenski, and M. K. Lindenberg. 2004. Enhanced submarine ground water discharge from mixing of pore water and estuarine water. Ground Water (special Ocean issue) **42:** 1001-1010.

Michael, H. A., A. E. Mulligan, and C. F. Harvey. 2005. Seasonal oscillations in water exchange between aquifers and the coastal ocean. Nature **436:** 1145-1148.

Moore, W. S. 1996. Large groundwater inputs to coastal waters revealed by Ra-226 enrichments. Nature **380:** 612-614.

---. 1999. The subterranean estuary: a reaction zone of ground water and sea water. Marine Chemistry **65:** 111-125.

Moore, W. S., and A. M. Wilson. 2005. Advective flow through the upper continental shelf driven by storms, buoyancy, and submarine groundwater discharge. Earth and Planetary Science Letters **235:** 564-576.

Morgan, P. P. 1994. SEAWATER: A Library of MATLAB® Computational Routines for Properties of Sea Water. CSIRO Marine Laboratories.

Nielsen, P. 1990. Tidal dynamics of the water table in beaches. Water Resources Research **26:** 2127-2134.

Pandit, A., and C. C. El-Khazen. 1990. Groundwater seepage into the Indian River Lagoon at Port St. Lucie. Florida Scientist **53:** 169-179.

Pasch, R. J., E. S. Blake, H. D. Cobb Iii, and D. P. Roberts. 2006. Tropical Cyclone Report: Hurricane Wilma, 15 -25 October 2005, p. 27. National Hurricane Center.

Precht, E., and M. Huettel. 2003. Advective pore-water exchange driven by surface gravity waves and its ecological implications. Limnology and Oceanography **48:** 1674-1684.

Prieto, C., and G. Destouni. 2005. Quantifying hydrological and tidal influences on groundwater discharges into coastal waters. Water Resources Research **41**, W12427, doi:10.1029/2004WR003920.

Robinson, C., B. Gibbes, and L. Li. 2006. Driving mechanisms for groundwater flow and salt transport in a subterranean estuary. Geophysical Research Letters **33**, L03402, doi:10.1029/2005GL025247.

Robinson, C., L. Li, and D. A. Barry. 2007. Effect of tidal forcing on a subterranean estuary. Advances in Water Resources **30:** 851-865.

Shaw, T. J., W. S. Moore, J. Kloepfer, and M. A. Sochaski. 1998. The flux of barium to the coastal waters of the southeastern USA: The importance of submarine groundwater discharge. Geochimica et Cosmochimica Acta **62:** 3047-3054.

Shum, K. T. 1992. Wave-Induced Advective Transport Below a Rippled Water-Sediment Interface. Journal of Geophysical Research-Oceans **97:** 789-808.

Simmons, Jr., G.M. 1992. Importance of submarine groundwater discharge (SGWD) and seawater cycling to material flux across sediment/water interfaces in marine environments. Marine Ecology Progress Series **84:** 173-184.

Smith, N. P. 1993. Tidal and nontidal flushing of Florida's Indian River Lagoon. Estuaries **16:** 739-746.

Stewart, S. R. 2006. Tropical Cyclone Report: Tropical Storm Tammy, 5 - 6 October 2005, p. 14. National Hurricane Center.

Toth, D. J. 1988. Saltwater intrusion in coastal areas of Volusia, Brevard, and Indian River counties, p. 160. Technical Publication SJ88-1. St. Johns River Water Management District.

United States Army Corps of Engineers, and Coastal Engineering Research Center (CERC). 1984. Shore protection manual, 4th ed. Dept. of the Army Waterways Experiment Station Corps of Engineers Coastal Engineering Research Center.

Urish, D. W., and T. E. Mckenna. 2004. Tidal effects on ground water discharge through a sandy marine beach. Ground Water **42:** 971-982.

Webster, I. T. 2003. Wave enhancement of diffusivities within surficial sediments. Environmental Fluid Mechanics **3:** 269-288.

Webster, I. T., and J. H. Taylor. 1992. Rotational dispersion in porous media due to fluctuating flows. Water Resources Research **28**: 109-119.

CHAPTER 4.

GEOCHEMICAL BEHAVIOR AND DISTRIBUTION OF $^{234, 238}$U, ^{226}Ra, AND ^{222}Rn IN A SUBTERRANEAN ESTUARY

Introduction

Radionuclides originating from uranium ($^{235, 238}$U) and thorium (^{232}Th) decay series have been used in a wide variety of environmental studies. The predictable decay rates of these radionuclides make them valuable in understanding transient processes (e.g. weathering, transport, and deposition) that occur on time-scales of hours to millions of years. For example, the conservative and relatively short-lived radon-222 (^{222}Rn; $t_{1/2}$ = 3.825 d) has been used effectively to study diagenesis in low permeability marginal marine environments (Hammond and Fuller 1979; Martens et al. 1980; Martin and Banta 1992) and transport across environmental boundary layers (i.e. air-sea and sediment-water) in fully marine environments (Broecker 1965; Broecker and Peng 1971; Peng et al. 1979). Similarly, the wide range in half-lives (11.4 d, 3.6 d, 1600 y, and 5.7 y) of radium isotopes ($^{223, 224, 226, 228}$Ra, respectively) have been used to investigate oceanic and estuarine mixing (e.g. Key et al. 1985; Crotwell and Moore 2003) as well as benthic exchange (e.g. Key et al. 1985). A number of the U and Th isotopes have been used in conjunction with one another to investigate water-rock interactions/weathering (e.g. Cochran et al. 1986; Tricca et al. 2001), surface water-groundwater interactions/mixing (e.g. Osmond and Cowart 1976), and geochronometers for rocks of variable age.

More recently, U-Th series radionuclides, especially ^{222}Rn and the Ra-quartet, have been applied as tracers for a transport vector commonly referred to as submarine groundwater discharge (SGD; e.g. Cable et al. 1996; Moore 1996; Windom and Niencheski 2003). This source has two distinct fluid end-members: 1) terrestrial-derived, fresh groundwater and 2) seawater recirculated through sediments as marine pore water and/or groundwater (e.g.

Taniguchi et al. 2002; Burnett et al. 2003); distinguishing these sources is important in evaluating material fluxes to the coastal ocean. A subsurface mixing zone, or "subterranean estuary" of Moore (1999), forms between the fresh groundwater and saline groundwater and/or surface water. Subterranean estuaries occur in all coastal aquifers that are either hydrologically connected to a saline surface water bodies or experience encroachment of saline groundwater. Material fluxes to coastal waters are likely to be enhanced by salinity gradients at the intersection of the coastal aquifer and surface water body. As suggested by Moore (1999), these subterranean estuaries can have a significant impact on the transformation and flux of geochemical constituents originating in both the fresh and saline waters, including the radionuclides commonly used to trace the water fluxes.

Although SGD has long been recognized as a pathway for nutrients and contaminants to coastal water bodies (Valiela et al. 1978; Johannes 1980; Valiela et al. 1990), only recently have studies examined how dissolved constituents are transformed in the subterranean estuary prior to discharging (e.g. Charette and Sholkovitz 2002; Testa et al. 2002; Snyder et al. 2004). The most comprehensive study of the biogeochemistry and redox (oxidation-reduction) framework of a subterranean estuary and the surrounding aquifer matrix was presented for Waquoit Bay, Massachusetts, USA (Charette et al. 2005; Charette and Sholkovitz 2006). Diagenetic alteration of amorphous and crystalline iron- and manganese-(hydr)oxides as well as other chemical constituents (e.g. U, Th, Ba, and P) bound to these grains of the subterranean estuary were investigated as well as dissolved pore water constituents (e.g. Fe, Mn, Ba, Sr, and U). Probably the most intriguing observation of their studies was made at the confluence of fresh and saline groundwater where the organic-carbon poor sediments (0.015 to 0.075 %) were coated with Fe- and Mn-(hydr)oxide. Stratification of these (hydr)oxides (Mn overlying Fe) indicated redox-controlled diagenesis, and implied redox controls significantly influenced the distribution of

dissolved and particulate constituents such as Ba, U, Sr, Th, and P (Charette et al. 2005; Charette and Sholkovitz 2006).

Following Charette and Sholkovitz (2006), the terms "groundwater" and "pore water" are used interchangeably throughout this study. However, the reference to a subterranean estuary in this study is slightly different than the more traditional view of a salinity transition zone between fresh groundwater and saline groundwater/surface water (Moore 1999). In this study, the "subterranean estuary" incorporates a portion of the fresh groundwater system (i.e. seepage face), the traditional mixing zone, and the saline groundwater system (beyond the mixing zone). As will be shown, the usage of the term "subterranean estuary" in this context reflects on the fact that the physical and geochemical processes occurring at the salinity transition zone originate beyond the actual mixing zone.

The geochemical framework of this hydrologic boundary between the fresh aquifer and marine sediments is examined for the Indian River Lagoon, Florida, both temporally and spatially, using the following: (1) pore water salinity, Eh, and pH; (2) texture, grain size, and composition of sediments; and (3) cation exchange capacity and reducible Fe- and Mn-(hydr)oxides) sediment characteristics. Within this background geochemistry the spatial and temporal distribution and behavior of ^{222}Rn, ^{226}Ra, U and $^{234}U/^{238}U$ activity ratio (UAR) in this subsurface mixing environment is discussed to elucidate the complex processes controlling their distribution. The complexity of this aquifer system may greatly influence the application of these radionuclides as tracers of water flow, especially SGD.

Background

Study Site

This study was conducted along the mainland shoreline of the Indian River Lagoon (IRL) near the town of Melbourne in east-central Florida. The lagoon is part of a larger well-mixed,

micro-tidal back-barrier lagoonal system of the same name (Smith 1993); the lagoonal system is comprised of Mosquito Lagoon, Banana River Lagoon, and Indian River Lagoon, from north to south. The Indian River Lagoon proper extends approximately 250 km along the east Florida coastline from Titusville to West Palm Beach (Figure 4.1). Lagoonal width averages approximately 3 km (maximum of 10 km) and depth averages 1.5 m (maximum 5 m). Three inlets connect Indian River Lagoon to the Atlantic Ocean and all are located greater than 50 km south of my study site. Maximum astronomical lagoon tidal range (spring-tide) at Sebastian Inlet is between 7 and 11 cm (Clark 2004); tidal dampening reduces the range to less than 0.5 cm at this field site.

In the area proximal to the field site, the Surficial aquifer consists of undifferentiated, Pliocene to Holocene interbedded coquina, sand, silt, and clay (Appendix A). However, a persistent Pleistocene coquina, known as Anastasia Formation, is observed within some sections of the surficial aquifer. Average aquifer thickness is 30 m and average saturated thickness is 25 m. The aquifer is heterogeneous and anisotropic; reported values of hydraulic conductivity range from 1.2 to 2 x 10^{-4} m sec^{-1} for the sandy portions to 0.5 to 1 x 10^{-3} m sec^{-1} for the shell-rich Anastasia Formation (Toth 1988). Local potentiometric highs occur along paleo-ridges forming groundwater divides within the surficial aquifer. Thus, meteoric waters recharging the surficial aquifer east of these paleo-ridges discharge directly into the Indian River Lagoon. The upper 3-4 m of the submarine portion of the surficial aquifer is characterized by moderately sorted, medium quartz sand (average d_{50} = 2.5 ϕ) with variable amounts of silt and clay and a mean porosity of 0.37±0.03 (Hartl 2006). Hydraulic conductivities determined from bail-down tests at this field site range from 10^{-3} to $10^{-1.7}$ cm s^{-1} within the upper 2.5 m below the seafloor (bsf) (Chapter 2; Hartl 2006). The sediments are a transitional sequence from a lacustrine or fluvial-

influenced, brackish-water environment to the modern back-barrier lagoon; this flooding has been estimated to have occurred over the last 10 ky (Hartl 2006).

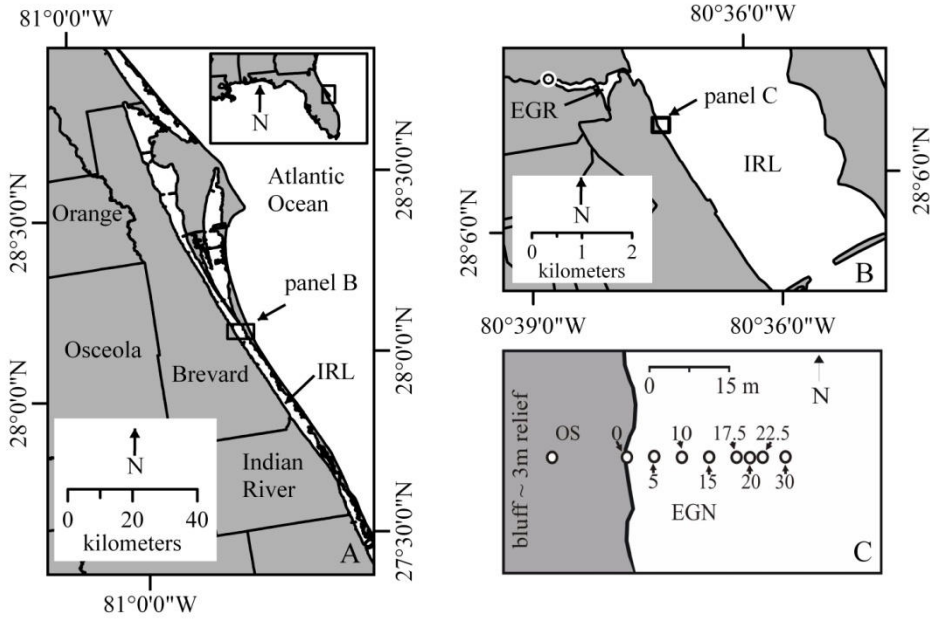

Figure 4.1. Map showing the field site location with respect to Indian River Lagoon (IRL), FL, and surrounding counties (A). Inset in (A) shows the location of the study site relative to the southeastern United States. A local view of the section of IRL where the study was conducted (B) is shown relative to Eau Gallie River (EGR). Plane-view of shore-normal transect of multi-samplers used to collect pore waters is provided in (C).

Submarine Groundwater Discharge to Indian River Lagoon

A number of studies have been conducted in Indian River Lagoon to quantify terrestrially-derived, fresh groundwater discharge and recirculated marine groundwater discharge using numerical groundwater flow models (Pandit and El-Khazen 1990), seepage meters and benthic flux chambers (Belanger and Walker 1990; Cable et al. 2004; Martin et al. 2006; Martin et al. 2007), geochemical tracers (Cable et al. 2004; Martin et al. 2004; Martin et al. 2006; Martin et al. 2007; Smith et al. in press), and temperature (Martin et al. 2006). Estimates of recirculated marine groundwater discharge (reported as specific discharge) are highly variable among the various studies and the techniques employed. For example, Martin et al. (2006) reports

recirculated marine groundwater discharge rates obtained from seepage meters (7.1 cm d^{-1}), pore water chloride concentrations (> 20 cm d^{-1}), and a pore water temperature model (150 cm d^{-1}) for a site 500 m offshore in the IRL. Martin et al. (2007) reports a similar range (13 to 116 cm d^{-1}) for a nearby site using excess pore water ^{222}Rn. Studies distinguishing fresh and marine groundwater discharge in IRL agree that fresh water inputs decrease linearly offshore, fresh water seepage occurs over a narrow zone proximal to the shoreline (less than 20 to 30 m offshore), and a subterranean estuary is present (Martin et al. 2007; Smith et al. in press). Smith et al. (in press) show that their estimates of total fresh groundwater seepage (1.01 to 1.89 m^3 d^{-1} m^{-1} of shoreline) obtained from a pore water transport model of ^{222}Rn were consistent with fluxes obtained from seepage meters (0.9 m^3 d^{-1} m^{-1} of shoreline; Martin et al. 2007) and from numerical groundwater flow models (0.43 to 2.60 m^3 d^{-1} m^{-1} of shoreline; Pandit and El-Khazen 1990).

The volumetric input of fresh groundwater, periodic and episodic surface water perturbations, and hydrodynamic dispersivity are credited as controlling the position and width of the subterranean estuary (Robinson et al. 2007; Smith et al. 2008). As with other studies of submarine groundwater discharge and subterranean estuaries, Martin et al. (2007) suggest the subterranean estuary beneath IRL could have a significant impact on the transport and transformation of dissolved constituents to IRL; however, their application of conservative tracers prevented them from making quantitative conclusions concerning the exact nature of such impacts. Smith et al. (in press) recognized that the heterogeneous distribution of sediment ^{222}Rn production throughout the subterranean estuary influences ^{222}Rn transport and hence accurate quantitative modeling. Processes controlling the distribution of ^{238}U series radionuclides include the sediment-mineral composition, sediment physical properties, groundwater flow dynamics and the distribution of the parent radionuclide.

Methods

Pore water samples and sediment cores were collected from a shore-normal transect along the mainland coast of Florida that extends approximately 30 m into Indian River Lagoon. For pore water sampling, eight multi-level piezometers (e.g. Martin et al., 2003) were installed along the transect; the multi-samplers are between 1.15 m and 2.30 m long and allow discrete sampling at eight port depths (approximately 10 to 40 cm apart) through 200 µm mesh screening. Pore waters were collected five times in attempt to capture wet and dry seasonal variability: 20-23 Nov-04, 9-12 May-05, 15-18 Sep-05, 6-8 May-06, and 5-6 Oct-06. Five sediment vibracores (O.D. 7.62 cm, thin-walled aluminum irrigation pipe) were also collected along the transect during the May-06 sampling trip. Pore water samples were pumped slowly (less than 1 L min^{-1}) into an open overflow cup using a peristaltic pump (Geopump, Geotech Environmental Equipment, Inc.) and silicone tubing. Oxidation-reduction potential (Ag/AgCl electrode), pH (Ag/AgCl electrode), conductivity, and temperature were monitored continuously using a YSI-556 multiprobe sensor (YSI, Inc.). Once these parameters stabilized, the values were recorded and pore waters were sampled. The oxidation-reduction potential (ORP) measured in the field was used to compute Eh by adding a constant 200 mV to the ORP value as suggested by manufacturer (YSI, Inc.). The resulting Eh values range between -115 and 250 mV for all sampling trips, where the higher Eh values (more oxic waters) were obtained from the surface waters. Natural surface waters generally have an Eh of approximately 400 mV; the discrepancy between this assumed value and that measured suggests that the probe was not accurately calibrated and the absolute value of Eh is questionable. However, surface water Eh measured at various points within the lagoon and during the different sampling trips had a mean and 2σ error of 192±34 mV (n=36; one-way ANOVA $p > 0.05$). This suggests that the instrument error was

fairly consistent among the various sampling trips and the resulting patterns of Eh for each sampling trip are comparable.

Water samples from each port depth were sub-sampled for ^{222}Rn (all trips), dissolved ^{226}Ra (May-05, Sep-05, May-06, and Oct-06 trips only), and total dissolved U concentration and isotopes ($^{234, 238}$U). Radon-222 was collected using standard field protocol for analysis by liquid scintillation counting (Clesceri et al. 1989; Smith et al. in press); measurements were performed at Louisiana State University (LSU) on a Packard Tri-Carb 3100 TR liquid scintillation analyzer with alpha-beta discrimination with a background of 3.05 counts per minute (cpm) and correction factor of 2.69 to 3.23. All measurements were made within the mean-life of ^{222}Rn ($^{1}/_{\lambda}$ = 5.5 days). Dissolved ^{226}Ra was extracted from approximately one liter of pore water collected in plastic bottles using a cryogenic radon extraction technique (Mathieu et al. 1988; Cable et al. 1996; Smith et al. in press). Approximately 60-mL of pore water was passed through a 0.45 µm filter (Geotech, Inc. Dispos-a-filter) into 60-mL, acid-washed Nalgene bottle and acidified to a pH less than 2 with distilled, concentrated HNO_3 acid. In the laboratory, approximately 20 g of pore water were spiked with ^{236}U, and the spiked water was pre-concentrated using Eichrom U/TEVA chromatographic exchange resin (Horwitz et al. 2002), and analyzed by inductively coupled plasma mass spectrometry (ICP-MS) at the Geochemistry Division of the National High Magnetics Field Laboratory at Florida State University (FSU-MAGLAB). A dilution of a certified NIST standard (SRM-4321C) was processed with each batch of samples to assess the accuracy and precision of pre-concentration and counting procedures; the average percent difference (n=24) between measured and diluted-certified U concentration and ^{234}U/^{238}U activity ratio were 6.4±3.0% and 1.1±0.8%, respectively.

Whole sediment cores were analyzed for bulk density, porosity, color intensity, and qualitative lithology as described in Chapter 2. Sediment sections (approximately 5 cm long)

were sub-sampled from the vibracores with mid-point depths of 7, 15, 25, 35, 55, 75, 95, 115, 145, 175, 205, and 230 cm bsf, which correspond to the pore water sampling depths. Sediments were partitioned out for various analyses including grain size, cation exchange capacity, major extractable cations (Na^+, K^+, Ca^{2+}, Mg^{2+}), iron and manganese (oxyhydr)oxide content, and sediment bound ^{226}Ra. Grain size was measured on 50 g of dry sediment using standard sieving techniques at 0.5 ϕ intervals (Folk 1974). An additional 20 g of dry sediment was wet sieved through a 4 ϕ (63 μm) sieve with 25% sodium metaphosphate ($Na_6O_{18}P_6$) solution to determine percent sand and mud.

Cation exchange capacity and total extractable cations of sediments were performed at the Coastal Wetlands Soil Characterization Lab, Department of Agronomy and Environmental Management, LSU. Cation exchange capacity was determined on 50 g sediment aliquots using a standard displacement after washing procedure with NH_4OAc buffered to a pH of 7.0 (Peech et al. 1947); NH_4OAc extract was analyzed by either an inductively coupled plasma optical emission spectrometry (ICP-OES) or atomic absorption spectroscopy (AAS) for total extractable cations.

Iron and manganese (oxyhydr)oxide concentrations were determined using two intermediate steps, “amorphous Fe oxyhydroxide” and “crystalline Fe oxide”, of the sequential leaching procedure proposed by Hall et al. (Hall et al. 1996). Following the nomenclature proposed by Charette and Sholkovitz (Charette and Sholkovitz 2002), we refer to the two extractions as “L3” (amorphous) and “L4” (crystalline). The total oxide concentrations are equal to the sum of the L3 and L4 extractions. Sediments (~1 g) were saturated with 20 mL of L3 solution (0.25 M hydroxylamine hydrochloride in 0.05 M HCl) in acid-cleaned centrifuge tube, heated at 60ºC in a water bath for 2 hours, centrifuged, and supernatant collected in a separate, acid-cleaned centrifuge tube. Sediments were washed twice with 5 mL of 18 MΩ deionized (DI)

water, centrifuged, and supernatant was added to L3 solution. Sediments were then exposed to 10 mL of L3 solution and heated for 30 min, washed twice with 5 mL of DI water, and all supernatant collected for a total volume of 50 mL. Sediment residue (~1 g) were then saturated with 30 mL of L4 solution (1 M hydroxylamine hydrochloride in 25% acetic acid, CH_3COOH) in acid-cleaned centrifuge tube, heated at 90ºC in a water bath for 3 hours, centrifuged, and supernatant collected in a separate, acid-cleaned centrifuge tube. Sediments were washed twice with 10 mL of CH_3COOH, centrifuged, and supernatant was added to L4 solution for a total volume of 50 mL. A second, full L4 leach was performed but the residence time in bath was only 1.5 hours. The L3 and both L4 solutions were diluted by a factor of 5 with 18 MΩ DI water and analyzed by ICP-OES at the Wetlands Biogeochemistry Institute Analytical Laboratory, Department of Oceanography and Coastal Sciences, LSU.

Sediment ^{226}Ra was measured using two different methods, batch-incubation (slurry), alpha scintillation to determine ^{222}Rn production, and gamma-ray spectroscopy to determine total sediment ^{226}Ra. For the batch-incubation measurements (referred to as $^{226}Ra_{eff}$), **e**ach sediment sample (approximately 50 g dry sediment) was placed in 500 mL Erlenmeyer flasks with approximately 300 ml of pore water (from consecutive sampling depths) of known dissolved ^{226}Ra activity and sealed to prevent exchange with the atmosphere. After a 30-day in-growth period for dissolved ^{222}Rn to equilibrate with the solid phase ^{226}Ra, the batch experiment flasks were analyzed directly for ^{222}Rn activities via the cryogenic extraction and counting procedures as described above. $^{226}Ra_{eff}$ (dpm g^{-1}) was determined by subtracting the total pore water ^{226}Ra activity from the total activity in the slurry and dividing the difference by the mass of the dry sediment. Radon emanation rates (E_{Rn}; dpm L_{pw}^{-1}) can be computed as

$$E_{Rn} = \left(\frac{(1-\varphi)\rho_g}{\varphi}\right) {}^{226}Ra_{eff} \quad (4.1)$$

where ρ_g is grain density (assumed 2.65 g cm^{-1}) and φ is porosity. ^{226}Ra ($^{226}Ra_{tot}$) was measured on approximately 2 g of dry sediment using a coaxial (well-type), high-purity germanium, (WeGe) gamma ray spectrometer (Canberra, Inc). The ^{226}Ra activity was determined indirectly from daughter isotopes ^{214}Pb (295.3 and 351.7 keV) and ^{214}Bi (609.3 keV).

Results

Geochemical Framework of the Subterranean Estuary

Salinity, Eh, and pH were measured during all sampling trips and provide the basic geochemical framework of the subterranean estuary (Figure 4.2 A-O; Appendix C). The salinity framework of this subterranean estuary has been described in detail by Smith et al. (in press) and Martin et al. (2007). They noted the presence of two distinct mixing zones: 1) vertical mixing of fresh groundwater and saline surface water that extends to approximately 35 cm below seafloor (cm bsf) and 2) lateral mixing of fresh and saline groundwater that occurs below 35 cm bsf and between 17.5 and 30 m offshore (Smith et al. in press; Martin et al. 2007). In addition to these general observations, the salinity distribution varies little between Nov-04 and Sep-05 (Figure 4.2 A-C) while a notable change occurs between the Sep-05 and May-06 sampling trips (Figure 4.2C, D). The lateral mixing zone appears to have migrated landward during this nine- month period as higher pore water salinities were observed at 17.5 and 20 m offshore during the May-06 sampling trip than during the Sep-05 sampling trip. Although the data set is more limited, the Oct-06 salinity distribution is similar to the May-06.

Oxidation-reduction (redox) potentials, or Eh, measured in pore waters from the subterranean estuary show a more spatially and temporally dynamic pattern than salinity. Because of uncertainties in the absolute Eh values, I focus on the general pattern in Eh. In general, the subterranean estuary appeared to become less oxidizing between Nov-04 and May-05 and more oxidizing through time for the remainder of the study (Figure 4.2F – J).

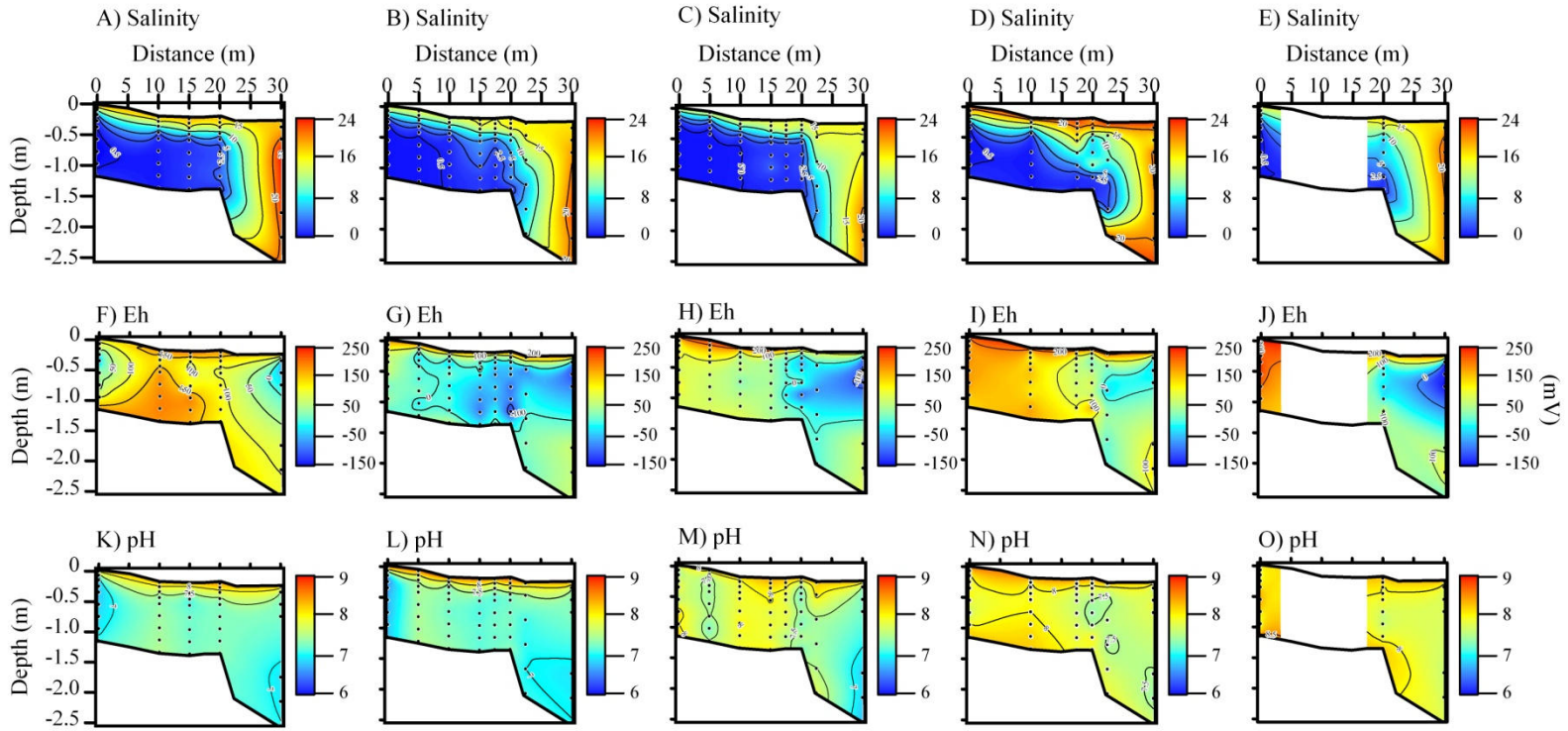

Figure 4.2. Cross-sectional views of the subterranean estuary/submarine aquifer complex showing the contoured, spatial and temporal distribution of (A – E) salinity, (F – J) Eh, (K – O) pH, (P – U) dissolved U concentration, (U – Y) $^{234}U/^{238}U$ activity ratio (UAR), (Z – BB) dissolved ^{226}Ra, (CC) ^{222}Rn emanation rates (E_{Rn}), and (DD – HH) total dissolved ^{222}Rn. Each column of data reflects a different sampling trip; they are from left to right: Nov-04, May-05, Sep-05, May-06, and Oct-06. We would like to point out that the contour scales for (P – U) dissolved U concentration and (Z – BB) dissolved ^{226}Ra vary among the various sampling trips.

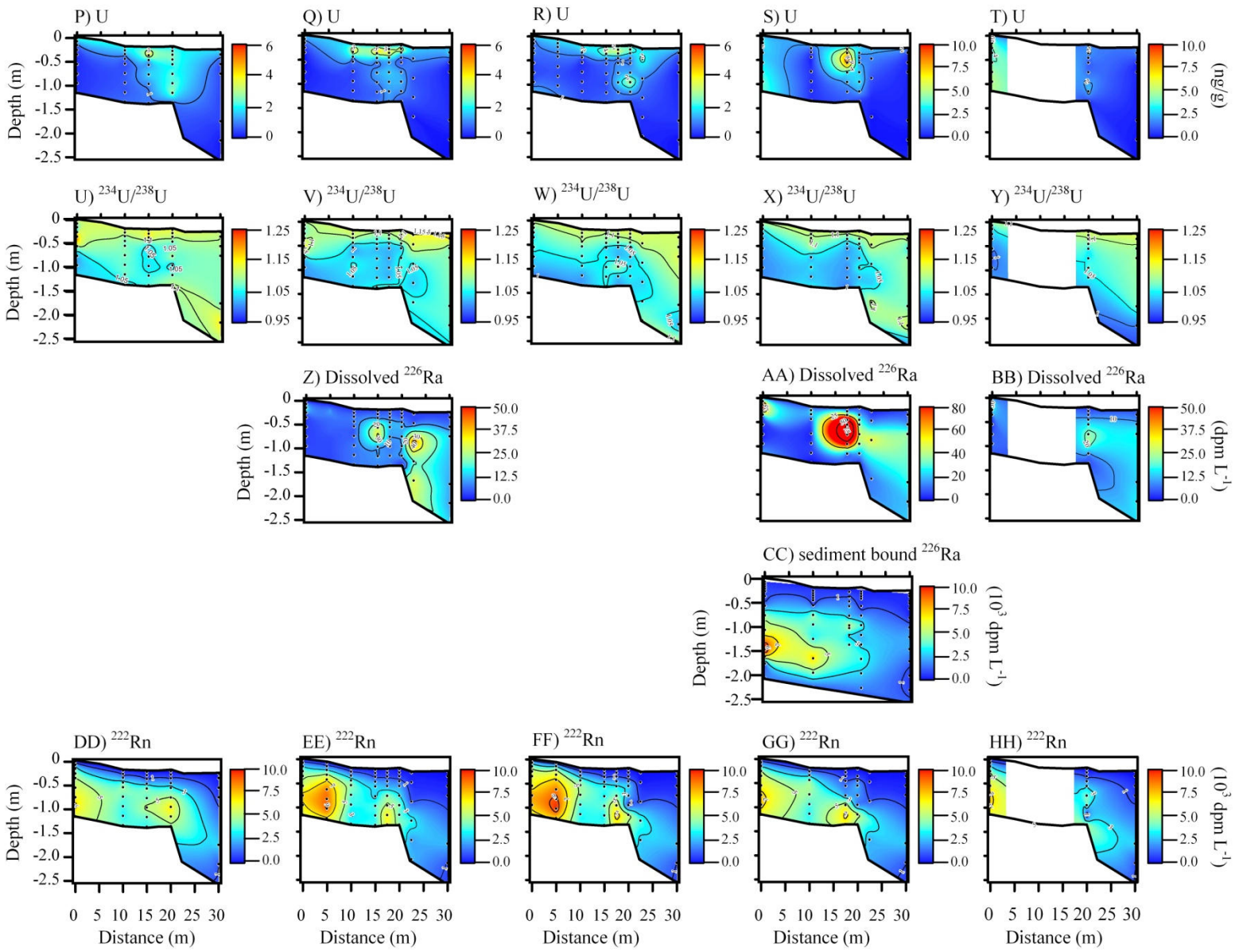
P) U
Q) U
R) U
S) U
T) U
U) $^{234}U/^{238}U$
V) $^{234}U/^{238}U$
W) $^{234}U/^{238}U$
X) $^{234}U/^{238}U$
Y) $^{234}U/^{238}U$
Z) Dissolved ^{226}Ra
AA) Dissolved ^{226}Ra
BB) Dissolved ^{226}Ra
CC) sediment bound ^{226}Ra
DD) ^{222}Rn
EE) ^{222}Rn
FF) ^{222}Rn
GG) ^{222}Rn
HH) ^{222}Rn
Depth (m)
Distance (m)
(ug/g)
(dpm L^{-1})
(10^3 dpm L^{-1})

(fig. cont'd)

The spatial distribution of Eh for Nov-04 is best described as a hyperbolic-paraboloid with minima at the shoreline and 30 m offshore, and a maximum occurring at mid-depths 10 to 15 m offshore. In contrast, Eh for May-05 and Sep-05 decreases with both depth below the sediment-water interface and with increasing distance offshore. Redox potentials measured during May-06 also show a deep (> 35 cmbsf) offshore decreasing trend similar to that observed during May-05 and Sep-05, however, the potentials are generally higher during May-06 than either of the previous two sampling trips. Although analysis of the Oct-06 data set is limited due to the sampling locations, the trend in redox potentials at EGN-0, 20, and 30 m offshore did not appear to change significantly from the previous May-06 trends.

Similar to Eh, the spatial and temporal distributions of pH within the subterranean estuary are more dynamic than salinity. In general, the subterranean estuary appears to become more alkaline with time with the mean pH increasing from 7.4 (Nov-04) to 8.0 (Oct-06) while the surface water pH (8.37±0.15; n=32) remains constant through space and over time. No significant difference occurs between the Nov-04 and May-05 pH distributions. Both sampling times are characterized by steep vertical pH gradients between the surface water and pore water collected from 25 cmbsf. Lateral pH gradients are relatively weak to non-existent during both sampling trips; the mean pH of all pore water samples collected below 25 cmbsf and between 5 and 22.5 m offshore is 7.3±0.2 (n=69). Slightly more acidic pH values (6.9±0.1; n=22) were observed at EGN-0 and at the base of EGN-30. The pH distribution during Sep-05 is more complex. In general, the pore waters are more alkaline than the previous sampling trips, with an average pH of 7.7±0.3 (n=67). The pore waters at EGN-0 were more alkaline than during the previous May-05, while samples at the base of EGN-30 remained relatively acidic. Pore waters at EGN-5 were slightly more acidic (less than 7.5) than the laterally adjacent pore waters (approximately 7.8). Also, a much stronger lateral pH gradient is observed between 10 and 30 m

offshore, with a decrease in pH of approximately 0.8 to 1.0. In May-06, the lateral gradient is still present but less pronounced with a pH change of 0.5 across the entire width of the transect. Samples from the base of EGN-30 remain more acidic than any other pore water locations; the most alkaline pore waters are observed at the base of EGN-0 and -10. In Oct-06, all pore waters sampled had a pH similar to the overlying lagoon water; even the samples at the base of EGN-30. The most alkaline pore waters were again observed at the base of EGN-0.

Aquifer Matrix

Macroscopic examination (1 cm resolution) of the sediments and quantitative measurements of color intensity, porosity, texture (mean grain size and percent mud), cation exchange capacity (CEC), major exchangeable cations, and total reducible Fe and Mn provide the basis for the sediment characterization presented in this section (Figure 4.3). Sediments collected from the field site can be qualitatively divided into three lithologic units (bottom to top): (LU-1) orange, thinly to thickly laminated (less than 1 cm), fine to medium quartz sand; (LU-2) gray to grayish-tan, massively bedded, moderately sorted fine quartz sand with an occasional burrow or root; and (LU-3) grayish-tan to black, normal graded, fine to coarse quartz sand with some shell fragments, mud, and organic matter. Although the lithologic contact between LU-1 and LU-2 is gradational, the apparent color contrast between the two units makes the contact easily discernible. The base of LU-3 consists of coarse-grained quartz sand with some shell fragments, which produces a sharp lithologic contact between LU-2 and LU-3.

The major distinction between LU-1 and LU-2 is fine-scale laminar bedding or laminations observed in LU-1. Although a detailed mineralogic study was not conducted on these sediments, the lamina are composed primarily of ferric-bearing, heavy minerals (e.g.magnetite or maghematite) as indicated by their attraction to a weak magnet. The effective

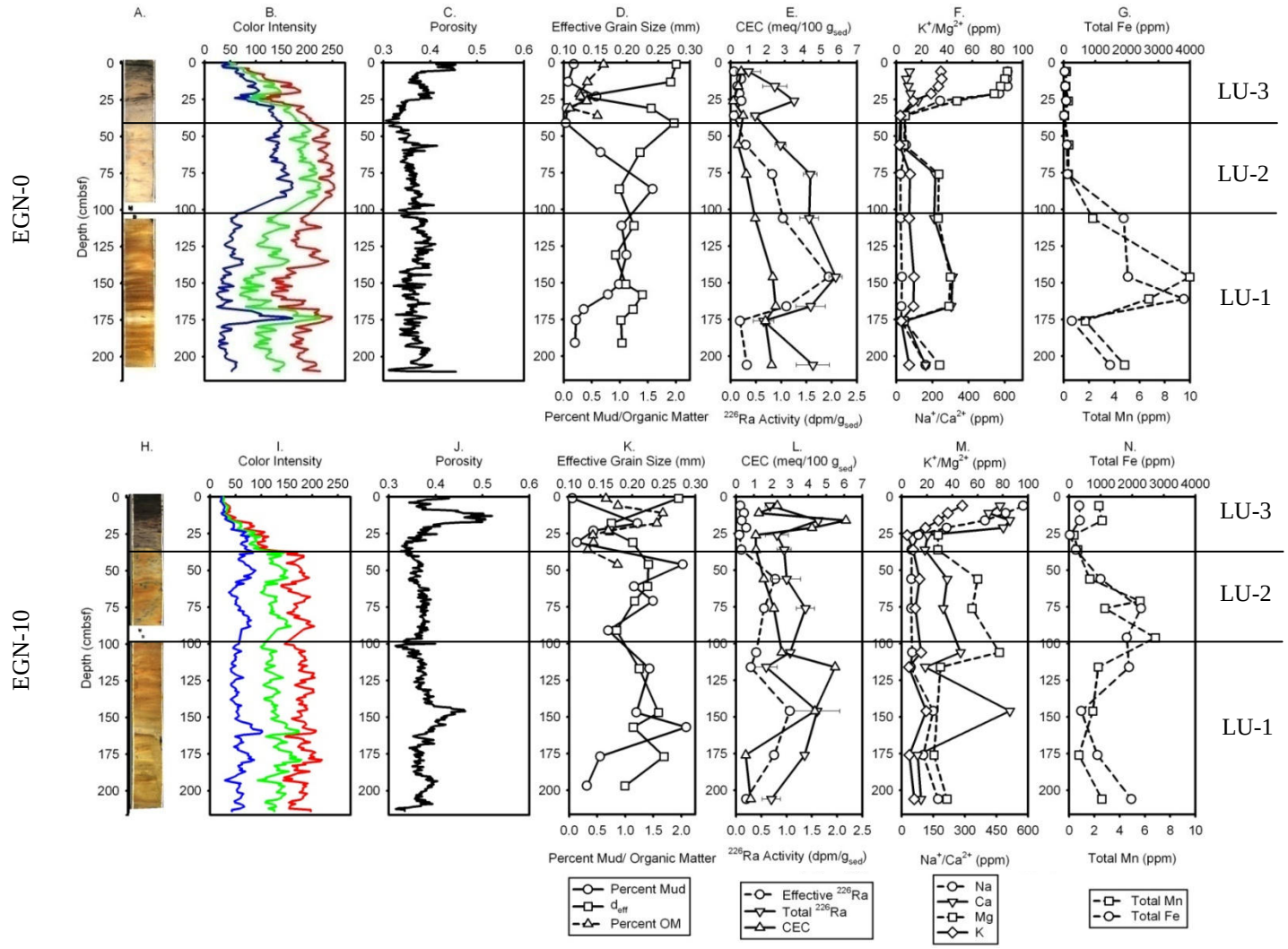

Figure 4.3. Vertical profiles showing the various physical and chemical properties of the sediments characterized in this study, including (A, H, P, V) core photographs; (B, I, O, W) color intensity; (C, J, Q, X) porosity; (D, K, R, Y) effective grain size/percent mud/percent organic matter; (E, L, S, Z) cation exchange capacity (CEC) and sediment ^{226}Ra; (F, M, T, AA) exchangeable Na^+, Ca^{2+}, K^+, Mg^{2+}; and (G, N, U, BB) total reducible Fe and Mn (hydr)oxides. Data are oriented such that each row represents a different coring location; that is (A – G) are for EGN-0, (H – N) are for EGN-10, (P – U) are for EGN-20, and (V – BB) are for EGN-30.

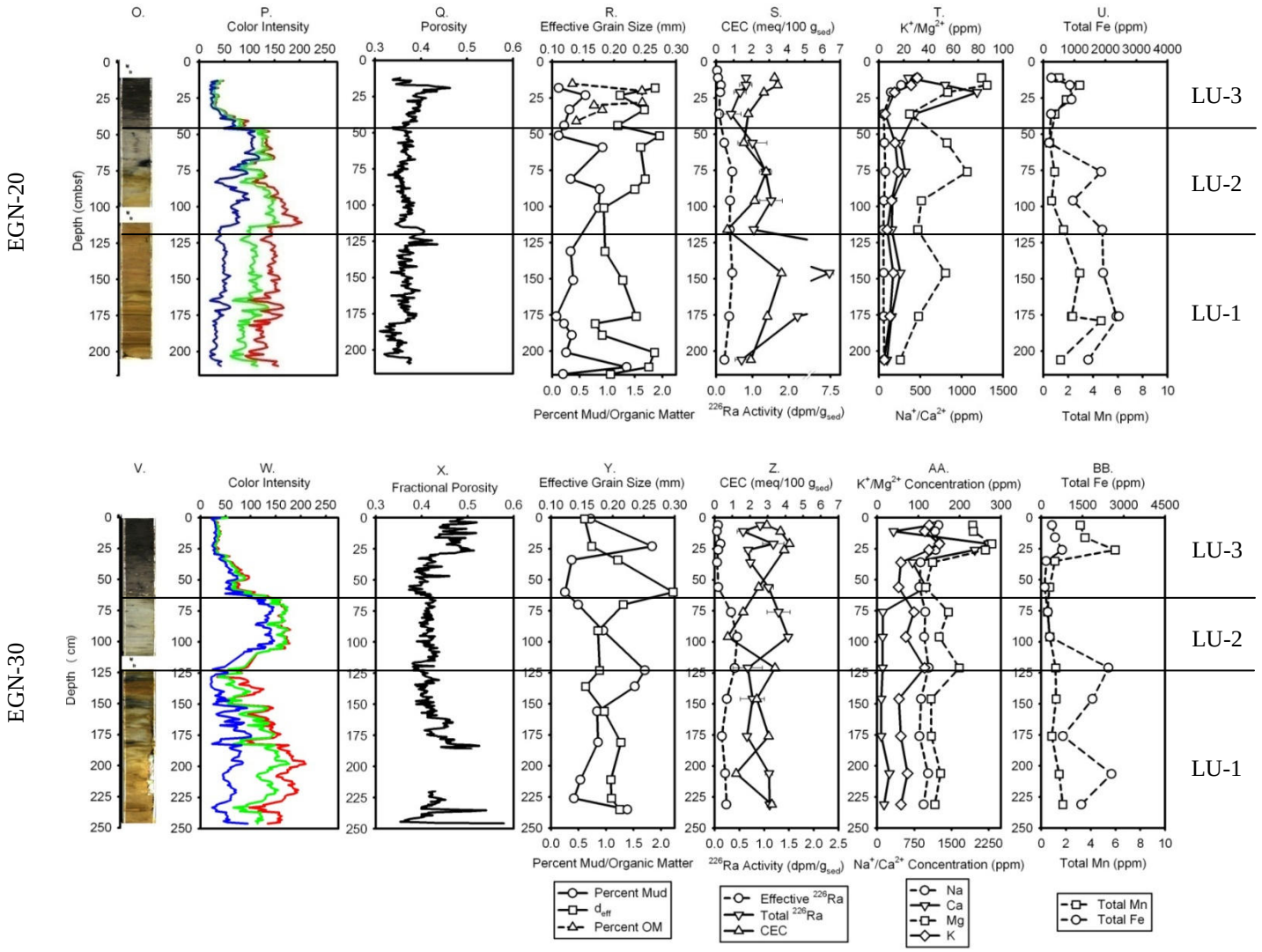
EGN-20
EGN-30
Depth (cmbsf)
Depth (cm)
O.
P.
Color Intensity
Q.
Porosity
R.
Effective Grain Size (mm)
S.
CEC (meq/100 g$_{sed}$)
T.
K$^+$/Mg^{2+} (ppm)
U.
Total Fe (ppm)
V.
W.
Color Intensity
X.
Fractional Porosity
Y.
Effective Grain Size (mm)
Z.
CEC (meq/100 g$_{sed}$)
AA.
K$^+$/Mg^{2+} Concentration (ppm)
BB.
Total Fe (ppm)
LU-3
LU-2
LU-1
Percent Mud/Organic Matter
^{226}Ra Activity (dpm/g$_{sed}$)
Na$^+$/Ca^{2+} (ppm)
Na$^+$/Ca^{2+} Concentration (ppm)
Total Mn (ppm)
Percent Mud
d$_{eff}$
Percent OM
Effective ^{226}Ra
Total ^{226}Ra
CEC
Na
Ca
Mg
K
Total Mn
Total Fe

(fig. cont'd)

mean grain size for samples collected from this unit range between 180 and 250 µm, which is a fine to medium sand. Mud content in LU-1 is generally less than 1% and is ferric-rich, strongly resembling the surface coatings on the sand. Porosity of the unit is fairly homogeneous, ranging between 0.37 and 0.4. In addition to these physical distinctions, LU-1 has chemical properties that distinguish it from LU-2 and LU-3. LU-1 has a larger CEC (2 to 5.5 meq/100g of sediment) and has higher concentrations of exchangeable Ca^{2+} and Mg^{2+} than the other two units. Similarly, the total reducible Fe and Mn are generally greater in this unit.

LU-2 has physical properties similar to LU-1. Porosity, mean grain size and percent mud are similar between LU-2 and LU-1; however, the absence of heavy mineral lamina in LU-2 distinguishes it from LU-1. The color of LU-2 sediments varies significantly among the four cores: orangish-yellow (high, closely spaced RGB intensities) at the shoreline; yellowish-orange to orange (high, closely spaced RG intensities and low B intensity) at 10 m offshore; and yellowish-gray to gray (low, closely spaced RGB intensities) at 20 and 30 m offshore. The CEC of the unit ranges between 1 and 3 meq/100g of sediment with Ca^{2+} being the dominant exchangeable cation near the shoreline and Na^{+} the dominant cation farther offshore; the contrast in the major exchangeable cation probably reflect differences in salinity and composition of major elements of the pore fluid. Total reducible Fe and Mn also varies spatially as suggested by the variability in LU-2 color. At 0, 20 and 30 m offshore, reducible Fe and Mn were less than 1000 ppm and 2 ppm, respectively; however, Fe and Mn concentrations averaged 1500 ppm and 5 ppm, respectively, at 10 m offshore.

LU-3 is the most lithologically distinct of the three units; it is normal-graded from slightly-shelly, medium quartz sand with trace amounts of mud at the base to a fine to medium grain quartz sand with variable amounts of mud and organic matter at the top. The sharp contact between LU-2 and LU-3 dips offshore and LU-3 thickness increases from 30 cmbsf at the

shoreline to approximately 55 cmbsf at 30 m offshore. Slightly higher porosities and mud content are observed in LU-3 relative to LU-1 and LU-2. CEC is generally lower than the other units, however, higher CEC (greater than 1 meq/100g of sediment) do occur in areas with high mud and/or organic matter. The highest concentrations of reducible Fe and Mn in LU-3 are observed at 25 to 30 cmbsf and tend to increase in an offshore direction. Given the coloration of the LU-3 sediments, I am uncertain whether the Fe and Mn obtained from these sediments were actually present as (hydr)oxides. Hall et al. (1996) noted that as much as 10% of the iron bound to organics and monosulfides can be released during the extraction of amorphous and crystalline oxyhydroxides. Thus, some of the Fe and Mn present in the LU-3 sediments may have originated from iron sulfides and organics.

$^{234, 238}$U Surface and Pore Water Distributions

While the magnitude of U concentrations and $^{234}U/^{238}U$ activity ratio (UAR) vary with time, the spatial distribution of total U and UAR within the subterranean estuary appears to remain consistent through time (Figure 4.2P – T and 4.2U – Y; Appendix C) with the exception of EGN-0 (see below). Pore water U concentrations range between 0.05 to 10.01 ng g^{-1} and average 1.54±3.34 ng g^{-1} (±2σ; n=205); pore water UAR range between 0.966 and 1.234 and average 1.062±0.081 (±2σ; n=205). Two zones of apparent U release are observed during all sampling trips: 1) high U concentrations (2 – 11 ng g^{-1}) with UAR slightly higher than the average (1.082) in shallow pore waters (7 – 15 cmbsf) collected from 0 to 20 m offshore and 2) high U concentrations (2 – 9 ng g^{-1}) with average UAR (1.061) in deeper porewaters (55 and 95 cmbsf) collected from 17.5 and 20 m offshore. The pore water U concentrations are generally below 1 ng g^{-1} outside of these enrichment zones. While UAR do not vary significantly between these release zones, the pore water UAR do exhibit general vertical and lateral gradients within the subterranean estuary (Figure 4.2U – Y). UAR increase offshore from approximately 1.02 at

EGN-0 to approximately 1.09 at EGN-30 during all sampling trips. Similar UAR gradients are observed in the vertical direction; however, the magnitude of these gradients depends on the lower UAR which tends to increase in the offshore direction.

In comparison, the average U concentration for the fresh groundwater (onshore well), saline groundwater (base of EGN-30), and surface water (~250 m offshore) end-members are 0.08±0.01, 0.11±0.06, and 1.84±0.52 ng g^{-1}, respectively (±2σ; n=4 for all) and the average UAR for end-members are 1.018±0.032, 1.061±0.061, and 1.121±0.018 (±2σ; n=4 for all), respectively (Table 4.1). Total U concentration versus salinity reveals most pore water samples fall above the conservative mixing line established using the fresh groundwater and surface water end-members (Figure 4.4A); this mixing line is indistinguishable from the oceanic U-salinity conservative mixing line proposed by Chen et al. (Chen et al. 1986). This observation is consistent with the release of U to the pore waters suggested by the spatial distribution of U. However, a group of pore water samples consistently fall below this line, which suggests a potential removal of U beyond the lateral mixing zone (EGN-22.5 and EGN-30; Figure 4.4A).

Table 4.1. Summary of fresh groundwater, saline groundwater, and surface end-members and associated constituents used in the development of mixing curves.

Constituent	**Fresh Groundwater**	**Saline Groundwater**	**Surface Water**
Salinity	0.18±0.2	20.4±1.0	20.8±3.6
U (ng g^{-1})	0.08±0.01	0.11±0.06	1.84±0.52
$^{234}U/^{238}U$ (UAR)	1.018±0.032	1.061±0.031	1.121±0.018
^{226}Ra (dpm L^{-1})	6.16±0.73	13.91±2.81	4.28±1.00
^{222}Rn (dpm L^{-1})			
Onshore Well	2790±590	-	-
Average Pore Water	6410±3530	960±510	130±130
Extrapolated Rn-Sal	4960±400	-	-
Extrapolated Rn-Ra_{eff}	1560±30	-	-

Surface water U concentrations are less variable than the pore water samples with a range between 1.39 and 2.38 ng g^{-1}. All but the May-05 surface water U concentrations plot above the U-salinity conservative mixing line between the fresh groundwater and surface water. The surface water U concentrations form a linear relationship with salinity ($r^2 = 0.57$; Figure 4.4B). Using this regression line, the effective fresh groundwater U concentration is 0.54 ng g^{-1} throughout the duration of the study, which is approximately six times greater than the measured fresh groundwater end-member and a third less than the average pore water uranium concentration.

As stated above, EGN-0 has the most temporal variability of all the sampling sites and for this reason, I describe the vertical distribution of U and UAR at this site independent of the

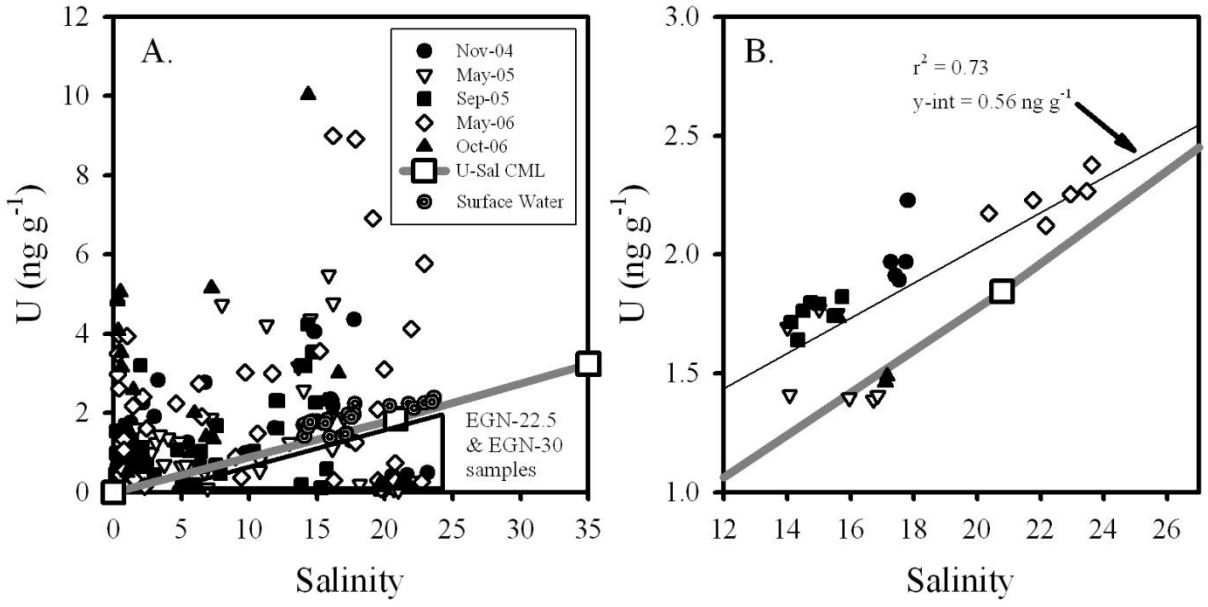

Figure 4.4. (A) Plot showing the relationship between dissolved U concentration and salinity for groundwater/pore water samples and surface water samples collected during the Nov-04, May-05, Sep-05, May-06, and Oct-06 sampling trips. Also shown is the U-salinity conservative mixing line (U-Sal CML; thick gray line) derived from the fresh groundwater and surface water end-members presented in Table 4.1; the line has been extrapolated out to full marine salinity. (B) A plot of surface water U and salinity data showing the long-term, general enrichment of U relative to that predicted by the CML. The y-intercept (y-int) shows the effective zero salinity concentration of U in fresh groundwater.

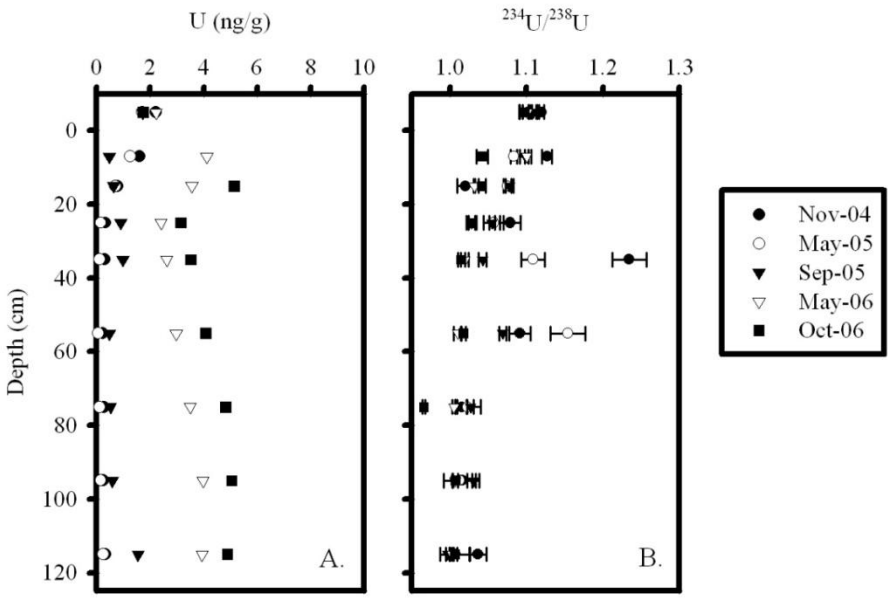

Figure 4.5. Vertical profiles of (A) dissolved U concentration versus depth and (B) $^{234}U/^{238}U$ activity ratio for EGN-0 (shoreline site) obtained during all five sampling trips.

transect-scale described above (Figure 4.5). A significant change in the U concentration and UAR occurs over the period between May-05 and -06 sampling trips. During Nov-04 and May-05, dissolved U decreases exponentially from surface water high of 2.23 and 1.71 ng/g, respectively, converging on average asymptotic values of 0.28±0.06 and 0.12±0.06 ng/g (±2; n=6 for both), respectively, at 25 cmbsf. UAR profiles during these sampling trips are defined by shallow water maxima (1.15 to 1.25) located between 35 and 55 cmbsf. During Sep-05, the dissolved U profile is more complex; concentration decreases from the surface water (1.71 ng/g) to a minimum at 7 cmbsf (0.48 ng/g), increases to a maximum at 35 cmbsf (0.99 ng/g), decreases and remains low from 55 to 95 cmbsf (0.53±0.05 ng/g; n=3), and increases yet again at 115 cmbsf (1.60 ng/g). The UAR profile still shows a mid-depth peak at 55 cmbsf, however, the magnitude of the peak is reduced to 1.09. The distribution of U during May-06 and Oct-06 follow the same general trend; U increases from the surface water to a maximum at 7 cmbsf, decreases to a minimum at 25 cmbsf, and increases and remains constant to the base of the

profile. The increase in dissolved uranium in deeper pore waters appears to have diluted the UAR making the lower portion of the UAR profile (below 35 cmbsf) near vertical.

^{226}Ra Pore Water, Surface Water, and Sediment Distributions

Similar to U, the spatial distribution of dissolved ^{226}Ra is characterized by an offshore, mid-depth release zone during the May-05, May-06, and Oct-06 sampling trips (Figure 4.2Z – BB; Appendix C). The ^{226}Ra activities range between 4.48 and 80 dpm L^{-1} and average 15.6 dpm L^{-1}. In May-05, the highest ^{226}Ra activity (45.11 dpm L^{-1}) is observed 60 cmbsf at EGN-22.5, while in May-06, this epicenter of dissolved ^{226}Ra (81.41 dpm L^{-1}) is located at 55 cmbsf at EGN-17.5. Also, high ^{226}Ra activities are observed at shallow depths (7 to 25 cmbsf) at EGN-0 during all three sampling trips. Outside of these enrichment zones, ^{226}Ra activities occur within a narrow range of 4 to 8 dpm L^{-1}.

The ^{226}Ra-salinity relationship is more ambiguous than the U-salinity relationship due to the lack of well-defined ^{226}Ra-salinity end-members (Table 4.1; Figure 4.6A). Average ^{226}Ra for the fresh groundwater, saline groundwater, and surface water end-members are 6.16±0.73, 13.91±2.81, and 4.28±1.00, respectively. Assuming conservative mixing between fresh and saline groundwater end-members, ^{226}Ra is enriched relative to the mixing line within the mid-salinity range of 5 – 15 and slightly depleted beyond a salinity of 15 (below mixing line). The behavior of ^{226}Ra within the subterranean estuary becomes more apparent when the data are separated relative to the two mixing zones delineated by salinity (Figure 4.6B). Within the vertical mixing zone (0 to 35 cmbsf), ^{226}Ra is released consistently with respect to time at a salinity between 2 and 7.5, while an additional release is observed during May-06 only and within the salinity range of 15 to 17.5. The inferred depleted zone observed when all data are considered is actually an artifact of chosen end-members. In comparison, samples collected

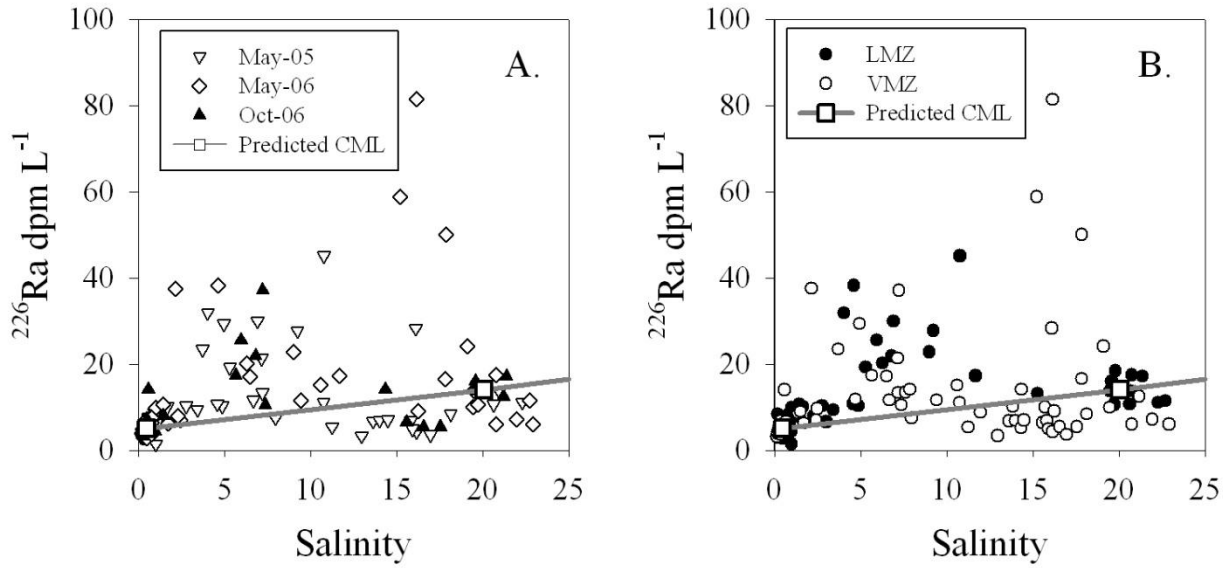

Figure 4.6. (A) Plot showing the relationship between dissolved ^{226}Ra and salinity for groundwater/pore water samples and surface water samples collected during the May-05, May-06, and Oct-06 sampling trips. Also shown is the ^{226}Ra-salinity conservative mixing line (Predicted CML; gray line) derived from the fresh and saline groundwater end-members presented in Table 4.1. (B) Plot showing the relationship between dissolved ^{226}Ra and salinity for groundwater/pore water samples within the lateral mixing zone (LMZ; > 35 cmbsf) and the vertical mixing zone (VMZ; < 35 cmbsf).

from within the lateral mixing zone (i.e. below 35 cmbsf) demonstrate a consistent release of ^{226}Ra across the entire mid-salinity range (5 – 15) of this system.

Radium may occur in a number of solid phase forms; batch equilibration experiments and gamma-ray detection measurements do not distinguish among these various sources. Batch measurements provide an estimate of ^{222}Rn emanation rates (E_{Rn}; Figure 4.2CC; Appendix D) from sediment ^{226}Ra located near the liquid-solid phase boundary ($^{226}Ra_{eff}$). The average $^{226}Ra_{eff}$ is 0.35±0.37 dpm g^{-1}_{sed} (E_{Rn} = 1850±1950 dpm L_{pw}^{-1}) and the range is from 0.05 to 1.95 dpm g^{-1}_{sed} (E_{Rn} = 260 to 10300 dpm L^{-1}_{pw}). $^{226}Ra_{eff}$ is most abundant in LU-1 sediments from EGN-0 and -10 and tend to decrease both vertically upward in LU-2 and LU-3 sediments from these cores as well as laterally offshore in LU-1 sediments between EGN-20 and -30. This general observation is further illustrated by the positive correlation between ^{226}Raeff and both total

reducible Fe and Mn (hydr)oxides (Figure 4.7) and the negative correlation between $^{226}Ra_{eff}$ and exchangeable cations (Figure 4.8).

The (WeGe) gamma-ray measurements reflect total ^{226}Ra present in the sediments ($^{226}Ra_{tot}$; Figure 4.3). The average $^{226}Ra_{tot}$ is 1.20±1.03 (1σ) dpm/g and the range in $^{226}Ra_{tot}$ is between 0.35 and 7.44 dpm/gsed. $^{226}Ra_{tot}$ shows a more uniform vertical distribution than $^{226}Ra_{eff}$ with the exception of the sample from 146 cmbsf at EGN-20 (7.44 dpm/gsed; Figure 4.3). No apparent relationship exists between $^{226}Ratot$ and any other sediment property such as total reducible Fe or Mn (hydr)oxide (Figure 4.7B) or exchangeable cations (Figure 4.8B). Removing the maximum $^{226}Ra_{tot}$ activity reduces the mean $^{226}Ra_{tot}$ to 1.05±0.43 (1σ), which is a 45% reduction in the relative standard deviation.

The ratio $^{226}Ra_{eff}/^{226}Ra_{tot}$, here referred to the emanation efficiency due to its reflection of radon emanation to pore waters, ranges between 6 and 93% and averages 28±21% (1σ); this average is consistent with estimates obtained from leach experiments (Amin and Rama 1986) and model experiments (Semkow 1990; Semkow and Parekh 1990). As with $^{226}Ra_{eff}$, emanation efficiencies exceeding 50% (n=9) are restricted to LU-1 sediments from EGN-0 and -10, while LU-1 sediments from EGN-20 and -30 have emanation efficiencies between 20 and 30%. The lower emanation efficiencies (below 15%; n=14) were observed primarily in LU-3 sediments from all four coring locations. The exception to this latter statement is observed at 146 cmbsf at EGN-20 (LU-3 sediment type) where the highest $^{226}Ra_{tot}$ results in the lowest emanation efficiency (6%).

^{222}Rn Surface and Pore Water Distributions

The spatial distributions of ^{222}Rn in this subterranean estuary (Figure 4.2P-U; Appendix C) shares strong similarities with the salinity distributions (Figure 4.2A-E); both exhibit a well-defined lateral gradient between fresh and saline groundwater and a well-defined vertical

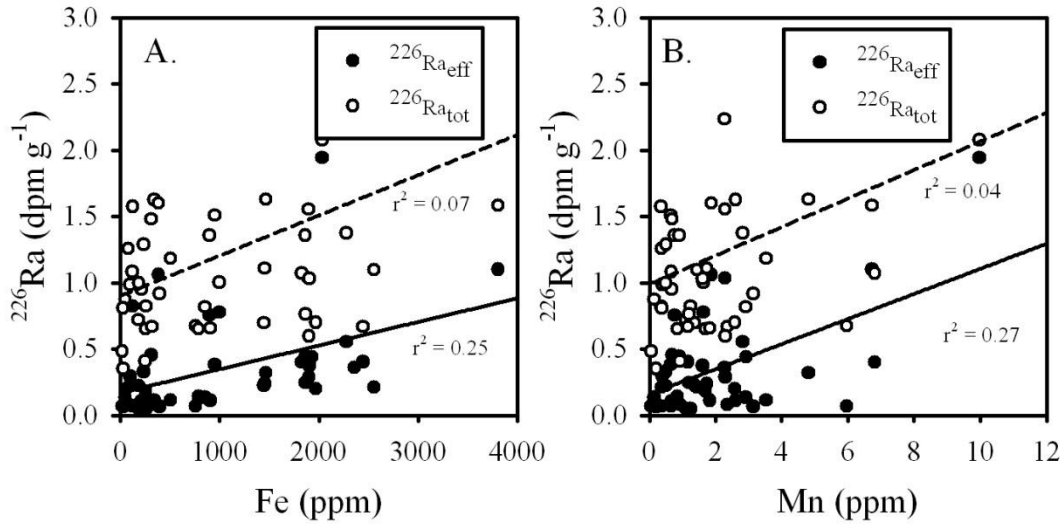

Figure 4.7. Scatter plot showing the relationship between sediment ^{226}Ra (total and effective) and total reducible (A) Fe and (B) Mn (hydr)oxides.

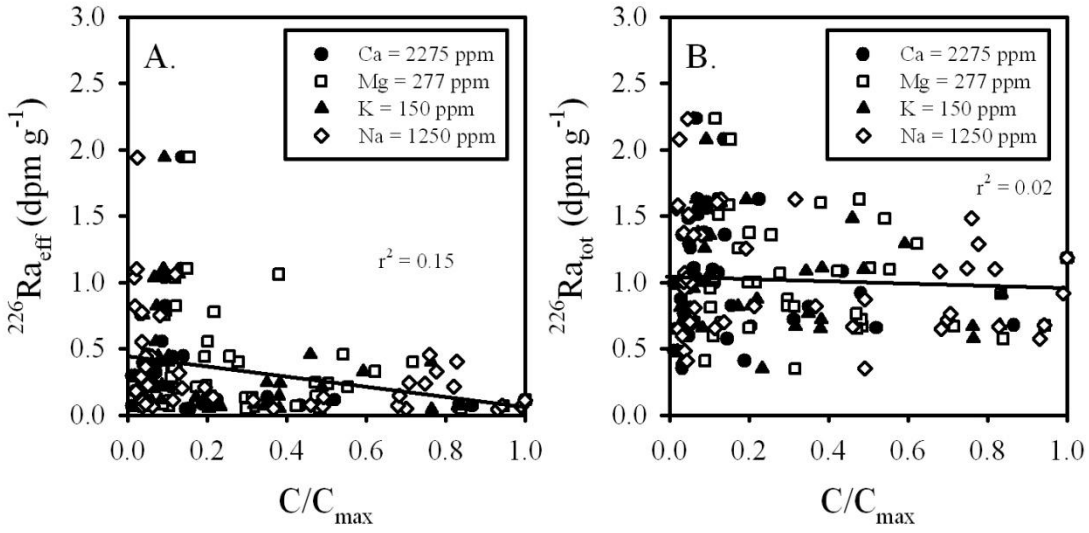

Figure 4.8. Scatter plot showing the relationship between (A) effective sediment ^{226}Ra ($^{226}Ra_{eff}$) and (B) total sediment ^{226}Ra ($^{226}Ra_{tot}$) to normalized exchangeable Na^+, Ca^{2+}, K^+, and Mg^{2+} concentrations. Cation concentrations are normalized to the maximum concentration defined in the legend.

gradient between fresher groundwater and the surface water. However, the ^{222}Rn distribution is an inversion of the salinity distribution. High ^{222}Rn activities (6410±3530 dpm L^{-1}; ±2σ, n =41) are observed in the fresher groundwater (salinity less than 0.5) located at depth within the aquifer and proximal to the shoreline. In comparison, the average ^{222}Rn from groundwater collected from the onshore well is 2760±590 dpm L^{-1} (2σ, n=4; Table 4.1). A plot of pore water ^{222}Rn versus salinity reveals a strong linear relationship ($r^2 = 0.75$) between a salinity of 2 and 15 suggesting conservative mixing across the subterranean estuary (Figure 4.9). Based on this linear fit, the ^{222}Rn activity of the incoming fresh groundwater would be 4960±400 dpm L^{-1} (±2σ), approximately 20% less than the average measured ^{222}Rn activity in fresh pore waters and 180% greater than groundwater ^{222}Rn from the onshore well (Table 4.1). Radon activities decrease offshore and vertically upward; the average ^{222}Rn activity for the saline groundwater end-member and the surface water are 960±510 and 130±130 dpm L^{-1}, respectively, which brackets most of the higher salinity pore waters (i.e. greater than 15; Table 4.1). Six samples are not bracketed by this range and have activities greater than 2000 dpm L^{-1}. Five of these six samples correspond to a mid-depth (150 cmbsf) maximum in ^{222}Rn at EGN-30; the maximum ^{222}Rn activity is two to three times greater than adjacent pore water samples collected from 50 and 190 cmbsf at the same site. The other high salinity-^{222}Rn sample was collected from the base of EGN-22.5 (160 cmbsf) during the May-06 sampling trip.

The similarity between pore water ^{222}Rn and ^{222}Rn emanation rates (E_{Rn}) suggest that sediment production plays a key role in the distribution of dissolved ^{222}Rn (Figure 4.10). In general, the average ^{222}Rn pore water activity (2965 dpm L^{-1}; n=249) is slightly higher than the average E_{Rn} (2005 dpm L^{-1}; n=30). Assuming production is the only source of radon (i.e. y-intercept of 0), linear regression ($r^2 = 0.40$) between E_{Rn} and ^{222}Rn pore water activity collected during May-06 suggests the average activity ratio ($^{222}Rn/E_{Rn}$) 21% greater than equilibrium

(Figure 4.10A). In comparison, a regression with no assumptions concerning source gives an effective activity ratio of 0.80 with a background (y-intercept) ^{222}Rn activity of 1530 dpm L^{-1} (Figure 4.10A). A similar comparison can be made for all pore water ^{222}Rn data assuming steady-state E_{Rn} with time (Figure 4.10B); the average activity ratio assuming production-only source is 1.24 and the activity ratio and additional radon source are 0.81 and 1590 dpm L^{-1}, respectively. The background ^{222}Rn activity estimated from this analysis is comparable to the fresh groundwater end-member measured from the onshore well, implying production or emanation from sediment ^{226}Ra is a major source of ^{222}Rn in this subterranean estuary/submarine aquifer complex.

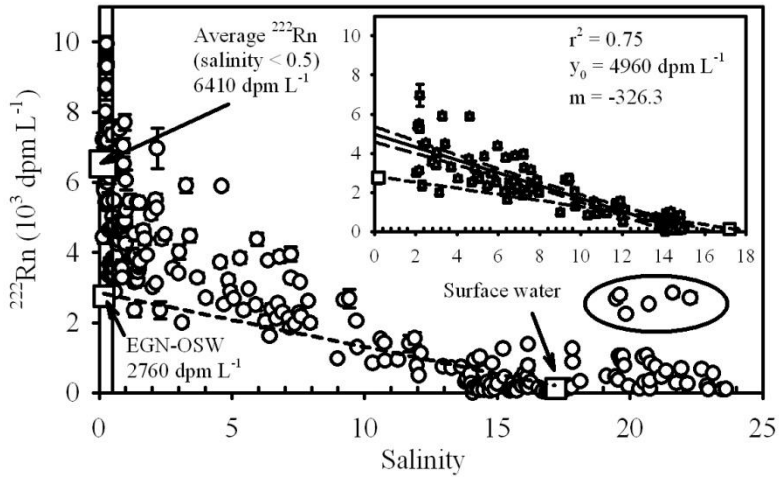

Figure 4.9. The relationship between salinity and total dissolved ^{222}Rn observed in the groundwater/pore water and surface water samples. Also shown are the average ^{222}Rn measured in water samples with a salinity less than 0.5 that were collected from the subterranean estuary, the average groundwater ^{222}Rn end-member from EGNW-OS, and from the surface water. A conservative mixing line (CML) extrapolated from these latter two end-members is shown as a short-dash line. Inset shows the quantitative linear relationship between ^{222}Rn and salinity between the salinity range of 2 and 15 relative to the CML expected between fresh groundwater in EGNW-OS and surface water.

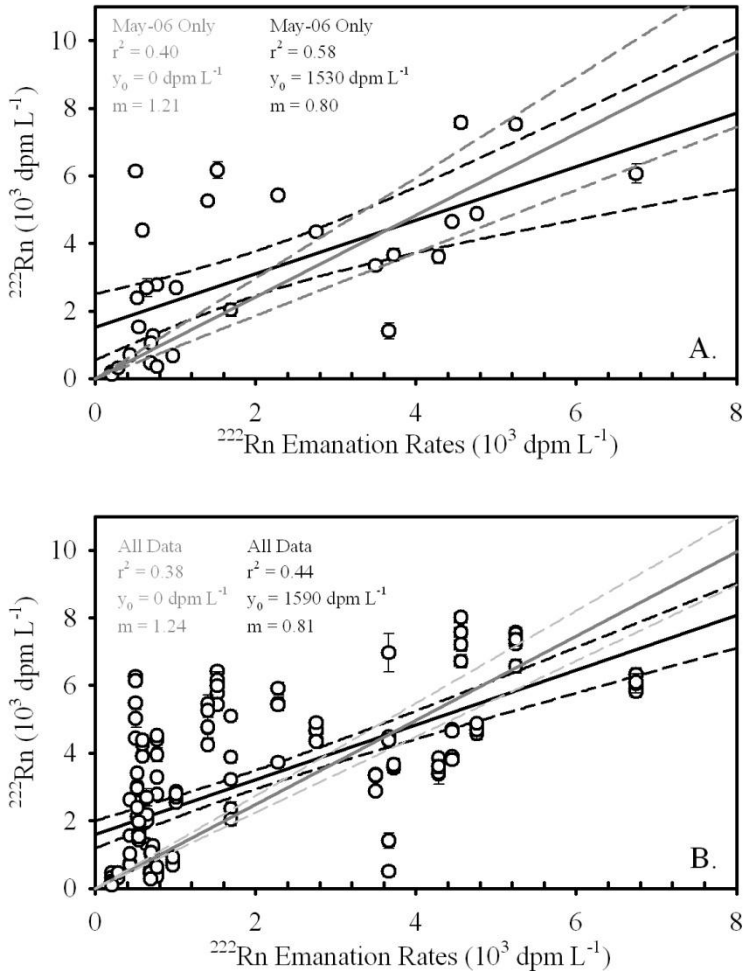

Figure 4.10. The relationship between ^{222}Rn emanation rates (E_{Rn}) and total dissolved ^{222}Rn assuming (A) non-steady-state production and (B) steady-state production. Within each plot, two different assumptions are also shown concerning sources of ^{222}Rn to the system; the first, shown in gray, is production-only (y-intercept = 0) and the second, shown in black, is assuming an additional source (i.e. groundwater, y-intercept determined).

Discussion

Non-conservative Behavior of Uranium

The subterranean estuary appears to act as a net source of U to the Indian River Lagoon. Stream and creek inputs of U were not quantified, but evidence from the pore waters strongly support a subterranean source. The spatial distribution of dissolved pore water U and the non-conservative source relationship observed in the pore water U-salinity data suggest the fresh water seepage face and associated subterranean estuary/aquifer complex are a U source to the

nearshore region (0 to 30 m offshore) of Indian River Lagoon. The spatial distribution of dissolved U in the subterranean estuary suggests two (temporally) stationary release zones that may act as sources for U (Figure 4.2P – T). A shallow (0 to 35 cmbsf) U maxima is observed at 5, 10, 15, 17.5 and 20 m offshore and a deep U maximum is observed at 20 m offshore.

Unlike the other radionuclides examined in this study, uranium has two commonly occurring oxidation states in natural waters, U^{4+} and U^{6+}, where the standard electrode reaction and associated potential for this reaction are:

$$U^{4+} + 2H_2O \rightarrow {UO_2}^{2+} + 4H^+ + 2e^-;\ E_0 = 270\ \text{mV}. \quad (4.2)$$

In oxic waters with a pH of 6 to 8, U occurs as a hexavalent ion found predominantly as the divalent uranyl cation (UO_2^{2+}) forming soluble complexes primarily with carbonate anions ($UO_2(CO_3)_3^{4-}$) but also to a lesser extent phosphate ($UO_2(HPO_4)_2^{2-}$) and hydroxides anions (UO_2OH^+) (Mckelvey et al. 1955; Langmuir 1978). In reducing environments, U occurs primarily as the uranous ion (U^{4+}) and is relatively immobile due to the formation of biogenic, amorphous, and crystalline uranium dioxides (UO_2) as well as insoluble hydroxides ($U(OH)_4$) (Gascoyne 1992). Measured Eh and dissolved U concentration appear to exhibit a positive relationship (Figure 4.11). Thus, the redox behavior of uranium is one of the fundamental controls on cycling in the subterranean estuary. Other factors controlling U cycling include sorption to iron (hydr)oxides and organic matter as well as changes in solubility due to changes in pH, alkalinity, and anionic complexes.

The shallow U maxima (0 to 35 cmbsf) occur within the vertical mixing zone between fresh groundwater and saline surface water. The U is released from LU-3 sediments, which have higher organic matter content (greater than 1% OM by weight; Figure 4-3K and R) and lower sediment iron and manganese content (Figure 4-3G, N, U, and BB) than either LU-1 or -2. The average $^{234}U/^{238}U$ activity ratio (UAR) of released U (1.082) is 2 to 5 % less than that of

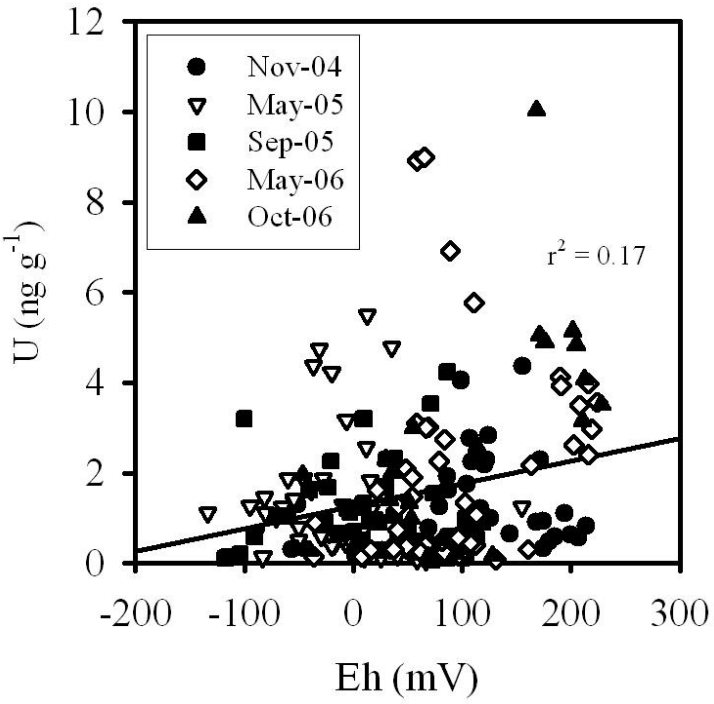

Figure 4.11. Linear relationship between Eh and dissolved U concentration obtained during Nov-04, May-05, Sep-05, May-06, and Oct-06 sampling trips.

average surface water (1.121). To account for this dilution of the UAR, the sediment U source must have a lower UAR than the lagoon water. This further suggests that the U released from the sediments is not derived from the reduction of lagoon water U rather a source where ^{234}U and ^{238}U is close to equilibrium. These observations suggest both redox and non-redox mechanisms may be influencing U release. Similar shallow pore water U maxima have been observed in other coastal marine environments (e.g. Cochran et al. 1986; Mckee et al. 1987; Barnes and Cochran 1993); however, most of these studies were conducted in fine-grained muddy sediments. Cochran et al. (1986) suggested that U release from muddy sediments from Buzzard Bay, MA, USA, originated from the diffusion of oxygen into the sediments and subsequent oxidation of organic matter and possibly uranous minerals. A similar argument can be made for the Indian River Lagoon. The steep salinity gradient observed from 0 to 20 m offshore suggests significant exchange occurs between fresh groundwater and saline surface water to depths as

great as 35 cmbsf. Smith et al. (in press; see also Chapter 5) estimated exchange rates at this site (0 – 30 m offshore) that were on the order of 3.6 to 123 cm d^{-1}. Such high exchange rates would favor the transport of dissolved oxygen and sulfate to greater depths than diffusion alone, especially given an opposing vertical advective flow from the fresh groundwater. Thus, the direct oxidation of uranous minerals by oxygen and/or desorption of U during the oxidation of organic matter by aerobic or sulfate-reducing bacteria may account for the shallow U release zone. McKee et al. (1987) and Barnes and Cochran (1993) suggested that the reduction of iron (hydr)oxides in Amazon and Long Island Sound sediments controlled U release to pore waters. Although the origin of "reducible iron" in my LU-3 sediments is not clear, if appreciable iron is present as (hydr)oxides then a similar process could account for the shallow release of U to pore waters of the Indian River Lagoon subterranean estuary. Finally, one could argue that the U release is mediated by an increase in anionic ligands or complexes as seawater is recirculated across the sediment-water interface. Gascoyne (1992) stated that work from Lemire (1988) indicated that in mildly reducing environments, the formation of uranium chloride and sulfate complexes increased U solubility several orders of magnitude, subsequently enhancing its mobility. In the subterranean estuary, the periodic exposure of sediments to both fresh and saline waters likely complicates U cycling. Given the complexity of the subterranean estuary all of these explanations are plausible and in fact the U release may be driven by any one or more of these processes. The relative depletion of U below the shallow release zone across most of the subterranean estuary (except for EGN-20 and EGN-0) favors this zone as the primary source of U to the lagoon.

The deeper (55 to 95 cmbsf) release of U at 20 m offshore shares similar complexity to that of the shallow maxima. While shallow recirculation of oxygenated lagoon water by waves and biota are unlikely at depths exceeding 55 cmbsf, large-scale convective-type recirculation

has been suggested as an important transport pathway for dissolved constituents in some subterranean estuaries (e.g. Smith 2004; Michael et al. 2005). However, the flow paths associated with these convection cells are generally much longer and penetrate to greater depths into the aquifer than those observed at the sediment-water interface. These longer flow paths would favor more reducing conditions (Roy et al. 2008), a setting in which U is not readily released. However, such reducing conditions have been observed at this site, Roy (in prep) noted the presence of apparent redox cycling of Mn, Fe, and S restricted to 55 to 95 cmbsf at20 m offshore (Figure 4.12) consistent with the release of U observed. In this zone, ferric (hydr)oxides surface coatings were reduced in the presence of dissolved sulfide, accounting for the color interface between L1 and L2 sediments. Roy's (in prep) observation implies U reduction may be controlling pore water distributions. However, similar releases of U in reducing conditions and in the presence of ferric (hydr)oxides have been observed in both field studies (Mckee et al. 1987; Barnes and Cochran 1993; Swarzenski and Baskaran 2007) and laboratory experiments (Barnes and Cochran 1993; Sani et al. 2005; Ginder-Vogel et al. 2006). Proposed mechanisms of U release follow one of two pathways: 1) desorption of U^{6+} during the reduction/dissolution of ferric hydroxides sediment coatings (Mckee et al. 1987; Barnes and Cochran 1993); or 2) abiotic/biotic (re)oxidation of U by ferric hydroxides (Barnes and Cochran 1993; Sani et al. 2005). While these two pathways cannot be differentiated here, it should be noted that recent controlled experiments have shown the desorption pathway is not required for the mobilization of U and in some cases is not favorable (Sani et al. 2004; Sani et al. 2005; Ginder-Vogel et al. 2006). For example, Sani et al. (2005) found under sulfate-reducing conditions containing reduced uranium and initially free of ferric hydroxides, that uranium release occurred upon the addition of ferric hydroxide and the subsequent precipitation of iron sulfides inhibited the reduction of U. This offshore, deeper release zone could ultimately provide a source of U to the

overlying water column; however, the subsequent removal of U directly above this release zone prevents it from being the dominant source.

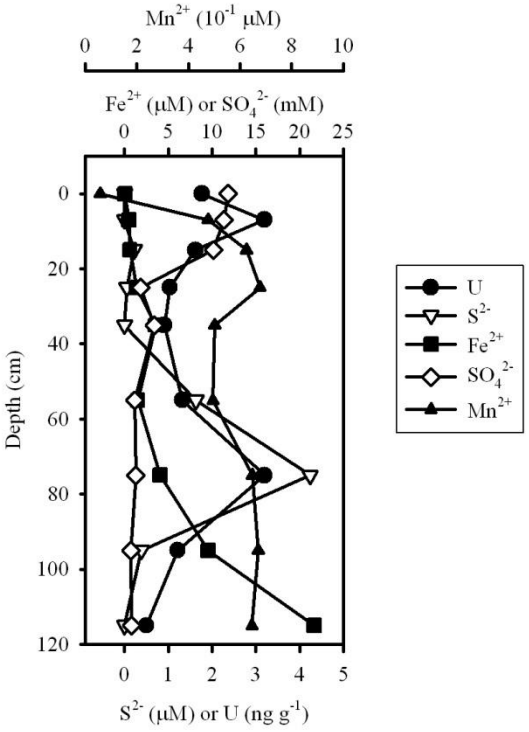

Figure 4.12. Vertical distribution of dissolved U, S^{2-}, Fe^{2+}, SO_4^{2-}, and Mn^{2+} obtained from EGN-20 during the Sep-05 sampling trip. Sulfide, iron, sulfate and manganese data are from Roy (in prep); speciation studies were not conducted and the oxidation state is assumed in this figure.

While the majority of U data supports a net source of U to the lagoon from the subterranean estuary/submarine aquifer complex, the implied removal of U seaward of the lateral mixing zone (22.5 and 30 m offshore) cannot be disregarded in the cycling of U in these systems (Figure 4.4A). The following characteristics were observed in these samples: 1) all UAR are bracketed by the lagoon water and secular equilibrium (UAR = 1.00), 2) all pore water U concentrations are less than the surface water concentrations, and 3) less than 50% of pore water U can be explained by ideal mixing between surface water and saline groundwater end-members (Figure 4.13). Assuming recharged lagoon water is the source of this saline groundwater, the first observation (diluted UAR with respect to lagoon water) disagrees with the redox front

model proposed by Osmond and Cowart (1976) where groundwater samples beyond a redox front (reduced conditions) are generally characterized by low U concentrations and high UAR. While a decrease in U concentration is observed, most UAR tend towards secular equilibrium which can only be explained by either mixing with a lower UAR solution, decay of ^{234}U, or

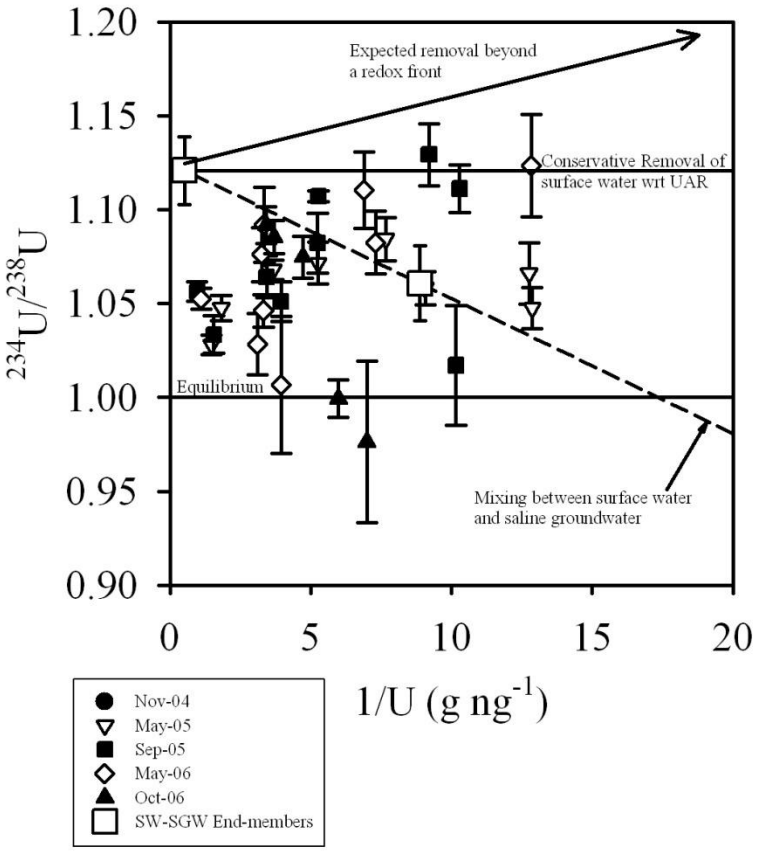

Figure 4.13. Plot of inverse U concentration (1/U) and $^{234}U/^{238}U$ activity ratio (UAR) for pore water/groundwater samples suggesting the subterranean estuary was removing U relative to the surface water. Also shown, as indicated by labels in figure, are lines showing conservative mixing between surface water and saline groundwater (dash line); conservative removal of surface water U with no affect on UAR (solid horizontal line with UAR = 1.13); the equilibrium ratio between ^{234}U and ^{238}U (solid horizontal line with UAR = 1.00); the expected removal behavior for samples collected beyond a redox front (i.e. in more reducing conditions; solid arrow).

samples deviate from the ideal mixing curve, simple mixing does not appear to be a reasonable mechanism. Also, the recirculation of lagoon water operates on much shorter time-scales than the half-life ^{234}U. Thus, the most probable mechanism for the dilution of UAR observed in most

of the pore waters is the dissolution or leaching of aquifer matrix with a lower UAR. This implies that these samples may not reflect active removal of U within the subterranean estuary but rather the slow weathering of the aquifer matrix by more reduced, recirculated lagoon water. Not to discount the apparent observation that U is being removed relative to the surface water, but the subterranean estuary (as defined by mixing between fresh and saline waters in a coastal aquifer) does not appear to be the site of removal. Thus, removal occurs seaward of the mixing zone where surface water is recharged to the aquifer. While the subterranean estuary may be easily defined by a lateral transition in salinity, the hydrodynamic processes of these subsurface mixing zones extend far beyond this well-defined interface, and the geochemical processes occurring at this interface reflect a combination of in situ cycling and external (residual) supply.

Cycling of U in the subterranean estuary/submarine aquifer at Indian River Lagoon is controlled by complex physical and (bio)geochemical conditions, with a resulting overall net source of U delivered to the lagoon. Assuming an average fresh groundwater discharge of 23.5 m y^{-1} (Martin et al. 2007; Smith et al. in press) and an average U concentration of 0.54 ng g^{-1} (2.35 μM), the net flux of U from fresh groundwater to the lagoon would be 54 μmol m^{-2} y^{-1}. In comparison, Charette and Sholkovitz (2006) noted the subterranean estuary beneath Waquoit Bay, MA, USA, removed U on the order of 150 μmol m^{-2} y^{-1}. Although both systems are classified as subterranean estuaries, notable differences between these two subterranean estuaries exist. They include salinity structure and its reflection on SGD sources, organic matter content (especially in shallow sediments), iron hydroxide source versus sink for dissolved iron, and local geology; I feel all of these may play a role in whether these mixing environments act as sources or sinks with respect to U.

At Waquoit Bay (see Figure 3 of Charette and Sholkovitz, 2006), the freshwater seepage face occurs landward of the shoreline, which suggests lateral mixing occurs landward of the

shoreline, shallow exchange (30 – 40 cm) between the surface water and the fresh portion of the subterranean estuary is limited, and recirculated seawater is the main component of SGD. In comparison, a fresh groundwater seepage face is present to approximately 20 m offshore at Indian River Lagoon causing the lateral mixing zone to occur between 20 and 30 m offshore and allowing for significant, shallow exchange between the lagoon and the freshwater portion of the subterranean estuary out to 20 m offshore. As suggested earlier, the exposure of sediments to significantly different ionic strength waters may contribute to U cycling. Also, the dark coloration of and organic matter content (greater than 1 %) in the shallow sediments (0 to 35 cmbsf) between 5 and 20 m offshore at Indian River Lagoon suggest organic matter is accumulating. Subsequent oxidation of the organic matter by aerobic or sulfate-reducing bacteria may release U to the pore waters. Such conditions were not reported at Waquoit Bay. Roy et al. (2008) noted that iron (hydr)oxides sediment coatings act as a source of dissolved iron in the Indian River Lagoon subterranean estuary. The release of low activity ratio U at depths between 55 and 95 cmbsf at 20 m offshore supports her observation.

In comparison, Charette et al. (2005) and Charette and Sholkovitz (2006) suggested that iron (hydr)oxides were a sink for dissolved iron, and subsequently U, originating from fresh and saline groundwater. The differences in conclusions regarding U source or sink in the subterranean estuary between Charette and Sholkovitz (2006) study and this study may also lie in the local geology of the two sites. Waquoit Bay is a glacial moraine dominated by poorly sorted, siliclastic sediments associated with glacial transport. The Surficial aquifer beneath Indian River Lagoon is also predominantly siliclastic sediments; however, adjacent inshore regions of the Surficial aquifer are comprised of the Anastasia Formation, an interbedded coquina and quartz sand deposit of Pleistocene age. The slow dissolution of these inshore, carbonate-rich sediments during recharge and seaward flow of fresh groundwater could supply uranium to the

subterranean estuary and the lagoon. However, the low U concentrations at the base of most pore water profiles and the implied reducing character for these waters suggest that any U supplied via groundwater has been removed prior to reaching the seepage face and subterranean estuary. Thus at local to regional scales, the location of the seepage face, fluid sources within the mixing zone and their control on redox conditions, and local geology control whether the subterranean estuary acts as source or sink of U to the coastal ocean.

The question remains to whether SGD and the interaction of the different components of SGD within the subterranean estuary have a significant impact on the global uranium budget. Dunk et al. (2002) estimated that SGD may deliver as much as 9.3×10^6 mol U y^{-1} to the global ocean, which is approximately 22% of the their total "pre-anthropogenic" uranium input. Charette and Sholkovitz (2006) suggested this was probably an overestimate based on their observation that SGD and the subterranean estuary favored U removal not supply. Extrapolating the Waquoit Bay U-removal (-5 nM) via SGD to a global scale, Charette and Sholkovitz (2006) suggested these environments may pose a sink on the order of 20×10^6 mol U y^{-1}. In comparison, extrapolating the U-source (0.54 ng g^{-1} or 2.35 nM) observed Indian River Lagoon to the global scale implies a net input of 9.5×10^6 mol U yr^{-1}. The local and global comparisons between these two studies further reflect the complexity of these dynamic coastal subsurface mixing zones and how different hydrogeologic settings may influence the coastal and global ocean uranium.

Controls on ^{226}Ra Distribution

The observations of sediment-bound and dissolved ^{226}Ra suggest a non-conservative behavior within the subterranean estuary/submarine aquifer complex. Radium (Ra^{2+}) can remain in solution under natural environmental conditions or it can be sorbed to sediment surfaces, co-precipitated with metal-(hydr)oxide surface-coatings, or bound in the mineral lattice (Semkow

1990; Tricca et al. 2001). In surface estuaries, dissolved radium exhibits a non-conservative behavior with respect to salinity between about 10 and 15, resulting in a release of radium from suspended and bottom sediments (Li and Chan 1979; Elsinger and Moore 1980; Elsinger and Moore 1983; Elsinger and Moore 1984; Webster et al. 1994). The general consensus from these studies is radium desorbs or is displaced from sediment surfaces by more favorable or abundant cations (e.g. Na^{+}) found in the higher ionic strength (saline) waters. Gonneea et al. (in press) suggests subterranean estuaries release radium from solid to aqueous phase by three different pathways: 1) weathering/dissolution of Ra-containing minerals; 2) reduction of metal-(hydr)oxides for which Ra has partitioned, and/or 3) surface exchange from negatively charged particles. All of these reaction-types favor radium release and are likely in the subterranean estuary/submarine aquifer complex observed at this site.

Surface exchange reactions are difficult to assess in field studies because the complexity of environmental conditions can easily mask such reactions. Such complications arise from variations in the size, valence state, and bonding character of competitive cations; physiochemical characteristics of the sorbing material (e.g. different types of clays, metal-(hydr)oxide coatings, etc); and solution or fluid chemistry (e.g. pH, Eh, ionic strength) (Krauskopf 1979). With such complications acknowledged, two observations in the presented data set support surface exchange of radium as a mechanism of its release to the pore waters. First, a landward shift in the main ^{226}Ra release zone between May-05 and May-06 coincides with a landward shift in the main lateral (salinity) mixing zone. Second, the observed negative relationship between effective sediment ^{226}Ra ($^{226}Ra_{eff}$) and exchangeable cations suggests these cations have effectively decreased the amount of sorbed ^{226}Ra. Considering a direct analogy to the surface estuary, the ^{226}Ra release could be associated with the exposure of sediments typically restricted to the freshwater portion of this system to higher ionic strength saline

groundwater. The sediments would in turn have exchangeable sites dominated by seawater cations rather than radium. Exposure to higher ionic saline groundwater is likely in the shallow sediments but I cannot determine which process (cation exchange or redox) drives Ra release below about 35 cmbsf.

While radium is strictly a divalent cation, its selective partitioning to redox sensitive metal (hydr)oxides (Krishnaswami et al. 1972; Moore and Reid 1973) causes an apparent redox cycling behavior in systems with strong Eh gradients (Gonneea et al. in press). The positive linear correlations of $^{226}Ra_{eff}$ with total reducible Fe and Mn (hydr)oxides reflects the selective partitioning of Ra to these redox-sensitive metal (hydr)oxides. While the diagenetic processes controlling the formation of these (hydr)oxides is beyond the scope of this study, their presence has a strong influence on the distribution of Ra in the sediments. The subsequent reduction of these (hydr)oxides would release Ra to the pore waters; vertical zonation of total reducible Fe and Mn (hydr)oxides was not observed, complicating which of these two is favoring the radium retention. Dissolved barium (Ba) exhibited a strong linear relationship with dissolved Mn yet lacked significant correlation with dissolved Fe (Roy in prep). Radium has a similar ionic charge (z) to ionic radius (r) ratio (z/r = 1.42) to that of barium (z/r = 1.48) resulting in similar geochemical behavior. In comparison, other alkaline earth metals have a z/r greater than 2 except for strontium, which is 1.76. Radium minerals (e.g. $RaSO_4$, $Ksp = 10^{-10.44}$) however are less soluble than similar barium minerals (e.g. $BaSO_4$, $Ksp = 10^{-9.97}$); therefore, radium tends to co-precipitate with barium minerals instead of forming its own mineral. Thus, it is not surprising that dissolved ^{226}Ra exhibits a similar relationship with dissolved Mn as observed with Ba (from Roy in prep) (Figure 4.13). Therefore, it is redox cycling of Mn not Fe that contributes to the non-conservative behavior of radium. The variability observed in the dissolved ^{226}Ra-Mn data may be attributed to surface exchange reactions described above. As suggested by Gonneea et

al. (in press), the presented data sets show a complex interaction between surface exchange and redox reactions control the behavior of radium in the subterranean estuary; such reactions greatly affect the application of Ra-isotopes as submarine groundwater tracers.

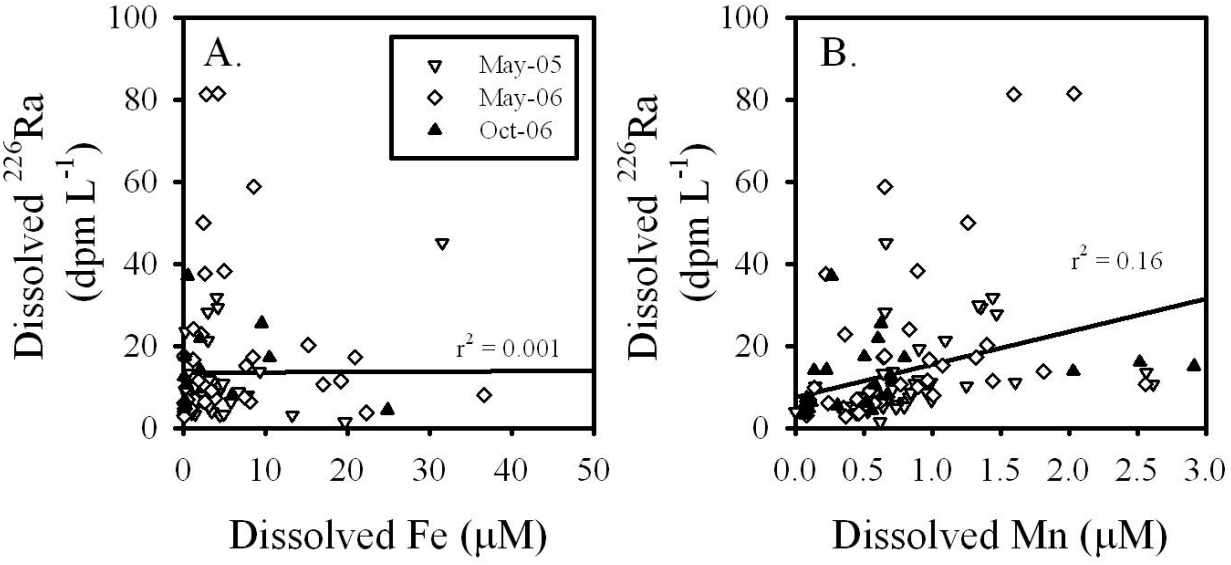

Figure 4.14. Plot showing qualitatively the relationship between dissolved ^{226}Ra and dissolved (A) Fe and (B) Mn. Figure legend is the same for both (A) and (B).

^{222}Rn Sources and Applicability as a Tracer

The applicability of ^{222}Rn as a tracer of benthic exchange and submarine groundwater discharge stems from its conservative behavior and general enrichment in the pore/groundwater relative to overlying surface water. The ^{222}Rn-salinity relationship suggests ^{222}Rn is behaving conservatively across the mid-salinity range (2 – 15) of the Indian River Lagoon subterranean estuary; however, the mixing line established in this salinity range is not consistent with that expected from simple fresh and saline end-member mixing. Burnett et al. (2007) recently reviewed some of the uncertainties in ^{222}Rn as a quantitative tracer for submarine groundwater discharge; they determined the largest uncertainty occurred in the estimation of an end-member activity used to convert radon flux to advective flux. This discrepancy is observed in the ^{222}Rn

data set where variance among ^{222}Rn activity measured in fresh groundwater from the onshore well, measured in fresh groundwater obtained from the offshore portion of the transect, and predicted from the conservative mixing line varied by almost an order of magnitude, which would result in a similar uncertainty in advection rate. The relationship between dissolved ^{222}Rn and E_{Rn} suggests that the spatial distribution of ^{222}Rn results from in situ production in heterogeneously distributed sediment $^{226}Ra_{eff}$ (E_{Rn}) and further, that fresh groundwater accounts for only a small fraction of total ^{222}Rn (~20%). It is common to for emanation to be a major control on ^{222}Rn distribution especially in slow-flowing groundwater systems (Cable et al. 1996; Corbett et al. 2000), the more important consideration is the linkage between factors influencing the distribution of sediment ^{226}Ra and the resulting impact to ^{222}Rn as a tracer. Release of radium is common in the subterranean estuary and its cycling between dissolved and solid phases will affect the distribution of ^{222}Rn.

Temporal Changes in the Subterranean Estuary

Subterranean and surface water salt wedge estuaries share similar structures when salinity is used to outline the systems, and they appear to migrate laterally based on hydraulic gradients driven either by aquifers or rivers. However, biogeochemically the subterranean estuary is more complex and dynamic due to the range in time-scales for flow, geological framework, microbial processes, and longer residence times for pore water transport. Interactions between redox and surface exchange processes affect, both directly and indirectly, the spatial distribution of U, Ra, and Rn, and subsequently, the application of these radionuclides as submarine groundwater tracers. While controls on spatial distributions are important for understanding radionuclide cycling, contrasts in salinity, Eh, U, and Ra between 2005 (May and Sep) and 2006 (May and Oct) also suggest a temporally dynamic subterranean estuary. The mixing zone dynamics respond as the 1) lateral mixing zone migrates landward; 2) subterranean estuary becomes more

oxidizing; 3) ^{226}Ra release zone migrates landward; 4) total pore water U and Ra between 17.5 and 22.5 m offshore increase 89 and 76%, respectively; and 5) total depth-integrated U at the shoreline site increased 550%. Lateral migration and oxidation of the mixing zone are likely driving the U and Ra geochemical behavior we observe between May-05 and May-06. The landward shift in the mixing zone results in Ra and U release offshore due to changes in ionic strength and/or redox potential, while the more oxidizing conditions observed in May-06 relative to May-05 appear to favor U transport at the shoreline site. Insignificant changes in the spatial distribution of ^{222}Rn between 2005 and 2006 are not surprising since the ^{222}Rn distribution is controlled primarily by sediment production. Total dissolved ^{226}Ra in these three sites during May-06 is only about 5% of the average $^{226}Ra_{eff}$ (sediment production rate). It is instructive here to understand the underlying mechanism(s) driving the dynamic responses of the subterranean estuary and the control these processes have on applications of tracers for quantifying groundwater discharge or simply quantifying the elemental flux to coastal waters.

The position of the subterranean estuary represents the hydraulic balance between seaward-flowing fresh groundwater, landward-flowing saline groundwater, and dispersive mixing at the interface of these two water masses. The width of these subterranean estuaries are ultimately determined by heterogeneity in the aquifer (dispersivity) as well as high frequency (waves and tides; Robinson et al. 2007), low frequency (seasonal recharge patterns; Michael et al. 2005), and episodic (storms; Anderson et al. 2005; Smith et al. 2008) variations in fresh groundwater inflow and sea-level. The Indian River Lagoon is a fetch-limited, event-driven system where non-tidal sea-level fluctuations, due primarily to meteorological forcing, are on the order of a 10 to 30 cm. In comparison, astronomical tides at this site are less than 1 cm. No significant meteorological events (i.e. frontal systems) were observed during or a week prior to

the various sampling trips, which indicates such events had little influence on the geochemical framework of the subterranean estuary.

Low frequency seasonal recharge is the primary force driving freshwater toward the shoreline and affects the temporal variability in the lateral position of the freshwater-saltwater interface. According to the steady-state, sharp freshwater-saltwater interface model of Glover (Glover 1959), the width of the seepage face is proportional to total fresh groundwater discharge; therefore, a decrease in recharge and subsequently discharge would cause the subterranean estuary to migrate landward and vice versa. A decrease in discharge would account for changes in the salinity distribution, but it would ultimately favor a more reducing environment created by the longer flow paths to discharge at the seepage face. However a more reducing environment is inconsistent with either Eh or U observations at the shoreline station. Seasonal estimates of total fresh groundwater discharge increase by 20% between May-05 and May-06 (Smith et al, in press). This increase favors a seaward migration of the subterranean estuary based on Glover's model, unless the system experienced some other type of perturbation between the 2005 and 2006 sampling trips.

Intense episodic events (e.g. hurricanes) could account for the transient mixing zone implied by Eh, salinity, and observations in the U and Ra geochemical behavior. Smith et al. (2008) documented a significant salinity perturbation at this site following two tropical cyclones in Oct-05 where fresh groundwater as head gradients were reversed by higher lagoon water levels during hurricane events. The slow rebound of the system back to pre-storm conditions (80 to greater than 160 d) was hypothesized to have lasting effects on the redox and geochemical framework of the subterranean estuary/submarine aquifer complex. The observed temporal and spatial variability in salinity, Eh, U, and Ra between 2005 and 2006 appear support this speculation. However, the question remains how this perturbation directly contributes to these

geochemical observations? Transient effects of the perturbation with respect to salinity are assumed to remain in the system after 200 days, which is slightly longer than predicted by Smith et al. (2008). Accepting this assumption, the more landward position of the lateral mixing zone in May-06 relative to May-05 is the residual effect of the Oct-05 hurricane perturbation, and subsequently, a redox and salinity framework conducive to U and Ra release offshore is present. As for the Eh and shoreline-U observations, two possibilities exist: 1) during the storm-event, the infiltration of lagoon water during storm surge may have introduced dissolved constituents to the fresh water portion of the aquifer, thus producing a residual effect on the redox chemistry (e.g. Anderson et al. 2005); or 2) an increase in discharge during May-06 following the hurricane events resulted in shorter, more oxic flow paths discharging from the shoreline (Smith et al. in press; see chapter 5). It is not possible to distinguish between these two possible explanations, and in fact, it is plausible that both mechanisms influenced the U flux. The temporal behavior of these dissolved constituents clearly reflects the complex and dynamic nature of the subterranean estuary.

Summary

The spatial and temporal complexity of dissolved U, $^{234}U/^{238}U$, ^{226}Ra, and ^{222}Rn is a reflection of the geochemical processes occurring within a subterranean estuary. In general, the freshwater seepage face and subterranean estuary/aquifer complex at Indian River Lagoon, FL, USA, is a net source for all of these radionuclides to the surface lagoon. Surface water and groundwater/pore water U data suggest three potential sources of U to Indian River Lagoon:

1) release during shallow, recirculation of lagoon water into the aquifer;
2) desorption during the reduction of ferric (hydr)oxides and/or oxidation by ferric (hydr)oxides;

3) release and transport due to temporal changes in the redox framework of fresh groundwater portion of the system.

The shallow release zone is the most prominent source of U to the lagoon. The other two release zones occur below a reducing zone, thus restricting their contribution to the net flux from this system. While the data support a net source, recycling of U in the lagoon is observed. Based on $^{234}U/^{238}U$ activity ratios (UARs), removal of U appears to occur seaward of the mixing zone as lagoon water is recharged to the saline portion of the aquifer. Contrasts in the behavior of U between this back-barrier lagoon study and the Waquoit Bay study (Charette and Sholkovitz 2006) demonstrates the presence of a fresh groundwater seepage face, whether iron (hydr)oxides are sources or sinks for dissolved iron, and geology influences whether the subterranean estuary environment is a net source or sink of U to the coastal ocean. This complex U cycling implies the general understanding of the global oceanic U budget with respect to subterranean mixing zones is incomplete.

The behavior of ^{226}Ra in this subterranean estuary is controlled by a complex interaction among surface exchange with seawater cations, redox cycling of Mn, and pre-existing sediment ^{226}Ra. As observed in this study, intrusion of saltwater into a previously freshwater environment and shifts in the redox framework of Mn can release radium to pore waters. The presence of Ra bound to the sediments is also crucial in its distribution in the pore waters. The lack of significant ^{226}Ra input from fresh groundwater suggests sediment ^{226}Ra, primarily surface-bound, is the result of processes unrelated to the presence of the seepage face or subterranean estuary. These observations beg the question "is Ra a reliable tracer for SGD in systems where a fresh groundwater seepage face and subterranean estuary are present?" I conclude no based on the presented data set. Not to discount the numerous studies where SGD rates obtain from Ra-isotope budgets agree well with other measurement techniques, it is that the complexity of this

environment limits Ra applicability as a tracer. In fact, environments where the main source of SGD is from recirculated seawater, the general conservative behavior of radium in high ionic solutions is favorable as a tracer. Also, measuring the dominant sister isotopes of Ra, which was not conducted in this study, may help elucidate some of the processes contributing to its cycling in the subsurface.

Radon-222 has the most conservative behavior in this subterranean estuary; and thus would be the most reliable for the quantitative SGD measurements. As suggested by Burnett et al. (Burnett et al. 2007), the uncertainty in ^{222}Rn as a quantitative tracer for SGD stems for the variability in the activity used to convert radon fluxes to fluid fluxes. In this site, estimates of fresh groundwater ^{222}Rn activities ranged over an order of magnitude; however, this variability was not associated with different water sources but rather with production. Based on the ^{222}Rn pore water activities and emanation rates, less than 20% of the observed ^{222}Rn is supplied by fresh groundwater inputs, while about 80% is emanated from sediment ^{226}Ra. This suggests that the parent isotopes behavior (e.g. ^{226}Ra) in the subterranean estuary can greatly influence the applicability of the daughter isotopes (e.g. ^{222}Rn) as a quantitative tracer.

The utility of these radionuclides in quantitative submarine groundwater studies depends on:

1) redox framework of the subterranean estuary,
2) impact of surface exchange reactions occurring within the subterranean estuary, and
3) the influence of 1) and 2) have on the parent isotopes behavior and distribution in the subterranean estuary/submarine aquifer complex.

Thus, future work applying these radionuclides as quantitative tracers of SGD should acknowledge whether a subterranean estuary is proximal to the site and if so, how the geochemical processes occurring within it may impact the estimated fluxes.

References

Amin, B. S., and Rama. 1986. Using Radon as Probe for Investigating Characteristics of Fractures in Crystalline Minerals. Nuclear Instruments & Methods in Physics Research Section B-Beam Interactions with Materials and Atoms **17:** 527-529.

Anderson, M. S., V. N. R. Jakobsen, and D. Postma. 2005. Geochemical processes and solute transport at the seawater/freshwater interface of a sandy aquifer. Geochimica et Cosmochimica Acta **69:** 3979-3994.

Barnes, C. E., and J. K. Cochran. 1993. Uranium geochemistry in estuarine sediments - controls on removal and release processes. Geochimica Et Cosmochimica Acta **57:** 555-569.

Belanger, T. V., and R. B. Walker. 1990. Ground water seepage in the Indian River Lagoon, Florida, p. 367– 375. Tropical Hydrology and Caribbean Water Resources: Proceedings of the International Symposium on Tropical Hydrology and Fourth Caribbean Islands Water Resources Congress. American Water Resources Association.

Broecker, W. S. 1965. The application of natural radon to problems in ocean circulation, p. 116-145. *In* T. Ichiye [ed.], Symposium on Diffusion in Oceans and Fresh Waters. Lamont-Doherty Geological Observatory.

Broecker, W. S., and T. H. Peng. 1971. Vertical Distribution of Radon in Bomex Area. Earth and Planetary Science Letters **11:** 99-108.

Burnett, W. C., H. Bokuniewicz, M. Huettel, W. S. Moore, and M. Taniguchi. 2003. Groundwater and pore water inputs to the coastal zone. Biogeochemistry **66:** 3-33.

Burnett, W. C., I. R. Santos, Y. Weinstein, P. W. Swarzenski, and B. Herut. 2007. Remaining uncertainties in the use of Rn-222 as a quantitative tracer of submarine groundwater discharge, p. 125-133. *In* W. Sanford, C. Langevin, M. Polemio and P. Povinec [eds.], A New Focus on Groundwater-Seawater Interactions. IAHS Publ.

Cable, J. E., W. C. Burnett, J. P. Chanton, and G. L. Weatherly. 1996. Estimating groundwater discharge into the northeastern Gulf of Mexico using Radon-222. Earth and Planetary Science Letters **144:** 591-604.

Cable, J. E., J. B. Martin, P. W. Swarzenski, M. K. Lindenberg, and J. Steward. 2004. Advection Within Shallow Pore Waters of a Coastal Lagoon, Florida. Ground Water **42:** 1011-1020.

Charette, M. A., and E. R. Sholkovitz. 2002. Oxidative precipitation of groundwater-derived ferrous iron in the subterranean estuary of a coastal bay. Geophysical Research Letters **29:** 85 (81-84).

---. 2006. Trace element cycling in a subterranean estuary: Part 2. Geochemistry of the pore water. Geochimica et Cosmochimica Acta **70:** 811-826.

Charette, M. A., E. R. Sholkovitz, and C. M. Hansel. 2005. Trace element cycling in a subterranean estuary: Part 1. Geochemistry of the permeable sediments. Geochimica et Cosmochimica Acta **69:** 2095-2109.

Chen, J. H., R. L. Edwards, and G. J. Wasserburg. 1986. ^{238}U,^{234}U and^{232}Th in seawater. Earth and Planetary Science Letters **80:** 241-251.

Clark, R. P. 2004. Sebastian Inlet -- Tidal Hydraulic Characteristics. Florida Department of Environmental Protection.

Clesceri, L. S., A. E. Greenberg, and A. D. Eaton [eds.]. 1989. Standard Methods for Examination of Water and Wastewater, 17 ed. American Public Health Association, American Water Works Association, Water Pollution Control Federation.

Cochran, J. K., A. E. Carey, E. R. Sholkovitz, and L. D. Surprenant. 1986. The Geochemistry of Uranium and Thorium in Coastal Marine-Sediments and Sediment Pore Waters. Geochimica Et Cosmochimica Acta **50:** 663-680.

Corbett, D. R., K. Dillon, W. Burnett, and J. Chanton. 2000. Estimating the groundwater contribution into Florida Bay via natural tracers, ^{222} Rn and CH_4. Limnology and oceanography **45:** 1546-1557.

Crotwell, A. M., and W. S. Moore. 2003. Nutrient and radium fluxes from submarine groundwater discharge to Port Royal Sound, South Carolina. Aquatic Geochemistry **9:** 191-208.

Elsinger, R. J., and W. S. Moore. 1980. Ra-226 Behavior in the Pee-Dee River Winyah Bay Estuary. Earth and Planetary Science Letters **48:** 239-249.

---. 1983. Ra-224,Ra-228, and Ra-226 in Winyah Bay and Delaware Bay. Earth and Planetary Science Letters **64:** 430-436.

---. 1984. Ra-226 and Ra-228 in the Mixing Zones of the Pee Dee River-Winyah Bay, Yangtze-River and Delaware Bay Estuaries. Estuarine Coastal and Shelf Science **18:** 601-613.

Folk, R. L. 1974. Petrology of Sedimentary Rocks. Hemphill Publishing Company.

Gascoyne, M. 1992. Geochemistry of the actinides and their daughters, p. 34-61. *In* M. Ivanovich and R. S. Harmon [eds.], Uranium series disequilibrium: applications to Earth, marine, and environmental sciences. Clarendon Press : Oxford, United Kingdom.

Ginder-Vogel, M., C. S. Criddle, and S. Fendorf. 2006. Thermodynamic constraints on the oxidation of biogenic UO2 by Fe(III) (hydr) oxides. Environmental Science & Technology **40:** 3544-3550.

Glover, R. E. 1959. The pattern of fresh-water flow in a coastal aquifer. Journal of Geophysical Research **64:** 457-459.

Gonneea, M. E., P. J. Morris, H. Dulaiova, and M. A. Charette. in press. New perspectives on radium behavior within a subterranean estuary. Marine Chemistry.

Hall, G. E. M., J. E. Vaive, R. Beer, and M. Hoashi. 1996. Selective leaches revisited, with emphasis on the amorphous Fe oxyhydroxide phase extraction. Journal of Geochemical Exploration **56:** 59-78.

Hammond, D. E., and C. Fuller. 1979. The use of Radon-222 to estimate benthic exchange and atmospheric exchange rates in San Francisco Bay. San Fransisco Bay: The Urbanized Estuary **The Pacific Division of the American Association for the Advancement of Science:** 213-229.

Hartl, K. 2006. Facies distribution and hydraulic conductivity of lagoonal sediments in a Holocene transgressive barrier island sequence, Indian River Lagoon, Florida. M.S. University of Florida.

Horwitz, E. P., M. L. Dietz, R. Chiarizia, and H. Diamond. 1992. Separation and preconcentration of uranium from acidic media by extraction chromatography. Analytica Chimica Acta **266**: 25-37.

Johannes, R. E. 1980. The ecological significance of the submarine discharge of groundwater. Marine Ecology Progress Series **3:** 363-373.

Key, R. M., R. F. Stallard, W. S. Moore, and J. L. Sarmiento. 1985. Distribution and Flux of Ra-226 and Ra-228 in the Amazon River Estuary. J Geophys Res-Oceans **90:** 6995-7004.

Krauskopf, K. B. 1979. Introduction to Geochemistry, 2nd ed. McGraw-Hill, Inc.

Krishnaswami, S., D. Lal, Somayaju.Bl, Stonecip.Sa, F. S. Dixon, and H. Craig. 1972. Silicon, radium, thorium, and lead in seawater - in-situ extraction by synthetic fibre. Earth and Planetary Science Letters **16:** 84-90.

Langmuir, D. 1978. Uranium solution-mineral equilibria at low-temperatures with applications to sedimentary ore-deposits. Geochimica Et Cosmochimica Acta **42:** 547-569.

Lemire, R. J. 1988. Effects of high ionic strength groundwaters on calculated equilibrium concentrations in the uranium-water system. Atomic Energy of Canada, Ltd.

Li, Y. H., and L. H. Chan. 1979. Desorption of Ba and Ra-226 from River-Borne Sediments in the Hudson Estuary. Earth and Planetary Science Letters **43:** 343-350.

Martens, C. S., G. W. Kipphut, and J. V. Klump. 1980. Sediment-water chemical exchange in the coastal zone traced by in situ Radon-222 flux measurements. Science **208:** 285-288.

Martin, J. B., J. E. Cable, J. Jaeger, K. Hartl, and C. G. Smith. 2006. Thermal and chemical evidence for rapid water exchange across the sediment-water interface by bioirrigation in the Indian River Lagoon, Florida. Limnology and Oceanography **51:** 1332-1341.

Martin, J. B., J. E. Cable, C. Smith, M. Roy, and J. Cherrier. 2007. Magnitudes of submarine groundwater discharge from marine and terrestrial sources: Indian River Lagoon, Florida. Water Resources Research **43:** -.

Martin, J. B., J. E. Cable, P. W. Swarzenski, and M. K. Lindenberg. 2004. Enhanced submarine ground water discharge from mixing of pore water and estuarine water. Ground Water (special Ocean issue) **42:** 1001-1010.

Martin, W. R., and G. T. Banta. 1992. The measurement of sediment irrigation rates: A comparison of the Br^- tracer and $^{222}Rn/^{226}Ra$ disequilibrium techniques. Journal of Marine Research **50:** 125-154.

Mathieu, G., P. Biscayne, R. Lupton, and D. E. Hammond. 1988. System for measurement of ^{222}Rn at low level in natural waters. Health Physics **55:** 989-992.

Mckee, B. A., D. J. Demaster, and C. A. Nittrouer. 1987. Uranium Geochemistry on the Amazon Shelf - Evidence for Uranium Release from Bottom Sediments. Geochimica Et Cosmochimica Acta **51:** 2779-2786.

Mckelvey, V. E., D. L. Everhart, and R. M. Garrels. 1955. Origin of uranium deposits. Economic Geology and the Bulletin of the Society of Economic Geologists **50:** Pages: 464-533.

Michael, H. A., A. E. Mulligan, and C. F. Harvey. 2005. Seasonal oscillations in water exchange between aquifers and the coastal ocean. Nature **436:** 1145-1148.

Moore, W. S. 1996. Large groundwater inputs to coastal waters revealed by Ra-226 enrichments. Nature **380:** 612-614.

---. 1999. The subterranean estuary: a reaction zone of ground water and sea water. Marine Chemistry **65:** 111-125.

Moore, W. S., and D. F. Reid. 1973. Extraction of Radium from Natural-Waters Using Manganese-Impregnated Acrylic Fibers. Journal of Geophysical Research **78:** 8880-8886.

Osmond, J. K., and J. B. Cowart. 1976. The theory and uses of natural uranium isotopic variations in hydrology. Atomic Energy Review **144:** 621-679.

Pandit, A., and C. C. El-Khazen. 1990. Groundwater seepage into the Indian River Lagoon at Port St. Lucie. Florida Scientist **53:** 169-179.

Peech, M., L. T. Alexander, L. A. Dean, and J. F. Reed. 1947. Methods of soil analysis for soil fertility investigations, p. 25. *In* U. C. 757 [ed.].

Peng, T. H., W. S. Broecker, G. G. Mathieu, and Y. H. Li. 1979. Radon Evasion Rates in the Atlantic and Pacific Oceans as Determined During the GEOSECS Program. Journal of Geophysical Research-Oceans and Atmosphere **84:** 2471-2486.

Robinson, C., L. Li, and D. A. Barry. 2007. Effect of tidal forcing on a subterranean estuary. Advances in Water Resources **30:** 851-865.

Roy, M. in prep. Iron and Manganese diagenesis in the seepage face: An indicator of Submarine Groundwater Discharge-A case study from Indian River Lagoon, Florida. Dissertation. University of Florida.

Roy, M., J. B. Martin, J. E. Cable, J. Cherrier, C. G. Smith, and A. Dorsett. 2008. Flow paths of submarine groundwater discharge (SGD) and its relation to Fe diagensis: A case sutdy from Indian River Lagoon, Florida. AGU Joint Assembly.

Sani, R. K., B. M. Peyton, J. E. Amonette, and G. G. Geesey. 2004. Reduction of uranium(VI) under sulfate-reducing conditions in the presence of Fe(III)-(hydr)oxides. Geochimica Et Cosmochimica Acta **68:** 2639-2648.

Sani, R. K., B. M. Peyton, A. Dohnalkova, and J. E. Amonette. 2005. Reoxidation of reduced uranium with iron(III) (hydr)oxides under sulfate-reducing conditions. Environmental Science & Technology **39:** 2059-2066.

Semkow, T. M. 1990. Recoil-emanation theory applied to radon release from mineral grains. Geochimica Et Cosmochimica Acta **54:** 425-440.

Semkow, T. M., and P. P. Parekh. 1990. The Role of Radium Distribution and Porosity in Radon Emanation from Solids. Geophysical Research Letters **17:** 837-840.

Smith, A. J. 2004. Mixed convection and density-dependent seawater circulation in coastal aquifers. Water Resources Research **40**.

Smith, C. G., J. E. Cable, and J. B. Martin. 2008. Episodic high-intensity mixing events in a subterranean estuary: Effects of tropical cyclones. Limnology and Oceanography **53:** 666-674.

Smith, C. G., J. E. Cable, J. B. Martin, and M. Roy. in press. Evaluating the source and seasonality of submarine groundwater discharge using a Radon-222 pore water transport model. Earth and Planetary Science Letters.

Smith, N. P. 1993. Tidal and nontidal flushing of Florida's Indian River Lagoon. Estuaries **16:** 739-746.

Snyder, M., M. Taillefert, and C. Ruppel. 2004. Redox zonation at the saline-influenced boundaries of a permeable surficial aquifer: effects of physical forcing on the biogeochemical cycling of iron and manganese. Journal of Hydrology **296:** 164-178.

Swarzenski, P. W., and M. Baskaran. 2007. Uranium distribution in the coastal waters and pore waters of Tampa Bay, Florida. Marine Chemistry **104:** 43-57.

Taniguchi, M., W. C. Burnett, J. E. Cable, and J. V. Turner. 2002. Investigation of submarine groundwater discharge. Hydrological processes **16:** 2115-2129.

Testa, J. M., M. A. Charette, E. R. Sholkovitz, M. C. Allen, A. Rago, and C. W. Herbold. 2002. Dissolved iron cycling in the subterranean estuary of a coastal bay: Waquoit Bay, Massachusetts. Biological Bulletin **203:** 255-256.

Toth, D. J. 1988. Saltwater intrusion in coastal areas of Volusia, Brevard, and Indian River counties, p. 160. Technical Publication SJ88-1. St. Johns River Water Management District.

Tricca, A., G. J. Wasserburg, D. Porcelli, and M. Baskaran. 2001. The transport of U- and Th-series nuclides in a sandy unconfined aquifer. Geochimica Et Cosmochimica Acta **65:** 1187-1210.

Valiela, I., J. Costa, K. Foreman, J. M. Teal, B. Howes, and D. Aubrey. 1990. Transport of Groundwater-Borne Nutrients from Watersheds and Their Effects on Coastal Waters. Biogeochemistry **10:** 177-197.

Valiela, I., J. M. Teal, S. Volkmann, D. Shafer, and E. J. Carpenter. 1978. Nutrient and particulate fluxes in a salt marsh ecosystem: Tidal Exchanges and inputs by precipitation and groundwater. Limnology and oceanography **23:** 798-812.

Webster, I. T., G. J. Hancock, and A. S. Murray. 1994. Use of radium isotopes to examine pore-water exchange in an estuary. Limnology and Oceanography **39:** 1917-1927.

Windom, H., and F. Niencheski. 2003. Biogeochemical processes in a freshwater-seawater mixing zone in permeable sediments along the coast of Southern Brazil. Marine Chemistry **83:** 121-130.

CHAPTER 5.

EVALUATING THE SOURCE AND SEASONALITY OF SUBMARINE GROUNDWATER DISCHARGE USING A RADON-222 PORE WATER TRANSPORT MODEL

Introduction

Groundwater aquifer systems connect recharge, storativity, transmissivity, and discharge; consequently understanding one or more of these hydrogeologic traits helps us better predict responses to perturbations (Bredehoeft 2007). For example, groundwater discharge to marine coastal regions, typically referred to as submarine groundwater discharge (SGD), can contain both marine and fresh water components, of which the fresh component is significant as a sink from terrestrial aquifers and source to surface waters. The relative fractions of these two components are critical considering approximately 23% of the world's population now lives within 100 km of the coast, stressing regional freshwater resources. This problem will likely be exacerbated considering the alarming predictions for climate change consequences to the hydrologic cycle (IPCC 2007). The marine component of SGD includes deep recirculating seawater and shallow pore water exchange across the sediment-water interface (Burnett et al. 2003; Mulligan and Charette 2006; Martin et al. 2007). Each component has a different geochemistry (i.e., pH, Eh, and ionic strength), and where these waters mix prior to discharging, they form reactive zones known as the "subterranean estuary" (Moore 1999). These dynamic interfaces affect the transport and transformation of dissolved constituents and impose source/sink limitations on the use of geochemical tracers to estimate groundwater discharge to coastal waters (Moore 1999; Gonneea et al. 2008; Dulaiova et al. 2008).

Comparing SGD from coastal aquifers with disparate characteristics requires using a method that is independent of climate and geological variability. Methods used include geochemical tracers (primarily radon and radium isotopes), water budgets, numerical models,

and direct measurements (e.g., seepage meters) and except for the water budget approach, no universal method has been found. The water budget approach has primarily been used to identify fresh submarine groundwater, although recently pore water composition also has been used to separate the components (Martin et al. 2007). When multiple methods are applied at the same site, estimated discharge rates may vary by an order of magnitude or more, likely because each method measures different processes (e.g. Taniguchi et al. 2002; Cable et al. 2004 and references therein). This problem has been studied systematically at several coasts over the past five years (Burnett et al. 2006; Mulligan and Charette 2006; Martin et al. 2007). In these studies, SGD rates estimated from a radon (^{222}Rn) water column mass balance model were similar to those measured with seepage meters and both methods appear to measure total SGD (fresh + marine sources). These studies also showed, however, that SGD rates from radium (Ra) tracers were an order of magnitude lower than estimates from ^{222}Rn mass balance and seepage meters at Waquoit Bay, MA, (Mulligan and Charette 2006), but were one to two orders of magnitude greater than ^{222}Rn mass balance and seepage meter estimates at Donnalucata, Sicily (Burnett et al. 2006). In contrast, radium (Ra), ^{222}Rn, and seepage meter-derived SGD estimates all fell within a narrow range at Cockburn Sound, Australia, and Shelter Island, NY, USA, (Burnett et al. 2006). These discrepancies, and the ubiquitous use of radioisotope tracers, point out the need to better understand how ^{222}Rn and Ra reflect SGD rates.

Radon-222 ($t_{1/2}$ = 3.825 d) has been used effectively in studies of diagenesis in low permeability marginal marine environments (Hammond and Fuller 1979; Martens et al. 1980; Martin and Banta 1992), for air-sea and sediment-water exchange in fully marine environments (Broecker 1965; Broecker and Peng 1971; Peng et al. 1979), and recently to evaluate advective fluxes in higher permeability coastal systems (Cable et al. 1996; Corbett et al. 1997; Corbett et al. 1999). Radon is an excellent tracer, because it is naturally enriched in pore water relative to

surface water, conservative (subject only to weak van der Waal bonds), easily measured at low activities, and production and decay can be measured precisely (Burnett et al. 1996). One problem with using ^{222}Rn as a tracer is that its parent, ^{226}Ra, is an alkaline earth metal and is heterogeneously distributed in sediments, occurring within minerals, on mineral surfaces (e.g. metal oxide coatings), and in solution. It also behaves non-conservatively in systems with strong salinity gradients (Li and Chan 1979; Webster et al. 1995; Hancock et al. 2000) and has been found to readily desorb when sediments are exposed to brackish waters (Webster et al. 1995). Non-conservative Ra behavior also results from its strong affinity for redox sensitive manganese (hydr)oxides (Moore and Reid 1973), causing release (or removal) of Ra in reducing (or oxidizing) environments. Both salinity and redox gradients are common at the seepage face of coastal aquifers (Moore 1999; Charette and Sholkovitz 2006) resulting in the heterogeneous distribution of ^{226}Ra, and consequently ^{222}Rn, complicating their use as tracers of SGD.

The most common ^{222}Rn approach for evaluating SGD is a water column mass balance, which assumes the surface water ^{222}Rn inventory is equivalent to advection of ^{222}Rn from underlying sediments, after correcting for production, decay, atmospheric evasion, lateral or vertical water column transport, and diffusion from surface sediments. The mass balance requires an end-member groundwater ^{222}Rn activity, typically acquired from onshore wells or from pore waters near the sediment-water interface, to convert the radon flux to a fluid flux (Cable et al. 1996; Corbett et al. 1997; Burnett et al. 2003). SGD estimates using onshore groundwater wells imply all SGD is derived from meteoric groundwater, although intercomparison studies suggest ^{222}Rn models often include the marine component. Using onshore groundwater end-members also assumes constant production of ^{222}Rn along a flow path; however, a number of studies have shown that surface-bound ^{226}Ra and subsequently ^{222}Rn emanation vary spatially within coastal submarine aquifers (Dulaiova et al. 2008; Gonneea et al.

2008; Chapter 4 of this document). Depending on the end-member chosen, fluxes calculated from this approach can span several orders of magnitude as a result of heterogeneous distribution of ^{226}Ra across the steep redox and salinity gradients of the seepage face (Burnett and Dulaiova 2003; Dulaiova et al. 2008).

This paper examines temporal and spatial distributions of pore water ^{222}Rn within the subterranean estuary of Indian River Lagoon, Florida (USA), to assess complexities with ^{222}Rn as a SGD tracer and to quantify fresh and marine advective fluxes from the sediments. Indian River Lagoon is a coastal water body where previous research provides a framework for the distribution and magnitudes of marine and terrestrial SGD (Cable et al. 2004; Martin et al. 2004, Martin et al. 2006; Martin et al. 2007; Smith et al. 2008). A one-dimensional transport model, which includes advection, diffusion, non-local exchange, and production/decay, is employed to quantify how groundwater advection and shallow sediment irrigation contribute to observed pore water ^{222}Rn distributions. Monte Carlo simulations are applied in the model to enhance statistical significance of predicted SGD rates. The model allows exploration of the role of non-local exchange in pore water ^{222}Rn distribution and separation of submarine groundwater discharge components.

Materials and Methods

Study Site

The Indian River Lagoon is a back-barrier, micro-tidal lagoon with an average length, width, and depth of 250 km, 3 km and 1.5 m, respectively (Smith 1993). In the field site, the lagoon is underlain by the heterogeneous and anisotropic surficial aquifer, a 30 m thick unit of undifferentiated, Pliocene to Holocene, interbedded coquina, sand, silt, and clay. The upper 3-4 m of the submarine portion of the surficial aquifer is characterized by moderately sorted, fine quartz sand (average d_{50} = 2.5 ϕ) with variable amounts of silt and clay, a mean porosity of

0.37±0.03, and hydraulic conductivities between 10^{-5} and $10^{-3.7}$ m s^{-1}. The sediments are a transitional sequence from a lacustrine or fluvial-influenced, brackish-water environment to the modern back-barrier lagoon (Hartl 2006).

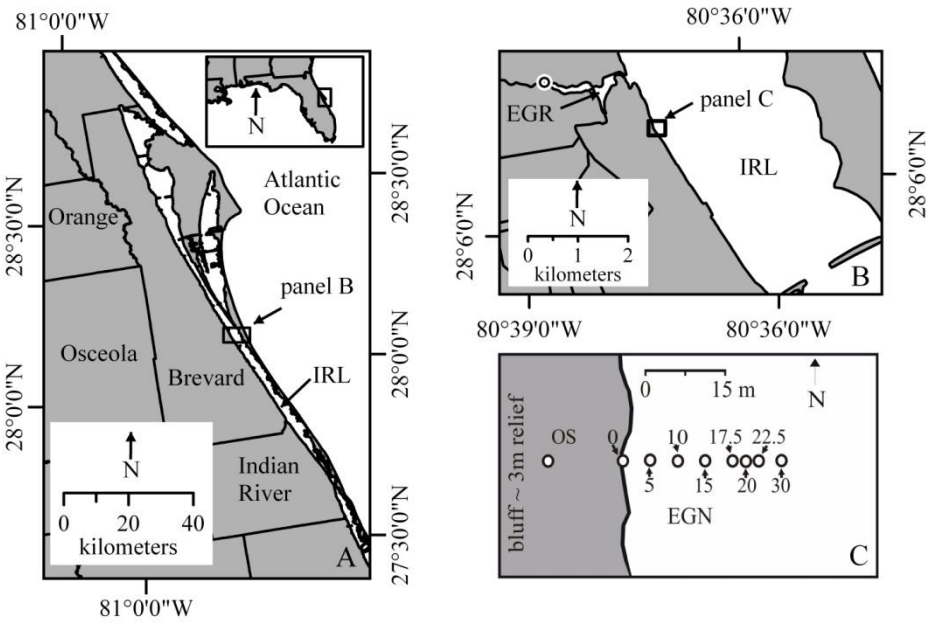

Figure 5.1. Map showing the field site location with respect to Indian River Lagoon (IRL), FL, and surrounding counties (A). Inset in (A) shows the location of the study site relative to the southeastern United States. A local view of the section of IRL where the study was conducted (B) is shown relative to Eau Gallie River (EGR). Plane-view of shore-normal transect of multi-samplers used to collect pore waters is provided in (C).

Methods

Pore water samples were collected from a shore-normal transect along the mainland coast of Florida between Eau Gallie River and Crane Creek (Figure 5.1; Appendix C). The transect extends approximately 30 m offshore into Indian River Lagoon and is comprised of eight multi-level piezometers ("multi-samplers"; Martin et al. 2003). The multi-samplers are between 1.15 m and 2.30 m long and allow discrete sampling at eight port depths (approximately 10 to 40 cm apart) through 200 µm screening. Pore waters were collected from each screened interval slowly (less than 1 L min^{-1}) using a peristaltic pump into an open overflow cup. Dissolved oxygen, pH,

conductivity, and temperature were monitored continuously using a YSI-556 multiprobe sensor until parameter values stabilized; values were recorded and pore waters sampled. Pore waters were collected six times: 20-23 Nov-04, 10-13 Feb-05, 9-12 May-05, and 15-18 Sep-05, 6-8 May-06, and 5-6 Oct-06. Sample nomenclature follows the convention, EGN-XX-MMYY, to differentiate among spatial (XX) and temporal (MMYY) pore water profiles; XX refers to the distance offshore in meters and MMYY refers to the month and year samples were collected.

Fluid from each port depth was sub-sampled for total ^{222}Rn (all trips) and dissolved ^{226}Ra (May-05, Sep-05, May-06, and Oct-06 trips only). Triplicate 10-mL samples of pore water were extracted using a gas-tight glass syringe from the bottom of the overflow cup and slowly injected into 20-mL glass scintillation vials pre-filled with 10 mL of high efficiency mineral oil. Samples were sealed, shipped back to Louisiana State University (LSU) within the mean-life of ^{222}Rn ($^{1}/_{\lambda}$ = 5.5 days), and counted on a Packard Tri-Carb 3100 TR liquid scintillation analyzer with alpha-beta discrimination with a background of 2.8 to 3.5 cpm and calibration factor of 2.69 to 3.23 cpm dpm^{-1} (Clesceri et al. 1989).

Approximately one liter of pore water was collected in plastic bottles for determination of dissolved ^{226}Ra ($t_{1/2}$ = 1620 y). At LSU the water was transferred into air-tight bottles designed for use in the cryogenic radon extraction technique (Mathieu et al. 1988; Cable et al. 1996). Each sample was de-gassed for at least fifty minutes, the bottle was re-sealed, and the sample was set aside to allow a five day ingrowth period for ^{222}Rn with ^{226}Ra. Samples were degassed using a cryogenic extraction line, and after this extraction step ^{222}Rn was transferred to alpha scintillation (Lucas) cells. After a three-hour ingrowth period when short lived daughters, polonium-218 (^{218}Po), polonium-214 (^{214}Po), and bismuth-214 (^{214}Bi) were allowed to equilibrate with ^{222}Rn, the Lucas cells were counted using photomultiplier tubes (Ludlum Instruments, Inc) to a counting error of < 3% (approximately four to six hours).

Sediment supported ^{222}Rn was determined from five vibracores (0, 10, 17.5, 20, and 30 m offshore) collected in May-06. Sediment sections (approximately 4 cm long) were sub-sampled with mid-point depths of 7, 15, 25, 35, 55, 75, 95, 115, 145, 175, 205, and 230 cmbsf, which correspond to the pore water sampling depths. Sediment equilibration batch experiments were performed to quantify radon production rates at depth in the sediments. Each sediment sample (approximately 50 g) was placed in 500 mL Erlenmeyer flasks with approximately 300 ml of pore water of known dissolved ^{226}Ra activity from depths consistent with sediment sample and sealed. Pore waters rather than Ra-free seawater were used to ensure that laboratory batch conditions were similar to environmental conditions (namely ionic strength). Dissolved ^{222}Rn was assumed to equilibrate with sediment-bound ^{226}Ra (primarily surface-bound radium) after a 30-day ingrowth period, and the water was analyzed for ^{222}Rn activities via the extraction and counting procedures described above. The total ^{222}Rn activity in the water, minus its dissolved ^{226}Ra activity, represents the production value for ^{222}Rn in the sediments. The activity per mass of sediment was converted to an equivalent activity per volume of pore water using measured porosity and grain density.

Results

A well defined subterranean estuary extends from the shoreline to approximately 20 to 30 m offshore, as demonstrated by strong lateral and vertical salinity gradients (Figure 5.2A). Pore water salinities range from 0.15 to 23.14 and display a slight temporal variation, while lagoon water salinities, controlled largely by precipitation and evaporation, are brackish (range = 14.01 to 23.47, mean ($\pm 1\sigma$) = 17.17±2.66). The steepest horizontal gradient occurs between 20 and 30 m offshore. Fresh water (salinity < 0.5) occurs 55 cm below the seafloor (bsf) at 0 and 5 m offshore during all sampling trips and at the same depth 10 m offshore during the Nov-04, Feb-05, Sep-05, and May-06 sampling trips. Salinities beyond this point (10 or 15 m) out to 22.5 m

offshore range from 0.7 to 9, reflecting dispersive mixing of fresh and saline groundwater. Steep freshening-downward salinity gradients are observed in pore waters collected from the upper 55 cmbsf at all sampling locations except for EGN-22.5 and -30. At 30 m offshore, salinities range from 17 to 23, freshening upward, suggesting limited transport across the seaward end of the subterranean estuary at 20 to 30 m offshore. These salinity distributions suggest that two distinct pycnoclines occur within the subterranean estuary of Indian River Lagoon. The first is associated with vertical mixing of surface water and groundwater in the upper 55 cmbsf and the second with horizontal mixing of fresh groundwater and deeper saline groundwater between 20 and 30 m offshore.

Total pore water ^{222}Rn activities are inverse of pore water salinity (Figure 5.2A – B). From the shoreline to 20 m offshore, all ^{222}Rn profiles exhibit a concave-downward shape, but beyond 20 m, the profiles display maxima at depths around 150 cmbsf (Figure 5.2B). The highest activities, approximately 8,500 to 10,000 dpm L^{-1}, occur in pore waters at 0 and 5 m and decrease offshore to approximately 2,500 dpm L^{-1} at 30 m. Radon-222 activities display steep vertical gradients within the upper 35 to 55 cm at each sampling location, but below this depth, little change occurs in activity with depth. In the upper 55 cm, vertical gradients average 160 dpm L^{-1} cm^{-1} at the shoreline and 5 m, but decrease steadily offshore from 10 to beyond 15 m. Overall, salinity and radon gradients vary little between sampling trips, with activities from successive sampling trips occurring within error of one another.

Within the subterranean estuary, three possible sources of ^{222}Rn exist: excess radon delivered with groundwater, in situ production from dissolved ^{226}Ra, and emanation from sediment ^{226}Ra. Sediment ^{226}Ra may be sorbed to sediment surfaces, co-precipitated with metal-(hydr)oxide surface-coatings, or bound in the mineral lattice (Semkow 1990; Tricca et al. 2001). These sources are not distinguished in our sediment equilibration batch studies; however, the

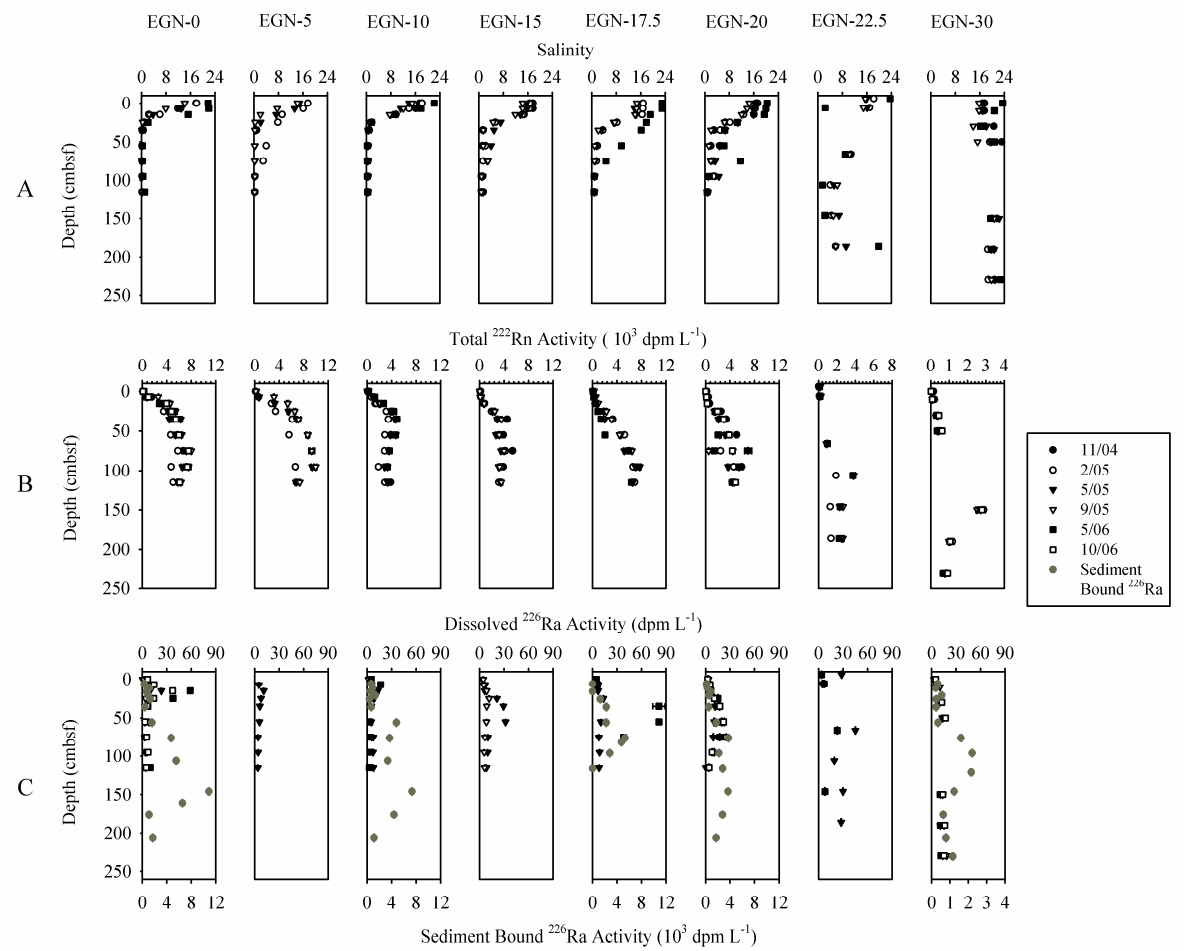

Figure 5.2. Pore water profiles of (A) salinity, (B) total ^{222}Rn, and (C) supported ^{222}Rn (i.e. dissolved and sediment bound ^{226}Ra) from the six sampling trips (Nov-04, Feb-05, May-05, Sep-05, May-06, and Oct-06) plotted vertically against depth and horizontally across the length of the transect (Fig. 5.1C). Note that the units for total ^{222}Rn and sediment bound ^{226}Ra are 10^3 dpm L^{-1} while dissolved ^{226}Ra is in dpm L^{-1}.

short recoil distance of radon (20 to 40 nm) suggests most radon emanation is associated with radium sorbed onto or co-precipitated with surface coatings. Dissolved ^{226}Ra profiles are characterized by mid-depth maxima, which decrease offshore at depths of between 15 and 75 cmbsf (Figure 5.2C). Dissolved ^{226}Ra activities range between 0.56 and 81.54 dpm L^{-1} with a mean of 10.84±23.36 dpm L^{-1} (±1σ). The activity ratio (AR) between pore water ^{222}Rn and the dissolved ^{226}Ra are on the order of hundreds to thousands, implying that dissolved ^{226}Ra has little influence on the distribution of pore water ^{222}Rn.

The vertical distributions of sediment-bound ^{226}Ra are roughly sigmoidal or concave-downward in shape with maximum activities observed between 95 and 150 cmbsf (Figure 5.2C). Similar to the spatial distribution of ^{222}Rn, the activity of sediment-bound ^{226}Ra decreases offshore. The maximum activity at the shoreline is approximately 11,000 dpm L^{-1} (145 cmbsf) while at 30 m offshore, the maximum activity is 2,200 dpm L^{-1} (95 cmbsf). Activity ratios (ARs) between ^{222}Rn and sediment-bound ^{226}Ra range between 0.068 and 14.23 for individual sampling depths with a mean (±1σ) of 2.02±2.22, suggesting that at a single point ^{222}Rn is generally out of equilibrium with the adjacent sediment-bound ^{226}Ra. However, ARs vary vertically with three well defined zones. At depths greater than 55 cmbsf, ARs are near equilibrium and average 1.21±0.46 (±1σ, n=60). While these ARs suggests approximately a 20% disequilibrium between ^{222}Rn and sediment ^{226}Ra, maxima of the sediment-bound ^{226}Ra occur 20 to 40 cm below the maxima of the ^{222}Rn activity indicating upward migration of produced Rn. Activity ratios of the pore water ^{222}Rn and sediment-bound ^{226}Ra maxima range between 0.54 and 2.89 with a mean (±1σ) of 1.34±0.60. EGN-30 (outside the freshwater plume of the subterranean estuary) has the largest ARs between ^{222}Rn and sediment bound ^{226}Ra maxima, with a mean (±1σ) of 2.67±0.18. Excluding EGN-30 from the analysis reduces the range in AR to 0.54 to 1.90 (mean (±1σ) of 1.12±0.25). These AR suggest most pore water ^{222}Rn at the base of the profiles can be explained by in situ sedimentary production within close proximity of the sampled port. The second zone occurs between 15 and 55 cmbsf. Activity ratios average 3.99±2.78 (±1σ, n=60) suggesting ^{222}Rn is in excess of sediment bound ^{226}Ra. The final zone occurs from the sediment-water interface to approximately 15 cmbsf. In this zone, ARs approach equilibrium (mean (±1σ) of 1.20±0.80, n=21). This zonation of radon and sediment bound radium (i.e. AR) suggests heterogeneous production contributes significantly to the distribution of pore water radon and such production must be accounted for in order to accurately use radon as a tracer.

^{222}Rn Transport Model and Model Parameters

Conceptual Model

In Chapter 2, I acknowledged that horizontal flow may be significant in this seepage face and subterranean estuary (i.e. 1:1 to 1:5 horizontal to vertical flow ratio for observations made at 150 and 250 cmbsf). However, horizontal flow would become increasingly negligible as the sediment-water interface is approached. Given the current scale of the model (i.e. less than 115 cmbsf) and these observations concerning flow ratios, a vertical one-dimensional model appears justifiable. Thus, assuming flow vectors along coastal seepage faces are vertically upward (Cooper Jr. et al. 1964) and lateral diffusive transport is negligible due to the stronger vertical gradients of Rn and Ra in the subterranean estuary, ^{222}Rn transport along the groundwater – seawater zone can be conceptualized as a one-dimensional problem in the vertical direction (Figure 5.3).

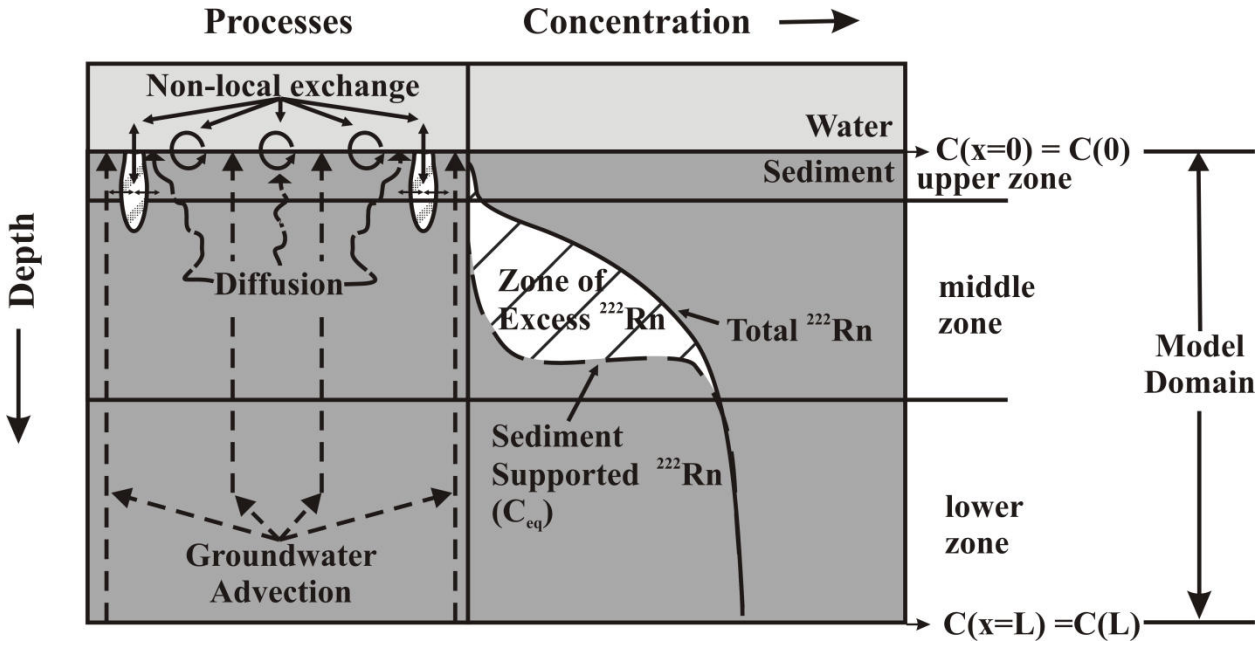

Figure 5.3. Schematic diagram of the conceptual model describing the various processes that occur at and below the sediment water interface.

Based on the activity ratios and radon distribution, the model consists of three zones: (1) a lower zone where ^{222}Rn is near equilibrium with sediment-bound ^{226}Ra suggesting ^{222}Rn transport is balanced by production (AR = 1.21±0.46, n=60); (2) a middle zone where ^{222}Rn is in great excess of sediment-bound ^{226}Ra from transport out of the lower zone into the middle zone (AR = 3.99±2.78, n=60); and (3) an upper zone where a near-vertical concentration gradient and AR approaching equilibrium (suggests that transport processes are effectively exchanging upper layer pore waters with the overlying, ^{222}Rn-depleted water column. This conceptual model highlights the complexity of the subterranean estuary and difficulties in determining submarine groundwater and recirculating seawater fluxes to the water column. In the case of ^{222}Rn, the processes governing its activity along the vertical flow path vary between three primary choices:

Table 5.1. List of constant and fitted parameters, their range and units, for the one-dimensional transport model (*indicates an observed value).

	Description	Range for First Monte Carlo Simulation	Units
Constants	Radon concentration, C	*	atoms cm^{-3}
	Time, t		d
	Depth, z	*	cm
	Sediment diffusion coefficient, D_s	*	cm^2 d^{-1}
	Radon concentration of flushing water, C_{fw}	*	atoms cm^{-3}
	Supported radon concentration, P	*	atoms cm^{-3}
	Radon decay coefficient, λ	0.181	d^{-1}
	Porosity, φ	0.37±0.04	-
Fitted Parameters	Seepage velocity, v	0 – 100	cm d^{-1}
	Depth-dependant mass transfer or irrigation coefficient, $\alpha(z)$		d^{-1}
	Irrigation intensity at z = 0, α_0	10^{-5} – 10^{3}	d^{-1}
	Irrigation depth-attenuation, α_1	0 – 5	cm^{-1}

shallow pore water exchange with the water column, in situ production and transport from depth, and terrestrial groundwater flow. Thus a model which captures only a few of the processes may over-simplify the system and fail to identify either the fluid source or magnitude of flow. We start here by applying a standard one-dimensional transport equation with first-order kinetic reactions and non-local source/sink terms to evaluate this conceptual model of ^{222}Rn

$$\frac{\partial \varphi C}{\partial t} = \frac{\partial}{\partial z}\left(D_s \varphi \frac{\partial C}{\partial z}\right) - \frac{\partial}{\partial z}(v\varphi C) - \alpha(z)\varphi(C - C_{sw}) + \lambda P - \lambda C \qquad (5.1)$$

where φ is porosity (unitless), C is the pore water concentration of ^{222}Rn (atoms cm^{-3}), t is time (d), z is depth (positive downward) (cm), D_s is bulk sedimentary diffusion coefficient (cm^2 d^{-1}), v is seepage velocity (cm d^{-1}), $\alpha(z)$ is a depth-dependant (non-local) mass transfer coefficient (d^{-1}), C_{sw} is the concentration of ^{222}Rn (atoms cm^{-3}) in the flushing water of the upper zone, λ is the decay constant for ^{222}Rn (0.181 d^{-1}), and P is the concentration ^{222}Rn emanated from the sediments (determined by sediment equilibration experiments) and dissolved ^{226}Ra (atoms cm^{-3}; Table 5.1).

The molecular diffusion constant for ^{222}Rn (in water) was estimated from a temperature-dependant equation (Janhne et al. 1987) and corrected for sediment properties by dividing by the tortousity factor obtained from Archie's Law (Boudreau 1997). The average sediment diffusion coefficient for all sampling trips and sites was 0.518±0.086 cm d^{-1}. The effects of hydrodynamic dispersion were not considered in this model under the assumption that diffusion dominates below a Peclet number of about 1 (i.e. Pe = v*d_{50}/D_s, where d_{50} is mean grain size; Bear 1972; Boudreau 1996). Given the average D_s and a mean grain size of 118 μm, advection rates would have to exceed 44 cm d^{-1} for dispersion to become significant. Based on previous estimates of advection rates obtained from seepage meters by Martin et al. (2007) during Sept-05 (less than 23 cm d^{-1}), we did not expect advection rates to exceed the 44 cm d^{-1} limit. In fact, only one

model simulation resulted in advection rates close to this limit (Table 5.2). The primary advective flow is vertical discharge of fresh groundwater, which is assumed to be constant over the model domain. Measured porosity from the sediment cores averaged (±2σ) 0.37±0.05 in the upper 150 cm; thus it was assumed in the model that porosity was constant over the model domain.

Irrigation is a spatially-averaged mixing of pore water with a flushing water (i.e. C(z = 0) = C_{sw} = C_0) caused by biological (bio-irrigation) or physical (e.g., waves and tides) processes (Aller 1977; Boudreau 1984; Meile and Van Cappellen 2003). In this study, irrigation is parameterized as a non-local mass transfer (Boudreau 1984), $\alpha(z)$, and is represented by an exponential depth-dependant irrigation term

$$\alpha(z) = \alpha_0 e^{\alpha_1 z} \quad (5.2)$$

where α_0 is the intensity of irrigation at the sediment water interface (d^{-1}) and α_1 is a depth attenuation coefficient (cm^{-1}). As shown in the conceptual model (Figure 5.3), irrigation, either physical or biological, represents the primary mechanism for which ^{222}Rn is exchanged from the pore waters to surface waters and the near vertical gradients observed near the sediment-water interface. Thus, we consider irrigation a reasonable measure of the magnitude of recirculated or marine SGD on the spatial scale of our study. Other investigators have identified much deeper (>3-10 m depth) recirculation processes, but these recirculation processes are often associated with locations farther offshore or different hydrogeologic regimes (Wilson 2005; Charette and Sholkovitz 2006).

Unlike conservative tracers (e.g. Cl^-, and Br^-), ^{222}Rn is subject to radioactive production and decay, but these sources and sinks are predictable and quantifiable. Previous work has shown ^{222}Rn deficits relative to supported radon in the upper 30 to 40 cm of fine-grained marine sediments (Hammond and Fuller 1979; Martin and Sayles 1987) are caused by diffusion or

Table 5.2. Summary of the input and output parameters for the 33 model runs used in the study.

Sampling Nomenclature	Seepage Velocity, v		Irrig. Intensity, α_0		Irrig. Attenuation α_1		Irrig. Rate v_{irr}	z_{90}	Optimal χ^2
	Optimal	Error	Optimal	Error	Optimal	Error			
	(cm d^{-1})		(d^{-1})		(cm^{-1})		(cm d^{-1})	(cm)	(-)
EGN-0-0205	-28.8	11.5	93.6	46.1	0.218	0.078	95.7	10.0	5
EGN-0-0505	-16.6	2.6	73.1	31.9	0.297	0.103	59.0	7.0	56
EGN-0-0905	-22.0	7.1	7.8	3.1	0.161	0.037	13.2	14.0	183
EGN-0-0506	-42.2	12.9	45.5	14.7	0.147	0.013	85.7	15.0	14
EGN-0-1006	-19.7	3.8	53.0	26.0	0.267	0.126	49.0	8.0	37
EGN-5-0505	-33.6	14.4	24.5	9.5	0.122	0.041	57.1	18.0	12
EGN-5-0905	-29.9	16.1	3.7	1.6	0.082	0.028	13.3	28.0	1
EGN-10-0205	-5.4	1.9	1.0	0.6	0.080	0.049	3.8	28.0	4
EGN-10-0505	-4.0	0.5	3.8	1.8	0.206	0.034	4.8	11.0	23
EGN-10-0905	-3.0	0.7	15.3	7.3	0.476	0.187	6.5	4.0	20
EGN-10-0506	-4.2	0.7	24.3	9.7	0.446	0.659	11.4	5.0	41
EGN-15-1104	-13.1	3.3	15.8	4.6	0.123	0.020	36.4	18.0	88
EGN-15-0205	-11.2	4.0	5.9	2.0	0.076	0.019	23.0	30.0	6
EGN-15-0505	-15.0	6.0	20.4	8.6	0.144	0.032	39.4	16.0	29
EGN-15-0905	-15.6	3.8	22.9	5.8	0.132	0.022	48.9	17.0	102
EGN-17.5-0205	-10.1	3.7	63.4	29.2	0.161	0.026	20.1	14.0	9
EGN-17.5-0505	-6.0	1.5	2.2	0.7	0.082	0.019	7.8	28.0	80
EGN-17.5-0905	-6.5	0.5	6.9	2.7	0.142	0.028	13.4	16.0	15
EGN-17.5-0506	-1.5	0.4	10.6	5.3	0.210	0.042	13.2	10.0	56
EGN-20-1104	-6.9	1.8	24.9	10.5	0.120	0.030	58.9	19.0	783
EGN-20-0205	-6.4	1.6	6.4	2.0	0.121	0.019	15.0	18.0	16
EGN-20-0505	-3.9	0.6	1.9	0.8	0.142	0.024	3.6	16.0	81
EGN-20-0905	-12.6	4.3	15.9	5.1	0.142	0.020	31.1	16.0	142
EGN-20-1006	-12.3	3.2	85.1	36.8	0.185	0.030	123.0	12.0	29
EGN-22.5-0205	-3.2	1.8	2.2	1.2	0.036	0.012	19.0	60.0	0
EGN-22.5-0505	-0.6	0.4	6.4	3.5	0.048	0.017	40.5	47.0	0
EGN-22.5-0905	-3.6	1.2	4.8	1.7	0.040	0.008	36.8	55.0	0
EGN-22.5-0506	-2.1	1.1	2.7	1.4	0.036	0.014	22.5	59.0	0
EGN-30-1104	-7.1	1.1	1.6	0.7	0.035	0.008	14.3	62.0	8
EGN-30-0205	-6.4	2.8	0.3	0.1	0.005	0.005	6.9	99.0	17
EGN-30-0505	-8.7	2.8	0.9	0.3	0.021	0.016	11.7	81.0	5
EGN-30-0905	-8.0	1.8	0.3	0.1	0.005	0.010	5.6	99.0	130
EGN-30-0506	-9.0	1.6	0.6	0.2	0.007	0.004	14.5	98.0	92

mixing of pore water containing elevated ^{222}Rn activities into surface water depleted in ^{222}Rn (Hammond and Fuller 1979). In contrast, our measurements (Figure 5.2) indicate excess radon at these depths, which we attribute to vertically upward advective transport of ^{222}Rn from a lower zone of in situ production (Figure 5.3). Contrasts in these two types of radon profiles indicate differences in the distribution of sediment-bound ^{226}Ra and in dominant transport processes in these environments rather than differences in the chemical behavior of ^{222}Rn. These differences in mean depth-dependent radon production must be included to accurately model pore water distributions and would represent a key improvement over the more widely employed ^{222}Rn water column mass balance model (Cable et al. 1996; Corbett et al. 2000), which neglects heterogeneous ^{226}Ra distributions.

Numerical Solution to the Model

Pore water ^{222}Rn variability was minor between sampling trips, thus allowing a numerical solution to the 1-D transport model (Eqn. 1) for steady-state conditions (Figure 5.2B). A second order, weighted finite difference scheme was used to solve the steady-state version (Fiadeiro and Veronis 1977). This model can handle a number of boundary conditions; we chose to use two Dirichlet boundary conditions: $C(z = 0) = C_0$ and $C(z = L) = C_L$ where L is the base of the model domain and C_L is the concentration (atoms cm^{-3}) at depth L (other parameters were described above).

The multivariate Nelder-Mead simplex minimization algorithm (Lagarias et al. 1998) was used to calibrate the model to observed ^{222}Rn activities using seepage velocity (v) and non-local exchange (α_0 and α_1) as fitting parameters. The following modified χ^2 function was used to test the goodness-of-fit between model and data

$$\chi^2 = \sum_{i=1}^{n} \left(\frac{C_{i,meas} - C_{i,calc}(v, \alpha_0, \alpha_1)}{\sigma_{i,meas}} \right)^2 + t \sum_{i=1}^{n} \left(\frac{C_{i,lim} - C_{i,calc}(v, \alpha_0, \alpha_1)}{\sigma_{i,meas}} \right)^2 \quad (5.3)$$

where C_{meas}, C_{calc} and C_{lim} are the measured, modeled, and the diffusion-only concentration profiles, t is a weighting parameter equal to zero when the parameters do not violate limits imposed or is set to 100 when the parameters fall outside of the limits (Table 5.1). The limits for v, α_0, and α_1 were 0 to -100 cm day^{-1}, 10^3 to 10^{-5} day^{-1}, and 0 to 5 cm^{-1}, respectively. The Nelder-Mead algorithm is sensitive to estimates of the initial fitting parameters and may converge on local minima rather than the desired global minimum. To overcome this sensitivity, an initial Monte Carlo (MC) simulation was performed where the initial parameters were normally-distributed (mean of 0 and standard deviation of 1) pseudorandom perturbations of the mid-point of each fitting parameter limit (i.e. v = -50, $\alpha_0 = 10^{-1}$, and α_1 = 2.5). For each initial-parameter MC simulation, an average of 71.5% of individual runs converged on the same minimum χ^2 and optimal fitting parameters; the remaining 28.5% of evaluations (i.e., local minima) resulted in χ^2 100 to 200% higher than the accepted global minimum.

After optimal fitting parameters were obtained, a Monte Carlo simulation was conducted to place 90% confidence intervals on the parameters given the variance in the measured ^{222}Rn activity. The data were corrupted using the same normally-distributed, pseudorandom number-generating algorithm and twice the standard deviation of ^{222}Rn measurements. Each Monte Carlo simulation consisted of 100 individual model runs calibrated with the Nelder-Mead algorithm. The upper and lower 5% of results were removed to obtain an overall 90% confidence in the estimated parameters. These confidence intervals provide estimates of uncertainty given the natural variability of ^{222}Rn in pore waters.

Model Performance

A total of 39 ^{222}Rn pore water profiles were analyzed using this model to obtain seepage velocity, irrigation intensity, and irrigation attenuation; 33 analyses provided unique and reliable results. The remaining six either converged on non-unique solutions (i.e. inconsistent merit

function χ^2 and/or fitting paramaters) or resulted in unnatural fitting parameters (i.e., negative irrigation intensities or positive seepage velocities) during the first Monte Carlo simulation. It is uncertain why the six model simulations failed; we speculate it had to do with numerous local χ^2 minima in the parameter space. No results are reported for these six model analyses.

The χ^2 fitting criterion used in the model ranges between 1.30×10^{-3} (EGN-22.5-0905 and EGN-22.5-0506) to 783 (EGN-20-1104) with a mean and standard deviation of 63±132 (Table 5.2). Twelve of the 33 calibrated model runs are shown to demonstrate typical model performance (Figure 5.4). These included the maximum (783), minimum (1.3×10^{-3}), approximate mean (63), and approximate median (21) χ^2 results. If these extreme cases (maxima and minima) are removed from the χ^2 data, then the mean and standard deviation of all data are reduced to 46±49, suggesting extreme cases cause much of the variability in model performance.

Steady-state Assumption

To validate the steady-state assumption, four transient-state model simulations were conducted and compared with the steady-state results (Figure 5.5). The following profiles were used in the comparison: EGN-0-0905, EGN-10-0505, EGN-15-0905, and EGN-20-1006. For these simulations, the model was run in a deterministic mode (i.e. no Monte Carlo routines) using the optimal parameters estimated during the respective steady-state simulation. For the transient-state model, two boundary conditions and an initial condition (i.e. one set of initial pore water concentrations) are required for the numerical solution. The same boundary conditions used for the steady-state model were used for the transient model. The concentrations measured during the sampling trip that preceded the actively modeled profile were selected as the initial condition (e.g. concentrations from EGN-0-0505 were used as initial conditions for EGN-0-0905) and the model was run for the length of time (d) between the two sampling trips.

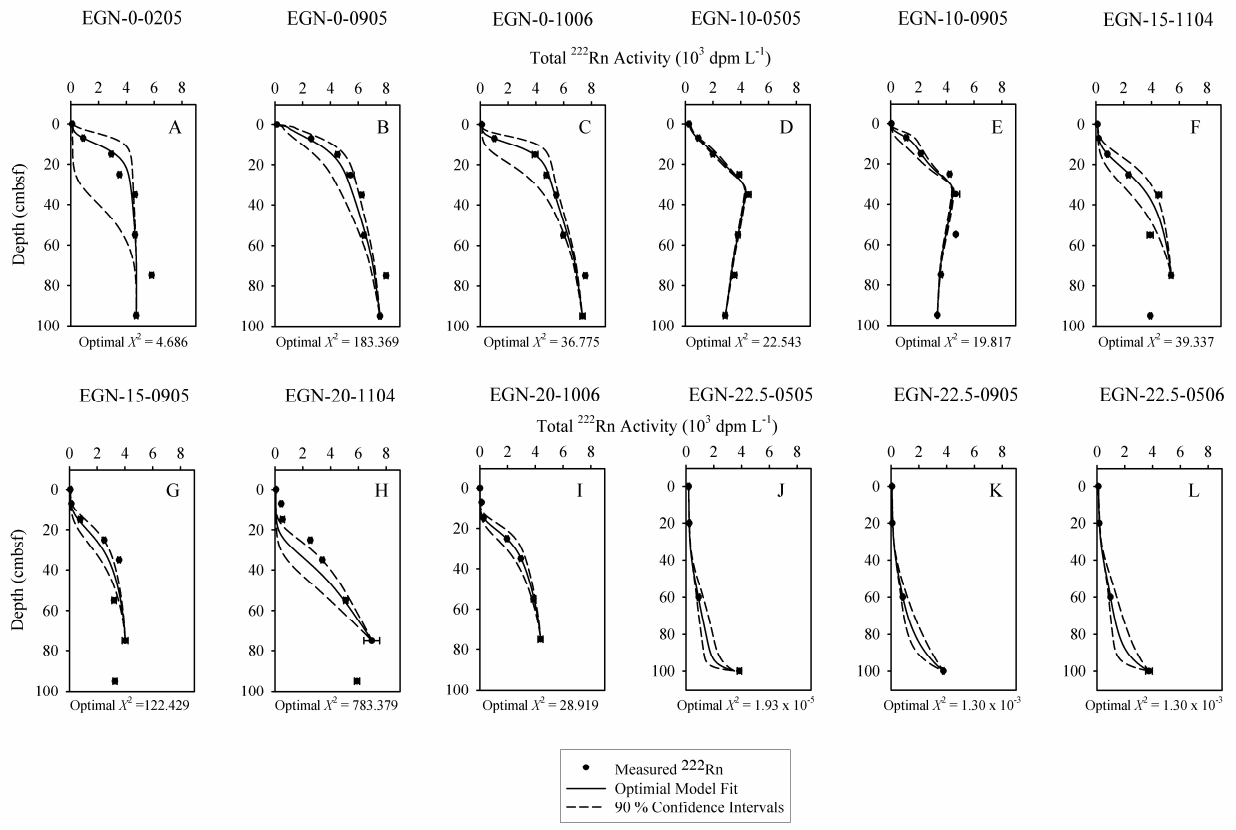

Figure 5.4. Measured and optimal (plus 90% confidence intervals) model predicted ^{222}Rn pore water activities (A – L) for a variety of merit function values including the (H) maximum, (A, J – L) minima, (B, G) mean, and (C – F, I) median.

Visual comparisons between the steady-state and transient-state model results for the four selected profiles show no significant difference (Figure 5.5). The average absolute and relative 2σ for all four simulations are 16 dpm L^{-1} and 0.59%, respectively, suggesting that statistically, the two models are virtually indistinguishable. Physically, the strong similarity between transient- and steady-state models reflects the large difference between time-scale of the concentration fluctuation, governed by the time lapse between sampling trips (82 to 233 d), and the dominate process (i.e. average advection time scale for the model domain is 19.2 d). This suggests that the steady-state assumption is valid given the temporal sampling resolution associated with this study.

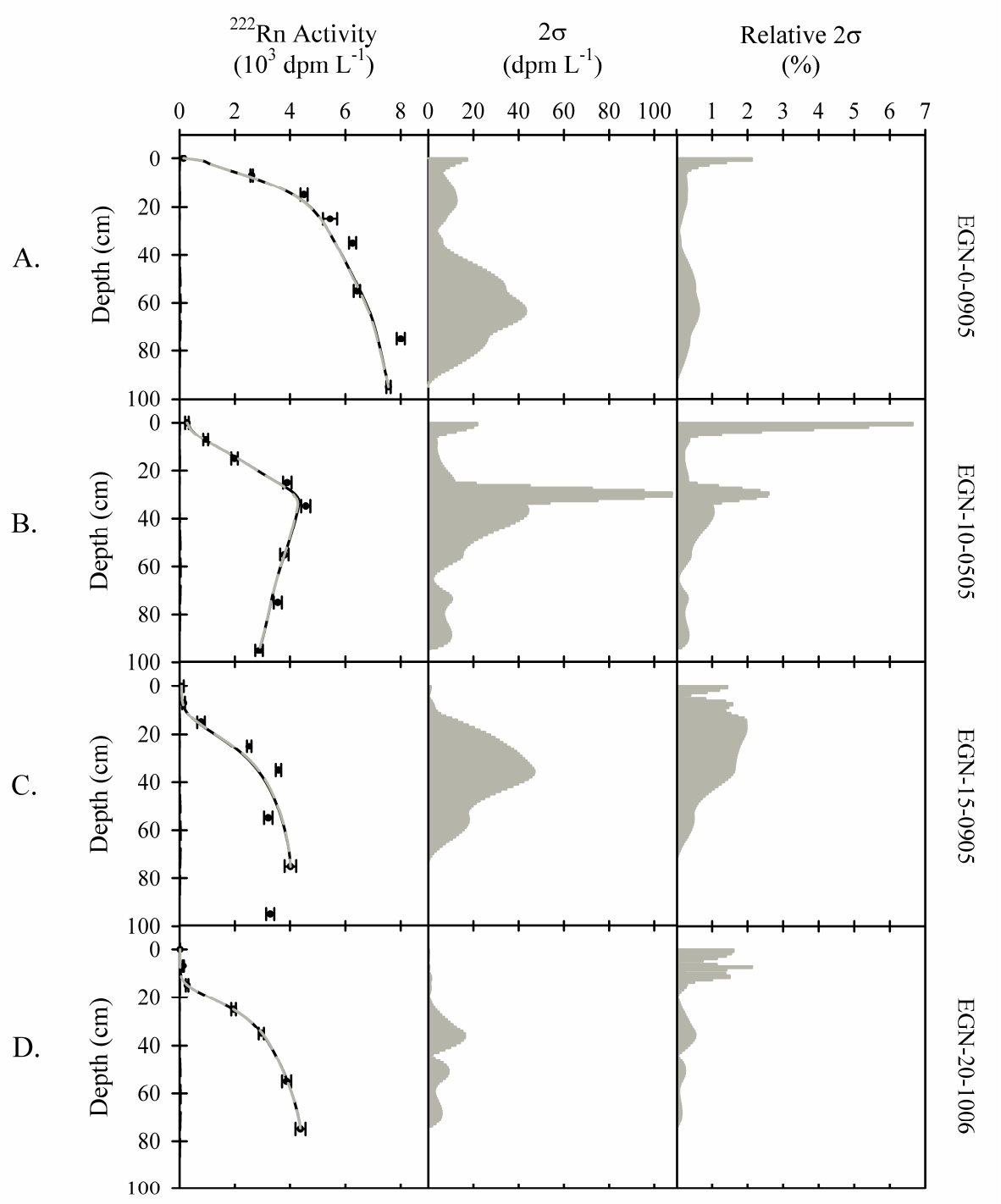

Figure 5.5. A comparison of model results obtained from the steady-state and transient-state simulation for four different pore water profiles: EGN-0-0905 (A), EGN-10-0505 (B), EGN-15-0905 (C), and EGN-20-1006 (D). The first column of graphs shows a qualitative comparison among the measured pore water concentrations, steady-state model results (solid black line), and transient-state model results (dash gray line). The second and third columns show the 2σ error and relative 2σ error, respectively, between the steady-state and transient-state models.

Discussion

Advection Rates

Estimates of submarine groundwater discharge derived from the water column mass balance approach can vary by one to two orders of magnitude at a single site primarily due to uncertainty in the groundwater radon activity needed to convert mass flux to fluid flux, derived either from ground water or pore water activities. Neither of these sources has produced consistently satisfactory SGD fluxes. By including our Ra activities in the 1-D transport model presented here, estimated advection rates vary by less than an order of magnitude and the observed variability can be placed in the context of potential hydrogeologic controls. Seepage velocities decrease with distance offshore (Table 5.2; Figure 5.6), which is consistent with expectations for seepage outflow where vertical head gradients decrease offshore (Glover 1959; McBride and Pfannkuch 1975). At individual sampling sites, the relative standard deviation of seepage velocities is less than 50%, considerably smaller than the one to two orders of magnitude variability observed in water column mass balance studies (Burnett and Dulaiova 2006; Dulaiova et al. 2006; Mulligan and Charette 2006).

Four sampling trips provided sufficient model results to evaluate spatial patterns of the seepage velocities (Figure 5.6). We use both linear and exponential regression models to describe variation in seepage velocities offshore; results are presented only when the regression coefficient (r^2) exceeded 0.50. A linear model was previously applied to pore water Cl^- concentrations and seepage meter data from this site (Martin et al. 2007)

$$v(x) = v_0 - mx \tag{5.4}$$

where $v(x)$ is the seepage velocity at distance x offshore (m), m is the rate of change of the seepage velocity moving offshore (m d^{-1} m^{-1}), and v_0 is the seepage velocity at the shoreline (m d^{-1}). The traditional mode of spatial discharge is exponential where McBride and Pfannkuch

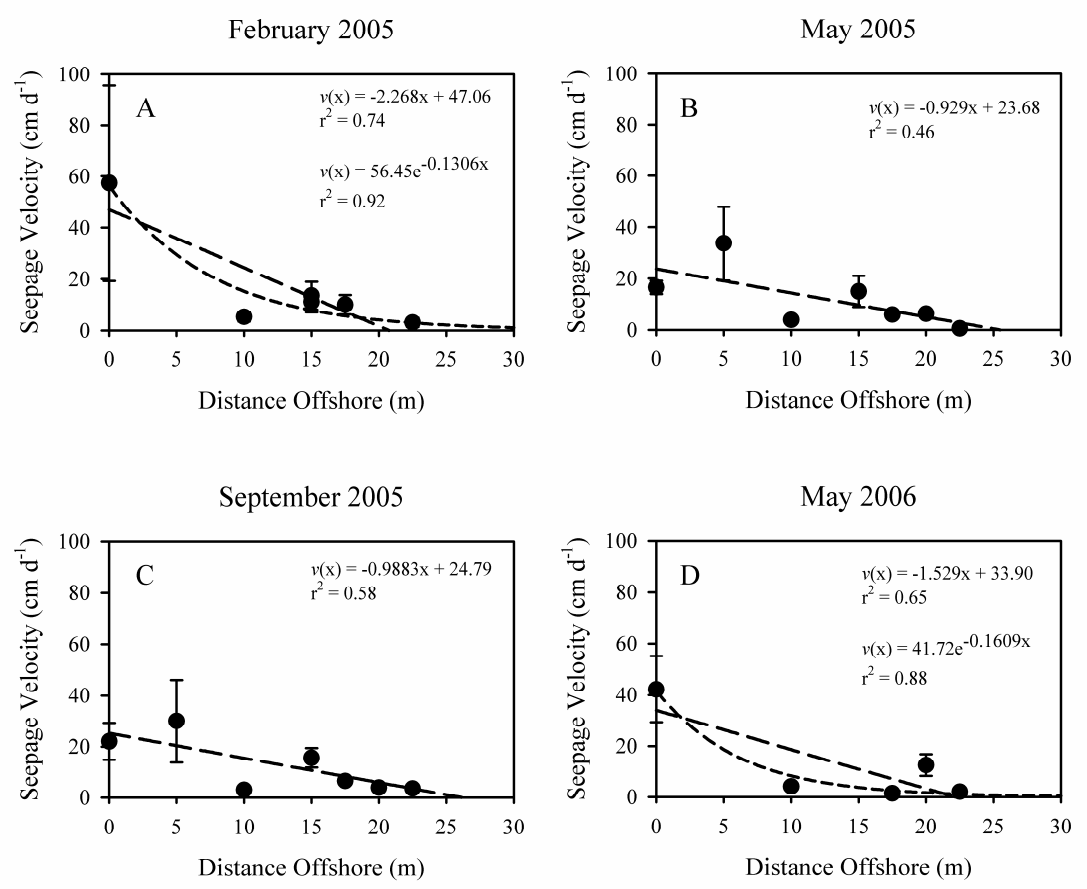

Figure 5.6. Seepage velocities (and 90% confidence interval shown as whiskers) obtained from the ^{222}Rn transport model plotted against distance offshore for the (A) Feb-05, (B) May-05, (C) Sep-05, and (D) May-06 sampling trips. Linear and exponential models are shown as dashed lines. Equations and regression coefficients (r^2) are shown for each model where $v(x)$ is the seepage velocity at x distance offshore.

(1975) showed seepage velocities in lakes conformed to an exponential function

$$v(x) = v_0 e^{-\beta x} \tag{5.5}$$

where β is an attenuation coefficient (m^{-1}) defining the rate at which seepage velocities decreased offshore. One drawback of the exponential model is the suggestion that fresh groundwater seepage extends infinitesimally offshore, which may be possible in an aquifer – lake connection where both water sources are fresh, but not possible in coastal aquifers where denser saline groundwater limits the width of the seepage face. Although this physical restriction exists, empirical exponential models can provide reasonable approximations to lateral changes in

seepage velocities and integrated groundwater fluxes from the seepage face (Lee 1977; Bokuniewicz 1980; Bokuniewicz 1995). One possible explanation to why fresh groundwater discharge decreases linearly offshore in this system rather than exponential may be due to enhanced vertical fresh groundwater advection associated with mixed convection close to the mixing zone. While pore water salinity suggests groundwater discharging out to 20 m is pre-dominantly fresh, mixed convection (i.e. free and forced convection) due to density gradients and variations in hydraulic gradients may enhance vertical discharge of fresh groundwater (Smith 2004). We test both linear and exponential regressions to describe lateral seepage patterns derived from this pore water transport model.

Table 5.3. Comparison of linear and exponential regression analysis of spatial distribution of seepage velocities obtained from the four different sampling trips.

Sampling Period	**Linear Regression**				**Exponential Regression**			
	m (cm d^{-1} m^{-1})	v_0 (cm d^{-1})	r^2	**Q** (m^3 d^{-1} m^{-1} shoreline)	β (m^{-1})	v_0 (cm d^{-1})	r^2	**Q** (m^3 d^{-1} m^{-1} shoreline)
Feb-05	2.27	47.1	0.74	1.59	0.131	56.5	0.92	1.89
May-05	0.929	23.7	0.46	1.16	-	-	-	-
Sep-05	0.988	24.8	0.58	1.19	-	-	-	-
May-06	1.53	33.9	0.65	1.45	0.161	41.7	0.88	1.01

Only the linear regression model provided consistent results (r^2 > ~0.5) for all four sampling trips. Exponential model r^2 values were less than 0.5 for May-05 and Sep-05 but provided statistically more significant fits than the linear model during Feb-05 and May-06 (Table 5.3, Figure 5.6). Based on the linear model, the terminus of freshwater outflow occurs between 20 and 25 m offshore, a location consistent with the measured salinity distribution (Figure 5.2A) and Martin et al. (2007). The differences in the fits between the models appeared

to be related to variations in velocity calculated at EGN-5. These seepage velocities were greater than anywhere else along the transect in May-05 and Sep-05, but lower than at EGN-0 during Feb-05 (Table 5.3; Figure 5.6B – C). Despite these variations, an estimate of total volumetric fresh groundwater discharge per unit length of shoreline, Q ($m^3\ d^{-1}\ m^{-1}$ of shoreline), can be estimated by integrating the regression model, $v(x)$, from the shoreline (0 m) to the terminus of the seepage face (x_t), as defined by the linear model,

$$Q = \frac{\varphi}{100}\int_0^{x_t} v(x)dx \tag{5.6}$$

where φ is average porosity (0.37) across the entire transect, dx is the width over which the function is integrated in meters, and 100 is to convert rates from centimeters to meters. Estimates from equation 6 suggest a 31% decrease between Feb- and May-05, relatively no change between May- and Sep-05, and a 20% increase between Sep-05 and May-06 (Table 5.3). This integrated flux represents the total fresh groundwater available for discharge to the offshore.

Temporal variations in total fresh groundwater discharge are ultimately controlled by changes in certain hydrogeologic characteristics (e.g., recharge, storativity, and extraction). Local recharge via precipitation provides the main source of fresh groundwater to the surficial aquifer. A qualitative comparison between total fresh groundwater discharge from the seepage face and cumulative monthly precipitation from the NOAA station at Melbourne, FL, reveals discharge is out-of-phase with precipitation. Elevated discharge occurs in Feb-05 and May-06 while elevated precipitation occurs Jun-04 to Sep-04 and Aug-05 to Oct-05 (Figure 5.7A). Too few discharge estimates are available to perform a statistical cross-correlation analysis with precipitation, but a qualitative comparison between sampling trip discharge and precipitation reveals a first-order estimate of five to seven month time-lag (Figure 5.7B).

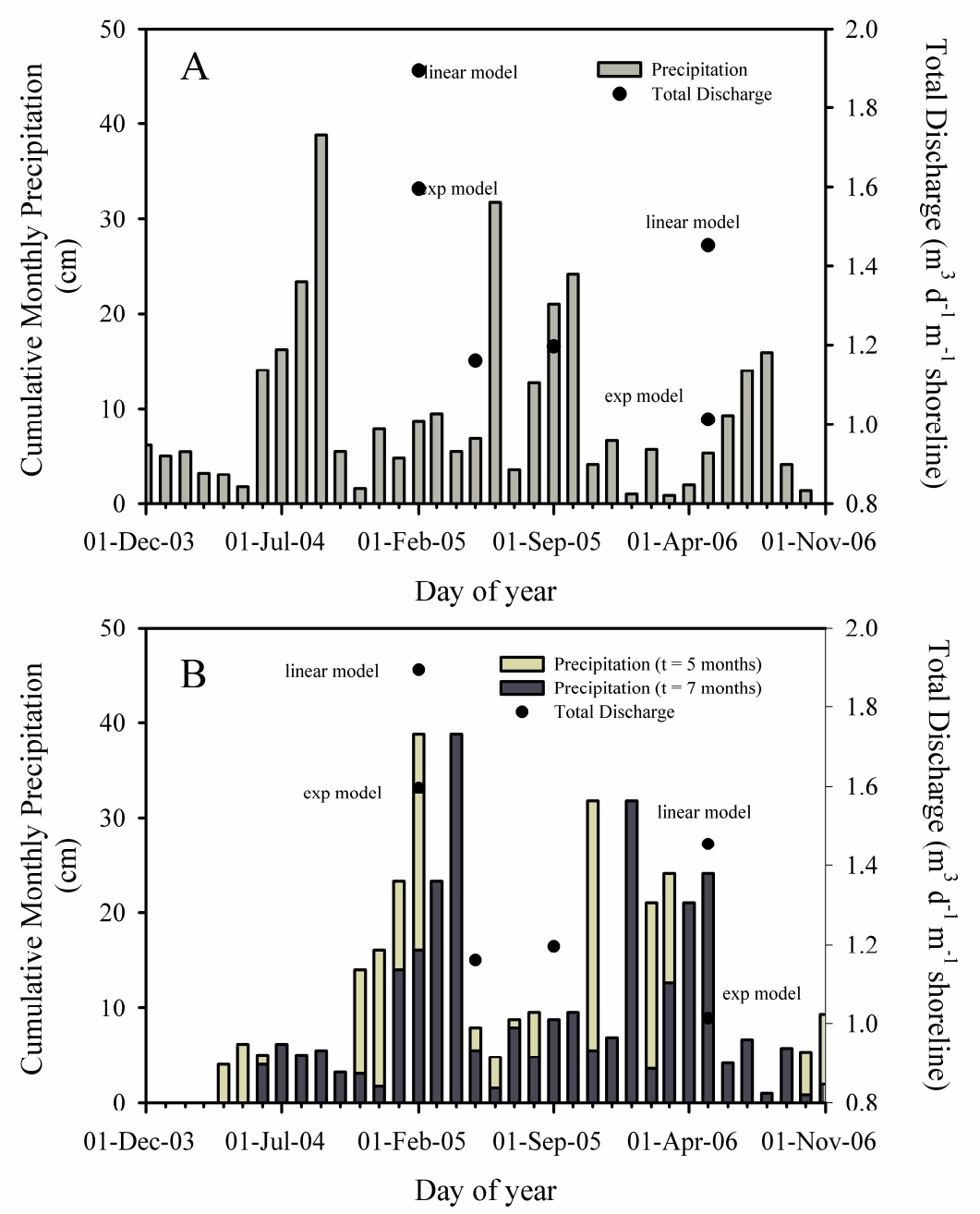

Figure 5.7. (A) Total fresh, groundwater discharge (m^3 d^{-1} m^{-1} of shoreline) and cumulative monthly precipitation (cm) are plotted versus day of year. (B) Same as (A) but with the precipitation data moved forward in time 5 and 7 months (i.e. time lag, τ) to show the similarity between temporal trend in discharge and precipitation; the imposed time lag suggests discharge follows precipitation by 5 to 7 months.

Similar semi-annual lag effects have been observed previously for SGD from coastal surficial aquifers, because the lag incorporates both the time needed for slow transport through unsaturated material and rapid response of the water table and the seepage face to mounded water (Michael et al. 2005; Hu et al. 2006). Michael et al. (2005) showed both fresh and saline groundwater discharge lagged peak recharge periods in Waquoit Bay, MA, by one to five months. Hu et al. (2006) postulated harmful algal blooms (HAB) in 2005 along the west coast of Florida may have resulted from excess recharge and subsequent nitrogen enrichments in SGD from a particularly active hurricane season in the fall of 2004, with a lag time between precipitation and HABs of four to six months. Differences in time lags between our site and other areas likely result from different flow path lengths, aquifer transmissivity, and recharge volume.

Comparison between ^{222}Rn Model Based Advection Rates and Other Techniques

Submarine groundwater discharge to the Indian River Lagoon has been quantified using seepage meters (Belanger and Walker 1990; Martin et al. 2004; Martin et al. 2006; Martin et al. 2007), temperature (Martin et al. 2006), Cl^- (Martin et al. 2004; Martin et al. 2006; Martin et al. 2007), Rn mass balance (Cable et al. 2004; Martin et al. 2006 ; Martin et al. 2007), and hydrologic mass balance or numerical models (Pandit and El-Khazen 1990), and hydraulic gradients (Chapter 2). Technique intercomparisons are often difficult because each method tends to measure different components of submarine groundwater discharge (recirculated seawater or fresh groundwater; e.g., Taniguchi et al. 2002; Cable et al. 2004). Other than the Darcy derived fluxes estimated in Chapter 2, only two other studies have explicitly measured fresh groundwater discharge to Indian River Lagoon (Pandit and El-Khazen 1990; Martin et al. 2007).

Pandit and El-Khazen (1990) used a cross-sectional finite element model to quantify an annual average fresh groundwater discharge from the mainland and barrier island surficial

aquifer to Indian River Lagoon, FL, near St. Lucie Inlet (approximately 100 km south of our field site). They used two general conceptual models: 1) a homogeneous, anisotropic aquifer and 2) a three layer aquifer comprised of an upper sand layer (10 m thick), a middle clay layer (3 m thick), and a sand and shell layer (37 m thick). The models predicted discharge ranging from 0.43 to 2.60 $m^3 d^{-1} m^{-1}$ of shoreline (mean of 1.51 $m^3 d^{-1} m^{-1}$ of shoreline; Pandit and El-Khazen 1990); approximately 95% of this discharge originated from the mainland. These estimates included fluxes from both the mainland and barrier island portion of the Surficial Aquifer; however, the barrier island portion of the aquifer contributed only about 5% of the flow. The lower estimates were obtained from the homogeneous, anisotropic aquifer while higher estimates were obtained from the three layer model. Estimates based on the distribution of ^{222}Rn of 1.01 to 1.89 $m^3 d^{-1} m^{-1}$ of shoreline are in good agreement with those provided by the hydrogeologic model.

Martin et al. (2007) estimated fresh groundwater discharge using seepage meters and Cl^- concentrations. The seepage meter study, which coincided with our Sep-05 ^{222}Rn measurements, demonstrated a linear trend offshore with a total fresh groundwater discharge of 0.9 $m^3 d^{-1} m^{-1}$ of shoreline or approximately 20% less than our estimate using the ^{222}Rn model for Sep-05. These seepage meter data were converted from specific discharge to seepage velocities by dividing by porosity to directly compare advection rates from seepage meters to those of the ^{222}Rn model (Figure 5.8). Because seepage meters are installed in the upper 7 cm of sediments, the shallow sediment porosity of 0.45 is used for this conversion rather than depth-averaged (upper 1 m of sediment) porosity (0.37) used in the ^{222}Rn model. Variability in flow at EGN-5 and lack of data from May-06 limits its use in statistical comparison with seepage meters. Neglecting EGN-5, a compelling relationship is observed ($r^2 = 0.78$, slope = 1.017) between the average seepage velocities from the seepage meters and the ^{222}Rn model (Figure 5.8). A slope of approximately 1

indicates fresh groundwater seepage velocities from the ^{222}Rn model and seepage meters are statistically indistinguishable.

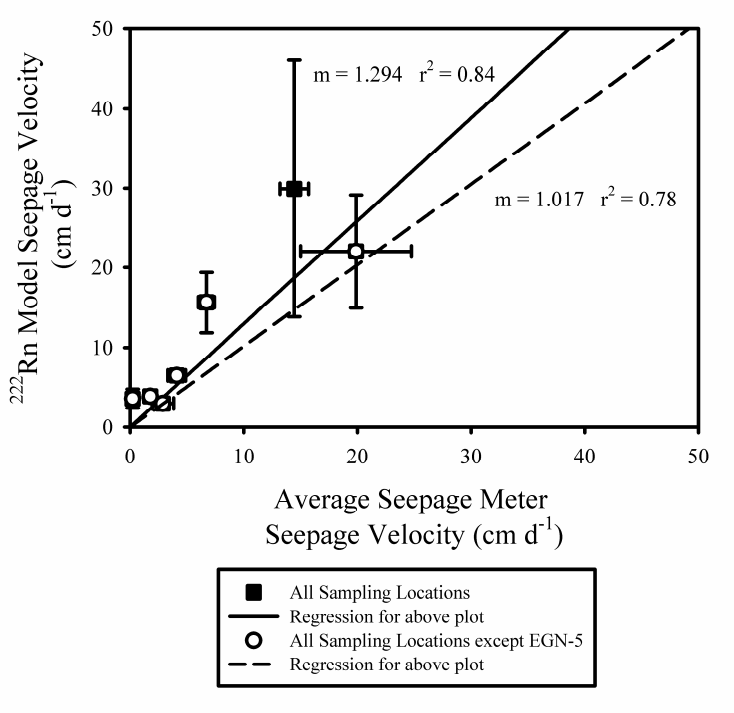

Figure 5.8. Comparison of fresh, groundwater seepage velocities obtained from seepage meters (SM; Martin et al. 2007) and the ^{222}Rn transport model for the Sep-05 sampling trip. SM-16 and -17 refer to the seepage meter measurements made on 16 and 17-Sep-05, respectively. Linear regression between two seepage velocity data sets shows that the radon model is about 50% higher than the seepage meters. However, if only temporally consistent measurements are used (i.e. seepage meter and radon data obtained on the same date, 16 or 17-Sep-05) then the regression is suggests that the radon model is only about 7% higher.

In Chapter 2, I presented specific discharge estimates derived from hydraulic gradients between groundwater and surface water along a piezometer transect. Based on these measurements, discharge from the seabed was generally restricted to the shoreline piezometer; however, the piezometer at 15 m offshore experienced both recharge and discharge. I argued that small head differences between groundwater at 15 m offshore and surface water prevented accurate measurements of the magnitude and direction of discharge at this site. For this reason, I

compare only the seepage velocities/advection rates for the shoreline site. This comparison can be made for the Feb-05, May-05, and Oct-06 sampling trips due to consistent observations from both the radon model and head measurements. The average ($\pm 2\sigma$) Darcy-based seepage velocities for Feb-05, May-05, and Oct-06 are 65.0±11.5, 77.5±10.8, and 55.7±13.8 cm d^{-1}, respectively. The average (with 90 % confidence intervals) radon-based seepage velocities for Feb-05, May-05, and Oct-06 are 28.8±11.5, 16.6±2.6, and 19.7±3.8 cm d^{-1}, respectively. Thus, the Darcy-based advection rates are 2.5 to 5 times higher than those obtained from the radon model. This may seem to be a large discrepancy however Darcy-based estimates are highly sensitive to the vertical hydraulic conductivity (K_v) used in the computation. In Chapter 2, the hydraulic conductivity used for the computation was $10^{-2.3}$ cm sec^{-1} (Hartl, 2006). By reducing the hydraulic conductivity by only a half an order magnitude ($K_v = 10^{-2.8}$ cm sec^{-1}), the Darcy-based advection rates for Feb-05, May-05, and Oct-06 reduce to 20.8±3.7, 24.8±3.5, and 17.8±4.4 cm d^{-1}, respectively, which are within error of the model. Relative to the large variability of hydraulic conductivity observed in natural materials (12 orders of magnitude), a half an order magnitude change is considered negligible in most traditional hydrogeologic studies. Thus, fresh groundwater advection rates and total discharge estimates derived from the radon model are comparable to different measurement techniques; further encouraging radon and radon pore water models to quantitatively tracing fresh submarine groundwater discharge.

Irrigation

Irrigation is a non-local exchange of a dissolved constituent between surface and pore waters which occurs as a bi-directional transfer. Implied fluid exchange is conservative, resulting in a piston-like exchange across the sediment-water interface. Irrigation rates are estimated by integrating the mass transfer coefficient, $\alpha(z)$, over the entire model domain (L) and

reporting the transfer velocity (e.g. irrigation rate), v_{irr} (cm d^{-1}) (Meile et al. 2001; Haese et al. 2006)

$$v_{irr} = \int_0^L \alpha(z)\mathrm{d}z \tag{5.7}$$

Transfer velocities enable us to describe irrigation concisely to compare them with groundwater seepage velocities. This comparison must be made carefully, however, since these rates are driven by different processes.

Irrigation velocities vary significantly with space and time; the complete range of values is from 3.60 to 123 cm d^{-1} (mean $\pm 1\sigma$ = 35.5±32.0 cm d^{-1}; Figure 5.9). Although seepage and irrigation velocities fall within a similar range, the mean irrigation velocity is approximately three times greater than the mean seepage velocity (12.8 cm d^{-1}). These irrigation rates are similar, but slightly lower than previously estimated based on variations in Cl^- concentrations and diurnal temperature variations several hundred meters offshore of our transect (Cable et al. 2004; Martin et al. 2004; Martin et al. 2006). Greater than 90% of the total exchange occurs within the upper 15 to 20 cm (Table 5.2), which is consistent with observations that the upper 15 cm of radon profiles are well mixed. The exception to this generalization is observed at the distal edge of the fresh seepage face (22.5 - 30 m offshore), where 90% of exchange occurs over depths of 47 to 99 cmbsf. The nearshore mixing depth is significantly shallower than the 60 to 70 cm mixing depths found offshore (Cable et al. 2004; Martin et al. 2004; Martin et al. 2006). Greater transfer depths may also reflect deeper biological activity or a lateral dispersive mixing of fresh groundwater and deeper saline groundwater not well-represented in a uni-directional model.

Transfer velocities acquired from individual stations have a high degree of temporal and spatial variability. For example, shoreline irrigation rates (EGN-0) vary by almost an order of magnitude from 13.6 to 95.6 cm d^{-1} while rates from EGN-15 differ by about a factor of two (23

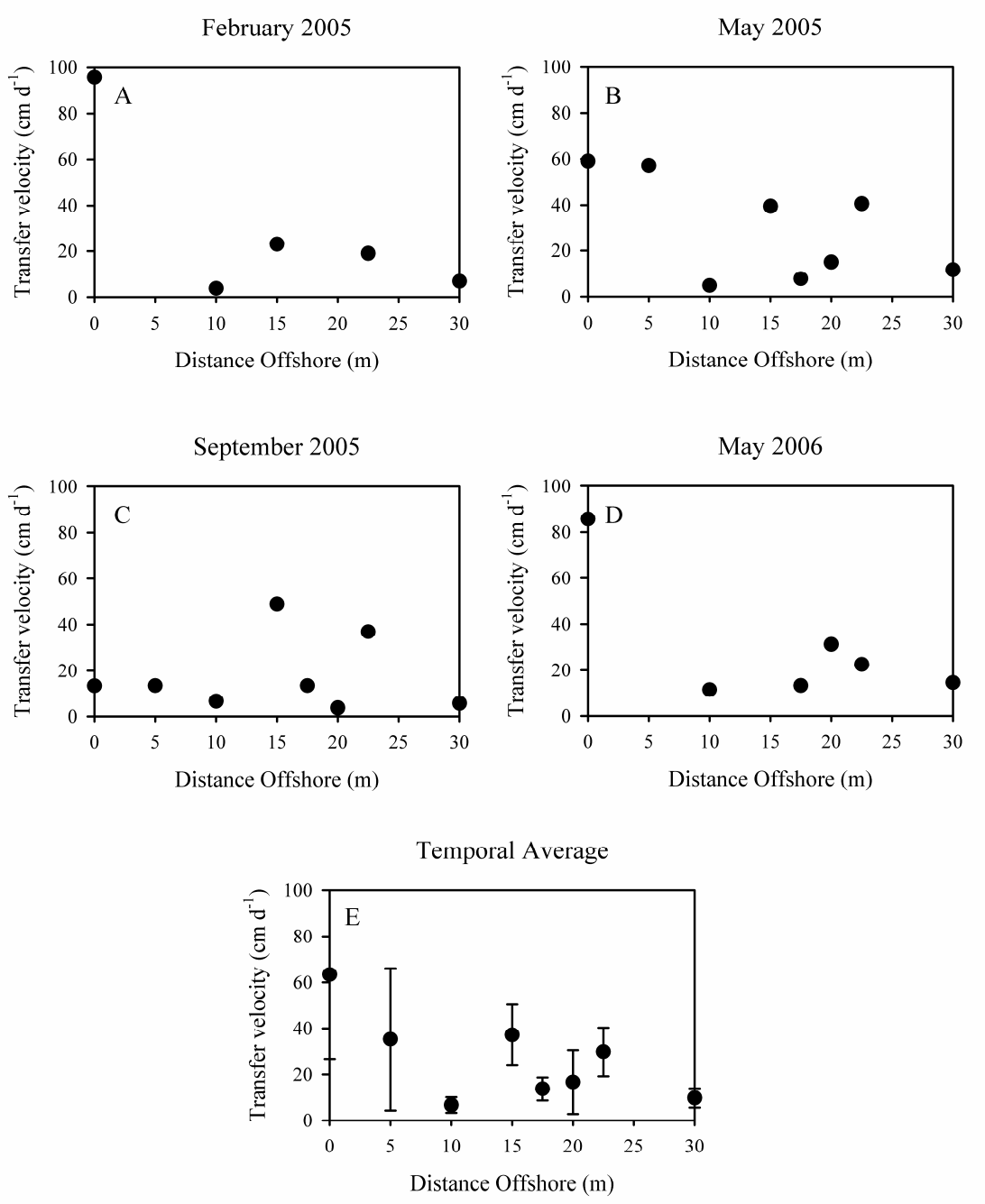

Figure 5.9. Irrigation velocities obtained from the ^{222}Rn transport model plotted against distance offshore for the (A) Feb-05, (B) May-05, (C) Sep-05, and (D) May-06 sampling trips and the (E) temporal average of all sampling trips. Irrigation velocities were computed by integrating the mass transfer coefficient, $\alpha(z)$, over the entire model domain.

and 48.9 cm d^{-1}; Table 5.2). Irrigation velocities show no definite spatial pattern (i.e. linear or exponential); offshore peaks are common 15 to 17.5 m offshore but vary through time so that a pattern is not obvious (Figure 5.9). This lack of any clear trend in irrigation makes it difficult to identify specific biological or physical processes responsible for exchange. Higher rates close to the shoreline (0 and 5 m offshore) and at depths less than 10 cm below the seafloor suggest a physical irrigation by dispersion, convective mixing, or wave pumping over sediment ripples. The steep salinity gradients at these locations (Figure 5.2A) could enhance density-driven convective mixing. In shallow water, the seafloor is often covered with small ripples with approximately 5 to 8 cm wavelengths and 2 to 3 cm amplitudes which can interact with waves to drive mixing to depths generally less than 5 cm within the sediment (Precht and Huettel 2003). Both convection and ripple bed effects are limited in their spatial extent to less than 15 cmbsf, and thus a mechanism is required to drive deeper mixing and cause our observed concentration gradients

Increases in irrigation rates 15 to 17.5 m offshore are speculated to be biologically mediated. The only notable difference between this area and the rest of the transect is a dense seagrass bed. Seagrasses generally have root systems extending less than 5 cm below the sediment-water interface and should not directly contribute to the irrigation, but these marine seagrasses tend to concentrate epi- and infaunal species (Everett 1994; Corona et al. 2000). Fauna would need to irrigate the sediments intensely to maintain a habitable, internal osmotic pressure since the seagrass bed is within the brackish groundwater plume (Figure 5.2A). Beyond this zone (20 to 22.5 m offshore), salinities are elevated closer to the sediment-water interface and thus fauna could irrigate less intensely to maintain internal osmotic pressure (Stanzel and Finelli 2004).

Irrigation may explain the distribution of numerous dissolved pore water constituents in estuarine environments with little to no groundwater flow (e.g., Hammond and Fuller 1979; Martin and Sayles 1987; Martin and Banta 1992). Meile et al. (2001) revisited a few of these studies, applied a non-local mass transfer parameterization for irrigation similar to our model, and reported irrigation velocities for various environments. Their re-calculated transfer velocities varied significantly among various sites with the highest rates, 79.8±78.0 cm d^{-1}, obtained from an intertidal region of Sapelo Island, GA, (Koretsky et al. 2003) and the lowest rates (0.38 cm d^{-1}) obtained from Buzzards Bay, MA (~15 m water depth; Martin and Banta 1992). Hammond et al. (1979) examined radon in pore waters from San Francisco Bay and estimated transfer velocities on the order of 100±50 cm d^{-1} were required to explain the ^{222}Rn deficit relative to ^{226}Ra 20 to 30 cmbsf. These models did not allow for terrestrial groundwater advection, but their irrigation rates are similar in magnitude to ours in Indian River Lagoon.

Calculated irrigation rates reflect shallow recirculation of seawater into and out of the sediments; integrating the irrigation rates using eqn. 6 over the entire seepage face provides a first order estimate of volumetric marine or recirculated submarine groundwater discharge to this portion of the lagoon (i.e. Q_{rsgd}; Table 5.4). Since the spatial distribution of the irrigation rates were not well-represented by a simple analytical expression like that observed for fresh groundwater seepage velocities, eqn. 6 must be solved using a numerical integration. Using this approach, the total flux recirculated seawater into and out of the sediments ranged between 1.69 and 3.43 m^3 d^{-1} m^{-1} of shoreline for the same four consistent sampling trips (Table 5.4). Total SGD is the sum of the fresh groundwater discharge and the marine or recirculated discharge (Table 5.4). It appears recirculated or marine SGD contributes 50 to 70% of the total SGD while fresh groundwater constitutes the remaining 30 to 50%. As with the fresh discharge estimates,

Table 5.4. Comparison between fresh, recirculated/marine, and total SGD as derived from the ^{222}Rn transport model.

Sampling Period	Fresh SGD		Recirculated or Marine SGD	Total SGD	
	Linear Regression	Exponential Regression		Linear Regression	Exponential Regression
	$\mathbf{Q_{fsgd}}$ (m^3 d^{-1} m^{-1} shoreline)	$\mathbf{Q_{fsgd}}$ (m^3 d^{-1} m^{-1} shoreline)	$\mathbf{Q_{rsgd}}$ (m^3 d^{-1} m^{-1} shoreline)	$\mathbf{Q_{sgd}}$ (m^3 d^{-1} m^{-1} shoreline)	$\mathbf{Q_{sgd}}$ (m^3 d^{-1} m^{-1} shoreline)
Feb-05	1.59	1.89	3.43	5.02	5.32
May-05	1.16	-	2.73	3.89	-
Sep-05	1.19	-	1.69	2.88	-
May-06	1.45	1.01	2.52	3.97	3.53
Sep-05 Seepage Meters*	0.91		1.55	2.46	

the ^{222}Rn-model estimates of total SGD and marine SGD agree well with the seepage meter measurements (Martin et al. 2007). The integrated total SGD and marine SGD from the seepage face as measured by the seepage meters is on the order of 2.46 and 1.55 m^3 d^{-1} m^{-1} of shoreline, respectively. These two independent and completely unrelated estimates provide similar estimates for the same processes at the same sampling location, and consequently suggest locations where fresh and marine submarine groundwater discharge contribute to total SGD, ^{222}Rn may be used effectively to quantify each source.

Conclusions

Spatial distributions of pore water ^{222}Rn activities and salinity outline a subterranean estuary at the mainland shoreline of Indian River Lagoon, FL. Distributions of ^{222}Rn within the subterranean estuary are controlled by fresh groundwater inputs and local production from sediment-bound ^{226}Ra. Using a one-dimensional transport model, we quantify spatial variations in average seepage velocities ranging from 24 cm d^{-1} at the shoreline to 2.5 cm d^{-1} at the seepage face edge. This model has advantages over traditional water column mass balance models to

estimate SGD because it incorporates of local production variability from solid phase ^{226}Ra, it reflects fresh groundwater discharge rather than total SGD, and recirculated seawater is described as irrigation or non-local exchange, which is more appropriate in this shallow microtidal lagoon. As a result, seepage estimates are less variable than those obtained from water column mass balance models.

Lags between coastal discharge and inland precipitation events suggest mean residence times of fresh groundwater in the aquifer are 5 to 7 months. Thus, effects of subtropical wet season precipitation are not reflected in offshore groundwater flow for half a year. Modifications in offshore discharge rate may occur between initial recharge and offshore discharge due to droughts or groundwater withdrawal along the flow path.

Seepage velocities obtained from the ^{222}Rn model suggest fresh groundwater inputs decrease linearly to exponentially offshore, with terminus of fresh inputs occurring between 20 and 25 m. Estimated fresh groundwater plume volumes are about 1.01 to 1.89 $m^3\ d^{-1}\ m^{-1}$ of shoreline. These values agree with fresh groundwater fluxes obtained from both seepage meters and numerical models. Inclusion of irrigation allows separation of terrestrial (fresh) and marine components of submarine groundwater discharge. Possible physical and biological processes causing irrigation of sediments include density-dependent convection, dispersion, wave pumping, and bio-irrigation. A single process is unlikely to dominate at any site with their combined effect driving shallow recirculation of lagoon water through sediments.

References

Aller, R. C. 1977. the Influence of Macrobenthos on Chemical Diagenesis of Marine Sediments. Ph.D. Dissertation. Yale University.

Bear, J., 1972. Dynamics of Fluids in Porous Media. American Elsevier Publishing Co., New York, 764 pp.

Belanger, T. V., and R. B. Walker. 1990. Ground water seepage in the Indian River Lagoon, Florida, p. 367– 375. Tropical Hydrology and Caribbean Water Resources: Proceedings of the International Symposium on Tropical Hydrology and Fourth Caribbean Islands Water Resources Congress. American Water Resources Association.

Bokuniewicz, H. 1980. Groundwater Seepage into Great South Bay, New-York. Estuarine and Coastal Marine Science **10:** 437-444.

---. 1992. Analytical descriptions of subaqueous groundwater seepage. Estuaries **15:** 458-464.

Boudreau, B. P. 1984. On the equivalence of nonlocal and radial diffusion models for porewater irrigation. Journal of Marine Research **42:** 731-735.

---. 1997. Diagenetic Models and Their Implementation: Modelling Transport and Reactions in Aquatic Sediments. Springer.

Bredehoeft, J. 2007. It Is the Discharge. Ground Water **45:** 523-523.

Broecker, W. S. 1965. The application of natural radon to problems in ocean circulation, p. 116-145. *In* T. Ichiye [ed.], Symposium on Diffusion in Oceans and Fresh Waters. Lamont-Doherty Geological Observatory.

Broecker, W. S., and T. H. Peng. 1971. Vertical Distribution of Radon in Bomex Area. Earth and Planetary Science Letters **11:** 99-108.

Burnett, W., J. Cable, D. R. Corbett, and J. Chanton. 1996. Tracing groundwater flow into surface waters using natural ^{222}Rn, p. 10. Proceedings of the Groundwater Symposium, Land-Ocean Interactions in the Coastal Zone.

Burnett, W. C., P. K. Aggarwal, A. Aureli, H. Bokuniewicz, J. E. Cable, M. A. Charette, E. Kontar, S. Krupa, K. M. Kulkarni, A. Loveless, W. S. Moore, J. A. Oberdorfer, J. Oliveira, N. Ozyurt, P. Povinec, A. M. G. Privitera, R. Rajar, R. T. Ramassur, J. Scholten, T. Stieglitz, M. Taniguchi, and J. V. Turner. 2006. Quantifying submarine groundwater discharge in the coastal zone via multiple methods. Sci. Total Environ. **367:** 498-543.

Burnett, W. C., H. Bokuniewicz, M. Huettel, W. S. Moore, and M. Taniguchi. 2003. Groundwater and pore water inputs to the coastal zone. Biogeochemistry **66:** 3-33.

Burnett, W. C., and H. Dulaiova. 2003. Estimating the dynamics of groundwater input into the coastal zone via continuous radon-222 measurements. Journal of Environmental Radioactivity **69:** 21-35.

---. 2006. Radon as a tracer of submarine groundwater discharge into a boat basin in Donnalucata, Sicily. Continental Shelf Research **26:** 862-873.

Cable, J. E., W. C. Burnett, J. P. Chanton, and G. L. Weatherly. 1996. Estimating groundwater discharge into the northeastern Gulf of Mexico using Radon-222. Earth and Planetary Science Letters **144:** 591-604.

Cable, J. E., J. B. Martin, P. W. Swarzenski, M. K. Lindenberg, and J. Steward. 2004. Advection Within Shallow Pore Waters of a Coastal Lagoon, Florida. Ground Water **42:** 1011-1020.

Charette, M. A., and E. R. Sholkovitz. 2006. Trace element cycling in a subterranean estuary: Part 2. Geochemistry of the pore water. Geochimica et Cosmochimica Acta **70:** 811-826.

Clesceri, L. S., A. E. Greenberg, and A. D. Eaton [eds.]. 1989. Standard Methods for Examination of Water and Wastewater, 17 ed. American Public Health Association, American Water Works Association, Water Pollution Control Federation.

Cooper Jr., H. H., F. A. Kohout, H. R. Henry, and R. E. Glover. 1964. Sea Water in Coastal Aquifers, p. 84. United State Geological Survey.

Corbett, D. R., W. C. Burnett, P. H. Cable, and S. B. Clark. 1997. Radon tracing of groundwater input into Par Pond, Savannah River Site. Journal of Hydrology **203:** 209-227.

Corbett, D. R., J. Chanton, W. Burnett, K. Dillon, C. Rutkowski, and J. W. Fourqurean. 1999. Patterns of groundwater discharge into Florida Bay. Limnology and Oceanography **44:** 1045-1055.

Corbett, D. R., K. Dillon, W. Burnett, and J. Chanton. 2000. Estimating the groundwater contribution into Florida Bay via natural tracers, ^{222} Rn and CH_4. Limnology and oceanography **45:** 1546-1557.

Corona, A., L. A. Soto, and A. J. Sanchez. 2000. Epibenthic amphipod abundance and predation efficiency of the pink shrimp Farfantepenaeus duorarum (Burkenroad, 1939) in habitats with different physical complexity in a tropical estuarine system. Journal of Experimental Marine Biology and Ecology **253:** 33-48.

Dulaiova, H., W. C. Burnett, J. P. Chanton, W. S. Moore, H. J. Bokuniewicz, M. A. Charette, and E. Sholkovitz. 2006. Assessment of groundwater discharges into West Neck Bay, New York, via natural tracers. Continental Shelf Research **26:** 1971-1983.

Dulaiova, H., M. E. Gonneea, P. B. Henderson, and M. A. Charette. 2008. Geochemical and physical sources of radon variation in a subterranean estuary -- Implications for groundwater radon activities in submarine groundwater discharge studies. Marine Chemistry **110:** 120-127.

Everett, R. A. 1994. Macroalgae in marine soft-sediment communities: effects on benthic faunal assemblages. Journal of Experimental Marine Biology and Ecology **175:** 253-274.

Fiadeiro, M. E., and G. Veronis. 1977. Weighted-Mean Schemes for Finite-Difference Approximation to Advection-Diffusion Equation. Tellus **29:** 512-522.

Glover, R. E. 1959. The pattern of fresh-water flow in a coastal aquifer. Journal of Geophysical Research **64:** 457-459.

Gonneea, M. E., P. J. Morris, H. Dulaiova, and M. A. Charette. 2008. New perspectives on radium behavior within a subterranean estuary. Marine Chemistry **109:** 250-267.

Haese, R. R., C. Hensen, and G. J. De Lange. 2006. Pore water geochemistry of eastern Mediterranean mud volcanoes: Implications for fluid transport and fluid origin. Marine Geology **225:** 191-208.

Hammond, D. E., and C. Fuller. 1979. The use of Radon-222 to estimate benthic exchange and atmospheric exchange rates in San Francisco Bay. San Fransisco Bay: The Urbanized Estuary **The Pacific Division of the American Association for the Advancement of Science:** 213-229.

Hancock, G. J., I. T. Webster, P. W. Ford, and W. S. Moore. 2000. Using Ra isotopes to examine transport processes controlling benthic fluxes into a shallow estuarine lagoon. Geochimica et Cosmochimica Acta **64:** 3685-3699.

Hartl, K. 2006. Facies distribution and hydraulic conductivity of lagoonal sediments in a Holocene transgressive barrier island sequence, Indian River Lagoon, Florida. M.S. University of Florida.

Hu, C. M., F. E. Muller-Karger, and P. W. Swarzenski. 2006. Hurricanes, submarine groundwater discharge, and Florida's red tides. Geophysical Research Letters **33:** 5.

IPCC (Intergovernmental Panel on Climate Change) 2007. *Climate Change 2007: Impacts, Adaptation and Vulnerability. Contribution of Working Group II to the Fourth Assessment Report of the Intergovernmental Panel on Climate Change* [M.L. Parry, O.F. Canziani, J.P. Palutikof, P.J. van der Linden and C.E. Hanson (eds)], p. 976.

Janhne, B., G. Heinz, and W. Dietrich. 1987. Measurement of the diffusion coefficients of sparingly soluble gases in water. Journal of Geophysical Research **92:** 10767-10776.

Koretsky, C. M., C. M. Moore, K. L. Lowe, C. Meile, T. J. Dichristina, and P. Van Cappellen. 2003. Seasonal oscillation of microbial iron and sulfate reduction in saltmarsh sediments (Sapelo Island, GA, USA). Biogeochemistry **64:** 179-203.

Lagarias, J. C., J. A. Reeds, M. H. Wright, and P. E. Wright. 1998. Convergence properties of the Nelder-Mead Simplex Method in Low Dimensions. SIAM Journal of Optimization **9:** 112-147.

Lee, D. R. 1977. A device for measuring seepage flux in lakes and estuaries. Limnology and Oceanography **22:** 140-147.

Li, Y. H., and L. H. Chan. 1979. Desorption of Ba and Ra-226 from River-Borne Sediments in the Hudson Estuary. Earth and Planetary Science Letters **43:** 343-350.

Martens, C. S., G. W. Kipphut, and J. V. Klump. 1980. Sediment-water chemical exchange in the coastal zone traced by in situ Radon-222 flux measurements. Science **208:** 285-288.

Martin, J. B., J. E. Cable, J. Jaeger, K. Hartl, and C. G. Smith. 2006. Thermal and chemical evidence for rapid water exchange across the sediment-water interface by bioirrigation in the Indian River Lagoon, Florida. Limnology and Oceanography **51:** 1332-1341.

Martin, J. B., J. E. Cable, C. Smith, M. Roy, and J. Cherrier. 2007. Magnitudes of submarine groundwater discharge from marine and terrestrial sources: Indian River Lagoon, Florida. Water Resources Research **43:** -.

Martin, J. B., J. E. Cable, P. W. Swarzenski, and M. K. Lindenberg. 2004. Enhanced submarine ground water discharge from mixing of pore water and estuarine water. Ground Water (special Ocean issue) **42:** 1001-1010.

Martin, J. B., K. M. Hartl, D. R. Corbett, P. W. Swarzenski, and J. E. Cable. 2003. A multi-level pore-water sampler for permeable sediments. J. Sediment. Res. **73:** 128-132.

Martin, W. R., and G. T. Banta. 1992. The measurement of sediment irrigation rates: A comparison of the Br^- tracer and $^{222}Rn/^{226}Ra$ disequilibrium techniques. Journal of Marine Research **50:** 125-154.

Martin, W. R., and F. L. Sayles. 1987. Seasonal cycles of particle and solute transport processes in nearshore sediments: $^{222}Rn/^{226}Ra$ and $^{234}Th/^{238}U$ disequilibrium at a site in Buzzards Bay, MA. Geochimica et Cosmochimica Acta **51:** 927-943.

Mathieu, G., P. Biscayne, R. Lupton, and D. E. Hammond. 1988. System for measurement of ^{222}Rn at low level in natural waters. Health Physics **55:** 989-992.

McBride, M. S., and H. O. Pfannkuch. 1975. Distribution of seepage within lakebeds. Journal of Research of the US Geological Survey **3:** 505-512.

Meile, C., C. M. Koretsky, and P. V. Cappellen. 2001. Quantifying bioirrigation in aquatic sediments: an inverse modeling approach. Limnology and Oceanography **46:** 164-177.

Meile, C., and P. Van Cappellen. 2003. Global estimates of enhanced solute transport in marine sediments. Limnology and Oceanography **48:** 777-786.

Michael, H. A., A. E. Mulligan, and C. F. Harvey. 2005. Seasonal oscillations in water exchange between aquifers and the coastal ocean. Nature **436:** 1145-1148.

Moore, W. S. 1999. The subterranean estuary: a reaction zone of ground water and sea water. Marine Chemistry **65:** 111-125.

Moore, W. S., and D. F. Reid. 1973. Extraction of Radium from Natural-Waters Using Manganese-Impregnated Acrylic Fibers. Journal of Geophysical Research **78:** 8880-8886.

Mulligan, A. E., and M. A. Charette. 2006. Intercomparison of submarine groundwater discharge estimates from a sandy unconfined aquifer. Journal of Hydrology **327:** 411-425.

Pandit, A., and C. C. El-Khazen. 1990. Groundwater seepage into the Indian River Lagoon at Port St. Lucie. Florida Scientist **53:** 169-179.

Peng, T. H., W. S. Broecker, G. G. Mathieu, and Y. H. Li. 1979. Radon Evasion Rates in the Atlantic and Pacific Oceans as Determined During the GEOSECS Program. Journal of Geophysical Research-Oceans and Atmosphere **84:** 2471-2486.

Precht, E., and M. Huettel. 2003. Advective pore-water exchange driven by surface gravity waves and its ecological implications. Limnology and Oceanography **48:** 1674-1684.

Semkow, T. M. 1990. Recoil-emanation theory applied to radon release from mineral grains. Geochimica Et Cosmochimica Acta **54:** 425-440.

Smith, A. J. 2004. Mixed convection and density-dependant seawater circulation in coastal aquifers. Water Resources Research **40**: W08309, doi:10.1029/2003WR002977.

Smith, C. G., J. E. Cable, and J. B. Martin. 2008. Episodic high-intensity mixing events in a subterranean estuary: Effects of tropical cyclones. Limnology and Oceanography **53:** 666-674.

Smith, N. P. 1993. Tidal and nontidal flushing of Florida's Indian River Lagoon. Estuaries **16:** 739-746.

Stanzel, C., and C. Finelli. 2004. The effects of temperature and salinity on ventilation behavior of two species of ghost shrimp (Thalassinidea) from the northern Gulf of Mexico: a laboratory study. Journal of Experimental Marine Biology and Ecology **312:** 19-41.

Taniguchi, M., W. C. Burnett, J. E. Cable, and J. V. Turner. 2002. Investigation of submarine groundwater discharge. Hydrological processes **16:** 2115-2129.

Tricca, A., G. J. Wasserburg, D. Porcelli, and M. Baskaran. 2001. The transport of U- and Th-series nuclides in a sandy unconfined aquifer. Geochimica Et Cosmochimica Acta **65:** 1187-1210.

Webster, I. T., G. J. Hancock, and A. S. Murray. 1995. Modelling the effect of salinity on radium desorption from sediments. Geochimica et Cosmochimica Acta **59:** 2469-2476.

Wilson, A. M. 2005. Fresh and saline groundwater discharge to the ocean: A regional perspective. Water Resources Research **41:** W02016, doi: 2010.01029/02004WR003399.

CHAPTER 6.

SUMMARY AND CONCLUSIONS

Studies conducted over the last decade on submarine groundwater discharge have largely focused on the quantification of this input term to coastal water budgets without regard for the source of the benthic fluid. My investigation has taken the step to resolve how fresh groundwater and recirculated seawater mix prior to discharging (submarine groundwater discharge) within the zone known as the subterranean estuary and how this mixing interface varies through time and space. Specifically, I examined how fresh groundwater and recirculated seawater contributed to submarine groundwater discharge to the Indian River Lagoon, Florida, USA, and how the interaction of these distinct water sources within the subterranean estuary altered the spatial and temporal distribution of $^{234, 238}U$, ^{226}Ra, and ^{222}Rn. Submarine groundwater discharge is recognized as any and all water discharged from the continental margin seafloor to the coastal ocean (Burnett et al. 2003). The discharging water may be derived from fresh meteoric groundwater, recirculated seawater, connate water or some combination of these three (Burnett et al. 2003). While SGD has been recognized for some time as being comprised of numerous water sources, not until recently have studies began to identify and quantify both components of SGD (e.g. Mulligan and Charette 2006; Martin et al. 2007).

Rapid response of groundwater head during surface water disturbances suggests a strong hydrologic connection between Indian River Lagoon and the submarine groundwater-aquifer system. Similarities in variance in measured surface and ground water levels and strong linear relationship in the time-domain confirm this strong hydrologic connection. Even with this connection, the hydraulic gradients between groundwater and surface water, and subsequently, the physical flow regime remain fairly constant through time. These gradients indicate fresh groundwater consistently discharges at the shoreline, whereas shifts between recharge of lagoon

water to the aquifer and discharge of brackish water from the aquifer occur at 15 and 30 m offshore. Auto- and cross-spectra for groundwater head and surface water level suggest low frequency periodic forces observed in the surface water propagate into the aquifer with limited attenuation.

Additionally, the strong hydrologic connection between Indian River Lagoon and the submarine groundwater-aquifer system was shown to have a significant impact on the salinity framework of the subterranean estuary during high-intensity episodic events. During the 2005 Atlantic hurricane season, Tropical Storm Tammy and Hurricane Wilma passed over east central Florida and the Indian River Lagoon study site. These events reversed the vertical and horizontal hydraulic gradients, recharged lagoon water into the aquifer, and shifted the seepage face and subterranean estuary landward. The groundwater system took 80 (15 m offshore) to greater than 160 days (30 m offshore) to return to pre-storm conditions, suggesting these episodic events could have long-lasting effects on the (bio)geochemical framework of the subterranean estuary.

As a result, mixing of fresh groundwater, saline groundwater, and surface water within the subterranean estuary creates a complex and dynamic geochemical environment. The spatial and temporal distribution of dissolved $^{234, 238}$U, ^{226}Ra, and ^{222}Rn was shown to be highly dependent on the chemical and geological conditions of the subterranean estuary. The dominant processes affecting the distribution of these radionuclides included active redox cycling of U, desorption or release of ^{226}Ra (due to redox cycling of Mn and surface exchange by seawater cations), and emanation of ^{222}Rn from heterogeneously distributed sediment ^{226}Ra. The redox cycling U within the subterranean estuary resulted in a net flux of U to the system where the primary source of U originated from a shallow release zone. In comparison, a study conducted at Waquoit Bay, MA, suggested that these subsurface mixing zones act as net U sink (e.g. Windom and Niencheski 2003; Charette and Sholkovitz 2006). Contrasts in the salinity structure of these

subterranean estuaries (Brazil, Massachusetts, Florida) reveal the presence or absence of an offshore seepage (i.e. fresh groundwater discharge) and the location of this fresh-salt boundary within the sediments that ultimately controls whether the subterranean estuary will act as source or sink of U to the coastal ocean.

Shared similarities between dissolved ^{226}Ra and U suggests the distribution of dissolved ^{226}Ra was partially controlled by redox cycling. The strong linear relationship between dissolved ^{226}Ra and Mn as well as sediment ^{226}Ra and Mn/Fe hydroxides linked apparent redox behavior to the redox cycling of Mn. However, negative relationships between exchangeable cations and sediment ^{226}Ra suggest exchange processes also influence the distribution of dissolved ^{226}Ra. Since Ra can partition onto and be incorporated into Mn-hydroxides, it was not possible to identify which of these two processes dominates. The sorption of ^{226}Ra to the metal-hydroxides had an apparent affect on the distribution of ^{222}Rn in the subterranean estuary. While ^{222}Rn appeared to be a good qualitative indicator of fresh groundwater inputs to the system (i.e. strong correlation with salinity), the discrepancy between the fresh groundwater ^{222}Rn end-members measured from the onshore well, measured within the seepage face, and extrapolated from the ^{222}Rn-salinity relationship suggests fresh groundwater inflow is not the only source of ^{222}Rn. The linear relationship between dissolved ^{222}Rn and E_{Rn} suggests the spatial distribution of ^{222}Rn results from in situ production in heterogeneously distributed sediment $^{226}Ra_{eff}$ (E_{Rn}), and further, fresh groundwater accounts for only a small fraction of total ^{222}Rn (~20%). Identifying these sources is critical in applying ^{222}Rn as a tracer of fluid flux and most critical in selecting the radon source activity to apply in flux calculations.

The temporally dynamic nature of the subterranean estuary was observed by contrasts in salinity, Eh, U, and Ra between 2005 (May and Sep) and 2006 (May and Oct) sampling trips. Between May/Sep-2005 and May-2006, the lateral mixing zone migrated landward, the

subterranean estuary became more oxidizing, the ^{226}Ra release zone migrated landward, the total pore water U and Ra at 17.5, 20, and 22.5 m offshore increased 89 and 76%, respectively, and the total depth-integrated U at the shoreline site increased 550%. The most probable explanation for this temporal variability is the residual effect of storm events that occurred seven months prior to the May-2006 sampling trip.

As suggested above, the application of ^{222}Rn as a quantitative tracer of groundwater is highly dependent on the ability to resolve all sources whether from external supply or in situ production. These sources were resolved in this study by measuring total dissolved ^{222}Rn within the seepage face/subterranean estuary and from inflowing groundwater, ^{222}Rn emanation from the sediment ^{226}Ra, and dissolved ^{226}Ra in porewaters, groundwaters, and surface waters. The strong linear correlation between total dissolved ^{222}Rn and sediment ^{226}Ra (E_{Rn}) resulted in the following vertical relationship: 1) a lower zone where pore water ^{222}Rn and sediment ^{226}Ra are in equilibrium and concentration gradients are vertical; 2) a middle zone where ^{222}Rn is in excess of sediment ^{226}Ra and concentration gradients are concave-downward; and 3) an upper zone where ^{222}Rn concentration gradients are nearly vertical. These ^{222}Rn data were simulated in a one-dimensional numerical model including advection, diffusion, and non-local exchange to estimate magnitudes of submarine groundwater discharge components (fresh or marine). Simulation of both advection and irrigation allows the separation of submarine groundwater discharge into fresh groundwater and (re)circulated lagoon water.

The magnitude of fresh groundwater discharge was shown to decrease linearly to exponentially offshore, with the terminus of the fresh inputs occurring between 20 and 25 m offshore. Total discharge estimates obtained from the model suggest fresh groundwater discharge to the lagoon is on the order of 1.01 to 1.89 $m^3\ d^{-1}\ m^{-1}$ of shoreline, which is consistent with previous estimates from seepage meters, head measurements, and groundwater flow

models. Lags between coastal discharge and inland precipitation events suggest mean residence times of fresh groundwater in the aquifer are 5 to 7 months. Non-local exchange in the model was applied as a proxy for irrigation and allowed terrestrial (fresh) and marine components of submarine groundwater discharge to be distinguished and quantified. Processes thought to cause ventilation or irrigation of sediments include density-dependent convection, dispersion, wave pumping, and bio-irrigation. While no single process presents itself as the clear control of shallow porewater exchange, it is important to characterize the magnitude of this flow in relation to the fresh component. Additionally, in most cases it is likely the combined effect of several processes driving shallow recirculation of lagoon water through sediments. A crude comparison between fresh and marine seepage velocities suggests that approximately two-thirds of SGD is derived from recirculated seawater while only one-third is derived from fresh groundwater.

This distinction between fresh groundwater and recirculated seawater as components of SGD is important to better understand the role of groundwater discharge to coastal water budgets and water resource management. Assuming discharge is ubiquitous over the entire length of the lagoon (~250 km) then the average available water supply from the entire Surficial aquifer adjacent to the lagoon would be 65 to 125 million gallons per day (mgpd). It is still unclear what role groundwater discharge has in coastal ecosystem health. In cases where coastal aquifers may become polluted, groundwater discharge could have deleterious effects (Simmons 1992; Miller and Ullman 2004; Hu et al. 2006; Kroeger et al. 2006). However, it has also been reported by scientists over the past 40 years the groundwater discharge to coastal waters simply creates a biological zonation near the shoreline as organisms are sorted by salt tolerance (Kohout and Kolipinski 1967; Ullman et al. 2003; Miller and Ullman 2004). What is clear is that scientists and managers alike need to understand the magnitude of the fresh “new” groundwater versus

"recycled" seawater if they are to interpret biogeochemistry and ecology well and make sound judgments about available resources.

How SGD and the subterranean estuary contribute to local- to global-scale elemental budgets (e.g. U, Ra) is still being studied. Previous studies (e.g. Windom and Niencheski 2003; Charette and Sholkovitz 2006) identified SGD and subterranean estuaries as sinks for U. Charette and Sholkovitz (2006) suggested at the global scale that the interaction between recirculated submarine groundwater discharge and the subterranean estuary would cause a net global sink on the order of 20 x 10^6 mol U y^{-1}. Using the same global estimate of SGD as Charette and Sholkovitz (2006) used (~4000 km^3; Burnett et al. 2003) and a groundwater end member concentration of 0.54 ng g^{-1} (2.35 μM), I calculate a global source of U scaled up from the Florida subterranean estuary would be ~9.5 x 10^6 mol U yr^{-1}; this estimate is close to 9.7 x 10^6 mol U yr^{-1} used by Dunk et al. (2002). The large differences in estimates of flux and the source/sink determination for U seem to occur because of the differences in width of the seepage face at each location and the overall geological matrix of the subterranean estuary. This observation reiterates the complexity of the hydrogeologic setting and dynamic nature of the physical flow regime inevitably determines whether these coastal, submarine groundwater systems ultimately act as a net source or sink to the ocean.

References

Burnett, W. C., H. Bokuniewicz, M. Huettel, W. S. Moore, and M. Taniguchi. 2003. Groundwater and pore water inputs to the coastal zone. Biogeochemistry **66:** 3-33.

Charette, M. A., and E. R. Sholkovitz. 2006. Trace element cycling in a subterranean estuary: Part 2. Geochemistry of the pore water. Geochimica et Cosmochimica Acta **70:** 811-826.

Dunk, R. M., R. A. Mills, and W. J. Jenkins. 2002. A reevaluation of the oceanic uranium budget for the Holocene. Chemical Geology **190:** 45-67.

Hu, C. M., F. E. Muller-Karger, and P. W. Swarzenski. 2006. Hurricanes, submarine groundwater discharge, and Florida's red tides. Geophysical Research Letters **33:** 5.

Kohout, F. A., and M. C. Kolipinski. 1967. Biological zonation related to ground water discharge along the shore of Biscayne Bay, Miami, Florida. Estuaries **83:** 488-499.

Kroeger, K. D., M. L. Cole, and I. Valiela. 2006. Groundwater-transported dissolved organic nitrogen exports from coastal watersheds. Limnology and Oceanography **51:** 2248-2261.

Martin, J. B., J. E. Cable, C. Smith, M. Roy, and J. Cherrier. 2007. Magnitudes of submarine groundwater discharge from marine and terrestrial sources: Indian River Lagoon, Florida. Water Resources Research **43:** -.

Miller, D. C., and W. J. Ullman. 2004. Ecological consequences of ground Water discharge to Delaware Bay, United States. Ground Water **42:** 959-970.

Mulligan, A. E., and M. A. Charette. 2006. Intercomparison of submarine groundwater discharge estimates from a sandy unconfined aquifer. Journal of Hydrology **327:** 411-425.

Simmons, J., G.M. 1992. Importance of submarine groundwater discharge (SGWD) and seawater cycling to material flux across sediment/water interfaces in marine environments. Marine Ecology Progress Series **84:** 173-184.

Ullman, W. J., B. Chang, D. C. Miller, and J. A. Madsen. 2003. Groundwater mixing, nutrient diagenesis, and discharges across a sandy beachface, Cape Henlopen, Delaware (USA). Estuarine, Coastal and Shelf Science **57:** 539-552.

Windom, H., and F. Niencheski. 2003. Biogeochemical processes in a freshwater-seawater mixing zone in permeable sediments along the coast of Southern Brazil. Marine Chemistry **83:** 121-130.

APPENDIX A.

EAST-CENTRAL FLORIDA HYDROGEOLOGY

Hydrogeology

Three hydrostratigraphic units are common in east-central Florida; they include the Floridan, Intermediate, and Surficial aquifer systems (Figure A.1; Toth 1988; Toth 1993; Mcgurk and Presley 2002). The Intermediate aquifer system acts as both an aquifer as well as a confining unit for the Floridan aquifer (Miller 1986; Scott 1988; Tibbals 1990; Miller 1997). These units are equivalent to the regional-scale hydrostratigraphic units described by Miller (1986), Tibbals (1990), and Miller (1997).

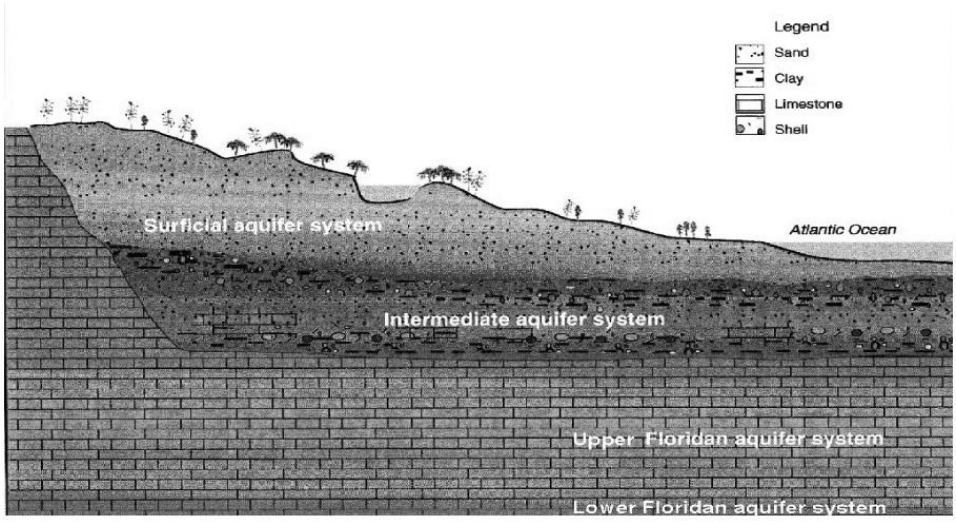

Figure A.1. A schematic shore-normal cross-section through east-central Florida showing the three dominant hydrostratigraphic units (Surficial, Intermediate, and Floridan) (modified from Toth 1998).

Floridan Aquifer

The Floridan aquifer is comprised of Eocene and late Paleocene age, calcareous rocks belonging to the following Stratigraphic Units (bottom to top): upper Cedar Key Formation (CKF), Oldsmar Formation (OF), Avon Park Formation (APF), and Ocala Limestone (OL). The Floridan aquifer system is divided into two sub-units, the Lower (upper CKF, OF, and lower

APF) and Upper Floridan (upper APF and OL). These sub-units are separated by a less permeable zone within the APF (Miller 1986; Tibbals 1990; Scott 1992; Miller 1997). As is common in karst settings, transmissivity of the Upper Floridan is highly variable in east-central Florida (110 to 49000 m^2 d^{-1}; Szell 1993; Mcgurk and Presley 2002). The top of the Upper Floridan aquifer (Ocala Limestone) dips to the south, controlling the thickness of the overlying units. Recharge to the Upper Floridan occurs via three directions: (1) downward flow from the Surficial aquifer where the Intermediate unit is thin (in the north); (2) direct recharge by precipitation where Surficial and Intermediate units are thin to absent (in the west and north); and (3) upward flow from the Lower Floridan aquifer (Miller 1986; Toth 1988; Toth 1993; Miller 1997; Mcgurk and Presley 2002). Regional flow in the Upper Floridan has been severely impacted by groundwater withdrawals. Recent models show a switch from a general eastward flow before 1936 (Toth 1988) to a more northeastern flow in 1995 (Mcgurk and Presley 2002).

Intermediate Aquifer/Confining Unit

The Intermediate unit is characterized by interbedded clay, sandy clay, and sand of the Miocene/Pliocene age Hawthorn Group. Although the unit acts as an aquitard between the Upper Floridan and Surficial aquifers, the lithologic heterogeneity produces localized zones of relatively high transmissivity (≤1900 m^2 d^{-1}). Hydrologic interaction between the Upper Floridan and Surficial aquifers is controlled by the thickness of this Intermediate unit. The unit thickness varies significantly within the Indian River Lagoon (IRL) region (Bermes 1958; Miller 1986; Scott 1988; Toth 1988; Miller 1997). Isopach maps show this unit is thin to nearly absent in Volusia, Seminole, and northern Brevard Counties and thickens southward down to 45 to 60 m (Boniol et al. 1993; Mcgurk and Presley 2002). Recharge to and flow within the Intermediate aquifer is highly localized and dependant on thickness of the more transmissible zones.

Surficial Aquifer

The Surficial aquifer system consists of one rock aquifer (Shallow Rock) and five overlying, shallow, interconnected clastic aquifers: Terrace, Inter-Ridge, Osceola Plain, Atlantic Coastal Ridge, and Ten-Mile Ridge (Figure A.2) (Toth 1988). The Shallow Rock aquifer is comprised of hard, limestone rock equivalent in age to the Pliocene Tamiami Limestone (Toth 1988; Szell 1993). Limited information exists on the Shallow Rock aquifer, but Toth (1988) suggested it is present in most of Brevard County, thickening eastward in the southern part of the county. Transmissivity values for the Shallow Rock aquifer at Malabar, Florida, range between 185 and 200 $m^2 d^{-1}$ (Szell 1993).

Of the five clastic Surficial aquifers (Figure A.2), only three are relevant to this study (Terrace, Atlantic Coastal Ridge, and Ten-Mile Ridge). In general, the aquifers are comprised of undifferentiated, Holocene interbedded coquina, sand, silt, and clay. However, a persistent Pleistocene coquina, known as Anastasia Formation, is observed within the Atlantic Coastal Ridge aquifer. Table A.1 summarizes aquifer transmissivity, storativity, and hydraulic conductivity for Volusia, Brevard, and Indian River County. Terrace aquifer forms the western (Pamlico Terrace) and eastern banks (barrier island chain) of Indian River Lagoon through most of central Brevard County. The Atlantic Coastal Ridge aquifer forms the west bank for the remainder of IRL (Figure A.2). The thickness of the Terrace aquifer ranges between about 9 and12 m (Szell 1993) and the water table is located 2 to 3 m below land surface (Toth 1988). In contrast, where land elevations reach 10 to 20 m above sea level, the ridge aquifers are 18 to 27 m thick with water table elevations between 6.7 and 19.5 m above MSL. Recharge to the Surficial aquifer is controlled by infiltration of meteoric water, upward flow from the Shallow Rock aquifer, and occasionally upward flow from the Upper Floridan (generally restricted to the northern portion of IRL). In general, the regional flow pattern on the mainland is eastward

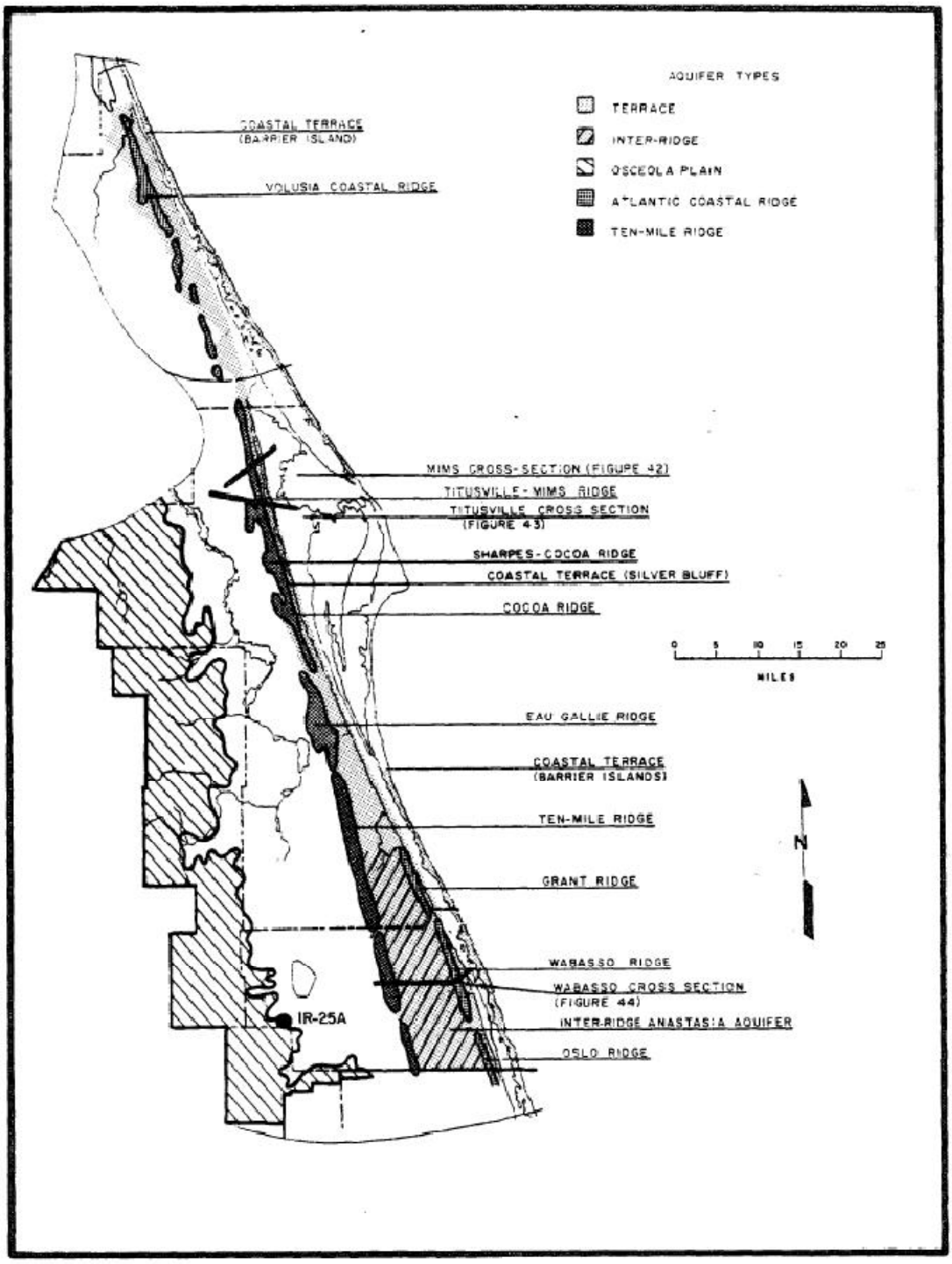

Figure A.2. Map of east-central Florida showing areal distribution of the five clastic aquifers that comprise the Surficial aquifer (modified from Toth, 1988).

Table A.1. Summary of the transmissivity, storage coefficient, and hydraulic conductivity for the clastic sub-aquifers of the Surficial aquifer system in Volusia, Brevard, and Indian River Counties (modified from Toth, 1988).

Area	Aquifer Type	Transmissivity (T)	Storage Coefficient	Hydraulic Conductivity (K)	Citation*
		($m^2 d^{-1}$)	Non-dimensional	($m d^{-1}$)	
N.E. Volusia	**Coastal Ridge**				
	shell deposits	3-1044	$1.6x10^{-4}$-$4.0x10^{-2}$	10-15	1
	water table	6-45	$1.9x10^{-1}$		2
North Brevard	**Coastal Ridge**				
	shell deposits	30-358	$2.5x10^{-4}$		3
	water table	69-343	$1.3x10^{-1}$		4
South Brevard	**Coastal Ridge**				
	shell deposits	113-256	$1.6x10^{-4}$-$2.0x10^{-2}$		5
	Coastal Terrace				
	water table	218		17	6
Indian River	**Coastal Ridge**				
	shell deposits	880	$1.4x10^{-2}$	41	7
	water table	172-216	$1.9x10^{-4}$	15-18	8
	Inter-Ridge				
	Anastasia Aq.	1185	$1.0x10^{-4}$	127	9
Vero Beach Area	**Coastal Ridge**				
	shell deposits	294-702	$2.3x10^{-4}$-$1.5x10^{-1}$	12-30	10

discharging into IRL and access canals (Toth 1988; Toth 1993; Mcgurk and Presley 2002), however, local flow patterns may be different. For example, in central Brevard County (near the proposed field site), the Atlantic Coastal Ridge is farther inland resulting in a local groundwater divide. Thus, a portion of the groundwater flows to the east discharging into IRL and a portion flows to the west and discharges into Lake Washington and the surrounding wetlands.

References

Bermes, B. J. 1958. Interim report on geology and groundwater resources of Indian River County, Florida, p. 74. Information Circular No. 18. U.S. Geological Survey.

Boniol, D., M. Williams, and D. Munch. 1993. Mapping recharge to the Floridan aquifer using a geographic information system, p. 41. Technical Publication SJ93-5. St. Johns River Water Management District.

Mcgurk, B., and P. F. Presley. 2002. Simulation of the effects of groundwater withdrawals on the Flordian aquifer system in east-central Florida: model expansion and revision, p. 196. Technical Publication SJ2002-3. St. Johns River Water Managment District.

Miller, J. A. 1986. Hydrogeologic framework of the Floridan aquifer system in Florida and parts of Georgia, Alabama, and South Carolina, p. 91. Professional Paper 1403-B. U.S. Geological Survey.

---. 1997. Hydrogeology of Florida, p. 69-88. *In* A. F. Randazzo and D. S. Jones [eds.], The Geology of Florida. University Press of Florida.

Scott, T. M. 1988. The lithostratigraphy of the Hawthorn Group (Miocene of Florida), p. 147. Bulletin 59. Flordia Geological Survey.

---. 1992. A Geological Overview of Florida, p. 78. Florida Geological Society.

Szell, G. P. 1993. Aquifer characteristics in the St. Johns River Water Management District, Florida, p. 495. Technical Publication SJ93-1. St. Johns River Water Management District.

Tibbals, C. H. 1990. Hydrology of the Floridan aquifer system in east-central Florida--regional aquifer system analysis--Florida aquifer system, p. 98. Professional Paper 1403-E. U.S. Geological Survey Professional Paper.

Toth, D. J. 1988. Saltwater intrusion in coastal areas of Volusia, Brevard, and Indian River counties, p. 160. Technical Publication SJ88-1. St. Johns River Water Management District.

---. 1993. Volume 1 of the lower St. Johns River basin reconnanissance hydrogeology, p. 52. Technical Publication SJ93-7. St. Johns River Managment District.

APPENDIX B.

GRAIN SIZE DATA AND HYDRAULIC CONDUCTIVITY

Derivation of the Modified Carmen-Kozeny Equation for Hydraulic Conductivity

In this appendix, I describe the modified version of the Carmen-Kozeny (CK) equation used to compute the hydraulic conductivity of sediments in Chapter 2 (i.e. Eqn. 2.4). This modification of the CK equation uses the particle size distribution (psd) to account for non-uniform psd as previously described in detail by Dullien (1979) and Panda and Lake (1994). The derivation and equations were obtained from Panda and Lake (1994). The traditional CK equation is

$$K = \left(\frac{\rho g}{\mu}\right)\left(\frac{\varphi^3}{2\tau(1-\varphi)^2 a_v^2}\right) \qquad (B.1)$$

where ρ is the density of water (g cm^{-3}), g is acceleration due to gravity (cm s^{-2}), μ is viscosity (g cm^{-1} s^{-1}), a_v is the specific internal surface area of the medium (i.e. ratio of exposed surface area to solid volume), φ is porosity, and τ is sediment tortousity. In the modified version presented in Chapter 2, an effective particle diameter (D_{eff}) is used to approximate a_v^{-1}. This approximation is valid for homogeneously packed, unconsolidated sediment with a number frequency distribution of psd given as

$$\int_0^\infty f(D_p)\,dD_p = 1 \qquad (B.2)$$

such that a_v for this assembly is

$$a_v = 6\frac{E_2}{E_3} \qquad (B.3)$$

where E_2 and E_3 are the second and third uncentered moments, respectively, of the psd. They are defined here as

$$E_2 = second\ moment = \int_0^\infty D_p^2 f(D_p) dD_p \qquad (B.4)$$

$$E_3 = \sigma^3 = third\ moment = \int_0^\infty D_p^3 f(D_p) dD_p \qquad (B.5)$$

The comparable centered moments are defined as

$$\sigma^2 = variance = \int_0^\infty (D_p - \overline{D_p})^2 f(D_p) dD_p \qquad (A.6)$$

$$\gamma = skewness = \frac{1}{\sigma^3} \int_0^\infty (D_p - \overline{D_p})^3 f(D_p) dD_p \qquad (B.7)$$

Recasting E_2 and E_3 in terms of the centered moments, we have

$$E_2 = \sigma^2 + \overline{D_p^2} \qquad (B.8)$$

$$E_3 = \gamma\sigma^3 + 3\overline{D_p}\sigma^2 + \overline{D_p^3} \qquad (B.9)$$

In equations B.6 through B.9, the term $\overline{D_p}$ is the mean particle size or first moment

$$E_1 = first\ moment = \overline{D_p}\ (mean) = \int_0^\infty D_p f(D_p) dD_p \qquad (B.10)$$

Thus, the formal modified Carmen-Kozeny equation as it appears in Chapter 2 is

$$K_{mCK} = \left(\frac{\rho g}{\mu}\right)\left(\frac{{D_{eff}}^2 \varphi^3}{72\tau(1-\varphi)^2}\right) \qquad (2.4)$$

or expanded with equations B.8 and B.9 is

$$K_{mCK} = \left(\frac{\rho g}{\mu}\right)\left(\frac{{\overline{D_p}}^2 \varphi^3}{72\tau(1-\varphi)^2}\right)\left[\frac{\left(\gamma C_{D_p}^3 + 3C_{D_p}^2 + 1\right)^2}{\left(1 + C_{D_p}^2\right)^2}\right] \qquad (B.11)$$

where C_{D_p} is the coefficient of variation of the psd, $\sigma/\overline{D_p}$. Based on the equivalence of Eqn. 2.4

and B.11, the effective diameter used in 2.4 is

$$D_{eff} = \frac{E_3}{E_2} = \overline{D_p}^2 \left[\frac{\left(\gamma C_{D_p}^3 + 3C_{D_p}^2 + 1 \right)^2}{\left(1 + C_{D_p}^2 \right)^2} \right] \qquad (B.12)$$

which shows that the effective diameter is the ratio of the skewness to variance in the psd and subsequently the hydraulic conductivity computed using this equation also accounts for non-uniformity in the sediments. Panda and Lake (1994) found that this modified CK model compared favorable well ($r^2 = 0.78$) with measured hydraulic conductivity when sediments had hydraulic conductivity greater than 9.8×10^{-4} cm s^{-1}. Below this hydraulic conductivity, the relationship was much weaker ($r^2 < 0.4$). My hydraulic conductivity measurements and grain-size based estimates exceed this lower limit (Table B.1). Table B.1 lists the data used to compute the modified CK hydraulic conductivity. Also presented is hydraulic conductivity computed using a empirically-modified Carmen-Kozeny equation presented by Hartl (2006),

$$K_{Hartl} = \left(\frac{\rho g}{\mu} \right) \left(\frac{\overline{D_p}^2 \varphi^3}{180(1+200 f_m - \varphi)^2} \right) \qquad (B.12)$$

where $200f_m$ is two hundred times the mud fraction (< 63 μm) and all other parameters have been described previously.

References

Dullien, F. A. L. 1979. Porous media: fluid transport and pore structure, p. 110-155. Academic Press.

Hartl, K. 2006. Facies distribution and hydraulic conductivity of lagoonal sediments in a Holocene transgressive barrier island sequence, Indian River Lagoon, Florida. M.S. University of Florida.

Panda, M. N., and L. W. Lake. 1994. Estimation of Single-Phase Permeability from Parameters of Particle-Size Distribution. Aapg Bulletin-American Association of Petroleum Geologists **78:** 1028-1039.

Table B.1. Grain size data and computed hydraulic conductivity

Vibracore	Depth (cm)	Mid-Depth (cm)	Porosity	Gravel (%)	Sand (%)	Mud (%)	E1 (mm)	E2 (mm^2)	E3 (mm^3)	D_{eff} (mm)	K_{mCK} (cm/s)	K_{Hartl} (cm/s)
EGN-0	0-2	1	0.42	0.04	99.78	0.18	0.115	0.022	0.006	0.278	0.114	0.043
	12-14	13	0.37	0.00	99.92	0.08	0.140	0.028	0.008	0.269	0.059	0.037
	22-24	23	0.38	0.00	99.42	0.58	0.091	0.010	0.001	0.131	0.016	0.002
	30-32	31	0.34	0.00	99.94	0.06	0.139	0.026	0.006	0.238	0.032	0.023
	40-42	41	0.33	0.00	99.96	0.04	0.156	0.033	0.009	0.275	0.038	0.031
	60-62	61	0.35	0.00	99.34	0.66	0.085	0.014	0.003	0.221	0.033	0.004
	85-87	86	0.36	0.00	98.42	1.58	0.064	0.008	0.001	0.188	0.026	0.001
	110-112	111	0.38	0.00	98.97	1.03	0.102	0.017	0.004	0.211	0.040	0.007
	130-132	131	0.37	0.00	98.88	1.12	0.075	0.010	0.002	0.182	0.027	0.001
	150-152	151	0.33	0.00	99.02	0.98	0.075	0.010	0.002	0.198	0.021	0.001
	157-159	158	0.34	0.06	99.15	0.79	0.078	0.012	0.003	0.225	0.031	0.003
	167-169	168	0.35	0.00	99.64	0.36	0.107	0.018	0.004	0.210	0.030	0.007
	174-177	176	0.36	0.00	99.78	0.22	0.123	0.020	0.004	0.191	0.028	0.010
	190-192	191	0.35	0.00	99.80	0.20	0.125	0.020	0.004	0.192	0.025	0.010
EGN-10	0-2	1	0.45	0.20	99.74	0.06	0.131	0.025	0.007	0.273	0.151213	0.101627
	17-19	18	0.41	0.00	98.78	1.22	0.073	0.008	0.001	0.167	0.037054	0.00141
	22-24	23	0.38	0.00	99.57	0.43	0.095	0.012	0.002	0.164	0.025798	0.004501
	30-32	31	0.34	0.04	99.82	0.14	0.118	0.018	0.004	0.201	0.025724	0.012608
	45-47	46	0.36	0.21	97.76	2.03	0.051	0.006	0.001	0.225	0.038904	0.000724
	60-62	61	0.36	0.00	98.84	1.16	0.065	0.009	0.002	0.224	0.038502	0.001802
	70-72	71	0.37	0.00	98.50	1.50	0.062	0.008	0.002	0.204	0.035542	0.001075
	90-92	91	0.37	0.00	99.30	0.70	0.091	0.013	0.002	0.175	0.026265	0.002535
	116-118	117	0.35	0.00	98.57	1.43	0.062	0.008	0.002	0.211	0.030385	0.001037
	146-148	147	0.35	0.02	98.78	1.20	0.061	0.009	0.002	0.242	0.039796	0.00181
	156-158	157	0.35	0.00	97.91	2.09	0.054	0.006	0.001	0.202	0.02777	0.000504

Table B.1 (cont'd)

Vibracore	Depth (cm)	Mid-Depth (cm)	Porosity	Gravel (%)	Sand (%)	Mud (%)	E1 (mm)	E2 (mm^2)	E3 (mm^3)	D_{eff} (mm)	K_{mCK} (cm/s)	K_{Hartl} (cm/s)
EGN-10	176-178	177	0.35	0.02	99.43	0.55	0.085	0.015	0.004	0.250	0.042734	0.005856
	196-198	197	0.35	0.00	99.68	0.32	0.110	0.017	0.003	0.188	0.024206	0.006159
	226-228	227	0.35	0.00	99.66	0.34	0.109	0.015	0.002	0.161	0.017672	0.004246
EGN-20	17-19	18	0.43	0.20	99.69	0.12	0.116	0.021	0.005	0.266	0.116242	0.058258
	22-24	23	0.39	0.64	98.75	0.60	0.083	0.011	0.002	0.210	0.04811	0.005396
	32-34	33	0.38	0.12	99.56	0.32	0.100	0.017	0.004	0.249	0.059403	0.014418
	43-45	44	0.36	0.02	99.76	0.22	0.112	0.017	0.004	0.206	0.032795	0.011462
	50-52	51	0.37	0.64	99.24	0.12	0.129	0.025	0.007	0.273	0.063265	0.033215
	58-60	59	0.37	0.00	99.08	0.92	0.069	0.011	0.003	0.243	0.050487	0.003311
	80-82	81	0.34	0.00	99.66	0.34	0.106	0.021	0.005	0.250	0.038829	0.009507
	87-89	88	0.36	0.00	99.14	0.86	0.073	0.012	0.003	0.233	0.04017	0.002954
	100-102	101	0.40	0.00	99.16	0.84	0.083	0.012	0.002	0.183	0.039726	0.002748
	130-132	131	0.37	0.00	99.66	0.34	0.113	0.018	0.003	0.185	0.0278	0.006508
	150-152	151	0.37	0.00	99.62	0.38	0.103	0.017	0.004	0.214	0.038346	0.007846
	175-177	176	0.39	0.00	99.92	0.08	0.157	0.032	0.008	0.236	0.059459	0.037263
	180-182	181	0.37	0.00	99.78	0.22	0.123	0.019	0.003	0.169	0.023527	0.008264
	188-190	189	0.34	0.00	99.64	0.36	0.110	0.017	0.003	0.181	0.018892	0.004351
	200-202	201	0.36	0.00	99.74	0.26	0.114	0.023	0.006	0.265	0.053712	0.016441
	210-212	211	0.40	0.00	98.65	1.35	0.057	0.007	0.002	0.256	0.078144	0.002586
	217-218	216	0.38	0.00	99.80	0.20	0.129	0.022	0.004	0.194	0.036076	0.013371
EGN-30	0-2	1	0.35	0.00	99.28	0.72	0.082	0.009	0.001	0.154	0.01621	0.001554
	22-24	23	0.35	0.00	98.16	1.84	0.063	0.007	0.001	0.166	0.018733	0.000423
	33-35	34	0.35	0.02	99.60	0.38	0.100	0.016	0.003	0.208	0.029523	0.006276
	59-61	60	0.35	1.21	98.53	0.25	0.106	0.021	0.006	0.297	0.060223	0.018964

Table B.1 (cont'd)

Vibracore	Depth (cm)	Mid-Depth (cm)	Porosity	Gravel (%)	Sand (%)	Mud (%)	E1 (mm)	E2 (mm^2)	E3 (mm^3)	D_{eff} (mm)	K_{mCK} (cm/s)	K_{Hartl} (cm/s)
EGN-30	69-71	70	0.35	0.00	99.51	0.49	0.096	0.016	0.003	0.217	0.032051	0.005061
	90-92	91	0.35	0.00	99.05	0.95	0.081	0.011	0.002	0.176	0.021143	0.001372
	122-124	123	0.39	0.00	98.29	1.71	0.063	0.008	0.001	0.178	0.034122	0.000783
	135-137	136	0.39	0.00	98.48	1.52	0.070	0.008	0.001	0.156	0.026031	0.000726
	155-157	156	0.42	0.00	99.16	0.84	0.083	0.012	0.002	0.186	0.05125	0.003374
	180-182	181	0.45	0.00	99.14	0.86	0.077	0.011	0.002	0.213	0.091672	0.005414
	210-212	211	0.45	0.00	99.47	0.53	0.096	0.015	0.003	0.197	0.078291	0.009056
	225-227	226	0.43	0.02	99.56	0.42	0.103	0.016	0.003	0.198	0.06425	0.010537

APPENDIX C.

PORE WATER DATA

Nov-2004												
MS	**Depth (cmbsf)**	**^{222}Rn (dpm/L)**	**2σ**	**^{226}Ra (dpm/L)**	**2σ**	**U (ng/g)**	**^{234}U/^{238}U**	**2σ**	**Temperature (^{o}C)**	**Salinity**	**Eh**	**pH**
EGN-0	0	182.86	15.81			2.228	1.120	0.003	24.71	17.81	111.7	8.11
EGN-0	7	1647.25	60.61			1.617	1.127	0.007	24.71	11.9	86.9	7.1
EGN-0	15	4393.59	160.14			0.778	1.020	0.010	25.48	2.36	69.1	6.74
EGN-0	25	4753.78	298.77			0.324	1.079	0.014	25.64	0.87	2.1	6.83
EGN-0	35	5021.91	268.51			0.309	1.234	0.022	25.95	0.52	-56.9	6.8
EGN-0	55	5770.20	140.56			0.238	1.091	0.014	26.32	0.21	52.8	6.84
EGN-0	75	6716.59	195.63			0.278	1.015	0.006	26.59	0.18	26.9	6.9
EGN-0	95	7239.97	79.72			0.263	1.017	0.012	26.86	0.19	96.3	6.92
EGN-0	115	5909.56	34.30			0.328	1.036	0.011	26.72	1.07	174.1	7.08
EGN-10	0	213.30	30.84			1.910	1.123	0.006	26.26	17.43	182.7	8.26
EGN-10	7	781.11	144.76			2.175	1.118	0.005	26.37	16.16	120.9	8.05
EGN-10	15	1298.10	78.43			0.990	1.091	0.006	25.61	9.73	125.7	7.53
EGN-10	25	3927.80	50.31			0.643	1.063	0.009	25.06	1.8	144.2	7.32
EGN-10	35	4816.68	52.41			0.468	1.084	0.011	25.11	0.97	180.1	7.36
EGN-10	55	3887.53	127.72			0.583	1.078	0.010	25.65	0.64	185.4	7.4
EGN-10	75	3565.83	59.65			0.626	1.067	0.009	26	0.58	199.9	7.42
EGN-10	95	3327.20	59.67			0.561	1.074	0.013	26.13	0.55	207.1	7.44
EGN-10	115	3853.38	135.06			0.824	1.039	0.008	26.26	0.54	214.5	7.49
EGN-15	0	141.72	29.98			1.967	1.114	0.010	26.45	17.75	207.2	8.17
EGN-15	7	230.08	28.61			4.354	1.201	0.015	26.13	17.71	156.0	7.88
EGN-15	15	839.18	55.18			4.049	1.120	0.018	25.59	14.81	98.8	7.37
EGN-15	25	2351.06	112.99			1.253	1.087	0.009	20.86	5.45	78.9	7.07
EGN-15	35	4534.38	200.93			1.212	1.022	0.012	24.66	1.34	116.9	7.12
EGN-15	55	3907.75	219.43			1.751	1.047	0.006	25.85	1.25	104.5	7.23
EGN-15	75	5426.34	133.74			1.107	1.039	0.006	25.05	1.51	194.1	7.2
EGN-15	95	3928.14	75.61			0.929	1.055	0.008	24.97	1.32	174.9	7.23
EGN-15	115	3444.85	161.62			0.906	1.062	0.011	25.22	1.47	168.5	7.25

Nov-2004												
MS	**Depth (cmbsf)**	**^{222}Rn (dpm/L)**	**2σ**	**^{226}Ra (dpm/L)**	**2σ**	**U (ng/g)**	**^{234}U/^{238}U**	**2σ**	**Temperature (^{o}C)**	**Salinity**	**Eh**	**pH**
EGN-20	0	51.89	9.37			1.970	1.142	0.008	26.78	17.28	171.0	8.48
EGN-20	7	448.64	83.40			2.296	1.113	0.009	26.29	16.12	171.7	8.16
EGN-20	15	621.25	27.30			2.350	1.103	0.008	26.39	16.02	116.3	7.86
EGN-20	25	2544.77	110.20			2.761	1.091	0.007	25.39	6.74	107.0	7.38
EGN-20	35	3408.18	109.25			1.913	1.041	0.012	24.23	2.99	86.1	7.25
EGN-20	55	5093.53	156.87			2.280	1.104	0.004	27.04	1.97	122.0	7.29
EGN-20	75	6972.29	569.99			2.256	1.033	0.006	25.65	2.19	109.1	7.28
EGN-20	95	5910.46	193.55			2.822	1.075	0.003	26.2	3.28	123.8	7.26
EGN-20	115	4642.13	189.70			0.786	1.104	0.022	25.19	0.94	112.5	7.33
EGN-30	0	113.45	18.31			1.891	1.115	0.005	25.66	17.54	158.8	8.34
EGN-30	10	119.06	12.02			1.293	1.101	0.003	23.77	17.51	-50.8	7.38
EGN-30	30	346.29	31.56			0.403	1.096	0.006	24	20.55	-49.0	7.27
EGN-30	50	553.52	22.07			0.488	1.080	0.003	23.87	23.14	-18.0	7.25
EGN-30	150	2856.16	117.93			0.428	1.076	0.011	25.16	21.62	87.6	6.91
EGN-30	190	1029.18	46.98			0.102	1.156	0.008	25.73	20.49	99.1	6.93
EGN-30	230	843.96	82.41			0.104	1.104	0.012	26.02	20.78		7.02

Feb-2005												
MS	**Depth (cmbsf)**	**^{222}Rn (dpm/L)**	**2σ**	**^{226}Ra (dpm/L)**	**2σ**	**U (ng/g)**	**^{234}U/^{238}U**	**2σ**	**Temperature (^{o}C)**	**Salinity**	**Eh**	**pH**
EGN-0	0	128.77	7.20						21.29	17.96	246.3	8.32
EGN-0	7	901.29	190.22						21.49	12.79	229.7	7.18
EGN-0	15	3387.29	441.63						21.98	6.02	231.2	6.65
EGN-0	25	3514.75	419.75						22.24	0.76	78.4	6.65
EGN-0	35	4634.42	259.89						22.97	0.2	157	6.72
EGN-0	55	4637.47	430.53						23.97	0.15	158.1	6.58
EGN-0	75	5825.68	1001.91						24.68	0.27	142.4	6.79
EGN-0	95	4717.32	1108.34						25.17	0.29	151.5	6.79
EGN-0	115	5048.48	670.81						25.17	0.23	87	6.88
EGN-5	0	195.28	59.38						19.3	17.6		
EGN-5	7	623.35	121.53						19	16.1		
EGN-5	15	2748.79	742.61						19.1	9.2		
EGN-5	25	3399.71	375.02						19.5	7.8		
EGN-5	35	6132.79	923.22						20.2	0.9		
EGN-5	55	6319.18	1447.27						21.4	4		
EGN-5	75	1712.11	121.32						20.6	3		
EGN-5	95	7529.83	2081.31						22.4	0.3		
EGN-5	115	6804.07	355.74						23.1	0.3		
EGN-10	0	232.51	22.28						20.71	18.22	187.8	8.31
EGN-10	7	858.24	30.12						20.9	13.98	10.3	7.66
EGN-10	15	1548.11	157.77						21.03	9.48	-13.1	7.37
EGN-10	25	3477.04	416.06						21.23	1.8	12.5	7.44
EGN-10	35	3481.69	257.81						21.44	0.71	20.1	7.49
EGN-10	55	3262.76	242.33						22.35	0.48	13.3	7.39
EGN-10	75	2864.06	202.02						23.14	0.48	34	7.41
EGN-10	95	1862.06	871.86						23.63	0.48	80	7.42
EGN-10	115	2908.42	275.24						24	0.49	83.8	7.49

Feb-2005												
MS	**Depth (cmbsf)**	**^{222}Rn (dpm/L)**	**2σ**	**^{226}Ra (dpm/L)**	**2σ**	**U (ng/g)**	**^{234}U/^{238}U**	**2σ**	**Temperature (^{o}C)**	**Salinity**	**Eh**	**pH**
EGN-15	0	196.51	25.68						17.85	16.62	191.8	8.21
EGN-15	7	230.55	78.09						16.65	16.51	162.8	8.11
EGN-15	15	646.76	58.89						16.88	14.29	76.8	7.80
EGN-15	25	1977.25	168.15						16.76	5.44	46.3	7.26
EGN-15	35	2994.48	118.46						18.08	1.44	53.3	7.29
EGN-15	55	3218.35	338.38						18.37	2.23	10.6	7.25
EGN-15	75	4222.42	104.44						18.31	1.48	-24.7	7.11
EGN-15	95	3492.41	342.44						19.19	0.85	-8.4	7.14
EGN-15	115	3159.02	321.10						17.72	0.94	-27.1	7.16
EGN-17.5	0	321.80	0.00						18.8	16.78	204.4	8.35
EGN-17.5	7	301.88	7.22						19.17	16.68	140	8.25
EGN-17.5	15	432.47	31.45						18.48	16.46	180.1	8.29
EGN-17.5	25	1845.04	249.95						18.53	8.25	130	7.53
EGN-17.5	35	3301.75	285.20						18.11	3.61	118	7.35
EGN-17.5	55	5220.65	316.25						19.02	1.83	105	7.32
EGN-17.5	75	5952.47	420.77						19.4	1.52	108	7.34
EGN-17.5	95	6621.62	169.97						20.67	0.84	123	7.30
EGN-17.5	115	6896.74	344.31						20.54	0.83	125	7.34
EGN-20	0	61.79	51.42						18.38	16.72	167	8.30
EGN-20	7	180.70	56.89						19.01	16.44	60.7	8.00
EGN-20	15	648.65	63.65						18.45	12.66	36.2	7.71
EGN-20	25	2043.31	88.02						18.88	8.23	21.4	7.38
EGN-20	35	2265.08	227.97						19.07	5.02	21.7	7.31
EGN-20	55	3708.34	233.23						19.3	4.92	3.9	7.28
EGN-20	75	2462.51	54.20						19.54	3.02	-33.9	7.30
EGN-20	95	4603.43	146.07						20.12	2.7	-48.8	7.28
EGN-20	115	4358.64	126.85						20.57	0.93	1.2	7.34

Feb-2005												
MS	**Depth (cmbsf)**	**^{222}Rn (dpm/L)**	**2σ**	**^{226}Ra (dpm/L)**	**2σ**	**U (ng/g)**	**^{234}U/^{238}U**	**2σ**	**Temperature (^{o}C)**	**Salinity**	**Eh**	**pH**
EGN-22.5	0	61.50	41.15						16.4	18.3		
EGN-22.5	20	163.06	74.53						15.9	16.9		
EGN-22.5	60	1099.13	23.37						18	10.8		
EGN-22.5	100	1903.67	127.94						17.7	4.1		
EGN-22.5	140	1277.48	131.42						18.6	4.5		
EGN-22.5	180	1363.71	174.55						18.9	5.8		
EGN-30	0	215.26	33.75						16.45	16.94	121	8.3
EGN-30	10	339.46	129.61						16.79	16.62	-72	7.44
EGN-30	30	501.02	79.53						17.48	17.71	-92	7.36
EGN-30	50	437.01	19.39						18.46	19.24	-93	7.29
EGN-30	150	2884.88	232.37						19.29	19.97	-44.9	6.99
EGN-30	190	1391.40	34.72						20.17	18.57	43	6.96
EGN-30	230	878.15	47.88						20.5	18.79	-16	7.03

May-2005												
MS	**Depth (cmbsf)**	**^{222}Rn (dpm/L)**	**2σ**	**^{226}Ra (dpm/L)**	**2σ**	**U (ng/g)**	**^{234}U/^{238}U**	**2σ**	**Temperature (^{o}C)**	**Salinity**	**Eh**	**pH**
EGNW-OS	225	2407.72	120.48			0.091	0.990	0.029	25.45	0.18	166.50	6.31
EGN-0	0	159.65	56.40	0.56	0.10	1.710	1.102	0.012	31.82	14.08	173.10	8.60
EGN-0	7	736.19	42.13	3.32	0.32	1.251	1.084	0.004	30.82	12.97	154.90	7.81
EGN-0	15	3436.04	129.19	23.47	0.29	0.700	1.075	0.005	29.30	3.71	103.90	6.57
EGN-0	25	4484.61	258.93	6.57	0.27	0.156	1.057	0.013	27.68	0.68	61.20	6.58
EGN-0	35	4680.15	128.05	3.13	0.35	0.117	1.108	0.015	27.97	0.16	71.00	6.63
EGN-0	55	5624.18	114.31	3.08	0.29	0.069	1.154	0.023	27.32	0.26	59.00	6.73
EGN-0	75	7497.56	146.08	3.29	0.03	0.119	1.023	0.017	22.56	0.15	10.00	6.71
EGN-0	95	6776.55	78.36	3.96	0.08	0.159	1.013	0.021	22.27	0.19	40.30	6.79
EGN-0	115	5944.76	195.96	4.22	0.23	0.255	1.007	0.020	22.65	0.20	2.40	6.77
EGN-5	0	242.85	80.37						31.20	14.76	185.00	8.61
EGN-5	7	704.37	66.14	5.19	0.11				29.29	13.28	-12.00	7.76
EGN-5	15	3195.13	147.29	10.92	0.39				27.91	7.23	-16.00	7.57
EGN-5	25	5469.40	186.68	7.82	0.45				27.08	2.14	-26.50	7.39
EGN-5	35	6845.56	327.09	6.35	0.39				27.44	0.60	10.00	7.48
EGN-5	55	8683.77	301.88	5.78	0.05				27.25	0.27	-4.00	7.39
EGN-5	75	8926.21	470.93	4.02	0.20				27.63	0.30	25.00	7.49
EGN-5	95	9259.82	219.26	4.10	0.12				27.22	0.29	-21.00	7.44
EGN-5	115	6751.16	124.59	3.70	0.09				27.69	0.26	18.00	7.50
EGN-10	0	270.28	25.07			1.692	1.125	0.005	31.09	14.01	166.00	8.60
EGN-10	7	946.52	101.50	5.41	0.07	4.217	1.116	0.005	29.71	11.26	-20.00	7.53
EGN-10	15	1990.56	83.11	7.50	0.24	4.737	1.110	0.004	29.16	7.96	-31.00	7.28
EGN-10	25	3897.14	94.66	8.57	0.29	0.395	1.073	0.006	27.71	1.39	-18.00	7.28
EGN-10	35	4567.77	291.04	5.17	0.14	0.995	0.989	0.004	27.74	0.72	19.00	7.36
EGN-10	55	3793.74	22.51	5.12	0.08	0.370	1.039	0.007	27.18	0.60	-20.00	7.17
EGN-10	75	3555.19	104.65	7.64	0.12	0.471	1.060	0.006	27.19	0.57	4.00	7.29
EGN-10	95	2876.54	37.42	7.24	0.18	0.441	1.030	0.005	27.63	0.59	-7.00	7.29
EGN-10	115	3369.39	335.54	7.76	0.17	0.529	1.033	0.007	26.90	0.57	54.00	7.38

May-2005												
MS	**Depth (cmbsf)**	**^{222}Rn (dpm/L)**	**2σ**	**^{226}Ra (dpm/L)**	**2σ**	**U (ng/g)**	**^{234}U/^{238}U**	**2σ**	**Temperature (^{o}C)**	**Salinity**	**Eh**	**pH**
EGN-15	0	146.87	2.94	3.99	0.35	1.751	1.103	0.004	29.12	15.58	163.60	8.58
EGN-15	7	274.89	48.75	6.89	0.29	5.488	1.076	0.003	29.17	15.83	13.00	8.05
EGN-15	15	722.30	137.77	6.76	0.36	3.163	1.054	0.005	28.29	13.64	-6.50	7.76
EGN-15	25	2110.78	81.30	21.37	0.06	1.824	1.053	0.005	27.66	7.15	15.10	7.29
EGN-15	35	2886.65	96.74	29.35	0.11	0.668	1.020	0.006	27.34	4.95	-22.80	7.16
EGN-15	55	2714.57	152.38	31.86	0.25	1.366	1.037	0.007	27.44	4.03	-54.10	7.10
EGN-15	75	3724.88	210.60	10.26	0.29	1.004	1.031	0.006	27.09	2.78	-70.80	7.15
EGN-15	95	3349.29	148.51	10.08	0.08	0.656	1.034	0.010	27.39	1.34	-90.00	7.15
EGN-15	115	3547.12	230.27	8.55	0.08	0.834	1.055	0.011	26.97	1.37	-30.50	7.15
EGN-17.5	0	271.80	43.84	4.31	0.11	1.769	1.109	0.002	32.68	15.01	145.10	8.50
EGN-17.5	7	530.64	50.09	6.92	0.10	2.566	1.091	0.003	31.33	13.99	12.00	7.77
EGN-17.5	15	581.54	73.55	7.01	0.15	4.378	1.087	0.002	30.56	14.49	-37.00	7.57
EGN-17.5	25	1896.74	76.37	13.35	0.38	1.869	1.032	0.003	28.11	7.19	-46.00	7.15
EGN-17.5	35	2067.60	62.12			1.247	1.023	0.005	26.75	3.13	-65.00	7.13
EGN-17.5	55	4601.54	128.80	10.09	0.30	1.610	1.016	0.004	27.18	1.67	-38.90	7.20
EGN-17.5	75	5241.58	158.89	7.75	0.43	1.423	1.023	0.005	26.78	1.02	-54.60	7.22
EGN-17.5	95	6980.14	220.92	8.78	0.28	1.276	1.018	0.004	26.60	0.91	-10.00	7.20
EGN-17.5	115	6381.10	117.83	8.04	0.07	1.169	1.064	0.006	26.06	0.92	16.00	7.22
EGN-20	0	74.92	15.11	3.58	0.10	1.389	1.117	0.004	30.37	16.72	167.00	8.79
EGN-20	7	166.75	19.43	4.34	0.24	4.777	1.096	0.003	29.48	16.16	35.00	8.06
EGN-20	15	413.93	50.60	4.95	0.17	1.869	1.118	0.003	28.90	15.92	-28.00	7.90
EGN-20	25	1431.56	42.97	11.05	0.22	0.793	1.065	0.006	2.70	10.75	-50.00	7.31
EGN-20	35	2138.34	95.77	11.65	0.13	0.510	1.028	0.008	26.58	6.69	-50.00	7.21
EGN-20	55	3147.94	194.07	10.28	0.33	1.274	1.056	0.006	27.76	4.87	-94.80	7.24
EGN-20	75	4467.86	72.82	9.41	0.30	1.448	1.060	0.006	27.02	3.42	-82.00	7.25
EGN-20	95	3866.91	203.88	10.78	0.28	1.117	1.057	0.007	26.40	4.57	-134.00	7.20
EGN-20	115	4388.76	252.04	1.43	0.14	0.604	1.048	0.009	25.74	1.00	-29.20	7.30

May-2005												
MS	**Depth (cmbsf)**	**^{222}Rn (dpm/L)**	**2σ**	**^{226}Ra (dpm/L)**	**2σ**	**U (ng/g)**	**^{234}U/^{238}U**	**2σ**	**Temperature (^{o}C)**	**Salinity**	**Eh**	**pH**
EGN-22.5	0	200.62	29.64	28.33	0.11	1.358	1.136	0.007	29.04	15.95	174.40	8.23
EGN-22.5	20	228.89	41.79	4.83	0.39	1.102	1.131	0.006	26.94	16.10	-81.00	7.42
EGN-22.5	60	888.74	55.18	45.11	0.31	0.549	1.048	0.007	26.98	10.77	-9.40	7.06
EGN-22.5	100	3489.51	47.81	19.24	0.03	0.679	1.028	0.005	26.08	5.31	8.00	7.03
EGN-22.5	140	2079.66	34.70	29.95	0.10	0.110	1.058	0.009	26.08	6.92	25.20	7.00
EGN-22.5	180	2402.71	155.62	27.75	0.24				25.18	9.23	8.00	7.04
EGN-30	0	17.15	7.43	2.94	0.10	1.405	1.164	0.004	28.57	16.86	209.80	8.55
EGN-30	10	99.70	4.59	3.66	0.32	1.877	1.157	0.005	26.26	16.97	-60.00	7.53
EGN-30	30	329.81	44.50	8.38	0.30	0.190	1.072	0.011	26.16	18.13	-115.00	7.29
EGN-30	50	375.99	82.23	13.76	0.13	0.131	1.084	0.012	25.99	19.56	-83.00	7.29
EGN-30	150	2455.03	75.58	11.10	0.28	0.273	1.068	0.005	25.39	22.28	68.00	6.91
EGN-30	190	962.57	72.88	10.71	0.15	0.078	1.066	0.016	25.13	20.64	59.00	6.96
EGN-30	230	676.90	23.65	13.59	0.03	0.046	1.048	0.011	24.79	20.97	66.50	7.01

Sep-2005												
Multisampler	**Depth (cmbsf)**	**^{222}Rn (dpm/L)**	**2σ**	**^{226}Ra (dpm/L)**	**2σ**	**U (ng/g)**	**^{234}U/^{238}U**	**2σ**	**Temperature (^{o}C)**	**Salinity**	**Eh**	**pH**
EGN-0	0	146.00	12.67	1.83	0.08	1.715	1.109	0.004	31.9	14.12	222.4	7.93
EGN-0	7	2610.31	84.65	14.16	0.72	0.478	1.099	0.007	30.05	7.88	56.1	7.22
EGN-0	15	4505.55	83.73	9.63	0.44	0.640	1.078	0.005	29.3	2.48	100.4	7.67
EGN-0	25	5446.14	224.99	3.70	0.15	0.908	1.055	0.004	28.61	0.35	118.9	7.67
EGN-0	35	6259.33	52.24	3.81	0.18	0.987	1.043	0.005	28.45	0.2	103	7.92
EGN-0	55	6420.90	159.23	8.43	0.20	0.482	1.069	0.005	28.22	0.18	64	7.57
EGN-0	75	8007.03	252.78	3.00	0.22	0.519	1.027	0.004	27.96	0.24	113.3	8.17
EGN-0	95	7563.67	237.40	5.72	0.02	0.591	1.030	0.008	28.1	0.29	87.4	8.01
EGN-0	115	6318.66	137.02	4.19	0.12	1.548	0.997	0.002	27.95	0.22	73.5	8.19
EGN-5	0	177.20	52.08						28.83	14.25	186	8.24
EGN-5	7	3148.90	80.95						28.81	7.57	-13.7	7.3
EGN-5	15	5381.85	980.08						28.82	2.09	45	7.38
EGN-5	25	6533.38	165.03						28.8	0.39	15	7.45
EGN-5	35	7172.43	536.28						28.65	0.31	-4	7.41
EGN-5	55	8645.65	525.30						28.8	0.25	25.2	7.42
EGN-5	75	9326.15	811.53						28.17	0.25	96	7.49
EGN-5	95	9937.25	281.72						28.36	0.28	-32	7.2
EGN-5	115	7346.70	144.47						27.88	0.25	106	7.52
EGN-10	0	45.82	4.21	1.83	0.08	1.792	1.121	0.003	30.6	15	231	8.16
EGN-10	7	1125.96	66.92			2.303	1.107	0.002	30.12	12.13	31.1	7.9
EGN-10	15	2171.92	176.57	13.45	0.10	1.681	1.106	0.004	29.42	7.61	30	7.83
EGN-10	25	4246.38	257.17			0.250	1.103	0.012	29.7	1.01	70.3	7.89
EGN-10	35	4680.04	268.46	4.29	0.23	0.230	1.063	0.012	29.07	0.56	58.4	7.9
EGN-10	55	4689.68	221.11			0.288	1.061	0.023	28.81	0.43	22	7.87
EGN-10	75	3614.85	101.93	5.45	0.07	0.423	1.046	0.010	28.59	0.44	53	8.02
EGN-10	95	3359.99	127.88			0.460	1.011	0.015	28.74	0.45	66.6	7.9
EGN-10	115	3414.40	454.08			0.516	1.012	0.007	28.34	0.49	90.4	7.94

Sep-2005												
Multisampler	**Depth (cmbsf)**	**^{222}Rn (dpm/L)**	**2σ**	**^{226}Ra (dpm/L)**	**2σ**	**U (ng/g)**	**^{234}U/^{238}U**	**2σ**	**Temperature (^{o}C)**	**Salinity**	**Eh**	**pH**
EGN-15	0	78.81	10.17	4.63	0.43	1.640	1.120	0.005	32.5	14.33	239.9	8.42
EGN-15	7	165.14	26.08	5.21	0.02	4.230	1.082	0.003	31.62	14.32	86.5	8.21
EGN-15	15	780.35	37.48	8.82	0.44	2.313	1.089	0.034	31.06	11.97	38.4	8.14
EGN-15	25	2518.85	82.40	11.85	0.18	1.063	1.076	0.008	29.42	4.71	38	7.96
EGN-15	35	3580.57	154.20	8.94	0.14	0.678	1.038	0.006	29.37	1.5	48.9	8.06
EGN-15	55	3213.60	86.34	8.64	0.22	0.622	1.048	0.006	29.23	1.44	41.1	7.77
EGN-15	75	4015.05	131.75	6.61	0.32	0.440	1.051	0.007	29.41	3.02	52.7	7.91
EGN-15	95	3282.37	463.24	5.89	0.38	0.589	1.057	0.005	28.97	0.87	41	7.82
EGN-15	115	3555.51	165.51	6.42	0.19	0.705	1.053	0.010	29.04	0.86	51	8.03
EGN-17.5	0	50.39	25.67			1.798	1.120	0.005	32.31	14.74	182	8.3
EGN-17.5	7	301.89	67.51			3.532	1.116	0.005	32.1	14.64	71	8.18
EGN-17.5	15	930.04	99.45			3.193	1.092	0.005	31.88	14.13	10	8.02
EGN-17.5	25	2268.62	128.91			0.697	1.079	0.010	30.48	7.54	0	7.9
EGN-17.5	35	3125.44	60.74			1.131	1.024	0.004	29.61	2.15	-3	7.78
EGN-17.5	55	4419.30	170.92			1.222	1.021	0.003	29.52	0.98	5	7.89
EGN-17.5	75	6444.43	297.70			1.678	1.096	0.003	29.36	0.88	-23	7.78
EGN-17.5	95	7709.86	89.89			0.961	1.026	0.006	29.11	0.96	15.7	7.51
EGN-17.5	115	6548.68	193.92			0.899	1.011	0.006	28.93	0.82	24	7.61
EGN-20	0	85.92	30.08			1.764	1.138	0.005	29.88	14.51	157	8.34
EGN-20	7	310.32	7.80			3.193	1.110	0.004	29.38	13.81	9	7.66
EGN-20	15	489.61	73.50			1.617	1.106	0.006	29.25	12.05	-40	7.4
EGN-20	25	1618.66	280.49			1.032	1.089	0.010	29.3	6.43	-59.6	7.17
EGN-20	35	3002.75	222.91			0.910	1.038	0.007	29.31	2.02	-25.6	7.23
EGN-20	55	2354.37	388.21			1.317	1.034	0.005	29.63	1.34	9	7.39
EGN-20	75	493.86	77.30			3.198	1.037	0.003	29.04	1.99	-100	7.25
EGN-20	95	5455.04	399.55			1.211	1.048	0.007	29.03	1.16	-5	7.51
EGN-20	115	4680.53	474.08			0.498	1.033	0.005	28.57	0.78	8	7.28

Sep-2005												
Multisampler	**Depth (cmbsf)**	**^{222}Rn (dpm/L)**	**2σ**	**^{226}Ra (dpm/L)**	**2σ**	**U (ng/g)**	**^{234}U/^{238}U**	**2σ**	**Temperature (^{o}C)**	**Salinity**	**Eh**	**pH**
EGN-22.5	0	68.35	12.99			1.742	1.120	0.005	30.47	15.48	85.8	8.25
EGN-22.5	20	116.89	16.41			2.260	1.115	0.005	29.74	14.9	-20.7	8.1
EGN-22.5	60	847.53	45.29			1.034	1.056	0.005	28.89	10.31	-70.5	7.44
EGN-22.5	100	3767.18	142.49			0.643	1.033	0.010	28.9	6.36	-13.3	4.42
EGN-22.5	140	2684.80	144.71			0.253	1.051	0.011	28.71	5.08	1.8	7.51
EGN-22.5	180	2502.11	133.17			0.191	1.082	0.016	28.75	5.9	2.5	7.75
EGN-30	0	65.44	7.50	3.75	0.08	1.822	1.116	0.006	31.12	15.74	170.1	8.4
EGN-30	10	131.27	38.04	10.04	0.03	0.587	1.121	0.008	29.66	15.7	-90.4	7.35
EGN-30	30	357.95	2.73	10.11	1.39	0.190	1.107	0.003	29.01	13.85	-104	7.22
EGN-30	50	499.37	26.79	13.17	0.14	0.109	1.129	0.016	28.86	15.28	-118	7.23
EGN-30	150	2530.18	45.59	13.72	0.50	0.291	1.064	0.011	29.26	20.72	325.2	6.83
EGN-30	190	995.60	117.37	15.35	0.18	0.058	1.017	0.032	29.11	19.69	72.3	6.85
EGN-30	230	777.97	83.47	18.45	0.78	0.097	1.111	0.013	29.09	19.79	85.5	6.76

May-2006												
MS	**Depth (cmbsf)**	**^{222}Rn (dpm/L)**	**2σ**	**^{226}Ra (dpm/L)**	**2σ**	**U (ng/g)**	**^{234}U/^{238}U**	**2σ**	**Temperature (^{o}C)**	**Salinity**	**Eh**	**pH**
EGNW-OS	225	2176.23	170.29			0.072	1.053	0.028		0.26		
EGN-0	0	281.25	2.83	6.09	0.00	2.229	1.101	0.006	31.63	21.76	229.1	8.61
EGN-0	7	691.96	19.89	7.22	0.09	4.126	1.100	0.002	31.32	21.94	132.3	8.41
EGN-0	15	2775.81	72.14	58.81	0.28	3.565	1.032	0.001	29.59	15.22	170.95	7.76
EGN-0	25	5255.69	53.54	37.55	1.04	2.407	1.028	0.007	28.86	2.17	184.75	7.82
EGN-0	35	6130.52	164.48	6.81	0.01	2.625	1.019	0.005	28.56	0.4	185.55	7.99
EGN-0	55	6156.44	246.40	5.09	0.17	2.980	1.010	0.005	28.43	0.31	168.35	7.94
EGN-0	75	7568.97	158.41	3.06	0.01	3.497	1.005	0.002	27.55	0.31	179	7.58
EGN-0	95	7520.73	172.01	5.53	0.19	3.979	1.007	0.003	27.54	0.41	149.4	8.06
EGN-0	115	6057.17	286.01	9.83	0.01	3.941	1.002	0.003	27.49	1.01	144.75	8.22
EGN-10	0	260.68	20.79	5.24	0.14	2.123	1.118	0.004	32.9	22.17	228.7	8.48
EGN-10	7	1251.84	28.91	16.58	0.47	1.258	1.078	0.006	30.98	17.84	101.7	7.86
EGN-10	15	2684.18	260.61	11.60	0.38	0.370	1.108	0.011	29.91	9.42	109.1	7.90
EGN-10	25	4377.46	163.67	6.33	0.33	0.252	1.099	0.013	28.71	1.72	144.2	7.99
EGN-10	35	4872.45	117.23			0.185	1.099	0.014	28.56	0.74	157.6	7.98
EGN-10	55	4641.18	65.21	3.49	0.12	0.493	1.017	0.010	27.86	0.37	141.6	8.00
EGN-10	75	3655.58	187.29	4.27	0.01	0.406	1.047	0.010	27.37	0.4	126.4	8.09
EGN-10	95	3339.50	64.60	4.84	0.03	0.406	1.018	0.011	27.11	0.38	172.5	8.18
EGN-10	115	3600.09	205.18	2.77	0.13	0.439	1.049	0.008	27.27	0.47	168.1	8.23
EGN-17.5	0	91.43	9.27	4.88	0.11	2.254	1.121	0.003	33.72	22.95	233	8.57
EGN-17.5	7	204.57	12.84	6.03	0.27	5.775	1.077	0.002	32.96	22.92	111.2	8.08
EGN-17.5	15	470.60	6.25	24.09	0.78	6.916	1.059	0.004	32.33	19.12	89.2	7.83
EGN-17.5	25	874.41	84.12	50.00	3.34	8.916	1.029	0.001	30.14	17.85	58.8	7.63
EGN-17.5	35	1385.07	50.40	81.41	7.47	8.994	1.008	0.003	29.35	16.17	65.6	7.64
EGN-17.5	55	2051.47	75.94	81.45	3.35	3.022	1.019	0.005	28.41	9.7	69.2	7.63
EGN-17.5	75	5890.84	108.03	38.23	1.03	2.250	1.004	0.004	28.54	4.61	79	7.77
EGN-17.5	95	7499.77	280.73	6.37	0.11	1.337	1.013	0.006	27.13	0.77	103	7.84
EGN-17.5	115	6382.26	200.28	7.49	0.62	1.066	0.995	0.007	27.59	0.76	113.3	7.91

May-2006												
MS	**Depth (cmbsf)**	**^{222}Rn (dpm/L)**	**2σ**	**^{226}Ra (dpm/L)**	**2σ**	**U (ng/g)**	**^{234}U/^{238}U**	**2σ**	**Temperature (^{o}C)**	**Salinity**	**Eh**	**pH**
EGN-20	0	112.26	30.76	5.77	0.77	2.174	1.134	0.007	34.09	20.365	225.7	8.48
EGN-20	7	195.09	9.08			3.106	1.105	0.004	32.35	19.955	58.3	8.04
EGN-20	15	458.99	18.48	9.96	0.06	2.094	1.090	0.003	31.55	19.46	18.3	7.85
EGN-20	25	1526.01	50.84	15.13	0.30	1.482	1.058	0.008	28.82	10.605	24.4	7.69
EGN-20	35	2380.23	160.10	17.17	0.34	1.910	1.038	0.007	27.81	6.5	54.2	7.46
EGN-20	55	2032.79	187.44	20.23	0.44	2.737	1.029	0.005	28.69	6.28	83.9	7.35
EGN-20	75	1404.78	231.30	17.25	0.39	2.999	1.057	0.005	28.43	11.685	67	7.45
EGN-20	95	5423.11	180.35	10.60	2.99	2.176	1.025	0.003	27.39	1.445	163.6	8.00
EGN-20	115	4336.89	142.77	3.67	0.07	0.565	1.043	0.011	26.08	0.755	96.69	7.90
EGN-22.5	0	101.65	24.33	3.55	0.004	2.377	1.112	0.004	32.08	23.62	221.0	8.24
EGN-22.5	20	172.61	27.83	6.95	0.43	1.616	1.112	0.004	25.83	12.43	22.2	7.42
EGN-22.5	60	973.17	45.16	22.83	0.29	0.895	1.052	0.006	27.33	8.99	-34.9	7.57
EGN-22.5	100	3739.70	239.67			0.322	1.028	0.016	27.13	5.54	34.2	7.42
EGN-22.5	140	2353.78	236.51	8.00	0.27	0.145	1.110	0.020	21.02	5.31	7.9	7.68
EGN-22.5	180	2245.84	89.99			0.137	1.082	0.017	31.18	19.85	-1	7.88
EGN-30	0	89.79	10.54			2.267	1.113	0.006	32.65	23.47	215.95	8.29
EGN-30	10	116.71	6.29	6.03	0.16	0.738	1.113	0.008	29.92	20.75	-17.55	7.55
EGN-30	30	308.21	9.03	9.09	0.04	0.301	1.046	0.009	27.64	16.26	-31.85	7.91
EGN-30	50	350.42	3.34	17.48	1.43	0.298	1.092	0.020	27.59	20.76	-9.85	7.77
EGN-30	150	2680.67	111.22	13.79	0.34	0.305	1.076	0.014	26.73	19.48	104.5	7.47
EGN-30	190	1043.65	66.17	10.64	0.15	0.078	1.124	0.027	25.62	19.74	129.15	7.38
EGN-30	230	668.04	23.98	11.50	0.32	0.253	1.007	0.037	25.77	22.71	97	7.67

May-2006												
MS	**Depth (cmbsf)**	**^{222}Rn (dpm/L)**	**2σ**	**^{226}Ra (dpm/L)**	**2σ**	**U (ng/g)**	**^{234}U/^{238}U**	**2σ**	**Temperature (^{o}C)**	**Salinity**	**Eh**	**pH**
CIRL-39	0	61.49	34.60			2.440	1.109	0.004	26.79	24.74	175.2	
CIRL-39	10	10.77	2.78			3.087	1.130	0.005	26.47	24.86	24.2	
CIRL-39	20	90.18	4.30			1.139	1.106	0.008	26.16	21.58	-29.5	
CIRL-39	30	55.91	31.50			0.762	1.124	0.009	15.84	20.64	-33.4	
CIRL-39	40	136.76	5.05			0.698	1.116	0.005	25.81	20.08	-44.4	
CIRL-39	60	175.39	33.68			0.510	1.106	0.009	25.77	18.1	-52.9	
CIRL-39	90	271.53	44.00			0.955	1.143	0.009	25.84	20.75	-74.8	
CIRL-39	140	225.05	10.26			1.818	1.123	0.005	24.81	20.91	-54	
CIRL-39	180	502.21	31.33			1.706	1.093	0.008	24.8	20.99	-29.5	

Oct-2006												
MS	**Depth (cmbsf)**	**^{222}Rn (dpm/L)**	**2σ**	**^{226}Ra (dpm/L)**	**2σ**	**U (ng/g)**	**^{234}U/^{238}U**	**2σ**	**Temperature (^{o}C)**	**Salinity**	**Eh**	**pH**
EGNW-OS	225	2366.57	185.89			0.081	1.012	0.009		0.18		
EGN-0	0	120.39	19.47	6.56	0.46	1.732	1.097	0.006	27.44	15.62	235.8	8.09
EGN-0	7	1019.32	79.97	14.14	1.02	10.033	1.042	0.007	27.4	14.35	168.5	7.84
EGN-0	15	3946.59	206.15	37.10	0.08	5.144	1.042	0.005	27.29	7.22	201.5	7.97
EGN-0	25	4766.66	150.84	14.08	0.03	3.158	1.029	0.004	27.12	0.58	210.6	7.72
EGN-0	35	5478.91	109.88	6.28	0.02	3.521	1.015	0.005	26.86	0.56	228.1	8.37
EGN-0	55	5983.65	123.26	3.26	0.02	4.074	1.018	0.003	26.86	0.32	212.5	8.29
EGN-0	75	7567.32	114.78	5.22	0.50	4.829	0.966	0.002	27.1	0.29	204.7	8.24
EGN-0	95	7355.37	192.50	7.20	0.11	5.050	1.007	0.003	27.27	0.5	171.4	7.72
EGN-0	115	6097.93	50.29	4.70	0.03	4.893	1.006	0.003	27.14	0.26	176	8.67
EGN-20	0	22.22	2.59	2.56	0.03	1.489	1.121	0.004	28.2	17.16	214.4	8.32
EGN-20	7	138.07	21.25	5.44	0.02	3.003	1.111	0.002	27.97	16.56	55.3	8.07
EGN-20	15	274.77	49.24	6.45	0.03	2.298	1.099	0.006	27.46	15.57	29.7	8.11
EGN-20	25	1958.23	84.67	10.55	0.04	1.333	1.088	0.009	27.16	7.37	51.1	7.7
EGN-20	35	2957.01	94.98	17.38	0.02	0.997	1.039	0.006	27.17	5.65	53.4	8.13
EGN-20	55	3873.42	167.08	21.88	1.36	1.403	1.047	0.003	27.37	6.8	33.8	7.6
EGN-20	75	4375.45	181.90	25.52	0.01	2.000	1.064	0.004	27.85	5.95	35.6	7.64
EGN-20	95			7.94	0.08	2.589	1.047	0.003	27.76	1.45	113.3	7.82
EGN-20	115	4897.51	94.53	4.37	0.03	0.502	1.026	0.006	28.14	0.98	82.5	8.25
EGN-30	0	16.62	1.35	5.05	0.02	1.464	1.126	0.002	27.6	17.1	231.8	8.35
EGN-30	10	86.83	3.49	5.49	0.04	1.955	1.123	0.002	26.48	17.55	-46.9	7.71
EGN-30	30	451.32	44.42	12.50	1.09	0.270	1.085	0.009	27.09	21.19	-40.5	7.77
EGN-30	50	620.80	90.14	17.18	0.42	0.293	1.092	0.010	27.4	21.37	-52.3	7.73
EGN-30	150	2792.31	108.94	13.78	0.60	0.212	1.075	0.011	27.98	19.63	94.2	7.62
EGN-30	190	1053.24	88.16	16.03	0.84	0.167	0.999	0.010	28.12	19.58	128	7.69
EGN-30	230	920.13	41.55	15.04	1.05	0.143	0.976	0.043	27.97	19.66	68.5	7.76

Oct-2006												
MS	**Depth (cmbsf)**	**^{222}Rn (dpm/L)**	**2σ**	**^{226}Ra (dpm/L)**	**2σ**	**U (ng/g)**	**^{234}U/^{238}U**	**2σ**	**Temperature (^{o}C)**	**Salinity**	**Eh**	**pH**
CIRL-39	-30	32.12	9.76	4.87	0.21	1.619	1.112	0.005	26.98	19.86	141.7	8.39
CIRL-39	10	32.69	1.20	4.97	0.02	1.485	1.114	0.006	26.84	20.83	-67.4	7.81
CIRL-39	20	62.36	7.46	3.56	0.01	1.194	1.137	0.009	26.68	21.95	-75	7.87
CIRL-39	30	76.15	15.65	4.62	0.03	1.318	1.108	0.011	26.99	21.45	-83.5	7.85
CIRL-39	40	80.94	22.15	4.89	0.05	1.328	1.136	0.006	26.95	21.56	-75.9	7.64
CIRL-39	60	195.20	3.00	4.22	0.08	0.872	1.124	0.005	27.16	21.16	-85	7.36
CIRL-39	90	182.71	14.53	11.06	0.00	0.775	1.138	0.008	26.83	21.08	-82.8	7.47
CIRL-39	140	220.33	17.36	9.24	0.02	1.540	1.132	0.005	27.24	21.34	-58.9	7.16
CIRL-39	180	469.43	40.64	8.22	0.41	0.728	1.101	0.005	27.2	22.25	-81.7	6.83

APPENDIX D.

SEDIMENT ^{226}Ra DATA

Core	Depth (cmbsf)	Total ^{226}Ra (dpm/g)	Error	Effective ^{226}Ra (dpm/g)	Error	^{222}Rn Emanation Rate (dpm/L)	Error
EGN-0	6	0.35	0.25	0.07	0.004	357	22
EGN-0	16	0.88	0.24	0.13	0.01	717	27
EGN-0	26	1.26	0.05	0.21	0.005	1311	29
EGN-0	36	0.48	0.09	0.07	0.004	422	26
EGN-0	56	0.99	0.11	0.30	0.01	1579	47
EGN-0	76	1.58	0.13	0.82	0.01	4720	79
EGN-0	106	1.56	0.19	1.04	0.01	5550	67
EGN-0	146	2.08	0.13	1.94	0.02	12229	97
EGN-0	161	1.58	0.29	1.10	0.01	6558	30
EGN-0	176	0.65	0.20	0.18	0.01	1093	37
EGN-0	206	1.63	0.32	0.32	0.01	1719	34
EGN-10	6	0.67	0.09	0.08	0.005	666	38
EGN-10	16	1.63	0.07	0.11	0.005	566	24
EGN-10	26	0.81	0.23	0.07	0.004	397	20
EGN-10	36	0.95	0.14	0.11	0.01	688	39
EGN-10	56	1.00	0.27	0.78	0.01	4802	69
EGN-10	76	1.38	0.18	0.55	0.01	3689	75
EGN-10	106	1.07	0.00	0.40	0.005	3391	38
EGN-10	116	0.60	0.22	0.29	0.01	2182	67
EGN-10	146	1.60	0.45	1.06	0.01	7354	40
EGN-10	176	1.36	0.04	0.75	0.005	4409	27
EGN-10	206	0.70	0.18	0.20	0.01	1157	44
EGN-17.5	6			0.09	0.004	479	21
EGN-17.5	16			0.21	0.01	1143	34
EGN-17.5	26			0.25	0.01	1267	36
EGN-17.5	36			0.28	0.01	2253	97
EGN-17.5	56			0.23	0.01	2236	72
EGN-17.5	76			0.68	0.01	5306	107
EGN-17.5	81.5			0.66	0.01	4734	94
EGN-17.5	96			0.49	0.01	2839	59
EGN-17.5	116			0.77	0.01	3729	59

Core	Depth (cmbsf)	Total ^{226}Ra (dpm/g)	Error	Effective ^{226}Ra (dpm/g)	Error	^{222}Rn Emanation Rate (dpm/L)	Error
EGN-20	6	0.82	0.01	0.05	0.004	287	24
EGN-20	16	0.82	0.17	0.13	0.004	796	25
EGN-20	21	0.66	0.17	0.11	0.004	549	20
EGN-20	36	0.41	0.28	0.08	0.01	522	52
EGN-20	56	1.00	0.40	0.22	0.01	1755	46
EGN-20	76	1.36	0.17	0.44	0.01	3763	71
EGN-20	96	1.51	0.31	0.38	0.01	2203	32
EGN-20	116	1.03	0.07	0.38	0.01	2789	65
EGN-20	146	7.44	0.21	0.44	0.002	3683	20
EGN-20	176	2.23	0.03	0.36	0.002	2780	17
EGN-20	206	0.70	0.18	0.23	0.002	1735	19
EGN-30	6	0.92	0.04	0.07	0.004	337	21
EGN-30	21	1.19	0.22	0.12	0.01	557	29
EGN-30	26	0.68	0.07	0.07	0.004	256	17
EGN-30	36	0.72	0.03	0.05	0.01	249	33
EGN-30	56	1.08	0.10	0.07	0.005	348	23
EGN-30	76	1.29	0.23	0.33	0.01	1598	35
EGN-30	96	1.48	0.03	0.46	0.01	2211	25
EGN-30	121	0.67	0.29	0.40	0.01	2160	52
EGN-30	146	0.76	0.25	0.25	0.004	1227	19
EGN-30	176	0.65	0.04	0.15	0.004	638	17
EGN-30	206	1.10	0.07	0.21	0.01	784	20
EGN-30	231	1.11	0.05	0.24	0.01	1154	37

APPENDIX E.

PERMISSION TO USE COPYRIGHTED MATERIAL

American Society of Limnology & Oceanography
5400 Bosque Boulevard, Suite 680 · Waco, Texas 76710 4446 · (254) 399 9635 or (800) 929 2756

June 4, 2008

Christopher G. Smith
Louisiana State University
Dept. of Oceanography & Coastal Sciences
RM 1223 Energy, Coast, & Environment Bldg.
Baton Rouge, Louisiana 70803

To Christopher G. Smith,

On behalf of the American Society of Limnology and Oceanography, we are happy to grant permission to use the following articles and/or figures from *Limnology & Oceanography*.

Author(s) Name(s): Christopher G. Smith, Jaye E. Cable, Jonathan B. Martin,

Journal Title: Limnology and Oceanography Publication Date: 2008

Volume: 53 Issue: 2 Page: 666-674 Figure:

Title. Elucidating marine pore water exchange and fresh aquifer sources in estimates of submarine groundwater discharge to a coastal lagoon.

Special Notes: The article will appear as part of my dissertation

When reproducing the article/figure(s), please cite according to the references that follow:

All copyrighted works, whether displayed electronically or in print, should be properly acknowledged as follows:

"Copyright (2008) by the American Society of Limnology and Oceanography, Inc."

Once permission is granted to use an article or any part thereof of a work from L&O, the full citation must include:
1. Name(s) of the author(s);
2. Journal title (Limnology & Oceanography or L&O)
3. Publication date
4. Volume number
5. Issue number
6. Chapter or article name
7. Pages on which the articles, data, and/ or figure(s) appear

For your records, the American Society of Limnology and Oceanography is a nonprofit organization (Taxpayer I D Number: 38-1710020)

If you have additional requests or have any questions in regard to this request, you can contact me directly via e-mail at jowood@sgmeet.com.

Sincerely,

Lysia Zavala
ASLO Business Office

VITA

Christopher Gerald Smith was born on August 1979 in Kinston, North Carolina. He is the son of Gerald (Jr.) and Myra Smith and the younger brother of Brad Smith. He is the husband of Jeanna Taylor-Smith and father of Alana Jolie Smith. He attended East Duplin High School in Beulaville, North Carolina, and graduated in 1997. It was during these early years and his interest in surfing that Chris truly became mesmerized by coastal systems. Chris enrolled at East Carolina University in Greenville, North Carolina, where he studied geology. He received a degree of Bachelor of Science in geology in December 2001. Chris entered the graduate program at East Carolina University in January 2002. He used sedimentological, paleontological, radiochronological, and geospatial data sets to decipher the late Holocene geologic development of two sections of the Outer Banks of North Carolina in his thesis research. He was awarded a Master of Science degree in geology in May 2004. On the 26 June 2004, Jeanna and Chris were married; one month later they packed up and moved to Baton Rouge, Louisiana. In August 2004, Chris enrolled as a doctoral student in the Department of Oceanography and Coastal Sciences at Louisiana State University. On 1 February 2007, Jeanna gave birth to their first daughter, Alana. He will earn a doctoral degree in oceanography and coastal sciences in August 2008. Chris has accepted a Mendenhall post-doctoral research fellowship with the USGS and will start around October 2008.